Commissioning and verification of compressed air yield on the hydraulic air compressor demonstrator

Justin Sivret

by

A thesis submitted in partial
fulfillment of the requirements for
the degree of Master of Applied
Science (MASc) in Natural
Resources Engineering

The Faculty of Graduate Studies
Laurentian University
Sudbury, Ontario, Canada

THESIS DEFENCE COMMITTEE/COMITÉ DE SOUTENANCE DE THÈSE
Laurentian Université/Université Laurentienne
Faculty of Graduate Studies/Faculté des études supérieures

Title of Thesis Titre de la thèse	Commissioning and verification of compressed air yield on the hydraulic air compressor demonstrator		
Name of Candidate Nom du candidat	Sivret, Justin		
Degree Diplôme	Master of Science		
Department/Program Département/Programme	Engineering	Date of Defence Date de la soutenance	mars 28, 2018

APPROVED/APPROUVÉ

Thesis Examiners/Examinateurs de thèse:

Dr. Dean Millar
(Supervisor/Directeur de thèse)

Dr. Brahim Chebbi
(Committee member/Membre du comité)

Dr. Ramesh Subramanian
(Committee member/Membre du comité)

Approved for the Faculty of Graduate Studies
Approuvé pour la Faculté des études supérieures
Dr. David Lesbarrères
Monsieur David Lesbarrères
Dean, Faculty of Graduate Studies
Doyen, Faculté des études supérieures

Dr. Hubert Chanson
(External Examiner/Examinateur externe)

Dr. Charles Ramcharan
(Internal Examiner/Examinateur interne)

ACCESSIBILITY CLAUSE AND PERMISSION TO USE

Explicit Declaration of Originality

I hereby certify that I am the sole author of this thesis and that no part of this thesis has been published or submitted for publication. The work I have presented in my thesis focuses on the commissioning activities and testing that has been completed at the Hydraulic Air Compressor (HAC) Demonstrator at Dynamic Earth in Sudbury, Ontario. This work includes the commissioning of the system, the calibration of the instruments, the understanding and checking of losses, and the verification of some of the assumptions made during the system design.

Following the major commissioning activities of the Demonstrator, the system was vigorously tested to record a wide range of data permitting the verification of some of the models used to predict the performance of the system before it was built using Young's (2017) model. The model, originally designed by Millar (2014), later upgraded to include solubility loss by Pavese et al. (2016), and finally refined by coupling solubility and psychrometric phenomena by Young (2017) was used to predict the efficiency and the compressed air yield of a HAC this size, which was going to be built at Dynamic Earth. Calculating these parameters using accurate measurements taken on a HAC of this size in real time permitted the verification of some of the assumptions previously made using Young's (2017) model.

Young's thesis (2017) focuses on the theoretical modelling of the HAC process using solubility kinetics which are important to consider in the design process of future HACs. Predictions made using Young's (2017) model can be compared to efficiency and free air delivery analysis on the HAC Demonstrator. These comparisons have revealed unexpected factors that have been found to affect HAC performance. One of these factors was the absolute roughness of rubber lined pipes, and another was the possible occurrence of detrainment in the downcomer pipe which is believed to account for significant head loss in the mixing process that was previously unaccounted for.

Further work on the HAC Demonstrator is looking to explore the performance of the system with other gases, as opposed to atmospheric gases. These trials will seek to evaluate the potential applications of HAC's as CO_2 separation systems. This is a specific research objective of Pavese, who also has a PhD thesis in preparation.

I certify that, to the best of my knowledge, my thesis does not infringe upon anyone's copyright nor violate any proprietary rights and that any ideas, techniques, quotations, or any other material from the work of other people included in my thesis, published or otherwise, are fully acknowledged in accordance with the standard referencing practices. Furthermore, to the extent that I have included copyrighted material that surpasses the bounds of fair dealing within the meaning of the Canada Copyright Act, I certify that I have obtained a written permission from the copyright owner(s) to include such material(s) in my thesis and have included copies of such copyright clearances to my appendix.

I declare that this is a true copy of my thesis, including any final revisions, as approved by my thesis committee and the Graduate Studies office, and that this thesis has not been submitted for a higher degree to any other University or Institution.

Abstract

The completion of the hydraulic air compressor (HAC) demonstrator at Dynamic Earth in Sudbury, Ontario marks the beginning of a series of research activities to increase the efficiency of compressed air production and build confidence in future commercial applications. Before any proper experiments could be conducted on the HAC Demonstrator a series of commissioning activities and testing was completed to i) calibrate the instruments, ii) check and understand losses, and iii) verify, or otherwise, some of the assumptions made during the system design.

The practical work associated with this master's thesis included the development of a human machine interface (HMI) to allow for automated control of the HAC. Instrumentation and control equipment was installed and routed to a control panel providing conditioned power and routes for signals. Within the control panel, these are digitised and transmitted using TCP/ IP/ MODBUS protocol, operating over a TopServer (Software toolbox, 2009) OPC backbone. The OPC Client toolbox in MATLAB was adopted to interface with the OPC Server, and MATLAB's App Designer adopted for authoring the HMI. All I/O functionality is thus routed to MATLAB in which a PID control loop was established between the HAC separator water level and the HAC's compressed air motorized globe valve. Thus, a reliable, flexible, scientific control interface and data storage infrastructure was established for this novel compression plant as part of the master's work. The HAC Demonstrator can now effectively run a variety of experiments while recording a wide range of data for analysis. To date, a series of 90 benchmark tests for compressor performance have been completed in a systematic manner on the demonstrator to create a database of real HAC operating conditions. This thesis thus represents the first formal publication of the HAC Demonstrator's complete performance under the baseline operating conditions.

Previous predictions of the compressed air yield and efficiency of a HAC of this size have been made by Millar (2014), upgraded to weakly couple solubility loss by Pavese et al. (2016) and refined using Young's (2017) detailed coupling of solubility and psychrometric phenomena. The predictions made by these models have been tested. The 1D hydrodynamic solubility models also predicted a small beneficial 'airlift' effect on compressor performance, due to exsolution of formerly dissolved compressed gas, that has also been reported upon.

One unexpectedly important factor that has been found to affect HAC performance that was not anticipated in any of the models included the absolute surface roughness of rubber lined pipe, in comparison to that of bare steel pipe. High precision experiments are reported upon that have produced reliable values for absolute surface roughness for rubber lining materials, that have now been adopted in the HAC models, and may be adopted more widely too. The occurrence of detrainment, water jet-free fall and air re-entrainment is speculated upon as the source of previously unreported loss in the air-water mixing process, based on pressure profiling observations undertaken over the complete performance envelope of the Dynamic Earth HAC Demonstrator.

Keywords: hydraulic air compressors, instrumentation, commissioning, air yield

Acknowledgments

I would like to thank Dean Millar for providing me with this opportunity and guidance through my research, the committee members Brahim Chebbi, Charles Ramcharan, Hubert Chanson and Ramesh Subramanian, the Northern Ontario Heritage Fund Corporation and MITACS for funding my research, my colleagues in the HAC Demonstration Project, my colleagues at MIRARCO and the Bharti School of Engineering at Laurentian University for your assistance with my research. Financial support for the construction of the Hydraulic Air Compressor that is the topic of this reseach is also gratefully acknowledged from the Ultra Deep Mine Network (UDMN), the Northern Ontario Heritage Fund Corporation (NOHFC), the Independent Electricity System Operator (IESO), MIRARCO Mining Innovation and Electrale Innovation Ltd.

Table of Contents

List of Figures

List of Tables

List of Appendices

Nomenclature

A	area, m^2
D	diameter, m
ε	absolute roughness
α	confidence interval
f	friction factor
F	irreversibility losses, J/kg
g	gravity, m/s^2
H	height, m
h	enthalpy, J/kg
$\hbar$	heat transfer coefficient, W/m^2K
k	thermal conductivity, W/mK
L	length, m
$\dot{m}$	mass flow rate, kg/s
n	molar mass, kg/mol
η	efficiency,
P	pressure, Pa
P_{air}	air pressure, Pa
ΔP	differential pressure, Pa
ρ	density, kg/m^3
Q	heat loss rate, W
q	heat loss, J/kg
R	thermal resistance, K/W
$\mathcal{R}$	gas constant, J/kgK
Re	Reynolds number
r	radius, m
S	objective function
T	temperature, K
t	time, s
u	velocity, m/s
μ	viscosity, Pa s
V	specific volume, m^3/kg
w	work, J/kg
z	elevation, m

1. Introduction

This section aims to provide background information on hydraulic air compressor technology followed by a brief overview of the Dynamic Earth HAC project. Objectives of the Dynamic Earth HAC project and personal research objectives highlighting the scope of this thesis are also discussed.

1.1 Hydraulic air compressors (HACs)

Hydraulic air compressors (HACs) are an old technology that take advantage of the potential energy of flowing water to compress atmospheric air. Old HAC installations would be installed near rivers which would provide the flowing water needed for the compression process with zero marginal cost as seen in Figure 1.

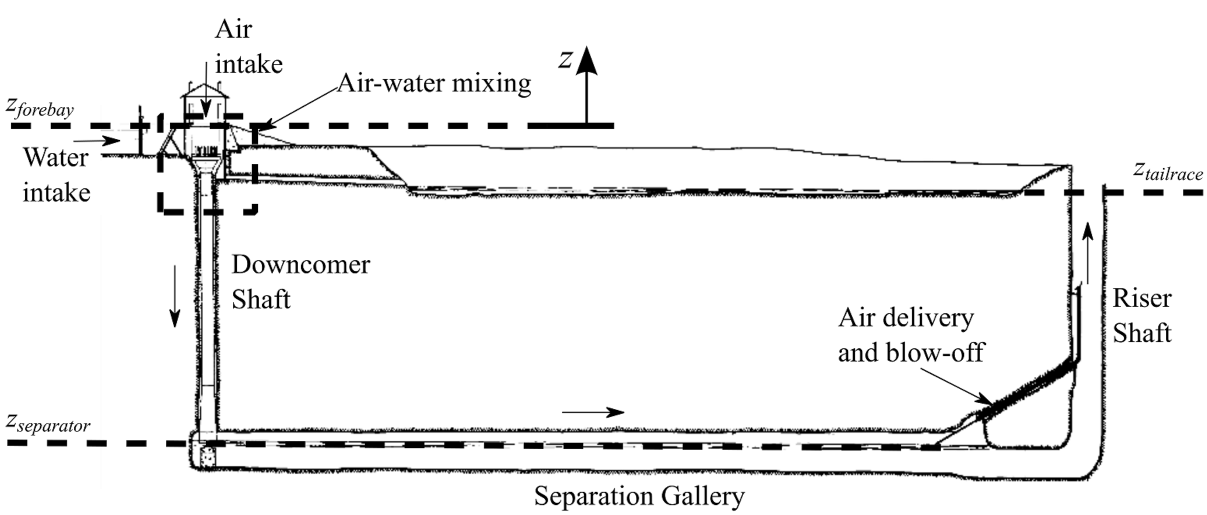

Figure 1: Conventional HAC from Schulze (1954).

The compressed air would then be routed to a location where it was needed. Unfortunately, this limited compressed air applications to locations near bodies of water. Recent research in HAC technology focused on decoupling dependence of the system on a natural water course so that it may be deployed anywhere. The process may still be regarded as energy efficient and the technology promises appreciable reductions in maintenance costs (Young *et al.*, 2016) in comparison to incumbent industrial stationary compressor designs. Modern HACs are designed to function independent of proximity to bodies of water but still meet compressed air needs by using a closed loop system to circulate the water with pumps. HAC adopters users can save on energy by taking advantage of a near-isothermal air compression process reported by Pavese et al (2016). The air transitions from atmospheric pressure to a desired working pressure with virtually no change in temperature. Further savings also arise from its simple, few moving parts arrangement which only needs to circulate water at low head in a closed loop and regulate the amount of compressed air being released from the system. This is expected to lead to high reliability. Typically screw compressors are the default for mine scale compression in Canada while centrifugal compressors are better for larger demand. Commercial scale testing of a modern HAC on a mine site would be required to confirm its energy efficiency in practice, but this aspect of HACs will not be discussed in this report as it falls outside of the scope of work.

The research mentioned has motivated the construction of the Dynamic Earth HAC Demonstrator, a project that has been underway for many years. Following the conceptualization, pilot scale testing, detailed engineering design and construction, the work outlined in this thesis will focus on the commissioning activities and operational aspects of the HAC Demonstrator project.

1.2 Dynamic Earth HAC

Before HACs can be taken to market for various full-scale applications a demonstrator has been commissioned and built at Dynamic Earth in Sudbury, Ontario in the old abandoned ventilation shaft at the former Big Nickel Mine as seen in Figure 2.

Figure 2: Dynamic Earth HAC (Electrale Innovation Ltd, 2017)

This demonstrator has been modelled after an old HAC installation at the Peterborough Lift Lock which ran from around 1903 to 1967 (Rice, 1976). Although it was modelled after such an installation, the demonstrator does not take advantage of a run-of-river configuration and instead utilizes pumps to operate in a closed loop environment by recirculating the water inside the system. The HAC Demonstrator at Dynamic Earth opened on 21st June 2017 and has since been running experiments to prove its energy efficiency and investigate its feasibility for other applications such as carbon capture and mine cooling as detailed by Millar (2014).

1.3 Research objectives

1.3.1 Dynamic Earth HAC program research objectives

The Dynamic Earth HAC program consists of a series of research objectives that need to be completed. Some of these research objectives include:

1. Acceptance testing
2. Verification of the HAC Demonstrator basic commercial readiness
3. Test applicability to deep mine cooling
4. Temperature cycling
5. Performance trials with alternative compression gases
6. Verification of the solubility loss models with Na_2SO_4
7. Performance trials with alternative co-solutes
8. Performance trials with a closed loop configuration

The acceptance testing is completed after the HAC commissioning phase, during the preliminary stages of the project. The HAC Demonstrator needed to be tested to verify that safety features work properly, the HAC is producing air at predicted pressures and air flow rates, and to familiarize the operators with the response time of the system when the pump speed is changed, or when the system is started up. This process constituted the first time an industrial scale hydraulic air compressor was started up in approximately one century and so was regarded a research task. The

Candidate was the person primarily charged with this responsibility and consequently, these aspects constituted a primary research objective.

The verification of basic commercial readiness seeks to prove the HACs compressor efficiency and air yield over a wide range of water mass flow rates. Repeated testing with varying head, a consequence of operating the HAC with varying amounts of circulating water had the objective of producing a HAC performance map of efficiency and free air delivery versus head and mass flow rate.

A final objective of this specific research was the preliminary verification of the nearly-isothermal compression process predicted by Millar (2014) and Pavese at al (2016), although this will be subject to far more detailed and rigorous verification in the PhD thesis under preparation by Clifford (2016).

Wider HAC Demonstrator Project objectives, that are not a specific part of this thesis include assessment of the potential for HACs to provide deep mine cooling. This has been reported by Rico (2017). By using the compressed air from a HAC and passing it through an expansion device and mixing it with the mine ventilation air, this test will seek to confirm the role of the HAC in potential mine refrigeration systems.

Also within the scope of this specific research, the HAC Demonstrator will also be put through long duration testing to verify the effects of temperature cycling on the system. By circulating the water in the HAC over an extended period we can report the increase in temperature over time and measure its effects on the gas solubility. Natural cooling of the system and possible active cooling techniques can also be tested.

Once enough tests have been run with atmospheric air the HAC performance will be investigated with other gases. Flue gas trials will be used to evaluate the potential application of HACs as CO_2 separation systems, potentially enabling the HAC technology to enter the carbon capture market. This is a specific research objective of Pavese who also has a PhD thesis in preparation.

Gas solubility increases with increasing pressure and leads to a loss of compressed gas in HACs. By dissolving certain co-solutes within the circulating water of the HAC it is hypothesised, as explained by Young (2017) that the loss of compressed gas can be reduced, and ultimately it is planned that this will be verified using the HAC Demonstrator too. Gas yield is monitored during testing and the gas composition is analyzed using a mass spectrometer to compare the experimental results with predictions.

Various co-solutes can also be tested on the HAC Demonstrator to verify the effects on air yield. Potential alternatives include sodium chloride sodium sulphate and organic solutes such as sucrose, or glycerol and a corrosion inhibiting co-solute such as ethylene glycol. Tests with these materials will help establish an optimum combination to obtain the maximum compressed air yield.

The HACs performance is also to be evaluated using a different mixing head based on the Clausthal (Schulze, 1954) head design. Performance trials in a closed loop configuration using this alternative head design will be undertaken and analyzed. The HAC can run in a closed loop configuration by routing the compressed air back into the forebay tank instead of pulling atmospheric air from the outside. Completing these research objectives is an essential part in concluding the HAC Demonstrator project.

1.3.2 Personal research objectives

Personal research objectives for the Dynamic Earth HAC include the calibration of instruments, installation of the instruments, commissioning of the HAC, design and programming of a human machine interface (HMI), checking and understanding losses in the system, and verifying some of the assumptions made during the system design. To reduce any potential delays in the commissioning of the HAC Demonstrator much of the testing and calibration of the instruments was performed off site before demonstrator construction was complete. The HMI was also programmed before commissioning and completed once the HAC Demonstrator was built and the communications infrastructure was in place. As soon as the system was operational the final objective was to check and understand the losses of the system by running the HAC Demonstrator through a series of tests and experiments. These tests would also serve as verification for the assumptions made on the system during the design process.

The scope of the research presented includes all tasks associated with the commissioning of the HAC Demonstrator and all work required to verify key assumptions made during the system design. Cost and efficiency analysis looking to compare HAC technology, or the HAC Demonstrator, to other air compression technologies do not fall within the scope of this research and shall not be discussed.

1.4 Thesis overview

Chapter 1 describes what a HAC is and what the goal for the Dynamic Earth HAC is along with a description of the personal research objectives.

Chapter 2 provides a brief overview for the HAC thermodynamic processes.

Chapter 3 presents the testing and calibration of the instrumentation and software at the Dynamic Earth HAC before starting with the experiments.

Chapter 4 describes work completed to automate the HAC Demonstrator system during operation and for post process data analysis.

Chapter 5 presents some of the acceptance tests performed on the HAC after commissioning of the system was complete.

Chapter 6 provides an overview of some established experimental procedures and quality control techniques used on site.

Chapter 7 describes the experimental program that is followed to prepare the HAC for commercial readiness.

Chapter 8 briefly summarizes any conclusions and describes any future work on the HAC Demonstrator.

2. HAC theory

This section examines the underlying HAC theory and provides an overview of the HAC process. Further attention is also given to the instrumentation that has been installed on the HAC Demonstrator that is used to verify the assumptions made during the system design.

2.1 Process flow diagram

A process flow diagram for a HAC can be seen in Figure 3. This diagram illustrates the relationship the various components of the HAC Demonstrator have with each other.

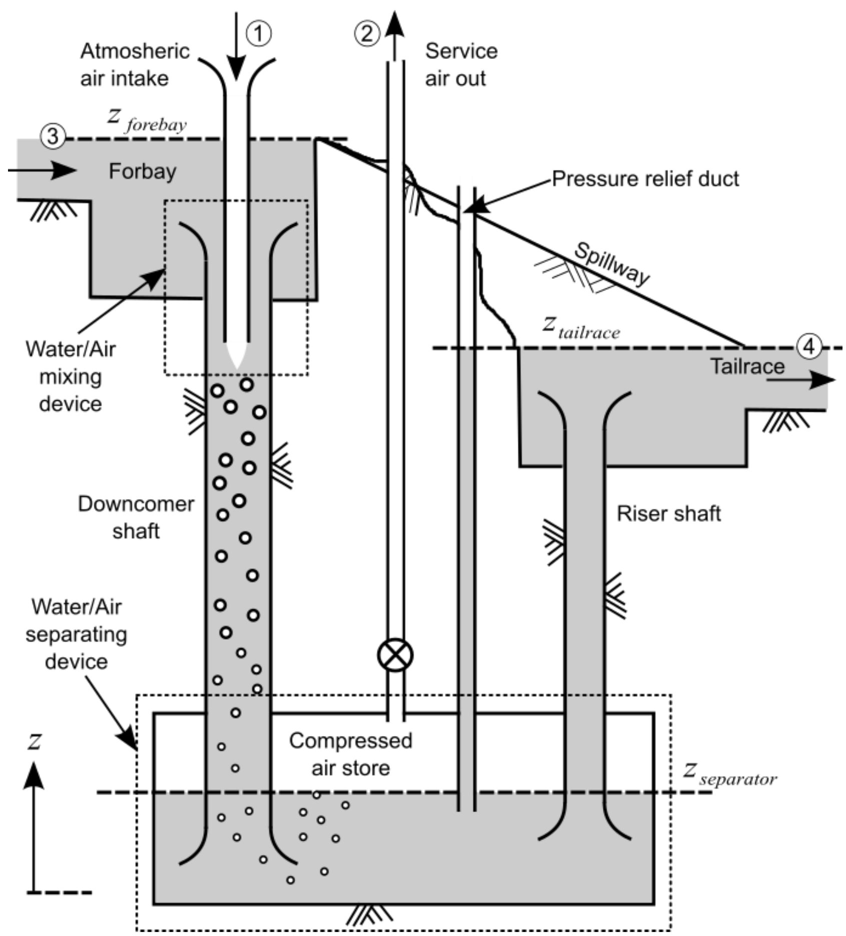

Figure 3: Process flow diagram

The air compression process inside the HAC begins when water initially enters the forebay tank and inducts atmospheric air into the tank. The water and air mix by passing through a mixing head in the forebay tank and they flow into the downcomer. The mixture of air bubbles and water in the downcomer flows downward towards the separator tank while compressing the air. The air is then separated from the water after circulating in the separator. The water then flows up the riser pipe into the tailrace. The mixing, circulation, compression and separation processes are driven by the difference in pressure head between the forebay and the tailrace, and this acts in a similar way to a siphon. The separated compressed air runs up the service air pipe and can now be delivered to the appropriate locations. The water level in the separator tank is dictated by the amount of compressed air that is stored in the separator at any given moment. By increasing or decreasing the amount of compressed air being inducted into the forebay tank the water level in the separator can change. If the water level in the separator falls below a designed level, the end of a so-called 'blow off' pipe becomes exposed and will release some of the air in the separator tank to the atmosphere, raising the water level in the separator back to acceptable levels. The blow off design level paired with the forebay and tailrace tank which are open to the atmosphere means the HAC will never be subjected to excessive pressures - by design. The water in the tailrace is pumped back up to the forebay tank to close the loop on the HAC Demonstrator.

2.2 Process instrumentation diagram

A full process instrumentation diagram for the HAC Demonstrator can be seen in Appendix A: Process instrumentation diagram and a simplified version of the process instrumentation diagram is presented in Figure 4.

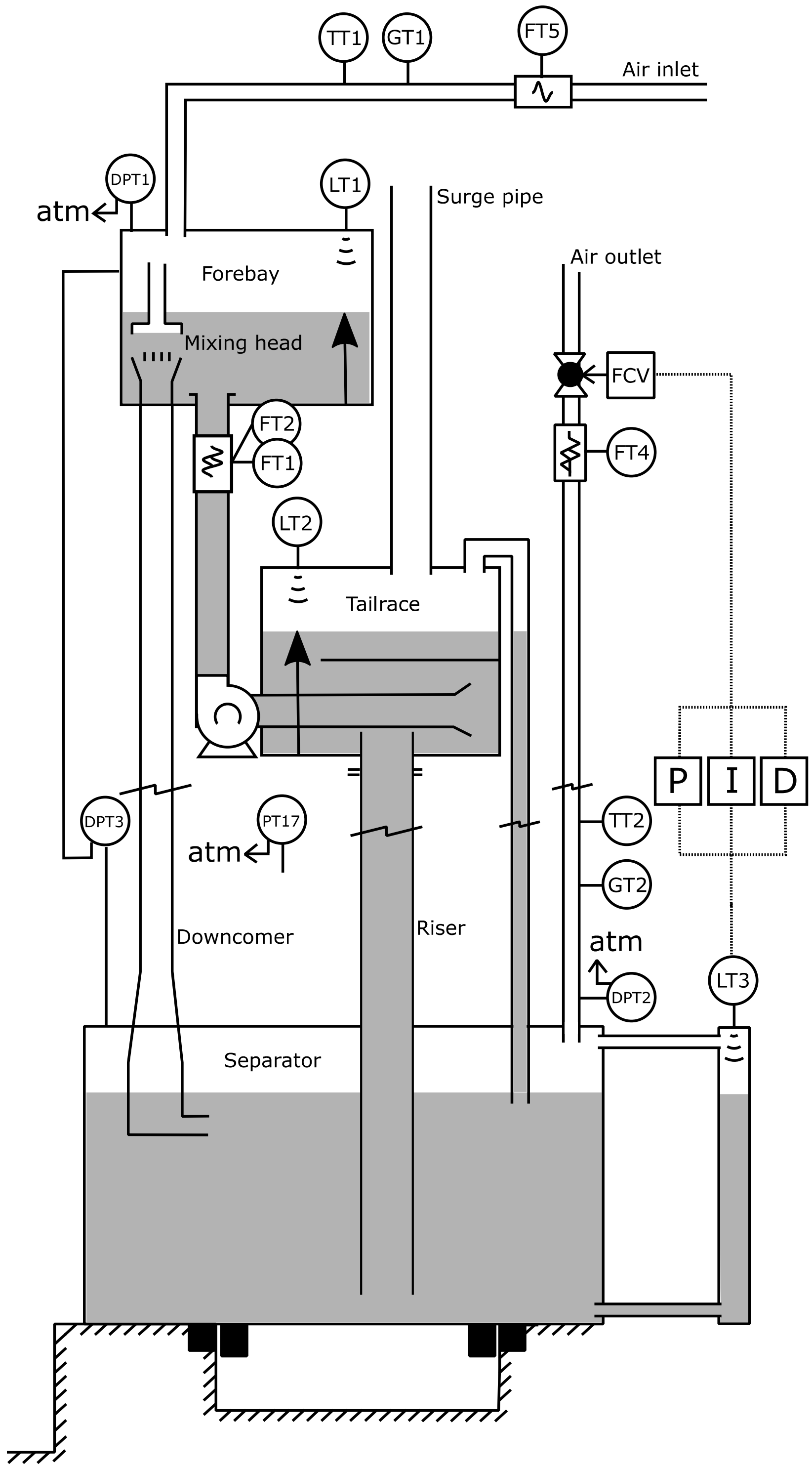

Figure 4: Simplified process instrumentation diagram of the Dynamic Earth HAC Demonstrator.

This section explains the instrumentation that has been installed on the HAC Demonstrator to monitor and characterize the processes and where the instruments are located. Starting at the forebay tank, there are two sensors installed. One is connecting the inside of the tank to atmosphere to measure the differential pressure (DPT1) and the second is installed on the top of the tank to measure the water level (LT1). The intake air pipe connected to the forebay tank has three sensors installed which measure the velocity of the air (FT5 – a sonic anemometer), the temperature of the air and the humidity (TT1, GT1) of the air entering the system. The downcomer pipe connected to the bottom of the forebay has a set of differential temperature sensors installed (D1P1, D1P2). The separator tank is also equipped with a differential pressure sensor (DPT2) and a water level sensor (LT3). The compressed air pipe is equipped with a temperature and humidity sensor (TT2, GT2), a motorized control valve (MCV1) and a Coriolis air mass flow meter (FT4). The tailrace tank is equipped with a guided wave radar water level sensor (LT2). Both pumps connected to the tailrace tank take the water up to the forebay through two water flow meters (FT1, FT2). The pumps are also equipped with differential temperature and pressure sensors (P1T1, P1T2, P2T2, P2T2, P1P1, P1P2, P2P1, P2P2). There is also a differential pressure sensor connected to the forebay and the separator tank installed on the collar level (DPT3). A barometer (PT17) is installed at the HAC collar level and elevation corrections are made to the separator level and to the forebay level so that thermodynamically absolute pressures can be estimated from the manometer observations.

2.3 Overview of the HAC process

The HAC operates in a similar fashion to a siphon. The water flows, between two approximately atmospheric tanks, from the higher forebay tank to the lower tailrace tank. For a HAC, the principal loss experienced by the process is the work done by the water to compress the gas. Figure 5 shows the HAC system and outlines a control volume along with three flow paths that are used to model the HAC process.

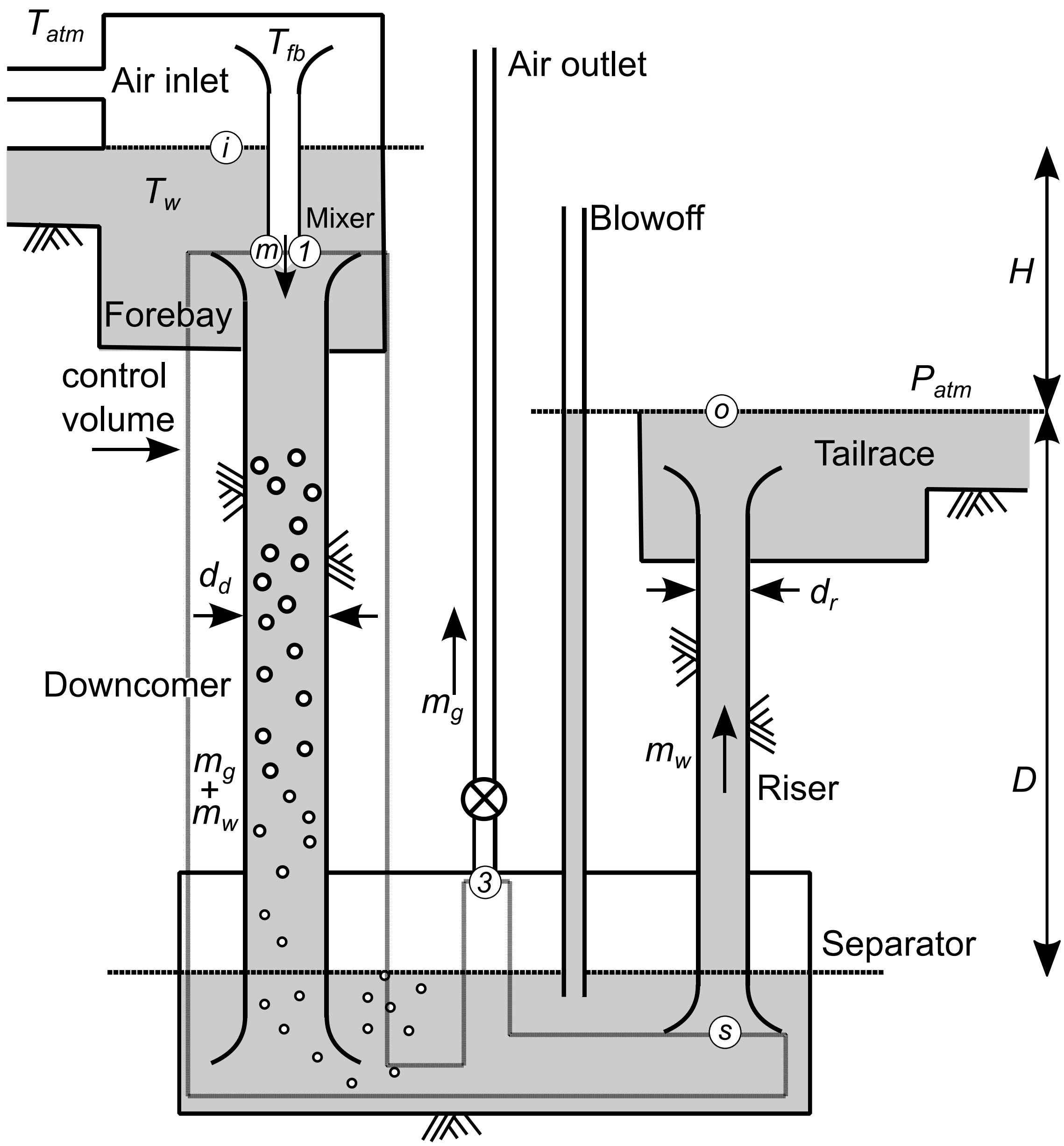

Figure 5: HAC control volume.

The first of these is the path for the water from *i* to *o* which are at different elevations and thus generate head, *H*, for the system. The second and third are nearly the same. Path *1* to *3* is for the air, and path m (mixer) to s (separator) is for the water. For the most part 1 to 3 and m to s share the same path in the downcomer and diverge only in the separator so that 3 lies at the air outlet and s lies at the water outlet. With this arrangement the velocities of the two phases can be estimated at the end of the compression and separation process.

At the inlet of the mixing head, the known geometry of the hydroplane horizon at m and the known geometry of the air inlet pipes permit the velocities of the fluids to be estimated before the mixing process.

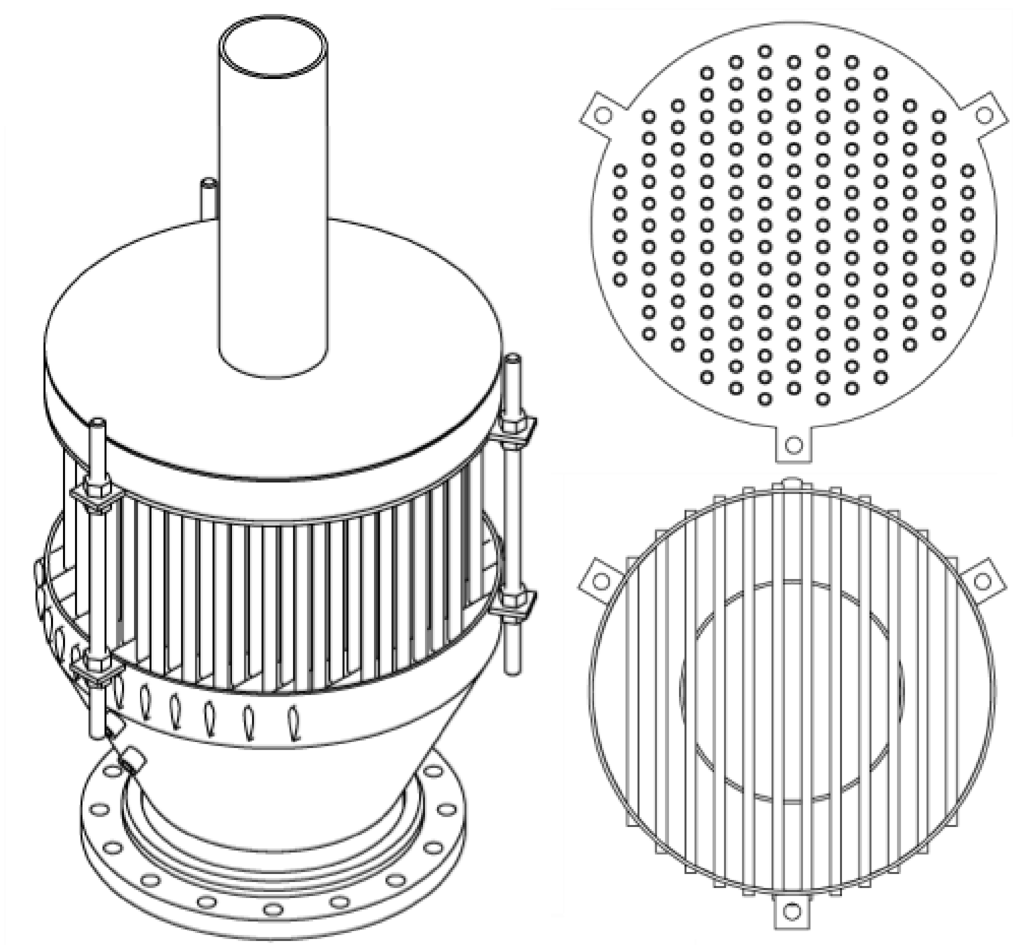

Figure 6: Isometric view of mixing head assembly (LHS). Cross sections of hydroplanes and inlet pipes. The open ends of the inlet pipes are positioned in the space remaining between the individual hydrofoils.

Figure 6 shows an isometric view of the air water mixing head (LHS) and a cross section of the hydrofoil plane. The hydrofoil itself is also shown in Figure 6 as the parallel bars, with a cross sectional shape resembling a tear drop, crossing the width of the mixing head horizontally. The ends of the pipes at the air inlet manifold are positioned at this low-pressure zone to provide a pressure potential that draws air into the downcomer. Air enters the head through the 188, ½" air inlet pipes and water enters the head through the open area of the conduit, accounting for the frontal area of the hydroplanes and the external diameters of the air inlet pipes. Importantly, at this point, the mass flow rates and densities of the water and air are known, so that the velocities of the fluids can be computed just before entry to the mixing head, m and 1.

The air leaves the separator through a 4" rubber lined pipe near the apex of the dome of the vessel. The pressure (DPT2), temperature (TT2) and humidity (GT2) of the air are measured at this point so that the density of the air is also known. As the Coriolis meter lies directly downstream of the separator air outlet, the mass flow of air at outlet is known accurately and the velocity of the air in the pipe can be computed.

The water leaves the separator via the riser pipe, which is equipped with a specially fabricated bell mouth inlet fitting. As the water is incompressible, and as its pressure and temperature are known at the point immediately after the bell mouth, the velocity of the water can be computed.

The distinctions of where precisely the velocities are determined are important as this defines the irreversibility considered within the system. These irreversibilities will reduce the compressor efficiency and as defined, will include those due to mixing, separation and compression as well as friction and minor loss in pipes containing water and bubble drag in the downcomer.

Downstream of *3* the air passes along a 4" rubber lined pipe to a high resistance Coriolis meter, a motorized globe control valve and a silencer. The specification of the Coriolis meter was selected so that the pressure drop expected was approximately equal to the pressure rise developed by the HAC that was expected. Dropping the HAC pressure in this way permitted the most accurate mass flow observations possible to be made. The Coriolis meter is thus the principal load that the HAC serves; there is no rock drill or air motor or tire inflator. The meter itself requires substantial work input to provide accurate measurements. The remaining parts of the downstream pipework offer up less resistance than the Coriolis meter but are also considered as part of the load of the compressor.

The 4" diameter rubber lined air inlet pipe produces pressure drops along its length of up to 2000Pa under maximum water flow conditions. Despite having unnecessary bends and turns designed out, the minor losses contribute approximately 50% of the loss associated with the inlet pipe. The other components of loss in this section of pipework are due to an inlet screen, the rubber lining material having higher absolute roughness than steel, and the loss of flow section due to the lining presence itself. The loss in this pipe, although small, is significant and is accounted for in analysis of the compressor efficiency. Compressor work is expended in inducting the air into the inlet pipe, and because this loss is in series with the downstream meter, valve and silencer, this work is conceptually considered as part of the external compressor load.

The inlet pipe modifies the atmospheric pressure at the forebay level so that the air pressure inside the forebay tank is a maximum of 2000Pa lower than atmospheric. The temperature of the atmospheric air is also modestly increased during its transit through the inlet pipe. The absolute humidity of the atmospheric air is assumed unchanged by the time it arrives inside the forebay tank. At this point the inlet air comes into contact with the surface of the water in the forebay tank, and the latter is highly agitated and turbulent (shown in Figure 7) such that it is assumed that there is a heat transfer between the air and the water so that the air temperature assumes that of the water.

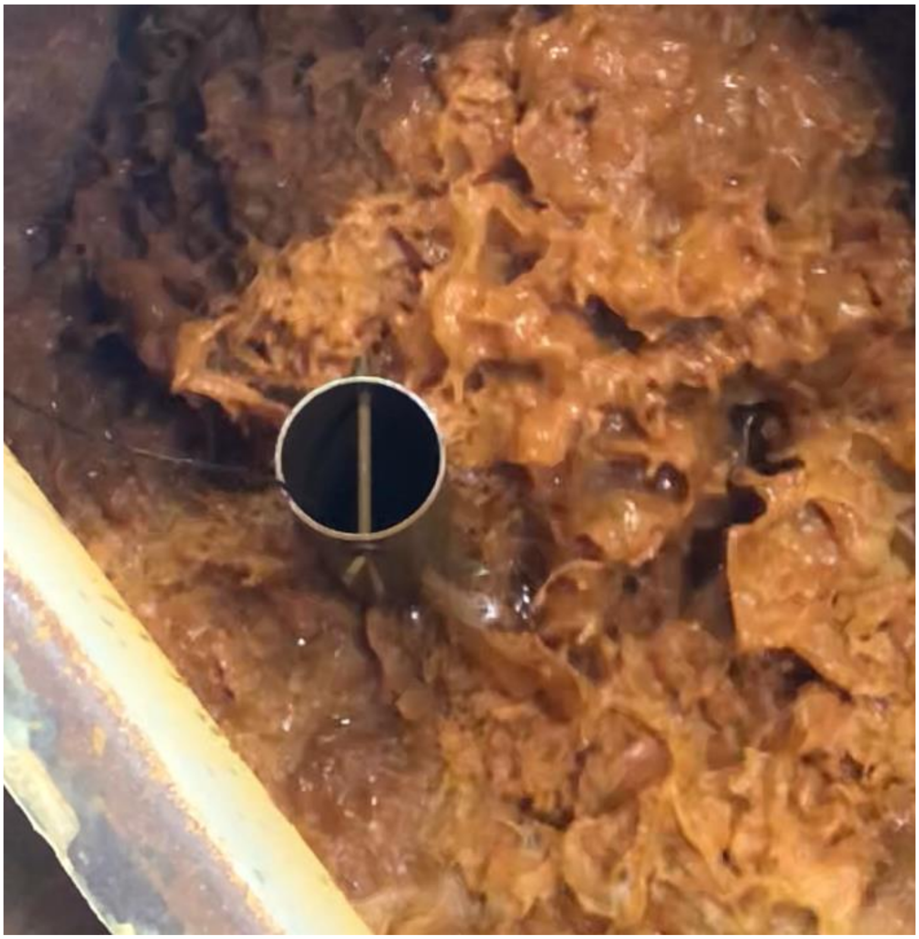

Figure 7: Water ‘sloshing around’ in the forebay tank during operation.

As described, all losses in the inlet pipe, the outlet pipe, the Coriolis meter, the control valve and silencer are considered load on the system and thus do not diminish the compression efficiency of the HAC. In contrast losses due to mixing, separation, friction and minor loss in pipes containing water, and bubble drag are taken to diminish the HAC compression efficiency. The compression ‘loss’ in the system is actually the useful flow work imparted to the inducted air by the compressor.

2.4 Thermodynamic description of the HAC process

The starting point for the determination of the HAC compression efficiency is to recognize that all flow processes can be represented using the steady flow energy equation (McPherson, 2009) under the assumption of 1D analysis:

$$\frac{u_n^2 - u_{n+1}^2}{2} + g(z_n - z_{n+1}) + w_{n,n+1} = \int_n^{n+1} VdP + F_{n,n+1} = h_{n+1} - h_n - q_{n,n+1} \quad (1)$$

where the terms have the units of J/kg and can be seen in Figure 8.

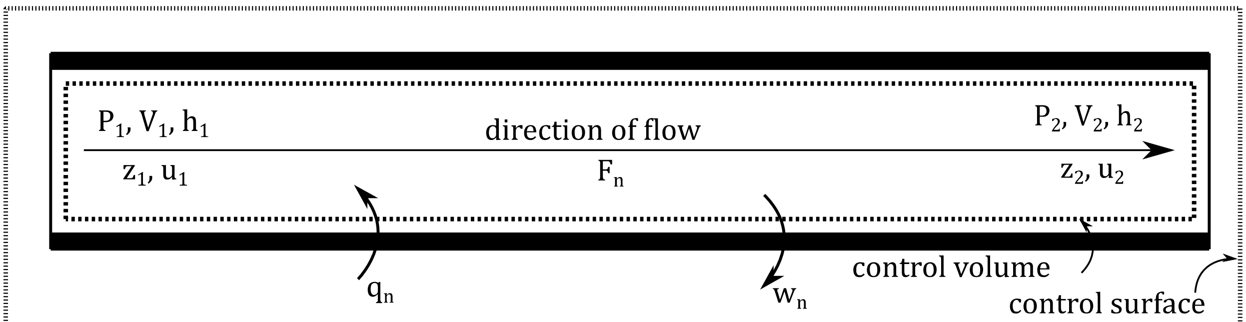

Figure 8: Steady flow energy equation

The term $\frac{u_n^2 - u_{n+1}^2}{2}$ represents the kinetic energy of the fluid, while the term $g(z_n - z_{n+1})$ represents the potential energy of the fluid. The term w is the external work input into the system, taken as positive from surroundings to the system. The integral term, $\int_n^{n+1} VdP$, defines the useful work imparted to the fluid (the flow work) and the term F represents the internal irreversibility of the flow arising from friction and minor loss. The term $h_{n+1} - h_n$ represents the mass specific enthalpy of the fluid and the term q represents the heat added to the system, again with positive sense from the surroundings to system.

The quantities measured by the instruments are used to calculate these terms and corresponding thermodynamic state variables at the inlet and outlet of the control volume. Using the steady flow energy equation with the three fluid flow paths, a system of equations and unknowns can be created. The path of air is defined from the initial mixing point above the mixing head, *1*, to the entrance of the compressed air pipe above the separator, *3*. The two paths of water are defined from the surface of water in the forebay, *i*, to the surface of water in the tailrace, *o*, and from the initial mixing point above the mixing head, *m*, to the entrance of the riser pipe in the separator, *s*.

The water's flow path from the forebay tank to the tailrace tank can also be defined using (1),

$$\frac{u_i^2 - u_o^2}{2} + g(z_i - z_o) + w_{io} = \int_i^o VdP + F_{io} \tag{2}$$

although this is not normally applied with a compressibility term for the flow work. In this analysis as the REFPROP equation of state is universally adopted for the lookup of thermodynamic properties, thermal expansion and liquid compressibility can be accommodated. In applying to the Dynamic Earth HAC where a maximum pressure difference between *i* and *o* is of order 2000Pa and the maximum temperature difference is of order 10mK, using REFPROP, the difference in density of the liquid is less than a 1/10th of a gram in 1000kg/m^3. As a consequence, the flow work term, $\int_i^o VdP$, always evaluates to near zero. Between *i* and *o* there is no mechanical work imparted to the HAC system from the surroundings and so, w_{io}, is also zero. At the Dynamic Earth HAC the same water flowrate passes from the forebay tank to the tailrace tank and these vessels have the same physical dimensions. Consequently, even though direct observation of the surface of the water at *i* in the forebay tank reveals that the water is in motion, a similar motion must be expected in the tailrace tank at o. As a result, the water velocities at i and o must also be similar and the kinetic energy term, $\frac{u_i^2 - u_o^2}{2}$, in (2) can be reliably neglected. Applying these simplifications,

$$g(z_i - z_o) = F_{io} \tag{3}$$

and it becomes clear that head set up between the forebay and tailrace tank is used to overcome all irreversibilities present in the system, including the work done to compress the air!

For the water, the second part of the tri-partite steady flow energy equation links the mechanical terms with the thermal terms:

$$g(z_i - z_o) = h_o - h_i - q_{io} \tag{4}$$

where the terms have the units of J/kg of water. Heat exchange across the process pipe work is expected to be low because the pipe work is effectively immersed in a bath of still air of constant temperature. Consequently, q_{io}, for the water may be principally attributable to compression heat transferred from the air.

The irreversibility in the HAC from the beginning of the process to the end of the process, F_{io}, can also be further defined to include losses from the water flowing into the mixing head, F_{im}, and the water flowing up the riser pipe, F_{so},

$$F_{io} = F_{im} + F_{mix} + F_f + F_d + F_w + F_{separator} + F_{so} \tag{5}$$

The losses between m and s for the water, F_{ms}, comprise the friction of the water rubbing on the rubber lined pipe, F_f, the viscous drag of the water on the bubbles drawn down the pipe, F_d, and the compression work done by the water on the air, F_w, the water mixing with the air, F_{mix} and the water flowing through the separator, $F_{separator}$,

$$F_{ms} = F_{mix} + F_f + F_d + F_w + F_{separator} \tag{6}$$

$$F_{ms} = F_{io} - F_{im} - F_{so} \tag{7}$$

$$g(z_i - z_o) = F_{io} = h_o - h_i - q_{io} = F_{im} + F_{mix} + F_f + F_d + F_w + F_{separator} + F_{so} \tag{8}$$

where the terms have the units of J/kg of water. From (5) as F_w is the only valued component of irreversibility for the water, an expression for the air compression efficiency is directly obtained thus:

$$\eta_{mech} = \frac{F_w}{g(z_i - z_o)} = \frac{F_w}{(h_o - h_i - q_{io})} \tag{9}$$

In the context of the air rather than the water, F_w is related to the useful flow work imparted to the air (units of J/kg of air), $\int_1^3 VdP$, so that:

$$F_w = \frac{\dot{m}_g \int_1^3 VdP}{\dot{m}_w} \tag{10}$$

and,

$$\eta_{mech} = \frac{\dot{m}_g \int_1^3 VdP}{\dot{m}_w g(z_i - z_o)} \tag{11}$$

To evaluate (8) for the Dynamic Earth HAC, the pressures and temperatures of the air at 1 and 3 need to be measured along with the head between the forebay and tailrace tanks and mass flow rates of air and water.

It is also instructive to revisit (5) to obtain insight for HAC design guidance:

$$g(z_i - z_o) = F_{im} + F_{mix} + F_f + F_d + F_w + F_{separator} + F_{so} \tag{12}$$

In order to maximize mechanical efficiency, water approach, mixing, friction, bubble drag and separator losses need to be minimized. The water approach losses can be minimized by designing a large forebay tank which will reduce the velocity of the water flowing within the vessel. The friction losses can be reduced by increasing the diameter of the pipes to reduce the velocity of the fluid. The bubble drag losses can be reduced by having smaller bubbles. The mixing loss can be minimized through engineering of an efficient mixing head. The separator losses can be minimized by increasing the size of the separator so that the velocities are low.

For the flow path of the air from 1 to 3, the steady flow energy equation can be defined and separated into two equations with three unknowns,

$$\frac{u_1^2 - u_3^2}{2} + g(z_1 - z_3) + w_{13} = \int_1^3 V dP + F_{13} \tag{13}$$

$$\frac{u_1^2 - u_3^2}{2} + g(z_1 - z_3) + w_{13} = h_3 - h_1 - q_{13} \tag{14}$$

where the terms have the units of J/kg of air. The terms for velocity, $u_1 and\ u_3$, elevation, z_1 and z_3, specific volume, V, pressure, P, and enthalpy, h_1 and h_3 are all known variables that can be measured or calculated using REFPROP (Lemmon, Huber and McLinden, 2013) with any two thermodynamic state variables. The three unknowns include the work, w_{13}, and heat, q_{13}, which are taken as positive when added to the system and the internal irreversibility, F_{13}, lying along the air flow path. Although there is no mechanical element present between 1 and 3 the work term, w_{13}, is retained as it is known that work is done on the air by the water.

The water's flow path from the mixing horizon, m, and to the riser inlet, s, can be similarly be defined without eliminating as many terms,

$$\frac{u_m^2 - u_s^2}{2} + g(z_m - z_s) + w_{ms} = \int_m^s VdP + F_{ms} \tag{15}$$

where the terms have the units of J/kg of water. The velocity at m can be determined at the hydrofoil plane as described earlier. The velocity at s can be determined at the riser pipe inlet as described earlier. Due to the small temperature rise the water flow work term is small enough to be neglected, so that:

$$w_{ms} = g(z_i - z_o) - F_{im} - F_{so} - \frac{u_m^2 - u_s^2}{2} - g(z_m - z_s) \tag{16}$$

Also,

$$\frac{u_m^2 - u_s^2}{2} + g(z_m - z_s) + w_{ms} = h_s - h_m - q_{ms} \tag{17}$$

where the terms have the units of J/kg of water. The thermal interaction between the two phases from m to s can be defined using the mass flow rate of air, $\dot{m}_g$, and the mass flow rate of water, $\dot{m}_w$:

$$\dot{m}_g q_{13} + \dot{m}_w q_{ms} = 0 \tag{18}$$

The mechanical interaction between the two phases from m to s can also be expressed:

$$\dot{m}_g w_{13} + \dot{m}_w w_{ms} = 0 \tag{19}$$

$$w_{13} = \frac{-\dot{m}_w w_{ms}}{\dot{m}_g} = \frac{-\dot{m}_w}{\dot{m}_g}\left[g(z_i - z_o) - F_{im} - F_{so} - \frac{u_m^2 - u_s^2}{2} - g(z_m - z_s)\right] \tag{20}$$

The mechanical efficiency of the HAC, η, can be defined as the quotient of the useful flow work, $\int_1^3 VdP$, divided by the work input, w_{13}, on the air to provide the useful flow work,

$$\eta_{mech} = \frac{\int_1^3 VdP}{w_{13}} \tag{21}$$

The overall efficiency of the HAC can be defined by including the air yield of the system and multiplying the mechanical efficiency by the ratio between mass flow of gas out, $\dot{m}_{g_{out}}$, and mass flow of gas in, $\dot{m}_{g_{in}}$,

$$\eta_{overall} = \frac{\dot{m}_{g_{out}} \int_1^3 VdP}{\dot{m}_{g_{in}} w_{13}} \tag{22}$$

The divisor can be simplified using the relationship between the work done on the mass of air by the water being equal to the irreversibility experienced by the mass of water,

$$\eta_{overall} = \frac{\dot{m}_{g_{out}}}{\dot{m}_{g_{in}}} \frac{\dot{m}_{g_{in}}}{\dot{m}_w} \frac{\int_1^3 VdP}{-\left[g(z_i - z_o) - F_{im} - F_{so} - \frac{u_m^2 - u_s^2}{2} - g(z_m - z_s)\right]} \tag{23}$$

The useful flow work on the air can also be simplified if the ideal gas assumption is held,

$$\int_1^3 VdP = \frac{n}{n-1} R(T_3 - T_1) = \frac{\ln(P_1/P_3)}{\ln(T_1/T_3)} \mathcal{R}(T_3 - T_1) \tag{24}$$

The final equation for the overall efficiency of the HAC can now be defined using only quantities that are directly measured on the HAC Demonstrator,

$$\eta_{overall} = \frac{\dot{m}_g \frac{\ln(P_1/P_3)}{\ln(T_1/T_3)} \mathcal{R}(T_3 - T_1)}{\dot{m}_w g H} \tag{25}$$

2.5 Heat transfer across pipe walls

The amount of heat transfer occurring during the compression process of the HAC, which is near isothermal, is minimally influenced by heat transfer from its surroundings. This section aims to quantify the magnitude of heat transferred into the system from the surrounding environment. Low air flow rates circulating around the HAC system and steel rubber lined pipes are both contributing factors to the small amount of heat transfer. Even with atmospheric temperatures ranging far above or below the temperature of the water in the HAC a small heat transfer coefficient leads to a negligible amount of heat transmitted into the system. Figure 9 shows an example of the conditions of the flow up the riser pipe when there is warm air flowing around the pipe. The thickness of the steel pipe and rubber lining in the riser are 17.5mm and 6.35mm respectively, with thermal conductivity's of 15W/mK and 0.009W/mK. Assuming the air flowing around the pipes has a velocity of 0.1m/s and a temperature of 15°C, the heat transferred to the air water mixture with a temperature of 10°C flowing in the riser pipe can be calculated using the following methodology.

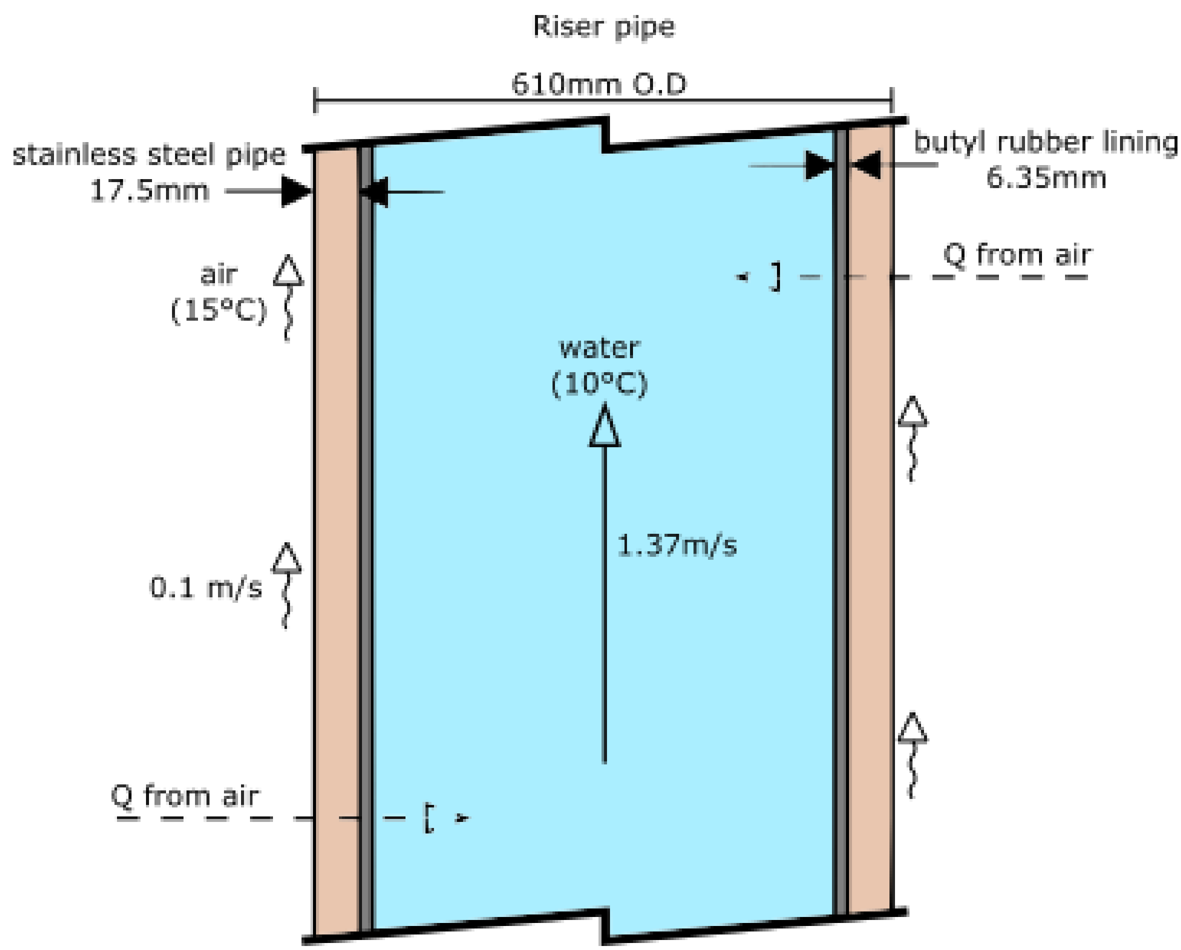

Figure 9: Heat transfer from air to the water in the riser pipe

The thermodynamic state variables of enthalpy, h, and pressure, P, can be calculated with REFPROP (Lemmon, Huber and McLinden, 2013). The heat transfer rate, Q, to the water from the air is calculated by dividing the difference in temperature, T, from the water inside the riser pipe and the air flowing outside the pipe by the sum of all the conductive and convective thermal resistances, R,

$$Q = \frac{\Delta T}{\sum R} = \frac{T_{air} - T_{water}}{R_{conv} + R_{cond}} \tag{26}$$

where each layer of material separating the water from the ambient air has its own convective or conductive resistance relative to its radius, r, length, L ,thermal conductivity, k, or heat transfer coefficient, $\hbar$,

$$R_{conv} = \frac{1}{\hbar_n(2\pi r_n L)} \tag{27}$$

$$R_{cond} = \ln\left(\frac{r_n}{r_{n-1}}\right)/(2\pi k_n L) \tag{28}$$

The mass specific heat transfer, q, can then be defined by dividing the heat transferred by the mass flow rate of the water, $\dot{m}$, in the riser pipe,

$$q = Q/\dot{m} \tag{29}$$

The specific enthalpy gained, h_{gain}, at steady state is defined as,

$$h_{gain} = q(t_2 - t_1) \tag{30}$$

The final temperature of the water, T_2, can then be defined using the final enthalpy and another thermodynamic state variable using REFPROP (Lemmon, Huber and McLinden, 2013). The calculations can then be repeated over periods of 24 hours to account for variables that change over time as the temperature of the water in the pipe and the air around the pipe approach equilibrium. By discretizing the calculations over a large period, the small amount of heat transferred to the water from the air in the riser pipe can be seen in Figure 10.

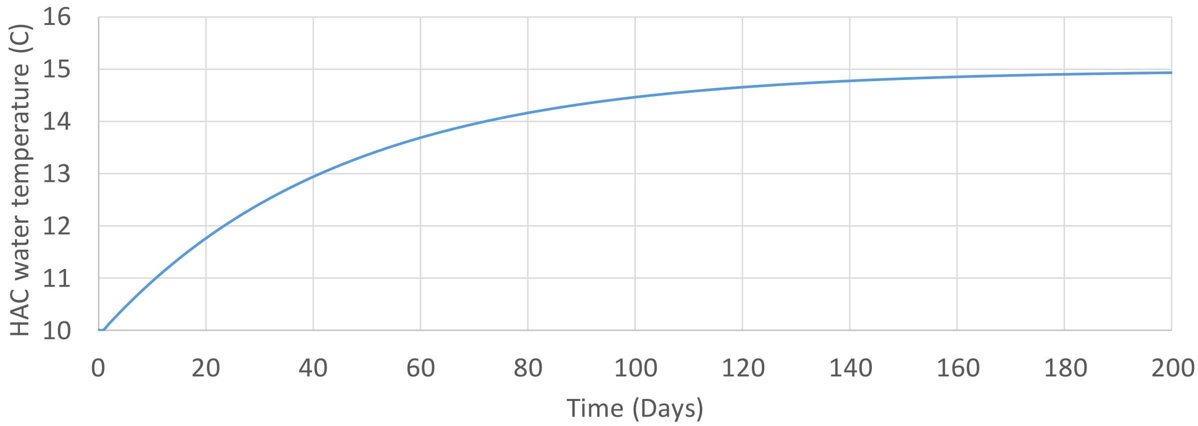

Figure 10: Temperature of water due to heat transferred from the surrounding environment only.

Assuming a starting 5°C temperature difference between the flowing water and the air circulating around the HAC, the water temperature would only rise 0.1°C per day at a decreasing rate over time since the differential temperature would be decreasing. These calculations confirm that the amount of heat transferred from the surrounding environment is negligible so that any change of temperature measured in the downcomer may be considered to be attributable to the near-isothermal gas compression process.

3. HAC Demonstrator instrumentation and software

This section aims to provide an overview of the instrumentation trials and the software used at the HAC Demonstrator. The construction of the human machine interface and the software used for data management can also be discussed.

3.1 Offsite instrumentation trials

During the construction of the HAC Demonstrator the instruments and control panel were delivered to a lab off site for testing to ensure functionality and reduce any potential delays if any problems were encountered. The lab also houses a pilot HAC called ‘Baby HAC’. The control panel is connected to a Server PC in the lab that hosts the OPC (Open Platform Communications) server software which readily permits communications with all the instrumentation and actuators.

Instruments were wired into the control panel and given trial runs to test for loop continuity and sensible measurements and to establish proper wiring procedures before full installation at the HAC Demonstrator facility. Some of the instruments that were tested include: two level sensors, two temperature and humidity sensors, three differential pressure sensors, a Coriolis meter, an Optisonic flowmeter, two power meters, and a barometric pressure sensor. The wiring procedures for the instruments can be found in Appendix B: Instrument wiring procedures. Most of the instruments followed the same general wiring procedure with the exception of the barometer and the temperature and humidity sensors. The instruments that could not be tested in the lab were delivered directly to the HAC Demonstrator and tested before the commissioning process began. Instruments tested on site include two water flow meters, a guided wave radar level sensor, and two variable frequency drives (VFDs). The wiring procedure for these instruments can also be found in Appendix B: Instrument wiring procedures. The establishment of specific wiring procedures allowed for quick troubleshooting when issues arise from one or multiple instruments.

Off site trials proved to be effective when problems with the barometer occurred during the initial testing of the instrument. Once the barometer was wired into the panel correctly and communicating with the Server PC, a constant maximum signal of 110mbar was reported which did not match the actual atmospheric pressure in the lab. It was later discovered that one of the fuses on the barometer had malfunctioned. The faulty barometer was returned to the manufacturer and quickly replaced. Further testing on the replacement barometer revealed no problems and the sensor was working as intended. After the instruments were properly tested the next step was to install everything on site before commissioning of the HAC. Had this testing not taken place offsite, there may have been appreciable time delays in commissioning and start up of the HAC Demonstrator.

3.2 Onsite instrument installation

When the HAC Demonstrator facility was near completion the instruments could be installed on site. Installation required running multiple armoured cables and CAT5 instrumentation cables from the control panel to various instrument locations around the system which can be seen in the process instrumentation diagram in Appendix A: Process instrumentation diagram and discussed in section 2.2. The instruments were installed and wired according to the wiring procedures outlined in Appendix B: Instrument wiring procedures. Some instruments required additional work to be installed, for example the differential pressure sensors required additional mounting plates to be installed at their specified locations, and the temperature and humidity sensors needed RJ45 to CAT5 adapters which are housed in weather proof boxes to protect the wiring from any water damage. Images for all the instruments installed at the HAC Demonstrator facility can be seen in Appendix C: Dynamic Earth HAC instrument .

3.3 HAC Demonstrator software map

The instruments installed and connected to the server in the control panel are controlled by the Server PC in the control room. The PC manages the software infrastructure required to run the HAC Demonstrator. Figure 11 shows a flow chart of the software used on the Server PC necessary to operate the HAC Demonstrator.

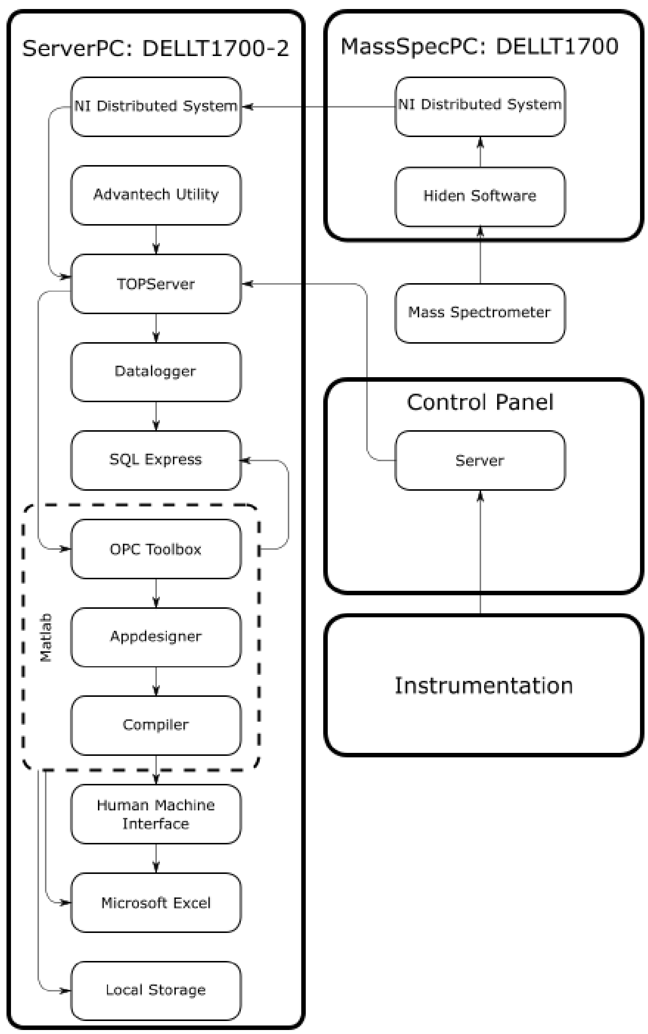

Figure 11: Softwareflow chart of the system created by the Candidate

There are two computers in the control room of the HAC Demonstrator. One computer is the Server PC and the other as the MassSpec PC. The MassSpec PC acts as a backup to the ServerPC but also is the future controller of the mass spectrometer once it is installed on site. The lab off site is currently housing the mass spectrometer for experiments being performed on the HAC pilot. The mass spectrometer will be communicating directly with the MassSpec PC and data will be transmitted to the Server PC through the OPC server.

3.4 OPC software

The backbone of the HAC Demonstrator software infrastructure is an OPC system that manages communications with the instruments. Multiple pieces of software like TOPServer, Datalogger, and MATLAB are used to read, store, and process information collected from the instruments on the OPC server.

3.4.1 TOPServer

TOPServer is an object linking and embedding process control (OPC) system and native HMI device connectivity software application (Software toolbox, 2009). This software serves as the hub for our instrument communication network. A physical server installed in the control panel communicates with the Server PC, located inside the control room by using the TOPServer application and relaying all necessary data and information from the instruments. Other applications will also connect to TOPServer through the Server PC to interact with the various instruments. TOPServer is required to configure the devices on the OPC network. From the TOPServer interface, the instruments and components connected to the OPC server can be identified, labeled, and addressed. An example of the TOPServer interface can be seen in

Figure 12.

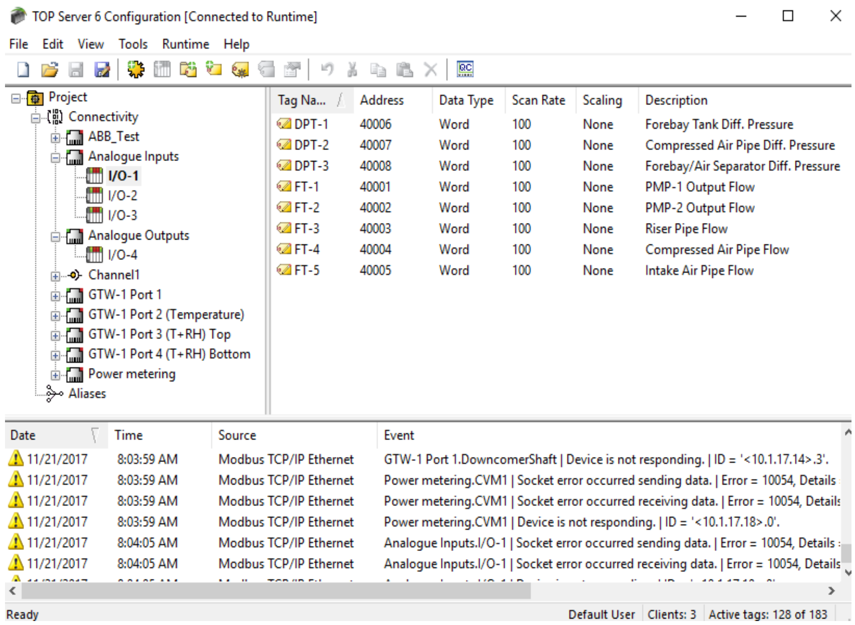

Figure 12: TOPServer configuration interface.

There are 13 devices connected to the server box inside the panel including three input modules, one input/output (I/O) module, and nine individual instruments. The nine instruments connected to the server directly do not need to pass through an input module to convert their signal since they communicate digitally. The remaining instruments are connected to the I/O modules that convert their analog signals to digital signals before sending the data to the server. Each instrument is assigned a tag or tags through TOPServer's interface which is configured with an address, a scale, and a data type. The digital instruments can have multiple tags. For example, the VFDs or the power meters transmitted much data to the server and require several tags each, but the analog instruments only have one tag since they can only transmit one signal at a time. Different instruments transmit signals in different scales which can be configured on the instrument itself by changing some of the on-board settings, but the scales can also be converted from TOPServer's interface. The analog instruments are functioning on 4-20mA or 0-10V signals which are then converted into a standard 16bit format ranging from 0-65536bits. The digital instruments go one step further and provide an already converted measurement to the OPC server matching the scales described in the instrument specifications.

3.4.2 Adam/Apax Utility

The Adam/Apax Utility software application allows configuration and control over the I/O devices in the control panel. The analog instruments pass through the I/O devices to have their data converted into digital form. Figure 13 shows an example of the Adam/Apax utility configuration interface.

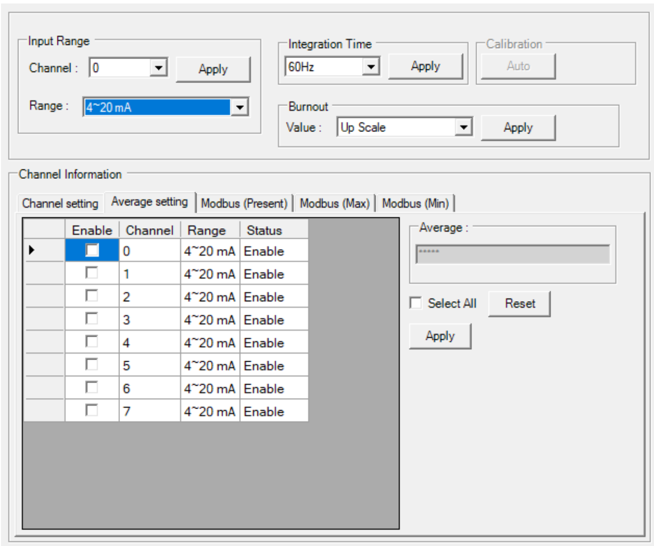

Figure 13: Adam/Apax Utility configuration interface.

The software allows the user to configure the IP address of the I/O devices and to configure the type of signal each device will be reading on each channel. For example, the I/O device shown in Figure 13 reads a 4-20mA signal for the instruments on all channels. The correctly addressed and configured devices are then found by TOPServer through the assigned IP address. Any connectivity issues with the I/O devices must be resolved through the Adam/Apax Utility software which also allows the operator to restart or reset the units remotely.

3.4.3 National Instruments

The National Instruments software is used to communicate with the mass spectrometer that will eventually be installed inside HAC Demonstrator control room but is currently in use off site, and was configured and tested off site. The mass spectrometer is used to analyse the chemistry of the air entering the system and leaving the system. Analysis of the air provides valuable information on the concentration of different gases at the inlet and the outlet depending on the type of mixture of water and co-solute in the system. The mass spectrometer will be running on a separate PC once it is on site and will need its data routed to the Server PC through this software by creating a clone of all of the tags which will be linked across both PC's

3.4.4 MATLAB

MATLAB has a software package named OPC Toolbox which provides a graphical interface to interact with OPC servers and the OPC objects located on those servers. The toolbox is used to configure and interact with objects on the OPC server setup by TOPServer from a MATLAB interface instead of using the TOPServer application. Figure 14 shows an example of the graphical interface.

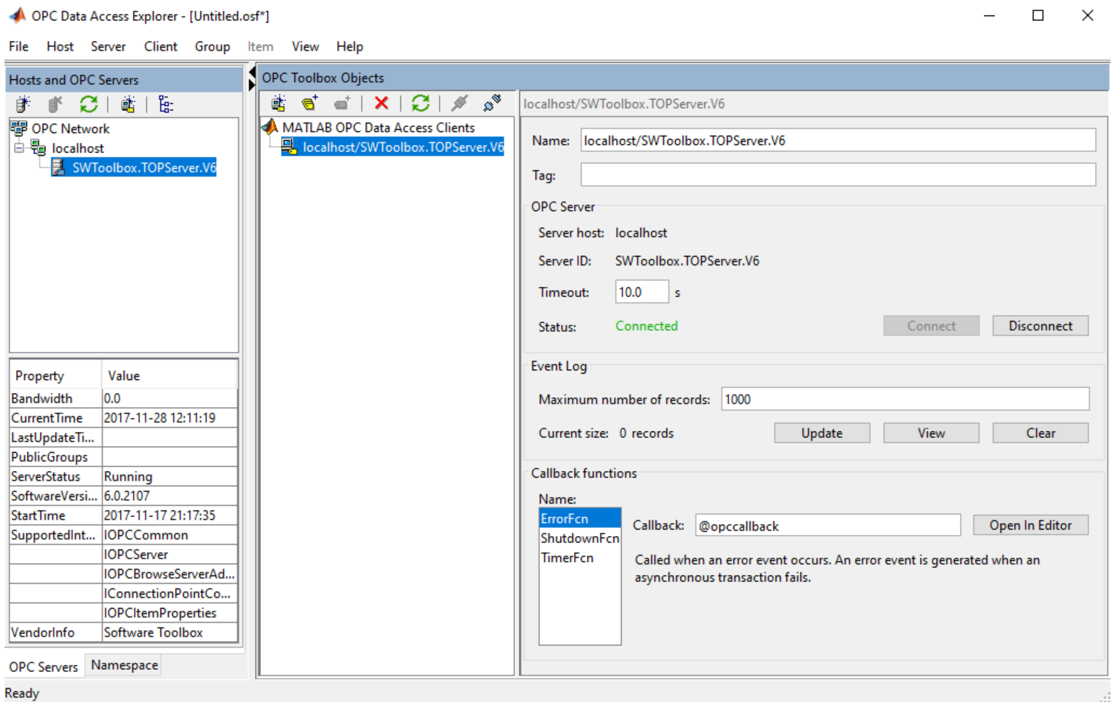

Figure 14: MATLAB OPC Toolbox configuration interface.

The toolbox also allows the user to execute MATLAB commands in the form of functions or scripts to the OPC server. Reading and writing data to the instruments on the OPC server can be done automatically and independent of the TOPServer software through MATLAB which is a recognized programming language and software application.

3.5 Human machine interface (HMI)

The HAC Demonstrator requires an HMI to monitor and control the system. Due to the Candidate's experience with MATLAB, the HMI was fully constructed and tested in a MATLAB environment and runs independently from the native MATLAB software through a compiled app using the Compiler Toolbox and Appdesigner. Figure 15 shows an updated image of the HAC HMI currently in use on site.

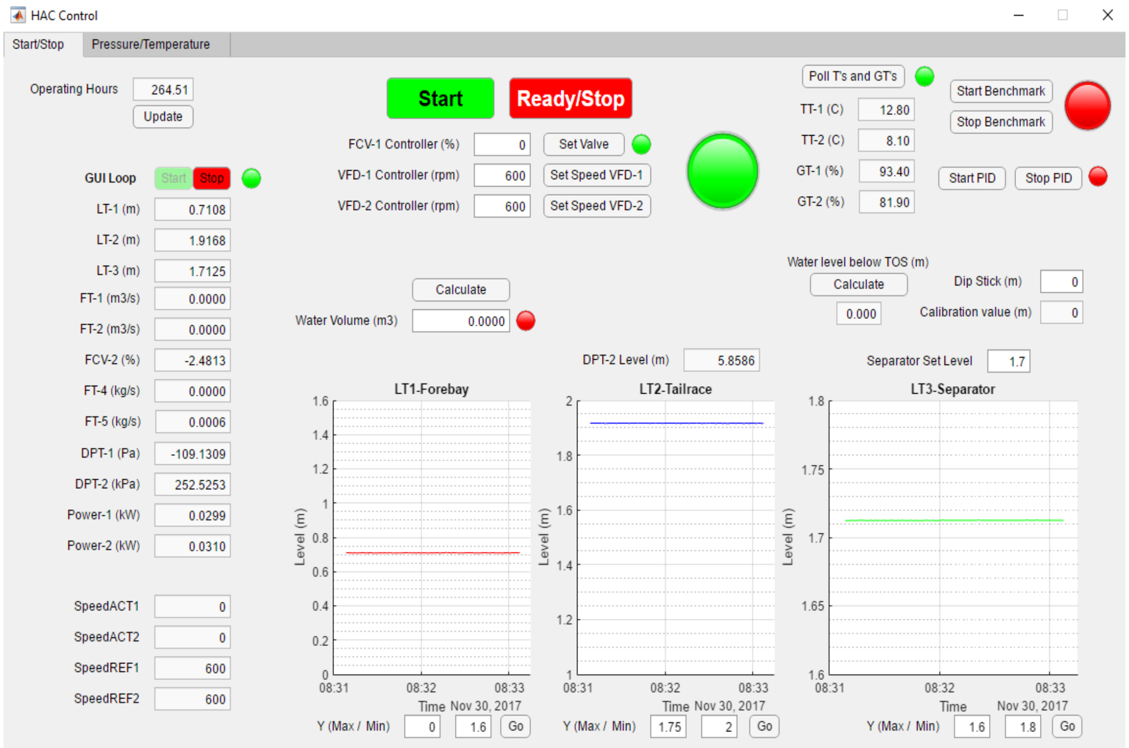

Figure 15: Dynamic earth HAC Demonstrator HMI.

The current iteration of the HMI allows the operator to monitor multiple quantities like differential pressure and flowrates on the left-hand side, control the speed of the VFD's in the upper center, check the temperature and humidity of the air at inlet and outlet of the system on the upper right, start and stop the different benchmark and PID protocols of the system, and graphically monitor the water levels in all three of the water tanks. The HMI is continuously evolving and improving over time with new features being added to suit the needs of the operator.

3.5.1 Using MATLAB to build an HMI

Taking advantage of a known programming language for students and researchers alike, MATLAB has decreased the time required to design and create the HMI. A similar process for the HMI for the BabyHAC using LabView took months. MATLAB has a built in graphical interface called

Appdesigner that permits the user to create apps in a drag and drop type environment and allows programming of the app ‘behind the scenes’ using MATLAB code. Appdesigner also allows the user to access other toolboxes within the app, such as OPC toolbox. These two apps combined enable the HMI to communicate with the OPC server to display, control or diagnose problems with the HAC system remotely. Apps designed through Appdesigner can also be compiled using the Compiler toolbox which then permits the HMI to run as a native application, independent of the MATLAB environment. This small decision has allowed various iterations of the HMI to run independently while further work or changes to the HMI were being completed on the native MATLAB software simultaneously.

3.5.2 HMI design philosophy

The HMI was designed with communication and ease of use in mind. The HMIs primary function is to control the HAC system remotely while simultaneously displaying important quantities that are necessary for monitoring the system in real time. The HAC can be controlled using a PID loop that has been programmed inside as part of the MATLAB scripting. Instead of using a PLC or a hardware controller the HAC Demonstrator operates with a software-based PID system which allows more flexibility in how to run the system, and results in a system more suited for research work, which will be further discussed in Chapter 4. The HMI also displays important quantities such as power consumption, air and water flow rates, temperatures, pressures and, most importantly, water levels which are necessary to assess the system’s current state at any given moment. It was critical during the commissioning stage to be able to quickly determine what part of the system may be behaving out of the ordinary, to ensure swift resolution of any problems.

3.5.3 Functionality and testing of the HAC Demonstrator HMI

The HMI design and testing process began before the HAC Demonstrator entered the commissioning phase. This amount of lead time allowed for robust testing of the HMI while paired with the control panel off site. This stage of the HMI design process allowed for testing of the limits and capabilities of the Appdesigner software. The HMI was firstly tested for speed and reliability. Originally the HMI was expected to display quantities from all instruments at any given moment at a frequency of 1Hz. Testing revealed that this wasn't going to be possible due to software limitations.

The HMI has been designed to function with two timer based control loops programmed in MATLAB. One loop focuses on displaying live values from the OPC server at a set frequency, known as the graphical user interface (GUI) loop. The second loop, known as the PID loop, focuses on automating the system. Further testing of the frequency on the GUI loop revealed certain functions and commands in MATLAB take significantly more time and processing power to execute. For example, reading over 20 individual devices from the OPC server through the OPC toolbox and displaying them on the HMI at a rate of 1Hz would require more computing power than available. However, executing hundreds of calculations on the values themselves once taken from the OPC server is virtually instantaneous. Multiple iterations of the HMI were tested for different GUI loop frequencies ranging from 0.2Hz to 4Hz that would be able to simultaneously control both loops at a reliable and effective rate. Ultimately a rate of 1Hz for both the GUI loop and the PID loop was settled upon. The total number of quantities monitored from the OPC server was later reduced from 20 to 13 tags to allow other calculations and functions to be run within the rate of 1Hz if necessary.

Extensive testing of the HMI in the lab also revealed that querying different objects within the OPC server takes different amounts of time to process. The difference in processing speed is due to the type of data that is being transmitted through different pieces of hardware. Instruments connected to the I/O units which use analog input and output signals could be written to and read from very quickly in comparison to instruments connected to the Gateway modules which communicate with a digital signal. As a consequence, instruments connected to the OPC server digitally are not monitored at a rate of 1Hz due to processing limitations but can be read on demand by the operator for a single reading if necessary. Nonetheless, most of the analog instruments can be displayed at a rate of 1Hz on the HMI while simultaneously running the PID loop for control.

Another important task when allocating processing time in the GUI loop was graphical representation of data being polled from the OPC server. An early iteration of the HMI displayed an image of the HAC with overlaying figures indicating the necessary components and quantities visually for operation. The figure highlighted the three water tanks and displayed graphically on a bar chart the water levels that would reflect the position of the water level relative to the height of the tanks. Although this display was appealing, it was inefficient and unnecessary due to processing limitations. Instead, scatter plots displaying the water level in all three tanks over a rolling three-minute period were added to the HMI and can be seen in Figure 15. The plots allow for easy assessment of trends in the water levels which was not possible in the previous iterations of the HMI. More functions and more complex calculations than were originally intended to be displayed at a rate of 1Hz on the HMI were also removed due to processing limitations such as water volume and HAC efficiency calculations. These types of calculations were relegated to post processing that could be completed outside of the HMI environment using the recorded data saved from the OPC server.

3.6 Data storage and data management

Controlling and monitoring the HAC is only the first step in the HAC Demonstrator software testing process. The data measured by the instruments on the HAC Demonstrator is also recorded for post process data analysis. TOPServer is unable to record data and is limited to reading from and writing to the instruments. A software application known as Datalogger from the same parent software company as TOPServer is used to manage and facilitate data storage. Datalogger's role in the software environment is to capture the readings taken by the instruments and transfer them to the appropriate data storage software. Datalogger is not responsible for storage, but instead is necessary to get the data from the OPC server to the desired storage location. The data is then stored in using a Standard Query Language (SQL) server which can be accessed and managed through SQL Express software. Furthermore, data from experiments or specific test times of the HAC Demonstrator can be queried from the SQL server and converted and stored locally in MATLAB .mat files or .txt files for quick and efficient post processing analysis.

3.6.1 Using Datalogger to collect data

The Datalogger software runs independently of the OPC server and needs to be configured and activated whenever data storage is required. Within the Datalogger interface the desired tags taken from TOPServer can be selectively logged at a desired rate into a storage application of choice. Figure 16 shows an example of the connection properties configuration interface within Datalogger.

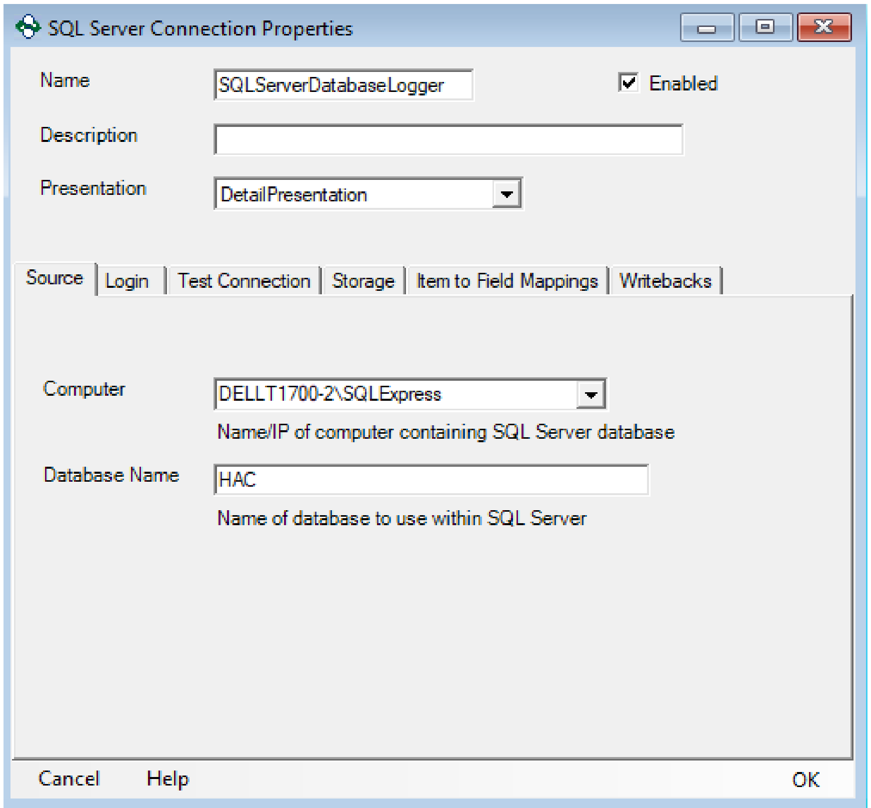

Figure 16: Datalogger SQL Server configuration interface.

Datalogger also allows for triggers to be configured which can enable the software to turn on and off when a holder tag set up in TOPServer on the OPC server changes its value. This type of functionality enables Datalogger to be automatically turned on whenever the HAC system is turned on, and off whenever it is not needed. This feature also allows for the arrangements of different logging groups. Different logging groups permit different tags to be recorded at separate times and intervals. Similarly, different logging groups can be configured to store data at different rates to differentiate storage between operating mode and standby mode. This type of configuration eases the management of the SQL Server which will not needlessly be filled with unnecessary data.

3.6.2 Using SQL Express to store data

SQL Express was chosen for data storage due to its compatibility with Datalogger. SQL Express allows for data to be stored in tables including the values, names and timestamps of millions of tags in an efficient format. Data from the database can be accessed at any time through SQL queries which can be completed through the SQL software or through MATLAB to make the process seamless. After a set amount of data has been saved into the database, SQL allows the user to remove unnecessary data easily to ensure query times stay quick and efficient. Queries can be automated to pull data from specific time frames and save data to local .mat files (see Appendix D: SQL Express procedure and automatic query script). This process enables the constant usage of SQL without having to worry about storage or memory limitations. Figure 17 shows an example of the SQL Express interface with the different tables in the HAC database listed on the left side of the image. The properties of the database can be seen in the window on the right.

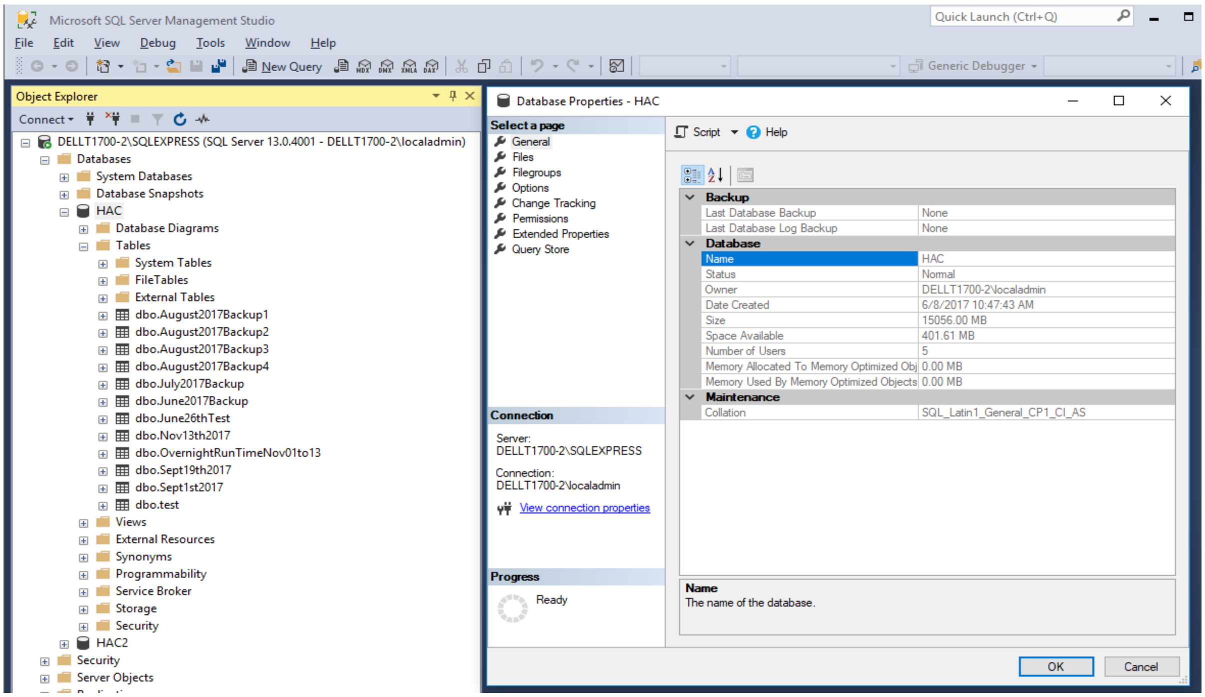

Figure 17: SQL Express configuration interface.

3.6.3 Local storage management

Data is regularly taken from the SQL server and saved in multiple .mat files as a backup and for post processing data analysis. The SQL server will log the measurements from the instruments in their respective formats, most of them as a 16bit digital number of the raw analog signal with a few using their own digital format. These direct analog and digital readings are known as the raw values which can later be converted into measurements based on instrument specifications and certificated calibration constant. Raw tags from every experiment and test are saved in separate .mat files. The raw values are then converted to process variable observations in engineering units and saved as a new file. These .mat files can directly interact with the MATLAB software for automated data analysis. The data is then converted and saved in a .txt format which can later be loaded into an Excel document for comparison to the HAC model which is used to analyse the predicted performance of the HAC.

4. Automation and data analysis

Once the framework for the software was established and the HAC system could operate as intended, the next step was to automate parts of the process. The first thing to be automated was the PID loop, which controls the entire system by regulating a motorized globe control valve through the MATLAB HMI. A procedure was also established to automate tests referred to as "benchmark tests". The benchmark tests were completed under consistent intervals over multiple days, weeks and months and the goal was to replicate operating times and conditions as closely as possible between trials. A process for collecting data for benchmark tests from the SQL server and converting them into .mat files was also automated to increase efficiency and simplify the procedure for the operator. Lastly, an automated procedure to calculate the KS statistic ('Kolmogorov–Smirnov Test', 2008) between two sets of benchmark test data was created to test for statistically significant differences between HAC Demonstrator operating states.

4.1 HAC Demonstrator automation using a PID loop

A proportional-integral-derivative (PID) control loop is frequently used in industrial settings to continuously and autonomously control a process. In the HACs case, the process that is controlled is the rate at which air is released from the separator tank. Controlling the amount of air being released from the system permits the HAC to run automatically without the need for human intervention. The HAC introduces different mass flow rates of air to the separator tank depending on different operating parameters such as the set point rotational speed of the VFDs or the total volume of water in the system. The mechanical control valve installed on the compressed air delivery pipeline will open by a certain amount to release the compressed air at a rate which closely matches the air production rate. Opening and closing the valve will raise and lower the water level in the separator tank as a consequence of delivering compressed air. By controlling the valve, the water level in the separator can thus be maintained at a desired setpoint.

The PID loop automatically controls the valve based on a set point water level in the separator chosen by the operator. The PID loop responds to changes in compressed air production rates created by increasing pump speed but is also tuned to keep valve actuations to a minimum. It is calibrated with three parameters: the proportional (P), integral (I) and derivative (D) terms. These three parameters shape the response time and behaviour of the water level when the system experiences a change in air production rate.

The P term controls the output proportionally with respect to the magnitude of the error by reading the current value of the error. The I term accounts for current and previous values of the error. By computing the cumulative value of the error, a controller with a fine tuned I term can eliminate any residual errors. The D term influences the controller by estimating future errors using the rate of error change.

The PID loop was firstly configured during the commissioning stage of the HAC Demonstrator simply by trial and error. The configuration process began with all three parameters set to zero within the code. The HAC was turned on and the proportional term of the PID loop was then increased until a desired response to a change in production rate was experienced by the valve. Once clear oscillations were established, as seen in Figure 18, the integral term was increased periodically to reduce the height of the oscillations.

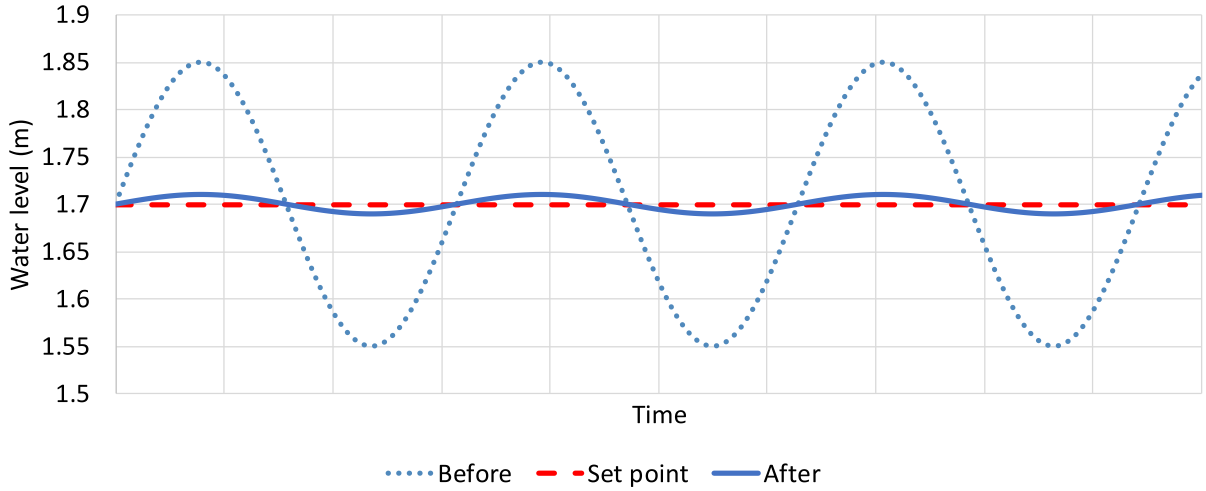

Figure 18: Example of oscillating behavior before and after PID loop tuning.

The integral term, responsible for ensuring the control loop does not slowly drift, can greatly increase the response of the valve if it is out of position for long enough. Following the integral term, the derivative term value was increased until a quick and steady response was observed when the PID loop was initially started up. Once the PID loop was able to operate within a small window and keep valve actuations to a minimum the parameters were saved in the HMI and the PID loop was ready for full scale testing. The PID controller polls the current water level in the separator from an I/O unit that is connected to the OPC server and makes adjustments to the position of the motorized control valve to control the HAC Demonstrator.. The function for the PID loop in the HMI can be seen in Appendix E: PID loop MATLAB script.

4.2 Establishing a benchmark test

To improve consistency in experiments being performed on different days of the week or times of the day a benchmark test procedure was established. During the preliminary stages of the HAC testing the benchmark procedure was completed manually by tracking the time spent on each setpoint and actively changing the speed of the VFD's at the correct intervals. Notes were then taken to track and record what the test was for and what the system conditions were for example: time of day, atmospheric pressure, temperature, water volume, lid setting, and other unique system parameters. This procedure did not allow the operator much time to perform any other tasks during any HAC trials and thus an automatic procedure was created.

This procedure is followed whenever an experiment or a test is run on the HAC Demonstrator and simply normalizes how long the pumps will run for at distinct set points for each test providing a performance curve of the HAC operation under those specific operating conditions. The pumps operate within a range of 220rpm to 880rpm. Early testing on the HAC revealed a minimum operating speed of 600rpm to ensure air production when operating at the the nominal water volume in the system. Consequently, the automatic benchmark test procedure starts at a minimum speed of 600rpm and ramps up to 880rpm in 50rpm intervals, with the last interval set to 30rpm. This procedure allows for 7 different setpoints with different pump speeds.

The time spent on each set point is 8 minutes. Of these 8 minutes, although all data is recorded, data captured during the first 3 minutes of operation at a specified set point is typically excluded from further routine analysis. This 3-minute allowance for the system to arrive at steady state between setpoint changes allows 5 minutes of data, logged at 1 Hz, for each setpoint to be collected and analyzed for HAC performance characterisation. The 3-minute allowance provides the PID loop with enough time to converge on the water level set point when the system makes a change. Commissioning and acceptance testing revealed that steady state operation is achieved early on in the 3 minute window, and the window length is very conservative.

Using MATLAB and the HMI a function was created to automate this process. When a benchmark test is needed a button on the HMI is pressed and a prompt is given to the operator to add any notes about the HAC system parameters that should be recorded which will automatically be saved in an Excel sheet on the Server PC. Time stamps for all benchmark tests are also automatically recorded in the same Excel sheet. The function for the benchmark test procedure in the HMI can be seen in Appendix F: Automated benchmark test MATLAB script.

The function uses a timer to start the test and sets the VFD's to the first setpoint speed: 600rpm. The function tracks the loop iterations and automatically changes the speed of the VFD's to the next setpoint every 480 loops, or 8 minutes. The PID loop runs parallel to the benchmark test loop and ensures the system remains stable throughout the test. After the final set point time has elapsed, the function ramps down the VFD's back to the first setpoint. This automated benchmark test procedure allows the operator to spend more time on other tasks.

As experience in operating the system was gained during the first six months of operations, a minor change was made to the benchmark procedure which monitors all instruments at high frequency when the system is in a quiescent state at the start of each benchmark test. During this period, zero values for every instrument are recorded before every test. This procedural change allowed for improved accuracy of values recorded by sensors that may suffer 'zero' drift. In particular, it was found that differential pressure sensors were particularly prone to drift, while remaining totally within their defined, and calibrated specifications. Zeros on these instruments could very effectively be reset before each benchmark test using water level observations when the HAC system was at rest.

4.3 Automatic data collection

Another automated function was created for collection of the benchmark test data from the SQL server. Initially, after benchmark tests were performed the operator would manually query the SQL server multiple times for data store to in .mat files for post processing analysis. The automatic data collection function was created to automatically read a desired benchmark tests timestamps, collect the appropriate data from the SQL server and save the raw values in a .mat file. It also converts the raw values into measurements and saves those in a separate .mat file. Furthermore, the function generates a matrix with values across all set points for the specified benchmark test and saves that matrix and some meta data in a third .mat file. The third file is also converted into a .txt file automatically for further post processing analysis in Excel. The functions used for the automated data collection procedure can be seen in Appendix G: Data collection and analysis MATLAB script.

4.4 Testing for consistency using the KS statistic

The Kolmogorov-Smirnov statistic, also known as the KS statistic is a method which compares the difference between two probability distributions. The null hypothesis for this statistical test is that the probability distributions are taken from the same source. By comparing the distance between two sample cumulative distributions taken from the same source, in this case any instrument recording a process variable in the HAC system, slight differences in the values of these operating parameters can be conclusively be proven to be either the same, or different than, the values from prior benchmark tests. The process of constructing cumulative distributions for the measurements taken by the instruments throughout each benchmark test was automated using a MATLAB function. The function compares two benchmark tests across all set points and instruments for the null hypothesis. The MATLAB function for the KS statistic can be seen in Appendix H: KS statistic MATLAB script. The function also plots a comparison of the CPDF plots for every instrument between both tests. The cumulative distributions are formed from the 5 minutes of recorded data of the HAC operating at steady state at each set point. Figure 19 shows the CPDF of two benchmark tests run on in October 9th and October 10th in 2017 and compares the intake air velocity (FT5) for the 600rpm setpoint of both tests.

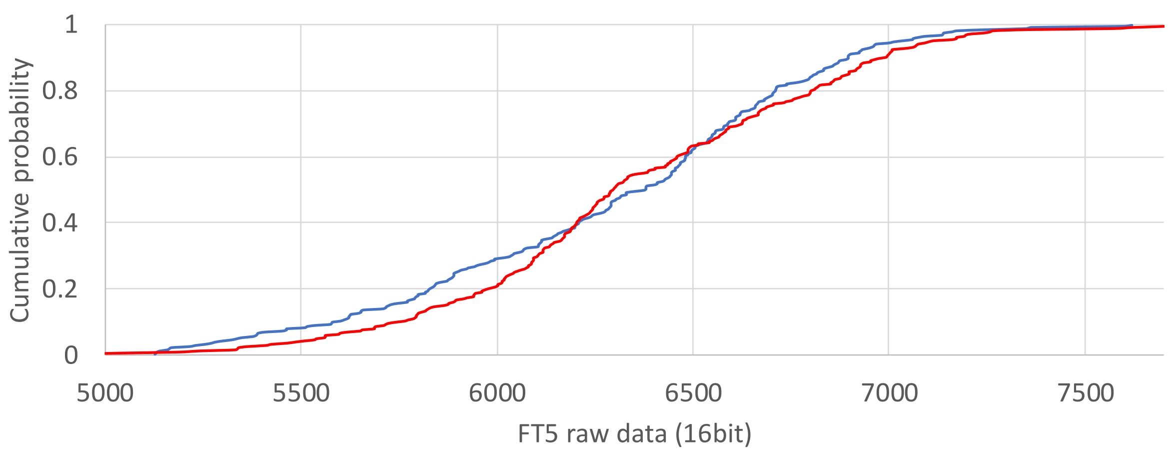

Figure 19: A chart showing good agreement between two CPDF plots.

The tests were run under similar conditions with an increased amount of water in the system for the second test. Although the intake air velocity seems to be consistent with different operating conditions, most of the instruments are much more sensitive to changes in the system. This can be seen in Figure 20 when the differential pressure measurements (DPT3) from both tests are compared.

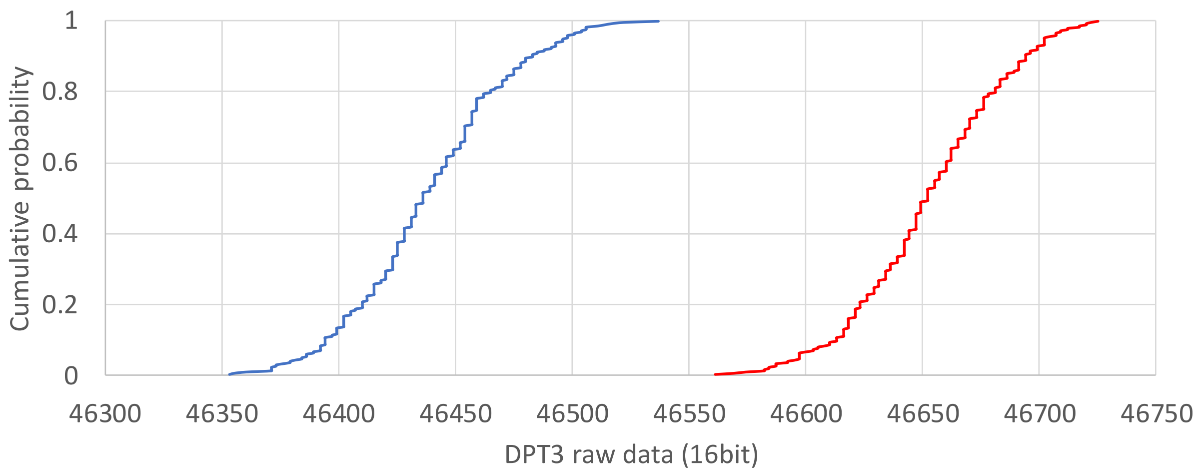

Figure 20: A chart showing poor agreement between two CPDF plots.

This differential pressure measurement is influenced by the volume of water in the system and is expected to be more sensitive to such a change. In theory, if the operating conditions are the same when performing benchmark tests the CPDF plots for the instruments should look like Figure 19 and not Figure 20. The automated KS statistic function is in place to ensure reliability and repeatability of our test results.

The KS statistic test for DPT3 with the data set shown in Figure 20 has been calculated and rejects the null hypothesis at a significance of 95% that the two sets of data come from the same distribution. The value of the KS statistic is equal to 1, representing the largest difference in cumulative probability between both data sets with a probability of 100% that the KS statistic would be as large or larger than its reported value. This result is expected due to the large discrepancy between the data sets recorded. However, running the same test for FT5 with the data shown in Figure 19 does not reject the null hypothesis at a significance of 95%. The value of the KS statistic is now 0.0906, and the test computes a probability of 83.564% that the two distributions would have a maximum difference as large or larger than its reported value. The KS tests reveal which instruments are more or less sensitive to minor changes in operating conditions such as temperature, humidity or water volume.

5. HAC acceptance testing

This section aims to describe testing that was required to fully commission the HAC Demonstrator. Verification of leaks in the system and calibration of certain instruments are also discussed.

5.1 HAC pressure testing

One of the first tests to run during the commissioning process after the HAC Demonstrator was built was the pressure test. To perform this test the HAC system was blocked at all exits and filled with pressurised water to ensure there was no leaks. The pressure of the water inside the system was then increased up to 90psi at the highest point in the system to ensure the system met or exceeded Engineer's specifications in the design. The HAC was successfully pressure tested to 90psi, a pressure that the HAC system will never reach in operation, by design.

5.2 Variable frequency drives (VFDs) commissioning

5.2.1 VFD bump test

Once the VFD's were installed and wired in by the contractors they had to be given a standard bump test. A bump test ensures the motors are rotating in the correct direction relative to the pumps. The VFD's are turned on for a short amount of time and the rotation of the shaft in the motor is monitored to ensure its turning in the correct direction. If the shaft is turning in the wrong direction, two of the phases of the 3 phase power lines have their terminals swapped over to correct the problem. In the case of the HAC Demonstrator, the bump test revealed one of the motors was rotating the wrong way which was immediately corrected by the electrician on site. A second bump test was performed to ensure the motors were turning in the correct direction.

5.2.2 Part load curve

The HAC Demonstrator's overall efficiency is dependent on the VFD's and the motors efficiencies. Figure 21 shows a generic part load curve for a 25HP motor, the same rating as that of the motors used at the HAC.

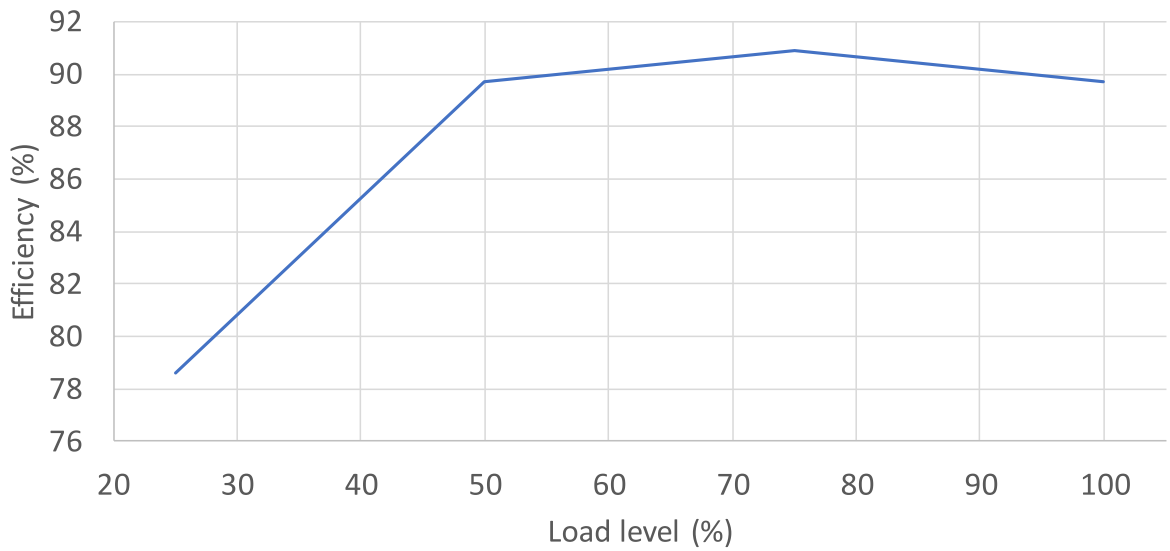

Figure 21: Part load efficiency curve for a 25HP motor from Chirakalwasan (2007).

The motors used at the HAC Demonstrator are three phase 25HP and running on 575V, 60Hz at a maximum speed of 880rpm. Although part load curves vary from motor to motor, the motors selected for the HAC Demonstrator (Baldor-Reliance 1256M) also have optimal operating efficiencies near 75% of rated load. To maximize the efficiency of the HAC it is critical to operate the motors at an optimal load in the range of 75%. The pumps and motors selected in the design of the HAC Demonstrator were selected due to their optimal efficiencies being in the expected operating range of the system. Similarly, in the design of future HACs, knowing the optimal operating point of the HAC will lead to the selection of a motor that will best match its intended operating range.

5.3 Investigation of air leakage into the system

During the first stage of benchmark testing the air flow rate entering the system the observations indicated a problem with the mass balance of air across the system. According to the instrumentation, the mass flow of compressed air the HAC was producing was greater than the mass flow of air that it was inducting from the atmosphere as seen in Figure 22. Over the length of the entire benchmark test a large gap between inlet mass flowrate and outlet mass flowrate of air can be observed.

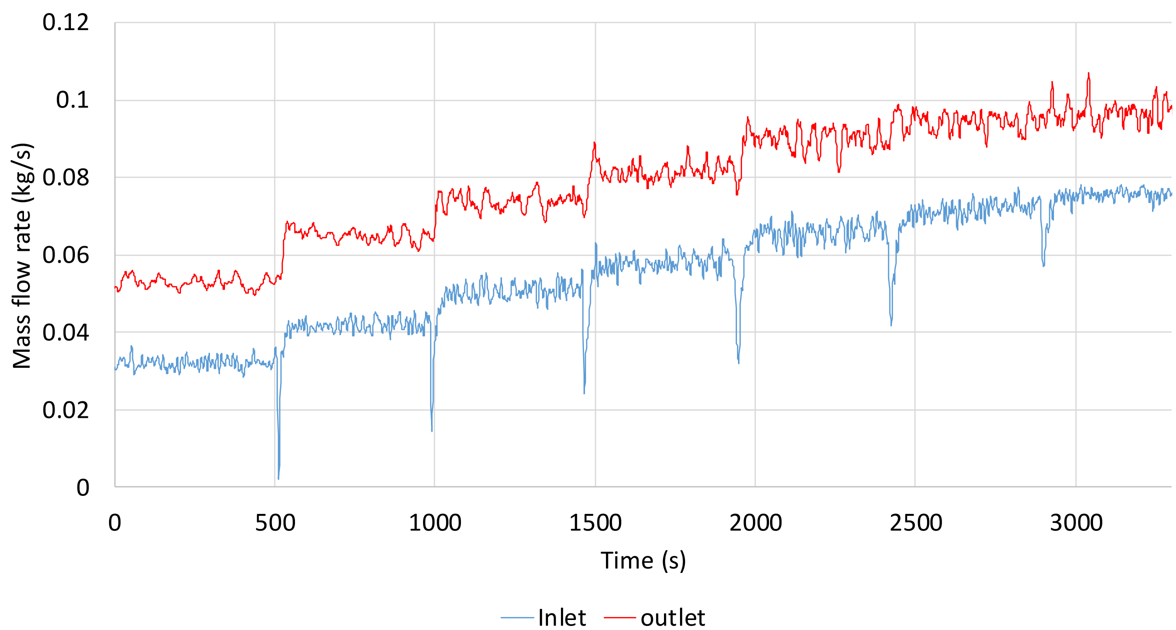

Figure 22: Early benchmark testing revealing a significant difference in inlet and outlet mass flow rate of air.

This was clearly physically impossible and indicated an error in the flow monitoring instruments or a possible air in-leak in the system. After placing the HAC in calibration mode by sending the compressed air through the Coriolis and the optisonic flow meters in series, Figure 23 shows that the air flow rates going through both instruments are similar, and the gap seen in the previous figure is no longer present. The oscillation behaviour recorded in the air mass flowrate data is a consequence of operating the HAC Demonstrator in calibration mode with the lid open.

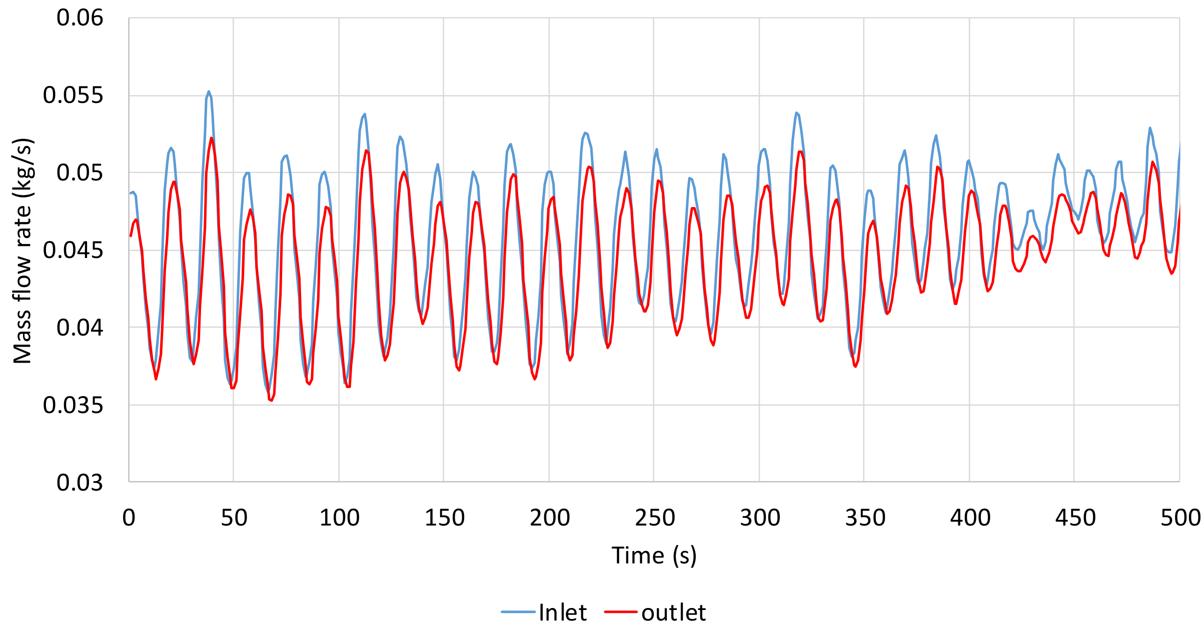

Figure 23: Comparison between inlet and outlet air flow rate when HAC is in calibration mode.

This confirms the problem does not lie with the instruments, since they are working as intended. The calculations required to reduce the raw observations to engineering quantities and units was also reviewed in detail and ruled out as a cause of the inconsistency leaving the only explanation as a leak in the system.

When the HAC isn't operating and the forebay tank lid is closed measurements taken by FT5 should be zero provided there is no leaks. This check could be used to confirm the presence of leaks in future benchmark tests. The velocity of air measured on FT5 should be zero if the forebay tank is sealed since air cannot flow into the intake air pipe if there is no where for the air to flow out. This can be further demonstrated by blocking the three-way valve immediately after the sonic anemometer and before the forebay which dead-heads the instrument, stopping air from flowing into the intake air pipe. Data collected over two separate two-hour periods can be seen in Figure 24 showing the expected behaviour of the sonic anemometer (when the three-way valve is closed) versus it's behaviour when the three-way valve is open.

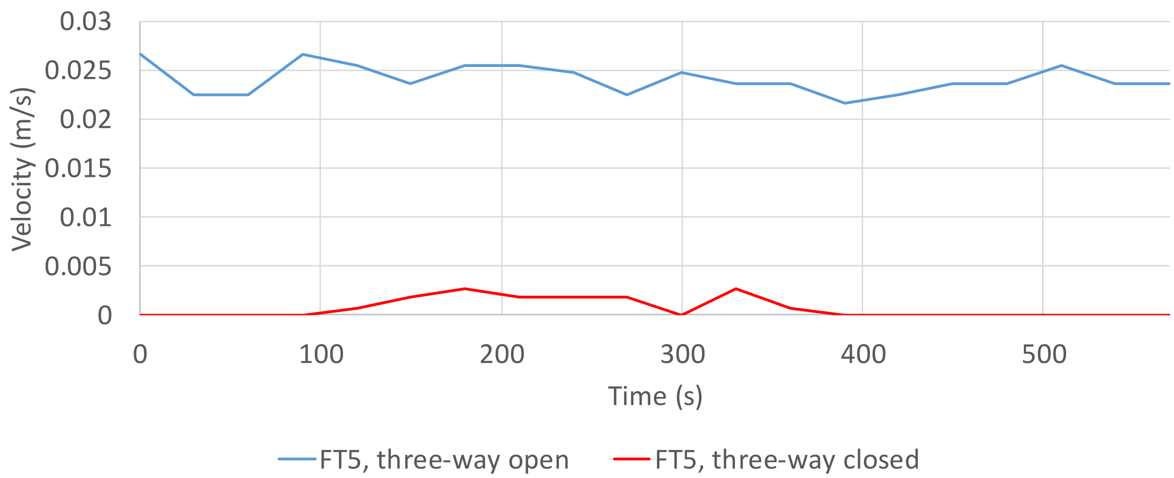

Figure 24: Difference between measurements taken by FT5 when the adjacent three-way valve is open or closed.

The velocity readings on FT5 when the three-way valve is open indicate air is flowing through the intake air pipe. Air flowing through this pipe is indicative of air leakage downstream of the three-way valve. Many days were spent tracking down, and eliminating the source of the leaks which ultimately lead to some more precise air flow rate measurements, and more precise leak detection methods.

5.3.1 Pressure vacuum relief valve (PVRV)

The first suspect of the air leakage investigation was the pressure-vacuum relief valve on the top of the forebay tank. The valve is designed to prevent any over pressure or under pressure of the forebay tank up to 2,000Pa or -2,000Pa respectively. It functions by lifting a sealed opening if the pressure in the tank ever exceeds 2,000Pa which will release some air and depressurize the system.

Similarly, if the vacuum pressure in the tank ever falls below -2,000Pa another sealed opening will be pulled up to suck air into the forebay tank and pressurize it. A drawing of the PVRV valve can be seen in Figure 25 showing the vacuum and pressure chambers and their mechanisms.

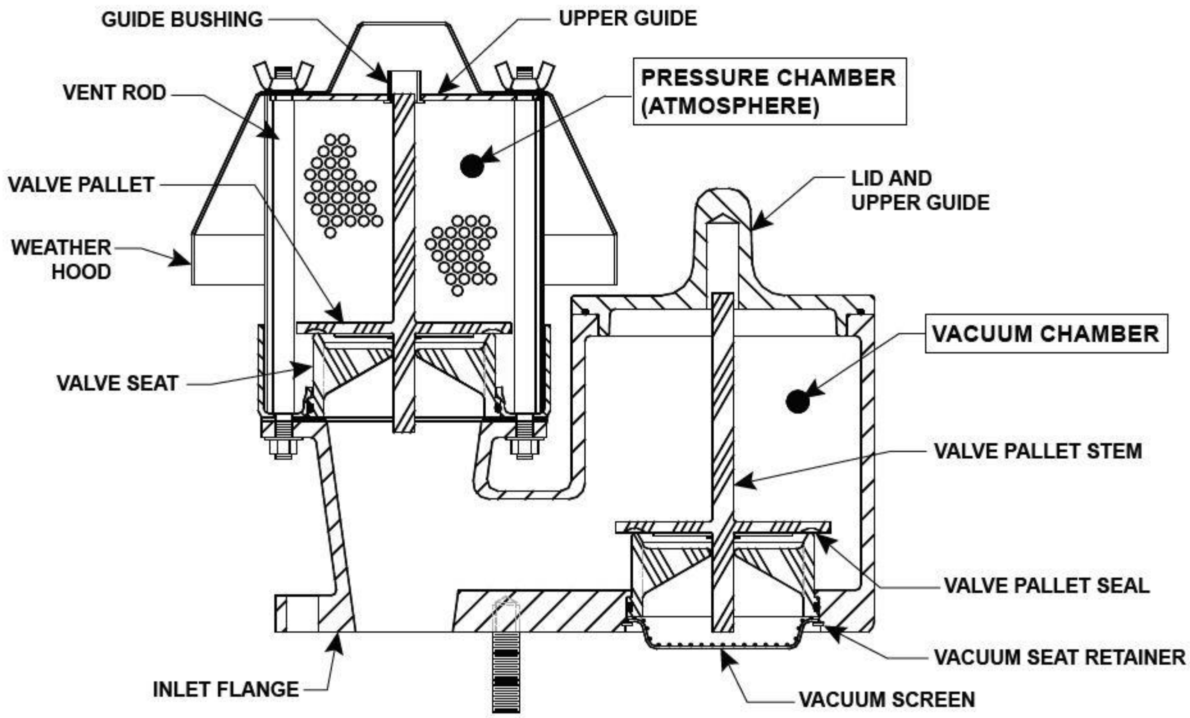

Figure 25: Drawing of the PVRV installed on top of the forebay tank.

This valve was thoroughly investigated for leaks when the system was operating at a variety of setpoints and was deemed to be leak free.

5.3.2 Spillway

Another suspect for leakage into the forebay tank was the spillway pipe coming up from the tailrace tank. It was believed atmospheric air inside the facility was entering the surge pipe, which is also connected to the tailrace, and flowing through the spillway shown in Figure 26 and into the forebay tank during operation.

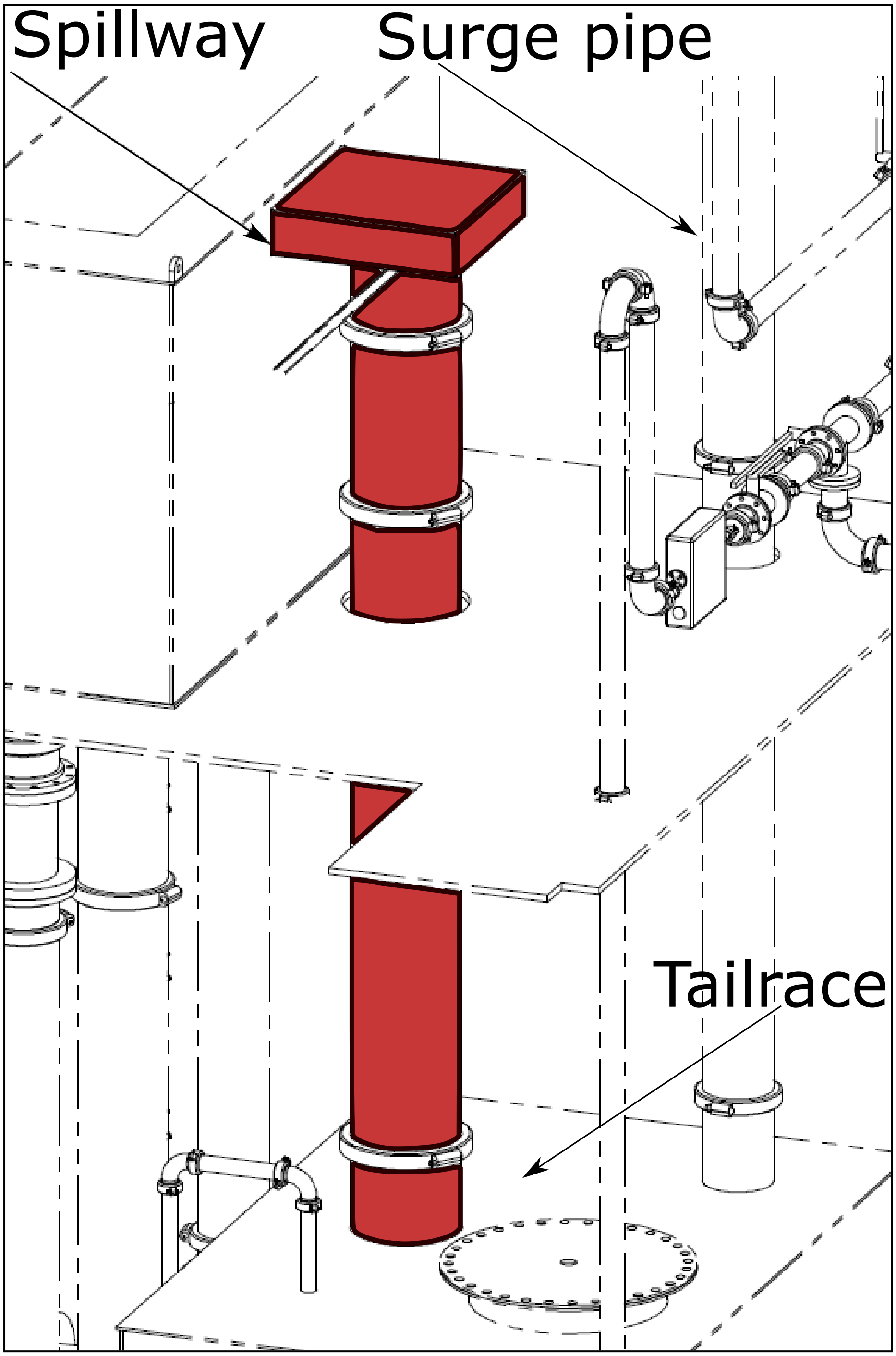

Figure 26: Drawing highlighting the spillway connecting the forebay tank to the tailrace tank.

Measurements taken during a benchmark test with a handheld anemometer measured a non-negligible air velocity entering the surge which confirmed the hypothesis. A wooden barrier is now installed on the forebay side of the spillway pipe to stop air from entering through the surge pipe. Operational experience established that blocking the spillway pipe was deemed safe since the HAC system will never contain enough water to use the spillway for its design purpose. More tests were later conducted on the system which revealed that the air entering the forebay tank through the spillway was only responsible for a small amount of air leakage and was not the primary problem. Figure 27 shows the difference between inlet and outlet air flowrates before the wooden barrier was installed and after.

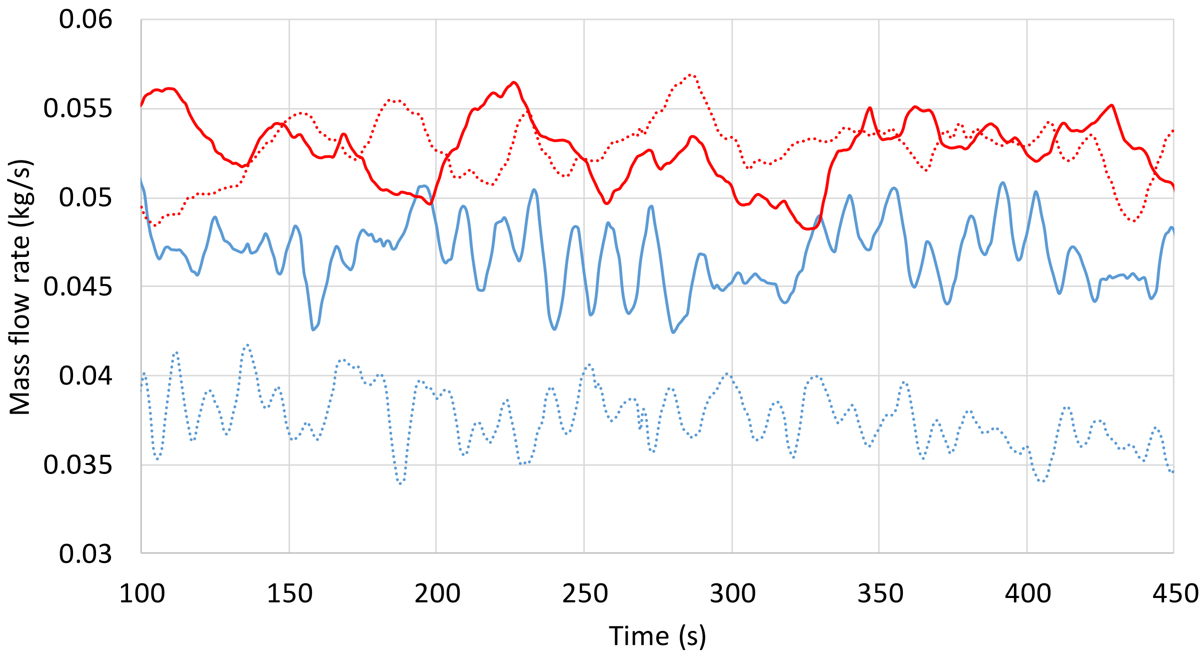

Figure 27: Difference between inlet (blue) and outlet (red) mass flow rate from before (dotted) and after (solid) the spillway was blocked.

Although blocking the spillway lead to an improvement in the measurement of air flowing into the system, it was still reading less than the outlet mass flow meter which meant there was another leak elsewhere in the system.

5.3.3 Smoke testing

The air pipe extending from the forebay tank to the exterior of the HAC facility that pulls atmospheric air into the system through the optisonic flow meter was also investigated for leaks. A smoke generating incense stick was lit up near the Victaulic pipe couplings. The generated smoke was used to visually identify if any of the Victaulic couplings were improperly installed and pushing or pulling any air at the couplings. As a consequence of this testing, the Victaulic couplings were eliminated for possible leaks after the test was complete due to zero signs of air leakage. Figure 28 illustrates some of the Victaulic couplings assessed.

Figure 28: Compressed air line showing some of the Victaulic couplings.

5.3.4 Forebay tank lid

The forebay lid was originally sealed with duct tape and a make shift rubber gasket. To properly assess if the lid was a source of air in-leak even more duct tape was applied to the lid. After multiple layers of duct tape were applied and more tests were done it became clear that the lid of the forebay tank was the primary cause of leakage of air into the system, even when ‘sealed’ with copious layers of duct tape and the gasket. A custom rubber gasket was ordered to replace the original gasket and g-clamps were purchased to ensure a tight seal on the new gasket. After installing the gasket and the g-clamps around the lid a final layer of duct tape was applied. This ultimately led to the most reliable measurements of air flowing into the HAC relative to the compressed air leaving the system as seen in Figure 29.

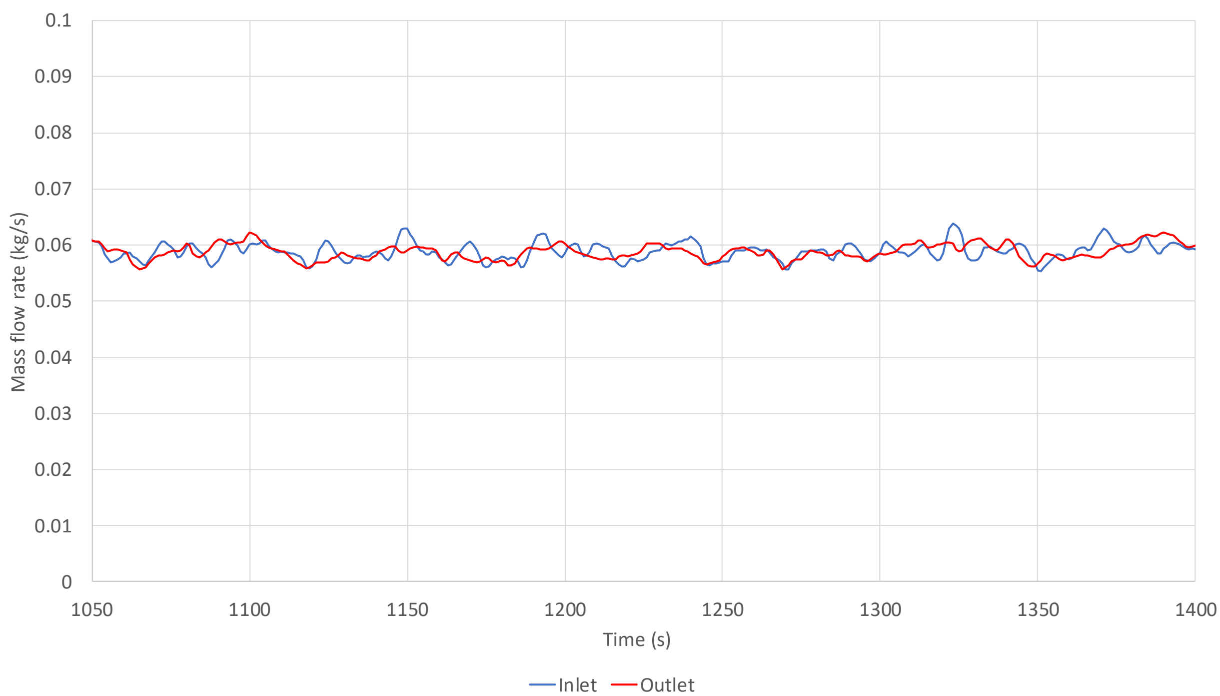

Figure 29: Comparison between inlet and outlet mass flowrate of air at the 700rpm setpoint during a benchmark test after the lid was sealed with a new gasket, g-clamps and tape.

After a few weeks of experimentation slight changes were made on the HAC system including 3 x 10mm holes that were drilled into the spillway pipe enclosure to allow air to be released during the filling and emptying processes. During prolonged benchmark testing to produce the performance map of the system it became clear that these small holes made to the system were enough to disrupt the mass balance of air entering the system, accounting for ~3 litres per second of leakage inflow. These holes have since been taped up to prevent any further leakage of air into the system.

5.4 Blow off testing

One safety mechanism built into the HAC Demonstrator is the blow off pipe. The end of the blow off pipe is positioned within the separator tank to ensure that the separator does not fill sufficiently with compressed air to expose the upper edge of the downcomer pipe discharge. During normal operation under PID control, the end of the blow off pipe is submerged in the swirling water in the separator. If the water level falls low enough to expose the end of the blow off pipe, air from the compressed air plenum above the water enters the pipe, leaves the separator vessel, and cause the the water level to rise to submerge the end of the blow off pipe again. During acceptance testing, this functionality needed to be tested. The blow of was tested using the level sensor in the separator tank. The HAC was turned on and compressed air was added into the separator tank until the blow off was activated. The level of water in the separator when the blow off activates was recorded at roughly 1.51m and the behaviour of the system was monitored.

During an experiment the HAC Demonstrator was left in operation continuously at a low flowrate for a period of three hours to test the behaviour of the blow off during a time when the PID loop was not operational. In theory, the blow off should self regulate the HAC and release any excess air stored in the separator when the water level falls below the blow off level. Figure 30 plots the data recorded for the water level in the separator over the course of the experiment.

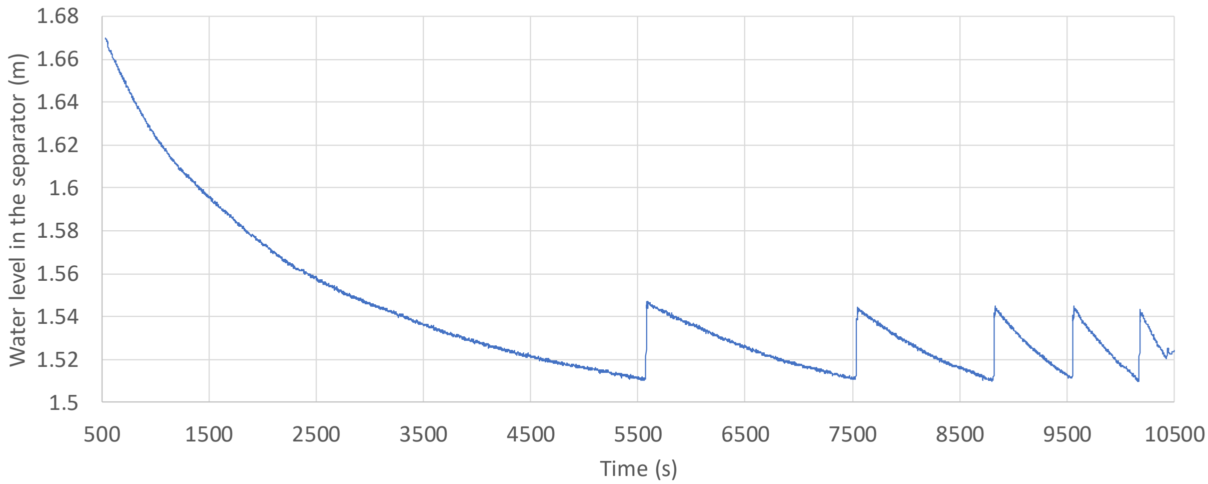

Figure 30: Time series plot of the level in the separator (LT3) when the blow off activated multiple times in succession.

The plot above shows the quick change in the water level in the separator when the blow off activates. This quick change is accompanied by a discernable rumbling noise coming associated with the blow off event. Although the events are clearly relatively violent, the blow off pipe performed entirely as expected. The increasing rate of blow off actuations however, was not expected. It can be seen in Figure 30 that the time between each blow off is decreasing. This decrease in time before each blow off must be a result from an increase in the rate at which compressed air was entering the separator. During this experiment, the violent blow off events caused water to flow up and out of the surge pipe resulting in a loss of water in the system. It can be surmised that the reduction of water volume in the HAC caused a small but incremental increase in the volume of air that was being inducted into the system due to a change in operating head.

Visual observation of sections of the blow off pipe during blow off events exhibited high amplitude vibrations in some of the pipe work at 90° elbows. As a consequence, a safety ‘whip’ line was installed across these couplings as an additional safety measure. Further testing has revealed that repeated activation of the blow off when the HAC is running while containing a relatively high volume of water (>41m^3) can lead to spilling of a small, but inconvenient volume of water from the surge pipe. As a consequence, a float switch was installed in the surge pipe that was connected to the hardware e-stop system.

5.5 Separator level calibration

The forebay tank and tailrace tank level are monitored with ultrasonic level sensors operating on a time of flight principle. They did not require much configuration to work properly and have proved very reliable, and accurate, returning water levels with sub-millimetre precision. The water level measurement for the separator uses an ultrasonic guided wave radar level sensor and required calibration to accurately measure the level of water in the tank. In fact, the observation is not made in the separator vessel at all, but in a stilling well connected in parallel with the separator seen in Figure 31.

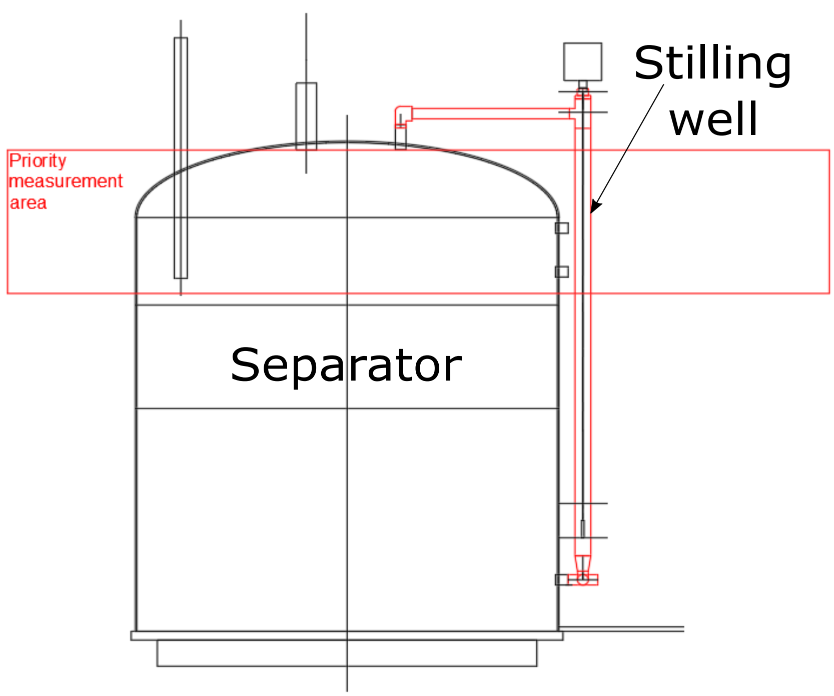

Figure 31: Schematic of the separator tank with the stilling well that houses LT3.

The rationale behind this was that it was anticipated that the surface of the water in the separator vessel was to be relatively dynamic, and perhaps frothy. As the signal for control of the whole HAC system is produced by this sensor, the measured value had to be as stable as possible, even if the value arising could only be considered an indication of the water level, rather than an accurate measurement of it at one point.

After configuring the unit, cutting the length of the wave guiding cable of the sensor to the appropriate length and installing it, a plastic sight tube was installed in parallel to the stilling well and the instrument offsets adjusted to produce accurate water level readings. The indicated water level values produced by this instrument were ultimately found to deliver reproducible levels to around 0.3mm: a highly satisfactory performance. Figure 32 shows a panoramic image of the separator tank at the bottom of the HAC facility with the stilling well, wave guided sensor and sight tube.

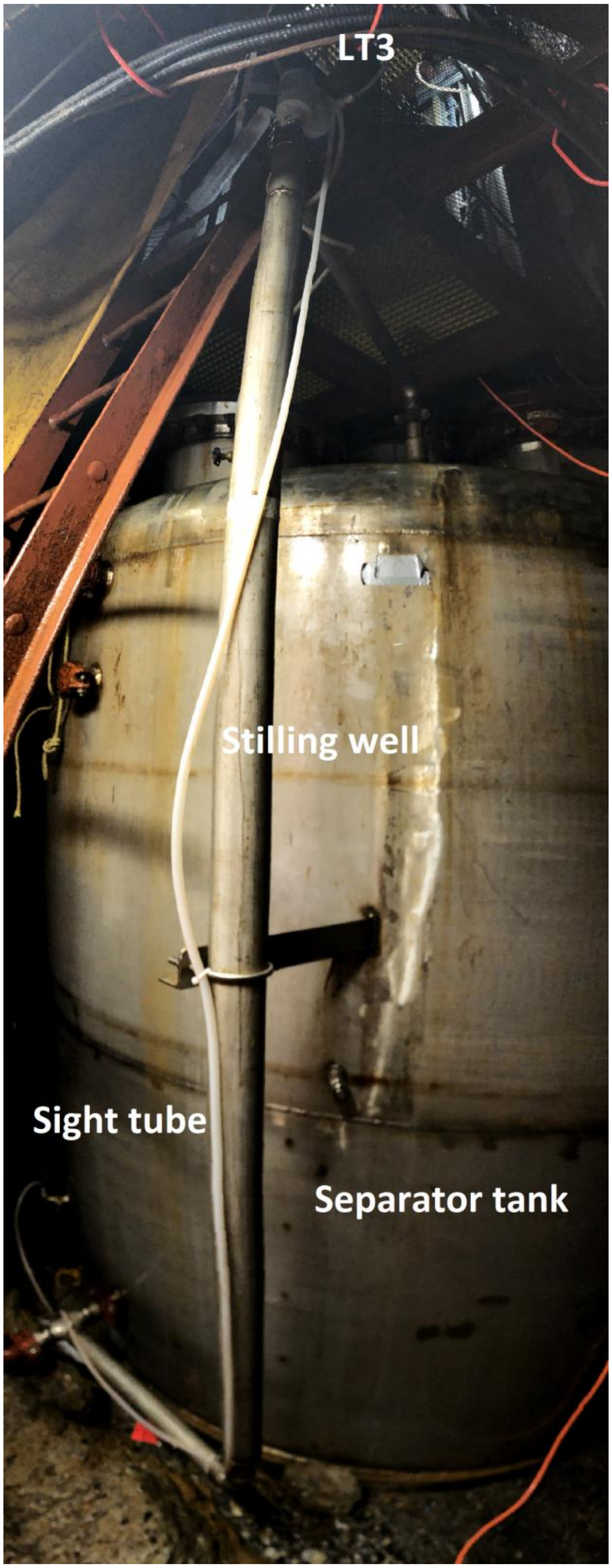

Figure 32: Panoramic photo of the separator tank, stilling well, LT3 and the sight tube.

Figure 33 shows a drawing of the same setup but includes key elevations at the separator floor, separator water level set point, DPT2, tailrace floor, and tailrace water surface. The water levels in this drawing also indicate the calibration that was necessary to render the measurements taken by LT3 accurate. Using the sight tube connected to the separator by two gateway valves an adjustment of 0.598m was measured as the offset between the LT3 measurement, 1.700m, and the floor of the separator tank. The drawing also shows some of the shock loss factors (x) that are used to calculate the water level in the tailrace tank using DPT2.

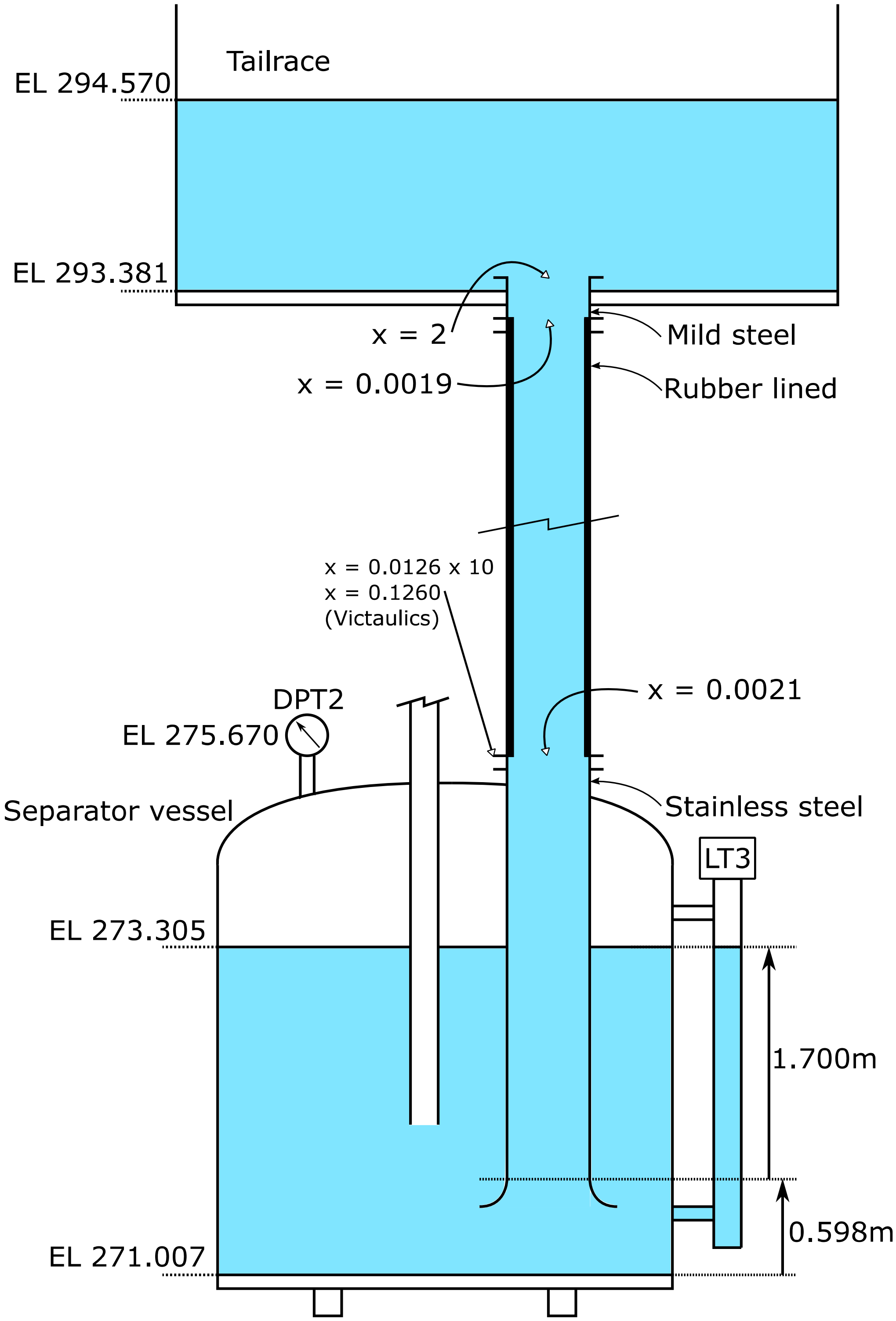

Figure 33: Drawing of the separator, level sensor, and stilling well, key elevations and shock loss factors (x).

Once the guided wave radar sensor is installed and calibrated its accuracy can be seen in Figure 34, capable of reading very small changes in water level. The PID loop is also capable of maintaining a set water level, 1.700m, with a maximum deviation of less than 0.01m by communicating with LT3.

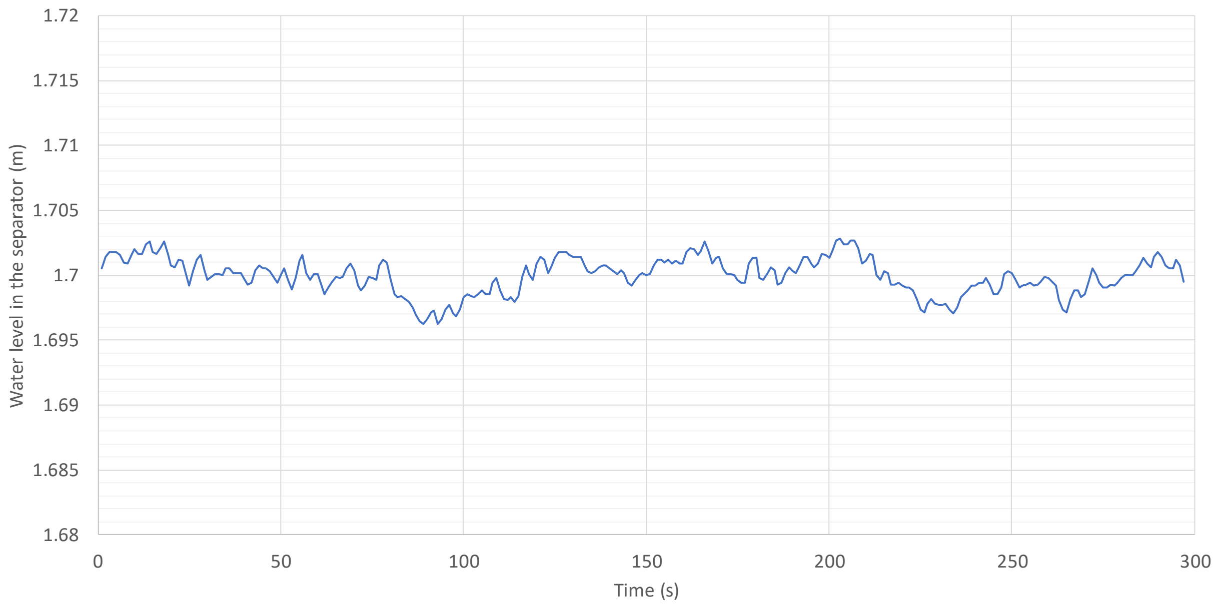

Figure 34: LT3 measurements over a 5-minute period during a benchmark test.

The precision of LT3 paired with the PID loop allows the HAC operator the freedom to experiment with different water level set points that can be maintained with no issues.

5.5.1 Description of system state transition from non-operating to operation condition.

One way of manipulating the head developed by the system, when the water flow rate circulating through it is 'held' steady is to increase the total volume of water in the system. In the current configuration, while water can be added or removed while the system is operating, this has to done through manual manipulation of fill and drain valves at the separator, and is not part of routine operating practice. Without filling or draining, when the circulation pumps are not operating, water levels in the pipe work and tanks are equal in the forebay tank / downcomer and the tailrace tank/surge pipe (as well as ‘auxiliary’ pump discharge pipes, blow off pipe, and spillway pipe). Under this condition, differential pressure sensor DPT2 measures the pressure of the air stored in the plenum above the (still) water level in the separator relative to atmospheric pressure at the separator elevation. The air pressure sensed by DPT2 arises due to the static column of water above the still water plane in the separator (at 273.305m in Figure 33) and can be used to estimate the elevation of the water free surface in the upper parts of the system, with knowledge of the water density.

In the non-operating condition, the precise elevation of the free water surface in the pipe work / tanks, depends on the total volume of water that has been admitted to the system. Figure 35 illustrates the two extreme fill states and an intermediate fill state.

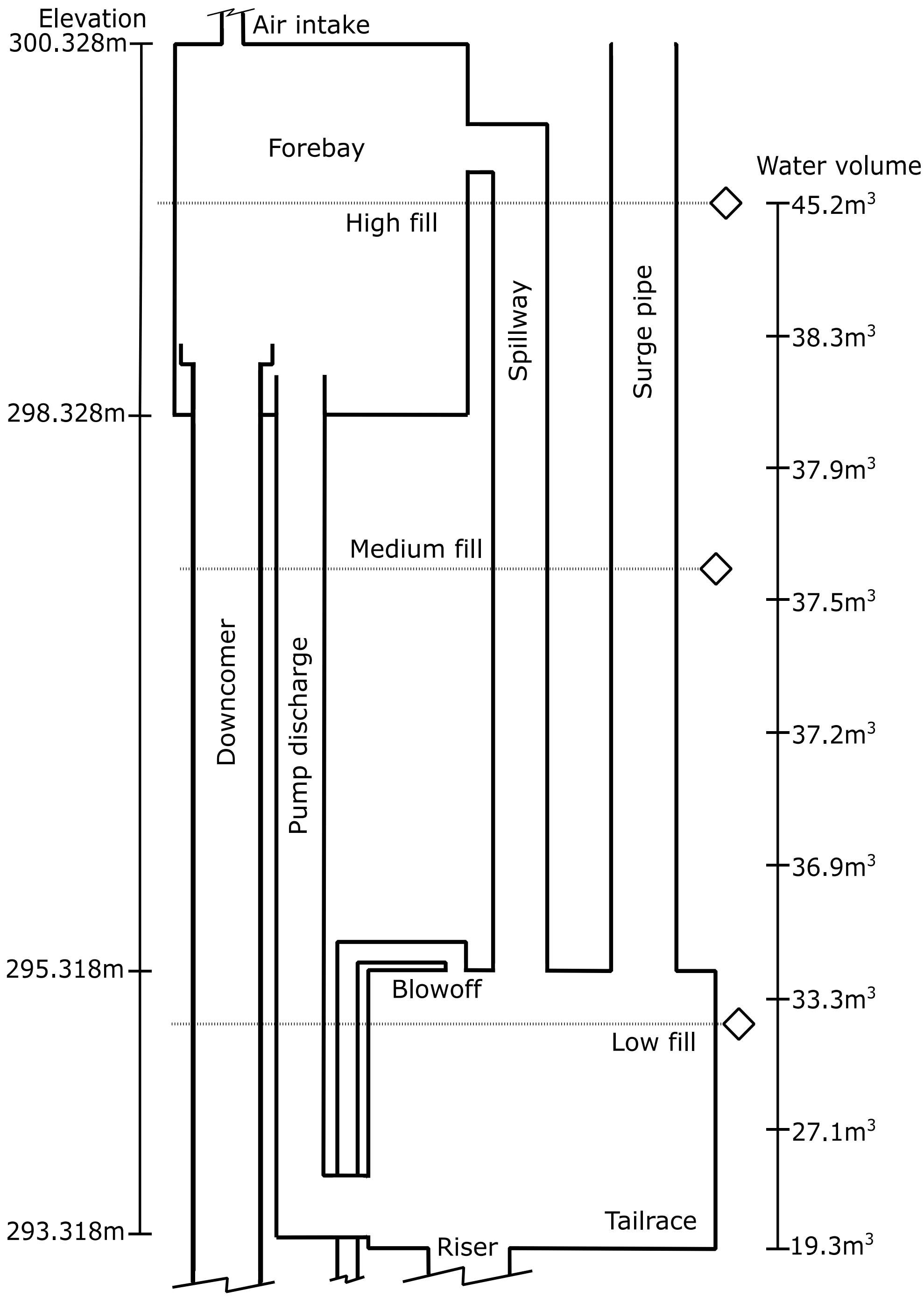

Figure 35: Non-operating condition water levels at high, medium and low fill in the tailrace/surge pipe/forebay.

Inspection of the 3 cases shows that in either of the two extreme fill states, either LT1 or LT2 are in range and their mm precision observations, from either sensor depending on the circumstance, can be used to determine the total volume of water in the system. The level measurement provides this by means of calculation, with knowledge of the precise internal geometry of the system. Also, the precise water level observation can be used to correct for zero drift of pressure sensors installed in the system before each operating test is performed. These pressure sensors include DPT1 to 3, and pressure sensors installed across the pumps, or in the downcomer or riser sampling ports. In the intermediate case, neither LT1 or LT2 is within range, and, with the current configuration of sensing equipment, it is not possible to know the level of water in the system, without manual measurement using a ‘dip stick’ in the surge pipe. The taking of this measurement is now a part of routine operating practice when the still water level in the system is out of range of both LT1 and LT2, so that zero drift corrections can still be applied to the pressure sensors.

When the circulation pumps operate, the free water levels in the upper parts of the system all change as seen in Figure 36. The water level in the forebay tank increases because the pumps lift water to this location from the tailrace tank. The water level in the forebay tank has to rise to an elevation above that of the hydroplane grill of the air water mixing head in order for water to be able to be admitted to the downcomer (compression) pipe. Thus, there is no longer any free surface in the pump discharge pipes leading to the forebay tank. As water is drawn from the tailrace tank, the elevation of the free water surface in the tailrace tank/surge pipe reduces. For almost all operating conditions, the tailrace tank water level falls within range of sensor LT2 – but not always, for high fill states. In these latter states, the water free surface remains in the surge pipe, and means it is not possible to establish the operating head of the HAC from a straightforward subtraction of water surface elevations derived from observations of LT1 and LT2. Another means of estimating the water surface elevation in the surge pipe is required. During HAC operation, i) the water level in the spillway pipe assumes that of the water in the tailrace tank, ii) there is no free water surface level in the pump discharge pipes, iii) the water level in the blow-off pipe also assumes that of the water in the tailrace tank.

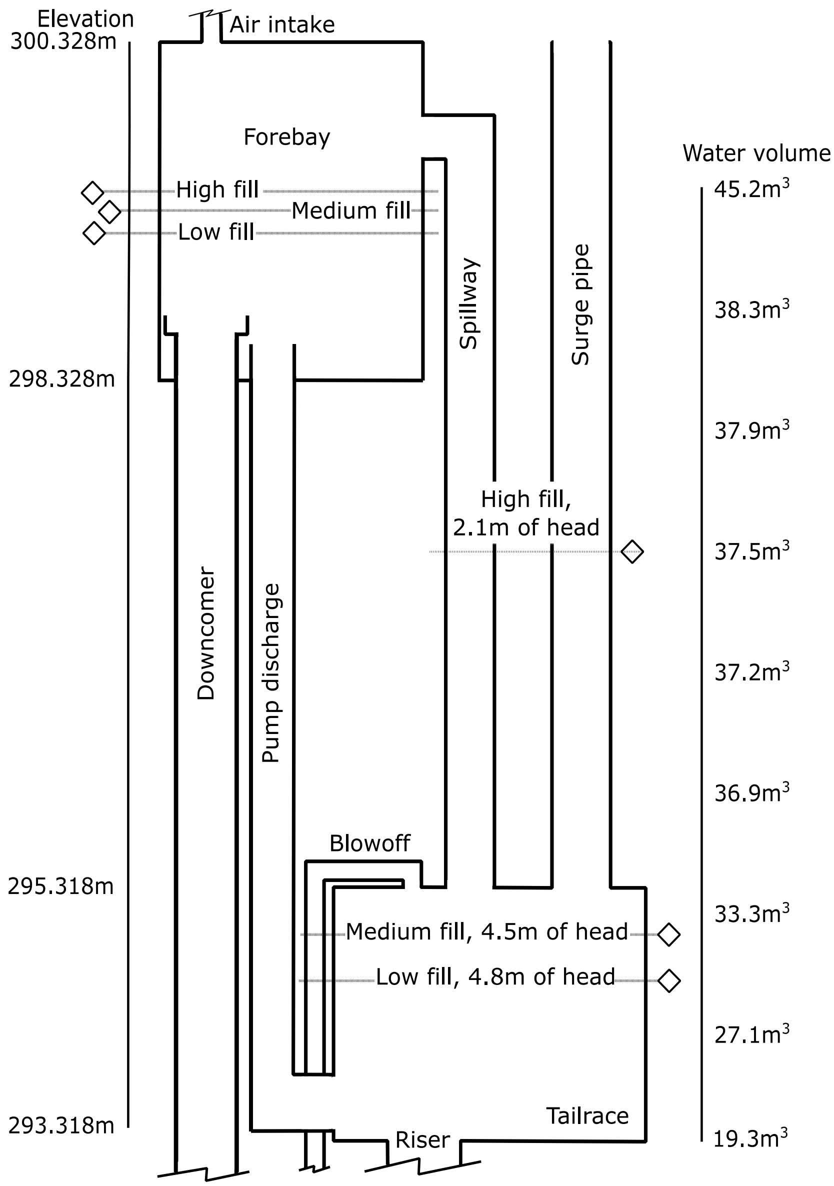

Figure 36: Operating condition water levels at high, medium and low fill in the tailrace/surge pipe/forebay.

5.6 Tailrace/surge pipe water level calibration with DPT2

The differential pressure sensor measuring the pressure in the separator tank can be used to back calculate the water level if it exceeds the height of the tailrace but remains below the forebay level (seen as the medium fill zone in Figure 35). The height of the water column above the separator tank when the HAC isn't operating is given by the DPT2 measurement, dP_{sep}. By substracting the frictional losses pressure losses, P_f, and the shock losses (denoted as x on Figure 33), P_s, and adding the elevation pressure difference, $P_{\Delta El}$, to the differential pressure measurement we can calculate the elevation of the water column.

$$El_{water\ column} = \frac{dP_{sep} - P_f - P_s + P_{\Delta El}}{g\rho} + El_{separator} \tag{31}$$

Once the elevation of the water column is known the level of the water in the tailrace is equal to the difference between the elevation of the water column and the elevation of the floor inside the tailrace,

$$DPT2_{water\ level} = El_{water\ column} - El_{tailrace} \tag{32}$$

To increase confidence in the calculations, data from a benchmark test where the water level was within the range of the level sensor was compared to the calculated value. Figure 37 shows the calculated water level using the pressure sensor versus the water level using the level sensor and there is a significant different between the values which increases with water flowrate.

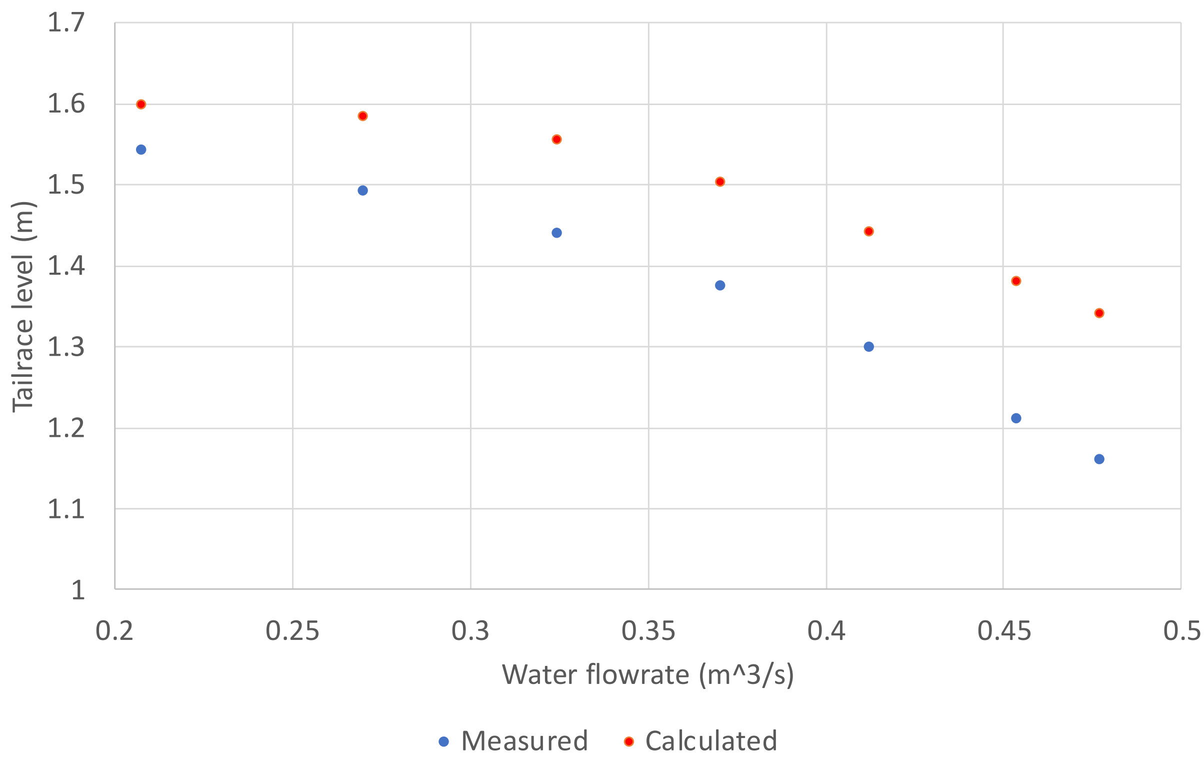

Figure 37: Level sensor reading (red) and pressure sensor level reading (blue)

Due to some of the geometries within the separator tank some shock losses, not seen in Figure 33, could still be unaccounted for in the original calculation. The level sensor (LT2) reading is considered accurate when the water level is within the boundaries of the tailrace tank and can be used as a calibration value. By using the sum of least squares between both values an unaccounted-for shock loss factor of 0.95 is necessary to make the pressure sensor (DPT2) level calculation accurate as seen in Figure 38.

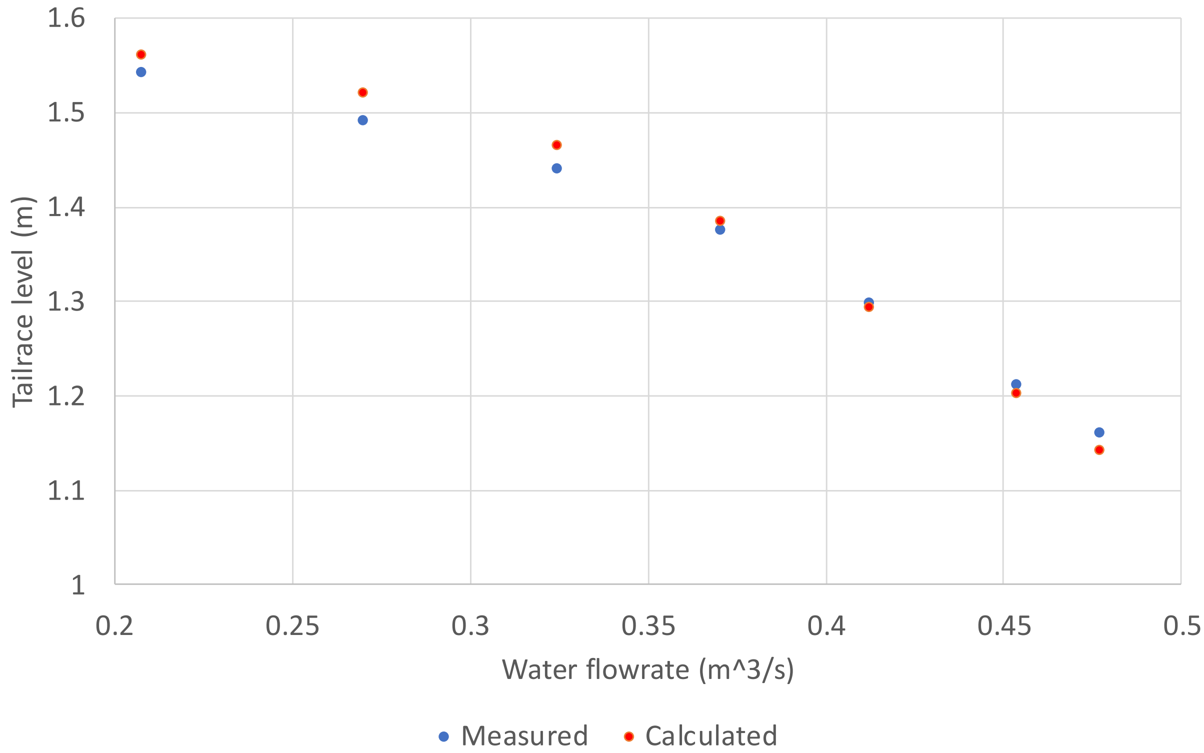

Figure 38: Level sensor reading (red) and pressure sensor level reading (blue) with calibration shock loss factor.

6. Operating procedures and quality control

This section identifies measures taken to reduce or prevent the occurrences of small or major problems with the HAC Demonstrator facility. Standard operating procedures to effectively and automatically track events at the HAC Demonstrator are also discussed.

6.1 Physical on site preventive measures

Before, during, and after the commissioning process for the HAC Demonstrator multiple preventative measures were put in place to prevent accidents or mitigate damages if an incident did occur.

6.1.1 Cloning the Server PC

In the event of an incident resulting in the loss of the current Server PC a clone has been prepared and is available if needed. The clone has all the necessary software installed on it and has access to backups that are regularly updated from the current Server PC onto an external hard drive. The only action required to replace the Server PC if it was put out of commission would be to transfer the software licences such as TOPServer and Datalogger to the clone and load any backup data required.

6.1.2 Spare sump pump and check valves

At the bottom of the HAC installation there is a sump pump that is responsible for draining the water that pools under the separator tank from condensed air humidity and rain and natural ground water inflows into the shaft. The sump pump is crucial to prevent flooding of the subsurface which is connected to Dynamic Earth. Sump pump inspection forms part of daily start up procedures to ensure it is always functioning as intended.

After system operations had commenced, it was determined that the check valves installed in the hose between the sump pump and the system drain line were not operating as intended when the HAC system was being drained (valve on the separator drain line in Figure 39 was opened). The back pressure faced by the check valves from the HAC (up to the forebay level) was high enough that water being drained from the HAC flowed to the sump pump, and water pooled in the sump. Figure 39 shows the piping arrangement of the drain line for the separator and the sump pump.

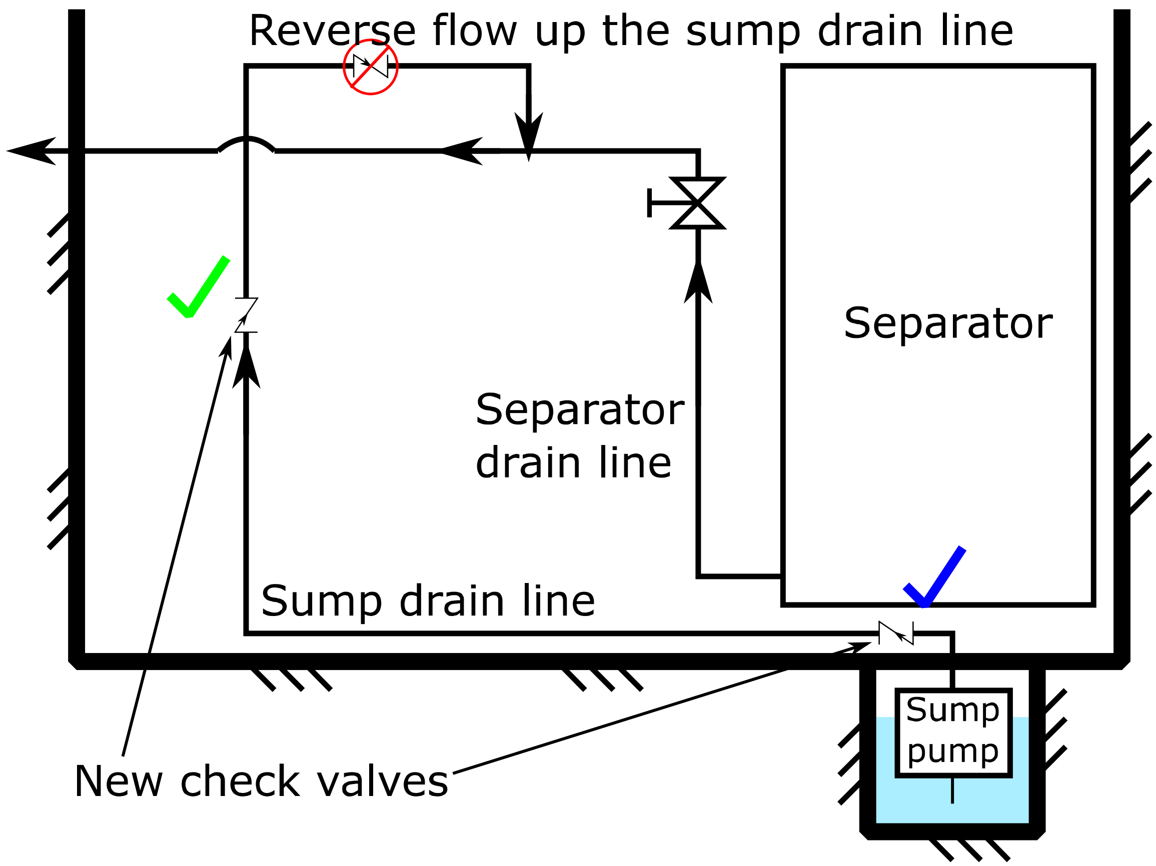

Figure 39: Water draining pipe arrangement connected to the separator tank showing the newly installed check valves (blue and green), and the malfunctioning check valve (red).

The sump pump operated as expected when valve on the separator drain line was closed. New check valves, seen in Figure 40, were installed which prevented the reverse flow in the hose. A backup sump pump was also purchased in the event of a malfunction or break in the current sump pump.

Figure 40: Check valve installed on the sump pumps drain line, also indicated on Figure 39 with a green checkmark.

6.1.3 Pump maintenance

Although the pumps are going to be operating at a reduced load and non-continuously there are still regular maintenance inspections that need to be followed. The pumps require routine, three-month and annual inspections. The pumps routine inspections consist of checking for i) leaks, ii) unusual noise, iii) oil levels and iv) for temperature and pressure levels at the discharge. Three-month inspection requires i) an oil change after 2000 operating hours minimum, ii) checking for the alignment of the shaft and iii) checking the foundation of the pump for loose bolts. The annual inspection of the pumps includes i) checking their power supply, ii) checking their capacity and pressure.

To complement routine inspections the pumps are also equipped with iALERT2 sensors. These sensors continuously monitor vibration experienced by the pumps and relay the data directly to the operator through a smart phone application. Any unexpected vibrations experienced by the pumps due to potential loosening of the bolts or a mechanical problem can be detected quickly before further problems occur. The pumps also operate while connected to the FREEFLOW (Riventa, 2018) thermodynamic pump monitoring system. This software effectively does the annual inspection of pumps listed above in real time. By measuring and monitoring the pumps hydraulic performance and efficiency data can be generated in real time to make optimisations.

6.1.4 Daily facility log

To keep track of the on goings at the HAC Demonstrator facility a daily facility log was created to track and monitor all changes, visits, experiments, and incidents that occur on site. The logbook provides the HAC operator with information about the current state of the system to avoid miscommunication between operators. If there is ever an incident at the HAC facility the daily facility log can help quickly identify the current state of the system, configuration of the valves, or indicate the last person to make a change to the system.

6.2 Benchmark test log

The automatic benchmark test function mentioned in section 4.2 also automatically populates metadata information from every test conducted in a benchmark test log constituting an Excel workbook. The benchmark test log contains the parameters of the HAC system during each set point of every benchmark test. Specific changes made to the HAC system from test to test are also noted and recorded in the log, after the operator notes them in the pop-up text box that prompts at the start of any benchmark test. This log is regularly accessed when searching for a specific set of data for post processing. Figure 41 shows an example of the benchmark test log. Starting from left to right, the entries in each record are i) the state of the lid of the forebay tank (0 = closed, 1 = open), ii) the volume of water in the system in m^3, iii) the set point level of water in the separator, iv) the speed of the VFD's, v) the circulating water temperature, vi) the atmospheric pressure, vii) the timestamp, viii) the benchmark test number, and ix) any additional notes.

	A	B	C	D	E	F	G–L	M	N–U
534	0	35.5622	1.7	700	0.521808267	981.2	2017_10_26_10_14_04	80	LT1 = ~0.165m, LT3 = ~1.7m, DPT2 = ~213.3kPa, Thirteenth test.
535	0	35.5622	1.7	750	0.521083713	981	2017_10_26_10_22_05		
536	0	35.5622	1.7	800	0.519984245	980.9	2017_10_26_10_30_06		
537	0	35.5622	1.7	850	0.518621147	980.9	2017_10_26_10_38_06		
538	0	0	1.7	880	0.516924739	980.9	2017_10_26_10_46_10		
539	0	0	0	0	0	0	2017_10_26_10_54_11		
540	0	35.1955	1.7	600	0.51831162	981.1	2017_10_26_12_39_35	81	LT1 = ~0.165m, LT3 = ~1.7m, DPT2 = ~213.3kPa. Single pump, first test.
541	0	35.1955	1.7	650	0.517655134	980.9	2017_10_26_12_47_36		
542	0	35.1955	1.7	700	0.517472744	980.9	2017_10_26_12_55_37		
543	0	35.1955	1.7	750	0.517130494	980.7	2017_10_26_13_03_38		
544	0	35.1955	1.7	800	0.516642451	980.7	2017_10_26_13_11_39		
545	0	35.1955	1.7	850	0.516030729	980.5	2017_10_26_13_19_40		
546	0	35.1955	1.7	880	0.515296996	980.4	2017_10_26_13_27_41		
547	0	0	0	0	0	0	2017_10_26_13_35_41		
548	0	35.6178	1.7	600	0.514825046	980.4	2017_10_26_13_56_12	82	LT1 = ~0.165m, LT3 = ~1.7m, DPT2 = ~216kPa. Single pump, second test.
549	0	35.6178	1.7	650	0.51473999	980.4	2017_10_26_14_04_13		
550	0	35.6178	1.7	700	0.514490664	980.4	2017_10_26_14_12_14		
551	0	35.6178	1.7	750	0.514096856	980.4	2017_10_26_14_20_15		
552	0	35.6178	1.7	800	0.513591468	980.4	2017_10_26_14_28_16		
553	0	35.6178	1.7	850	0.512953401	980.4	2017_10_26_14_36_16		
554	0	35.6178	1.7	880	0.512204587	980.4	2017_10_26_14_44_17		

Figure 41: Extract of the benchmark test log in Excel.

6.3 Start and stop log

To track total operating hours of the system the HMI has been equipped to directly log the start and stop times whenever the corresponding buttons on the HMI are pressed. Within Excel the total run time is calculated and provided to the HMI for display to the operator as seen in Figure 42. The total operating hours of the HAC for each month can be used to calculate the power consumption of the system and keep track of how many hours the pumps and motors have been operating since installation, for maintenance scheduling.

Start	2017_08_15_13_03_03	0
Stop	2017_08_15_13_03_20	0
Stop	2017_08_16_15_00_46	0
Start	2017_08_16_15_00_55	0
Stop	2017_08_16_15_20_37	0
Start	2017_08_16_15_21_00	0
Stop	2017_08_16_15_21_12	0
Stop	2017_08_16_15_21_55	0
Start	2017_08_16_15_22_34	0
Stop	2017_08_16_16_05_36	0
Stop	2017_08_17_14_50_36	0

Figure 42: HAC start and stop log snippet.

6.4 Instrumentation constants log

Each instrument installed on the HAC Demonstrator requires its own constants and conversion factors to permit conversion of raw data to engineering values with defined units of measurement. An excel file was created to keep the updated constants in one place. The HMI and other automated functions read data directly from this file to ensure all calculations are made using the same constants throughout for any post processing analysis. Figure 43 shows a screenshot image of all the constants used to convert the raw values into measurements.

A	B	C	D	E	F	G	H	I	J
Tags:	Raw Scale	Scale/Constants						CONSTANTS	
LT1	65536	0	2	m				DPT1	6000
LT2	65536	0	2	m				DPT2	300
LT3	65536	0	2.83464	m				DPT3	300
SpeedACT1	20000	0	880	RPM				FT1	0.35
SpeedACT2	20000	0	880	RPM				FT2	0.35
DPT1	65536	-3000	3000	Pa				FT4	0.35
DPT2	65536	0	300	kPa				FT5	25
DPT3	65536	0	300	kPa				LT1	2
FT1	65536	0	0.35	m^3/s				LT2	2
FT2	65536	0	0.35	m^3/s				LT3	2.83464
FT4	65536	0	0.35	kg/s				PT17	300
FT5	65536	0	25	m/s				FCV2	100
PT17	65536	800	1100	mbar				SpeedACT1	880
FCV2	65536	0	100	%				SpeedACT2	880
Power1	-	-	-	kW				FCV1	100
Power2	-	-	-	kW					
FCV1	4095	0	100	%					
P1P1	0.00003460	-0.994991592	bar	-1.038	0.04323	-0.99499159		Pump1 Suction	
P2P1	0.00003350	-0.96812261	bar	-1.011	0.04331	-0.96812261		Pump1 Discharge	
P1P2	0.00003220	-0.998605673	bar	-1.043	0.04429	-0.99860567		Pump2 Suction	
P2P2	0.00003160	-0.963234476	bar	-1.006	0.04261	-0.96323448		Pump2 Discharge	
T1P1	-264.5692733	1312.786196	-2802	3369	-2514.79	1218.993433	-407.564	86.86978845	C
T2P1	-261.9085075	1302.283354	-2784.8	3354	-2506.66	1216.276491	-406.83	86.74063142	C
dTP1			1000	mK					
T1P2	-263.4837718	1309.127235	-2797.5	3367	-2514.98	1219.522536	-407.729	86.91047617	C
T2P2	-268.8746857	1332.261666	-2837.6	3403	-2531.88	1223.321979	-407.835	86.88814214	C
dTP2			1000	mK					
T1D1	-276.5376214	1364.627299	-2896.1	3462	-2567.67	1236.547857	-410.674	87.0060449	C
T2D1	-271.9680403	1346.106589	-2865	3434	-2553.32	1232.314327	-409.827	86.87994828	C
dTD1			1000	mK					

Figure 43: File containing the constants used to convert the raw data into measurements.

7. Experimental program for basic commercial readiness

This section aims to identify all the experiments performed at the HAC Demonstrator facility up to this point in time. Future experiments that have yet to be performed can also be discussed.

7.1 Benchmark tests 1 to 68

Benchmark tests 1 through 68 did not follow a specific experimental program and were completed to commission and test the HAC facility. Benchmark tests 1 to 12 were performed to test the HACs automation and ensure the instruments were functioning properly. Benchmark tests 13 to 39 investigated potential air leaks in the system with some preliminary HAC performance mapping. This set of performance tests had a few deficiencies due to the air leaking into the system leading to inaccurate efficiency calculations, but they did help track down the source of the leaks and allowed the operators to learn a great deal about how the HAC Demonstrator operates. Benchmark tests 40 to 67 included experiments to calculate the absolute roughness of the rubber lined pipes and investigated the pressure profile of the air water mixture falling in the downcomer pipe underneath the forebay tank.

7.2 Environmental effects on the HAC

Sub 0°C temperfatures could lead to water freezing inside of the HAC when the lid to the forebay tank is open and atmospheric air cools the water inside the tank. Freezing of the water inside the HAC could lead to blocking of one or both pump discharge pipes preventing water from entering the forebay tank when the pumps are active. Freezing of the pipes on the mixing head within the forebay could also lead to disruption of HAC performance by altering the rate at which air can be inducted into the downcomer pipe. This potential hazard is only an issue when the lid of the forebay tank is open and allows heat transfer between the water in the system and the cold atmospheric air, when the lid is closed no stratification or drastic reduction in temperature could be observed as seen in Figure 44.

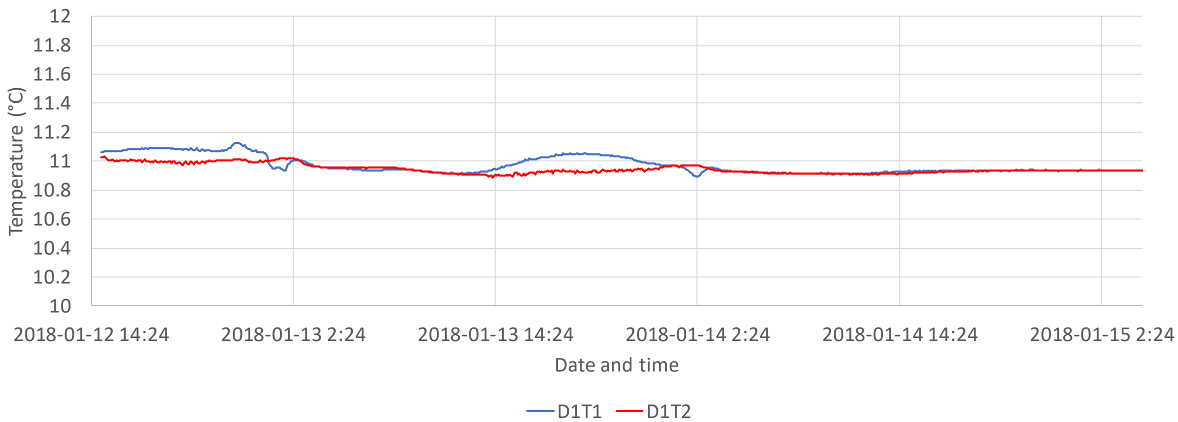

Figure 44: Temperature of the water inside the HAC with the forebay tank sealed in a 63-hour period.

The full scale of the system can be seen on Figure 45 showing the elevations of the ceilings of each tank, the locations of the differential temperature sensors used to collect this data, and other key elevations on the HAC Demonstrator.

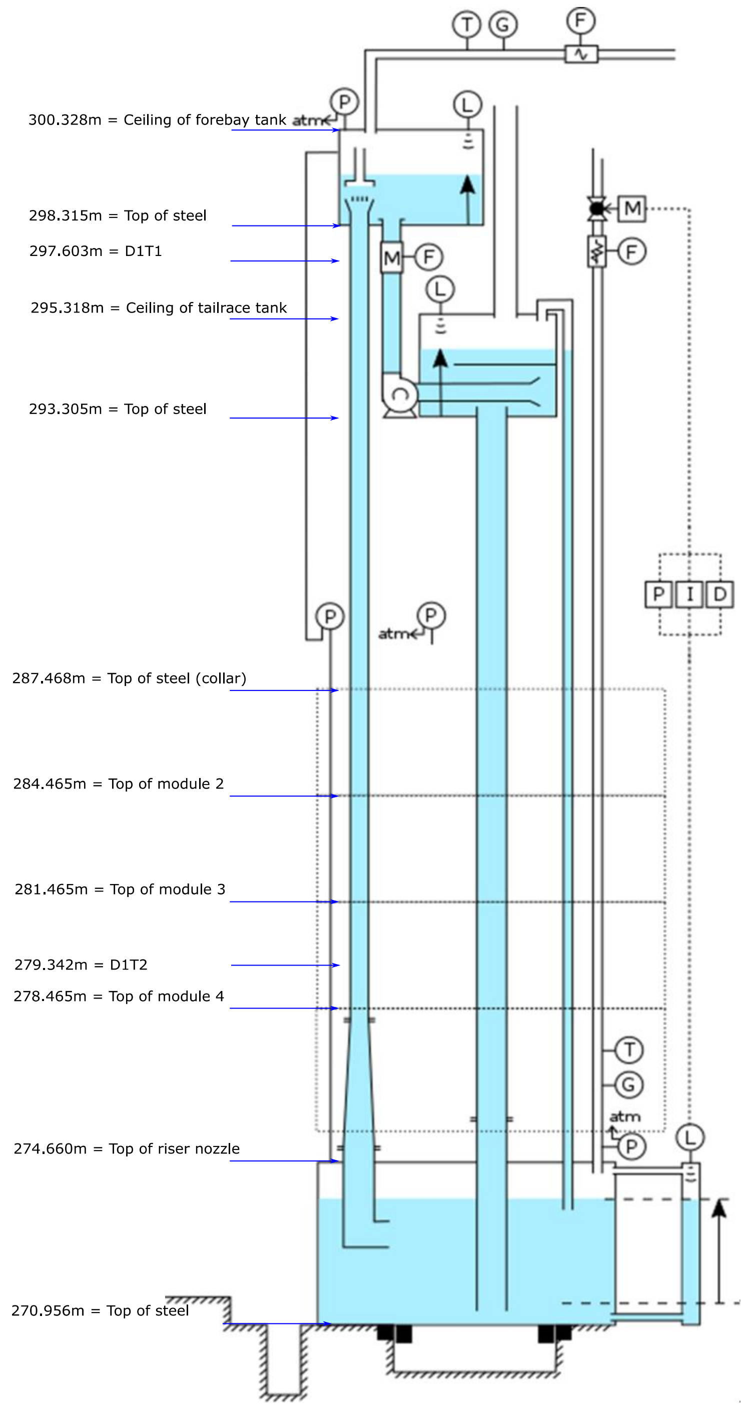

Figure 45: Schematic of the elevations of the HAC Demonstrator, indicating the locations of the temperature sensors on the downcomer pipe.

To prevent any freezing problems if the lid of the forebay tank was left open and to maintain the temperature inside the HAC Demonstrator facility two heaters have been installed. The heater inside of the control room is set to 20°C while the process side is set to 13°C. The extremely cold winter temperatures experienced by the HAC Demonstrator during December 2017, down to minus 30°C, has warranted investigation into the effects of environmental temperatures on the HAC water temperature. Figure 46 shows the outside temperature for the city of Sudbury, Ontario over a 96-hour period.

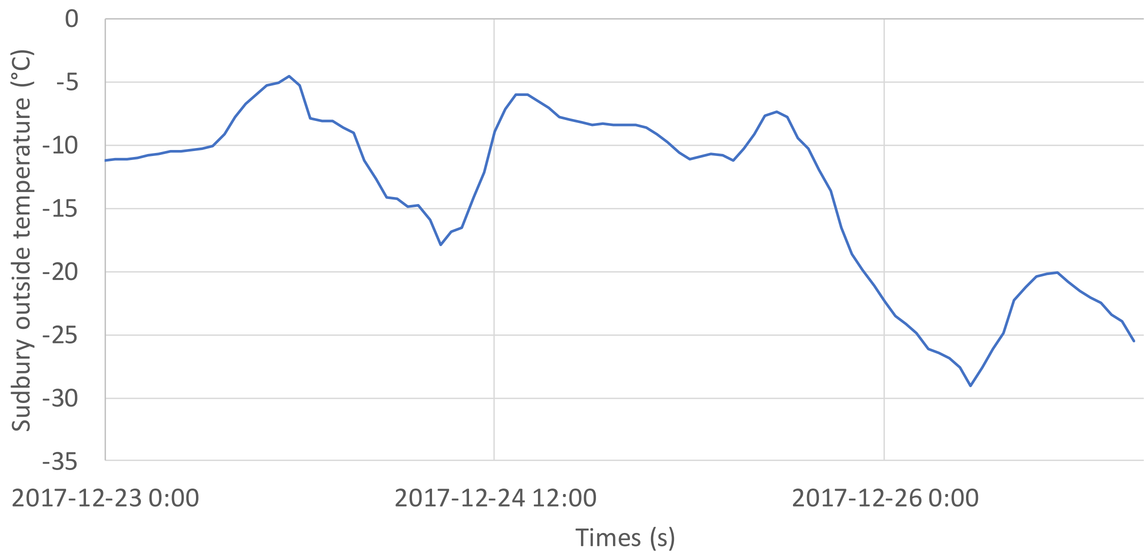

Figure 46: Temperature of Sudbury, Ontario over 96 hours.

The differential temperature sensors are separated by 18.261m and measure the water temperature at the upper level of the facility (D1T1, below the base of the forebay tank) and at the bottom of the shaft (D1T2, above the separator tank). The differential temperature sensors installed on the downcomer are calibrated together and record accurate temperature readings at both sensor locations. The difference between both readings can then be computed to obtain a very accurate differential temperature, but it is important to note that the differential temperature sensors both record individual readings, as opposed to a single differential temperature between the two sensor locations. The D1T1 and D1T2 sensors were monitored over the same 96-hour period with the lid of the forebay tank open to atmosphere and a louvre on the forebay level open to allow warm humid air to exit the facility. Figure 47 shows the temperature readings measured at the top of the downcomer pipe, D1T1, and the bottom of the downcomer, D1T2.

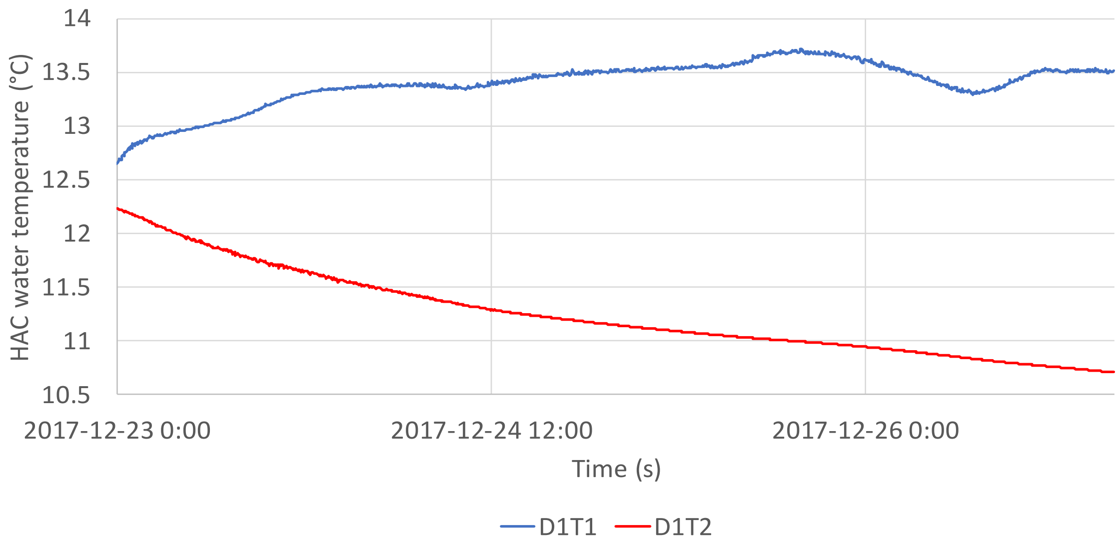

Figure 47: Temperature of D1T1 and D1T2 in the HAC over 96 hours.

It can be appreciated that D1T1 seems to be slightly influenced by environmental effects with slight fluctuations in temperature. D1T2 does not seem to be influenced by the temperature of the environment but does seem to decrease over time which indicates a lower temperature at the bottom of the facility than at the top of the facility. During the 96-hour monitoring period there was a 20°C temperature drop in environmental temperature which can be seen to correlate with an evident 0.5°C temperature drop for D1T1. Although temperatures dropped as low as -30°C the temperature of the water inside the HAC does stray far from the set point of the heater warming up the process side of the facility.

The heater on the process side of the HAC Demonstrator is not rated high enough to maintain a set temperature across the entire height of the facility due to air being forced up the shaft from Dynamic Earth and warm humid air exiting the facility. If temperature does become a problem in future the limiting factor of the HAC Demonstrator would be the temperature at the bottom of the facility instead of the temperature at the top near the forebay due to stratification.

7.3 Checking of magnetic water flow meter calibration

The magnetic water flow meters installed in the pump delivery pipes were supplied with factory calibration certificates, and there is no reason to think that these are in error. Nevertheless, from time to time it is necessary to confirm confidence in the measurement of the volume flow rate for the HAC demonstrator from these instruments. For these purposes, a special procedure was designed to permit verification of sensed values of these instruments, labelled FT1 and FT2. The accuracy and precision of this procedure is insufficient to be deemed calibration, but simply a check on calibrated values. The procedure involves an estimate of the volumetric flow rate of water derived from the change in water volume of the forebay tank while it is being filled during the initial start up of a benchmark test.

During the start of a benchmark test when the water level in the forebay is below the flanges (<0.16m) there is a brief period where water is added to the forebay by the pumps until it begins to spill into the mixing head. Level sensor LT1 is used to track the water level within the forebay tank during this period; A change in volume can be recorded and converted into a volume fill rate knowing the times of water level acquisition. Comparing the volume fill rate calculated using the LT1 measurements to the volume flow rates measured by FT1 and FT2 reveals, approximately, if the instruments are behaving within specifications together. To assess the flow meters individually, each pump must be operated individually and the pump discharge at the flanges of the line not containing the flow meter under test, must be blanked off.

The data for comparison is recorded when the pumps are operating at 600rpm, and the fill rate is low, providing more data for the estimate, given that the logging period is 1 Hz and to maximise the time when the water level is still increasing in the forebay without spilling into the mixing head. With two pumps running there is only a six second window where these conditions are met which leads to a very small-time window for comparison as seen in Figure 48.

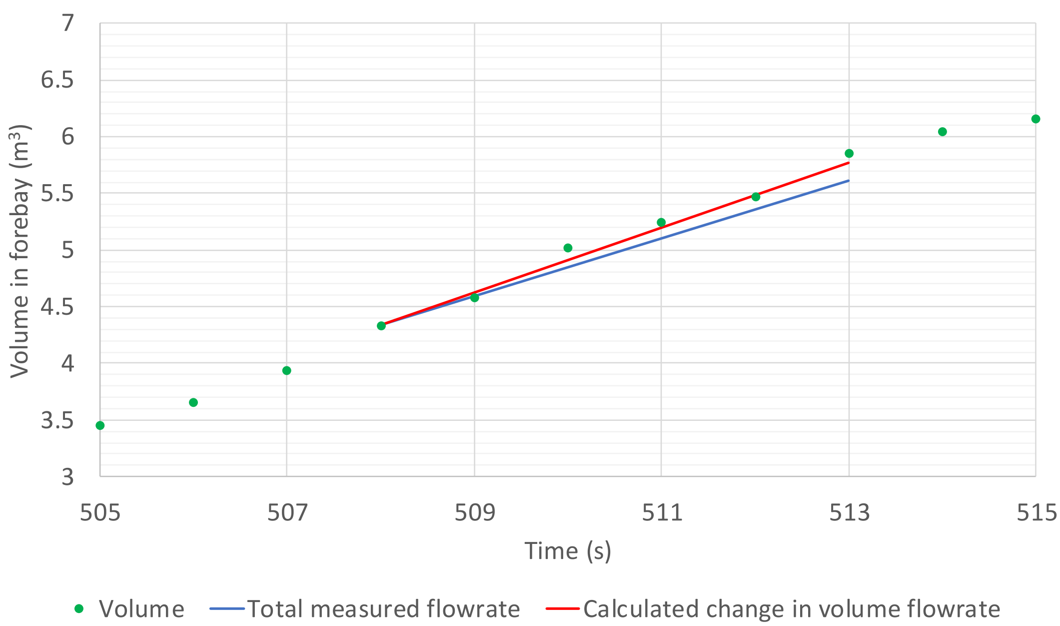

Figure 48: Volume of water in the forebay tank during initial startup of the HAC at 600rpm with the average water volume flowrate measured and calculated with 2 pumps.

A plot of the volume flowrate measured by FT1 and FT2 can also be compared to the volume fill rate calculated using LT1 measurements and can be seen on Figure 49.

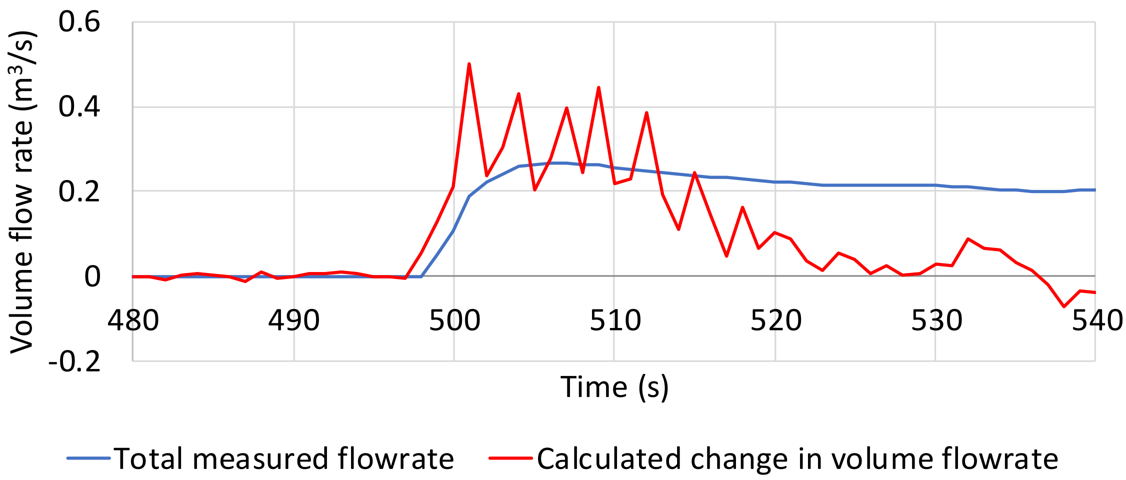

Figure 49: Water volume flowrate during steady operation at 600rpm with 2 pumps.

As expected the volume flowrates measured by FT1 and FT2 can be seen to increase when the pumps start up and eventually converge on a steady state value as the head established by the pumps stabilizes. The volume fill rate calculated using the LT1 measurements oscillate heavily during start-up before eventually dropping to zero once stability in the forebay tank occurs. That the volume flowrate determined from LT1 eventually oscillates around zero indicates that the water flowrate into the forebay from the pumps equals the water flow rate out of the forebay down the downcomer. The oscillation apparent in flow rates derived from the LT1 level sensors, is real; visual observations prove that the water surface is highly agitated as seen in Figure 7.

To increase confidence in the comparison the same test was performed but with a single pump set up. Reducing flowrate of water into the forebay tank should provide a longer period of comparison between the flowrate measured by FT2 and the fill rate calculated using LT1. Figure 50 shows a longer period of time where the single pump is running at 600rpm and water is still not spilling into the mixing head.

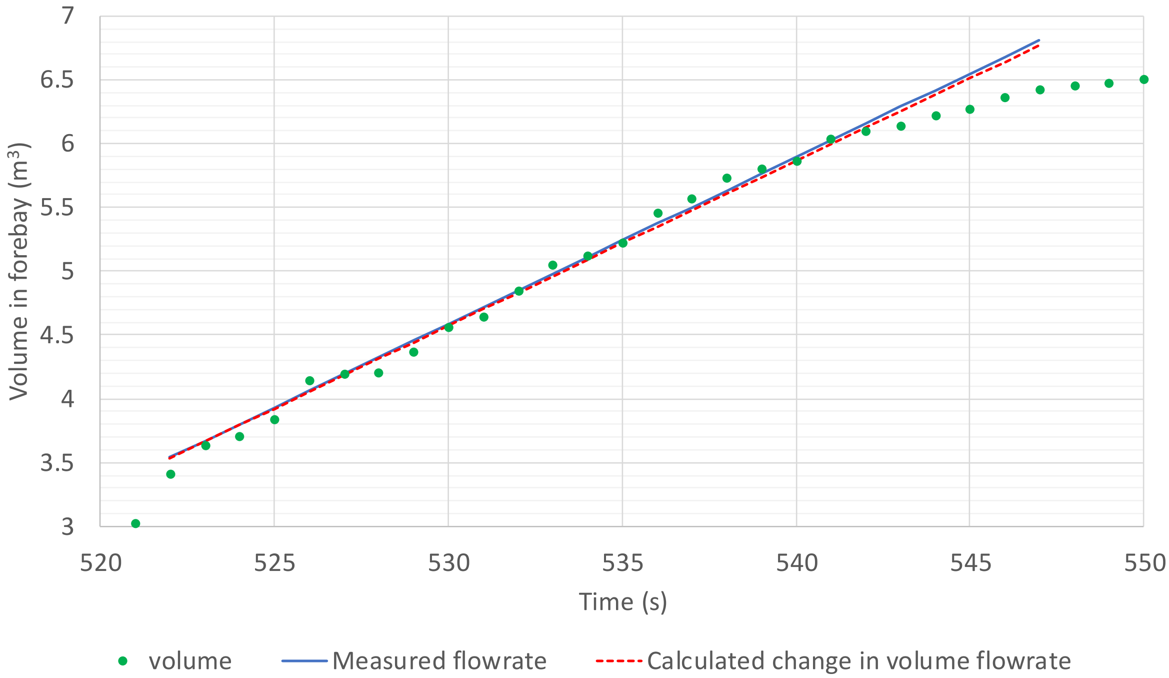

Figure 50: Volume of water in the forebay tank during initial startup of the HAC at 600rpm with the average water volume flowrate plotted in red with 1 pump.

This comparison using data from a single pump benchmark test makes the results much clearer. It can be seen that when the flow rate measured by FT2 and the fill rate measured by LT1 are applied to the increasing volume in the forebay the trends are nearly identical. Similarly, Figure 51 shows the single pump setup exhibiting the same behavior as the double pump setup but over a longer period before the volume of water in the forebay tank begins to spill into the mixing head.

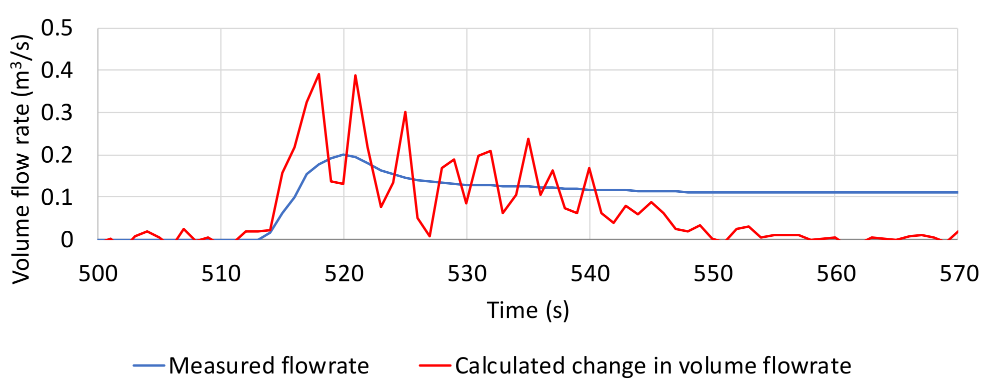

Figure 51: Water volume flowrate during steady operation at 600rpm with 1 pump.

By increasing the acquisition frequency from LT1 during this period, a greater degree of agreement may be able to be established between volume flow rate derived from LT1 observations and the flow rates obtained from the magnetic water flow meters. According to the calibration certificate and specifications for the latter instruments, they are accurate to 0.3% of full scale range – which is excellent.

7.4 Measurement of zero drift

The duration of a benchmark test is approximately 56 minutes. This long mensuration period can be subject to zero drift in the instruments. In order to account for drifting sensors, measurements are taken from the relevant instruments before the start of every benchmark test. The data recorded before the start of the test defines ‘zero’ for all set points for that specific benchmark test.

Due to its short span of measured values expected, DPT1 was the instrument investigated to assess the severity of zero drift for differential pressure sensors installed in the HAC Demonstrator facility. Over the same 96-hour period used in section 7.2 the data recorded on DPT1 was also tracked and is presented in Figure 52.

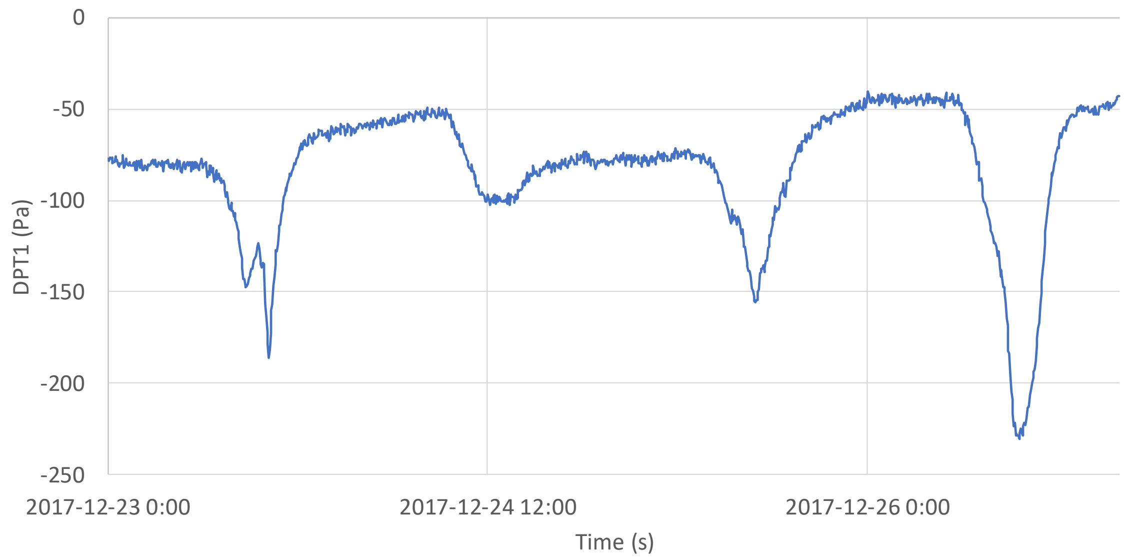

Figure 52: Differential pressure reading on DPT1 over 96 hours.

It should be noted that the low range of DPT1 cannot extend past -2000Pa in the forebay tank due to the setting of the PVRV. DPT1 measures the atmospheric pressure inside of the HAC facility to the pressure inside of the open forebay tank. This should provide a 0Pa differential pressure. DPT1 does not read 0Pa over the entire 96-hour period. There also seems to be a diurnal behavior over the 96-hour period where the magnitude of the drift seems to grow around 12:00. Also, these differential pressure observations do seem to be correlated with the temperature observations.

This magnitude of the zero drift can also be compared to the specifications of the instrument. According to the instrument specifications DPT1's accuracy can be calculated using its calibrated set span relative to its design span, also known as the turn down ratio. The turn down ratio is simply the quotient of the design span (300kPa to -300kPa) divided by the calibrated span of the instrument (3000Pa to -3000Pa). DPT1 has a turn down ratio of 100, is then multiplied by 0.005 and added to 0.015% for the accuracy of the instrument. DPT1 at its current calibrated span has an accuracy of + or – 0.515% of the set span, or + or – 30.9Pa. The calibrated accuracy of the instrument is within the same order of magnitude of the zero drift and so compensation clearly needs to be applied. This can be attributed to the high turn down rate of DPT1 which is set to a span of 6000Pa but is capable of measuring differential pressure across a 600kPa span. The DPT2 and DPT3 sensors do not have this problem as they are set to read in the full instrument specified span range of 600kPa giving them an accuracy of 0.02% of the design span.

7.5 Air flow calibration

7.5.1 Anemometer experiment

When investigating the possibility of air leaking into the system from the spill way pipe in section 5.3 an experiment was conducted to measure the speed of air flowing in or out of the surge pipe during operation. Duct tape was used to seal the surge pipe leaving only a small hole for the air to pass through. This reduction in area increases the velocity of any air passing in or out of the surge pipe to a suitable value to measure with a calibrated hotwire, hand held anemometer. The VelociCalc model 9535 has an operating range of 0 to 30m/s, an accuracy of plus or minus 3% of reading or plus or minus 0.015m/s, whichever is greater, and a resolution of 0.01m/s. The instrument is calibrated annually using a known air velocity in the range of 0.25m/s to 2.54m/s. The anemometer set up and mounted is diagrammatically depicted in Figure 53. During each test, velocity was logged by this device at regular intervals.

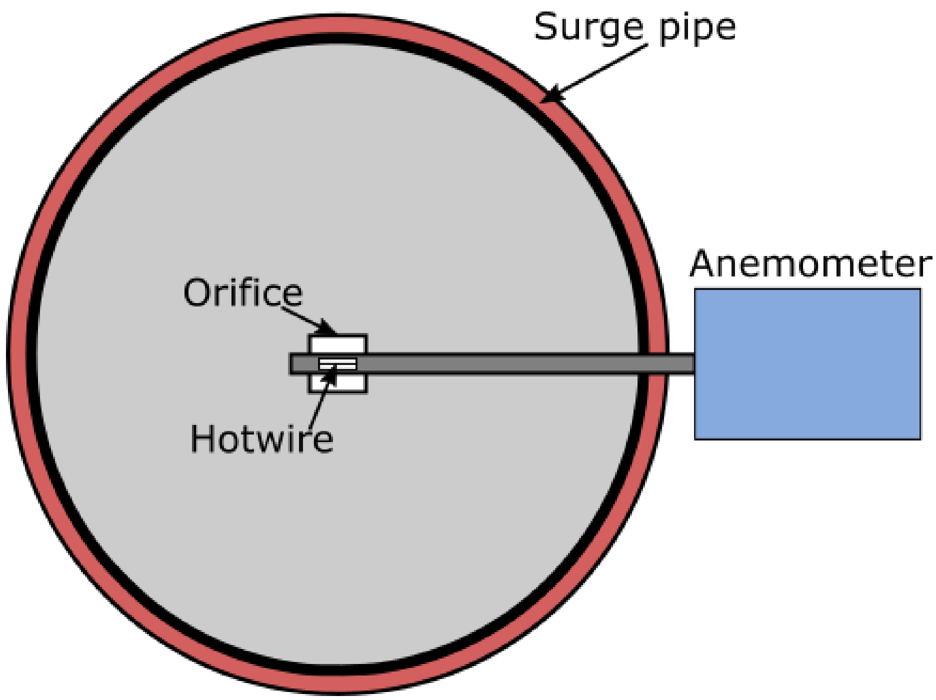

Figure 53: Experimental setup for air flow measurement on the surge pipe.

The data shown in Table 1 confirms that for this particular benchmark test, air was flowing into the HAC through the surge pipe. As the speed of the VFD's increased during the benchmark test the average airflow rate through the surge pipe also increased.

Table 1: Anemometer air speed data.

Speed	Average (m/s)	Min (m/s)	Max (m/s)	Area (cm^2)	V (m^3/s)	m (kg/s)
600	3.337	2.37	5.07	8.58	0.0029	0.0034
650	3.81	3.24	4.34	8.58	0.0033	0.0039
700	4.83	4.23	6.12	8.58	0.0041	0.0050
750	5.97	4.52	7.64	8.58	0.0051	0.0061
800	6.41	5.21	7.46	8.58	0.0055	0.0066
850	7.58	6.93	8.54	8.58	0.0065	0.0078
880	8.2	5.01	10.3	8.58	0.0070	0.0084

7.5.2 Calibration loop

As outlined in section 5.3, one of the most important experiments the HAC Demonstrator has been designed to undertake is one that assesses the yield of compressed air from the system. The modelling undertaken as part of the wider project predicts that there will be a reduction of air mass flow in the compressed air delivery line, in comparison to the air inducted at inlet. These differences are predicted to arise due to dissolution of compressed gas in the circulating process water. They may also arise as a consequence of air underflow in the HAC separator. As either of these factors are expected to introduce differences of measured mass flow that are of the order 1 to 2% of mass flow at inlet, in advance of tests aimed at detecting these differences in air flow, the so-called ‘calibration loop’ of the HAC permits the output mass flow of air to pass through Coriolis meter FT5 and sonic anemometer FT4 in series *after* the HAC process, rather than being in series *across* the HAC process. Through the manipulation of 2 three-way valves, the ‘calibration loop’ permits the meters to be connected in series after the process so that their observations can be directly compared, and the meters balanced without having to physically relocate either sensor as seen in Figure 54.

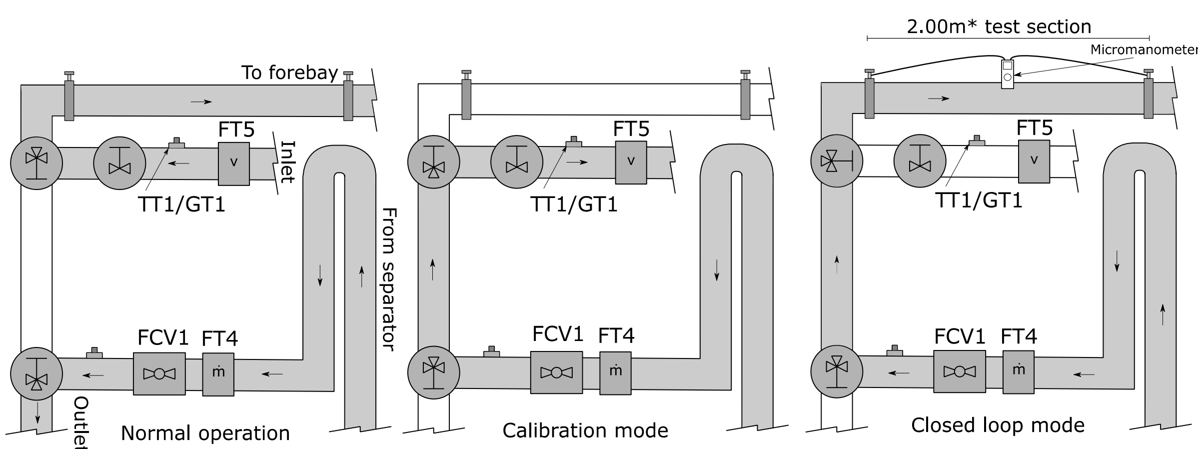

Figure 54: Schematic of the three configurations for the air inlet and outlet pipes. Normal operation (A), calibration mode (B), and closed loop mode (C).

When the system is running in calibration mode the air mass flow measurements on both instruments should in theory be identical. Any difference between the observations from each source may be attributed to instrumentation factors. It is assumed that due to its superior and more direct mensuration principle, that any disparities between observations are due to 'instrumentation factors' and corrections are applied to the sonic anemometer. In practice, both instruments have excellent repeatability/stability, sensitivity, and response time. Data from the instruments from a 500 second period of operation with 'calibration mode' applied, Figure 55, shows a small difference in the measured mass flow rate. A calibration factor of 1.0225 applied to the diameter of the Optisonic flow meter, produced the minimum difference between the observed values.

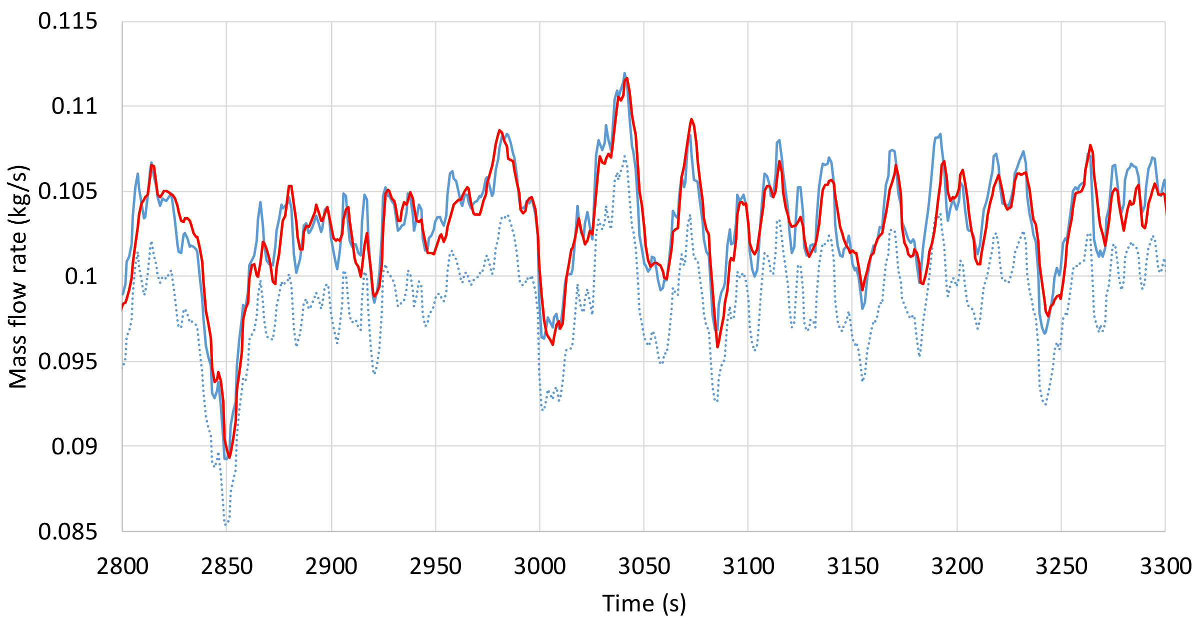

Figure 55: Comparison between inlet (blue) and outlet (red) flow rates on the Coriolis and the Optisonic sensors. Dotted line indicates the inlet flowrate before calibration (D x 1.0225).

Using the KS-test mentioned in discussed in section 4.4 the KS statistic before calibration and after calibration can be computed between the cumulative probability distributions of the data sets. Before calibration a KS statistic of 0.59082 is calculated, as seen in Figure 56, which rejects the null hypothesis at a significance of 95% that the two sets of data come from the same distribution. Once the diameter of the of the optisonic flowmeter is calibrated with a coefficient of 1.0225 the

KS statistic falls to 0.06986 which does not reject the null hypothesis at a significance of 95% and provides a probability of 83.3% that the data KS statistic would be as large or larger than the reported value. The probability of a maximum difference in cumulative distributions from both sensors being equal or larger than 0.06986kg/s is 83.3%.

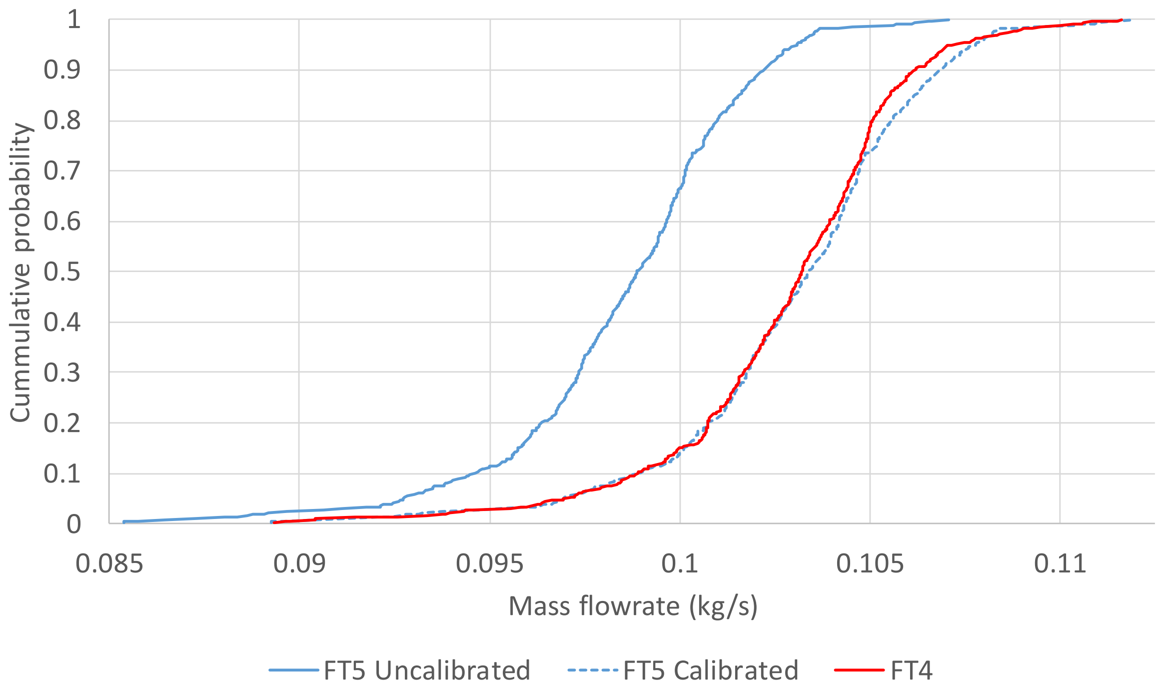

Figure 56: Cumulative probability distributions of the air mass flowrates at inlet (FT5) and outlet (FT4) before and after calibration.

After a full benchmark test with the HAC in calibration mode the sensors were confirmed to be working as intended since both instruments would read the same flowrates once the calibration factor was applied.

Lastly, as in calibration mode the sense of the air flow through the sonic anemometer is reversed in comparison to the sense during normal operations, as part of acceptance testing, the sonic anemometer installation was physically reversed in the air intake line to ensure that the balancing calibration held bi-directionally. The results of this special ‘one-off’ test confirmed prior reassurances from the flow meter manufacturer that the sonic anemometer operated equally effectively bi-directionally.

7.6 Estimation of absolute roughness for rubber lined pipes

The fundamental purpose of the HAC Demonstrator as a whole is to verify predictions made by two models of HAC processes, one developed by Millar (2014) that encapsulates the hydrodynamics only, and a more sophisticated model described in Young (2017) that also incorporates gas mass transfer from/to any system of aqueous solution and psychrometric aspects. If both or either of these models can be verified, then they may applied in design tasks for larger HACs with good confidence.

During the construction process, one compromise decision that was made on a cost basis was to utilize a ¼ inch thick butyl rubber lining for pipe work, rather than to use a 350µm polymer-ceramic coating. This decision meant that performance predictions of the HAC Demonstrator had to be recomputed with 'as-built' specifications for the rubber lined pipework, rather than values reflecting the friction performance of the ceramic polymer. As the rubber lining material was ~73 times thicker than the ceramic polymer coating, adoption of the former also constituted a significant loss of section available for flow that would also alter predicted performance.

One of the physical properties input into the model of the HAC performance is the absolute roughness of the pipe material used in the installation which is part of the friction factor calculation, required for every pipe installed in the system. A literature review undertaken to establish the absolute roughness of the rubber lining material identified a single accepted value for absolute roughness of rubber lined pipe of 0.15mm (Abulnaga, 2002), but this did not specify what type of rubber. As quantification of frictional, drag and other losses in the HAC system were of paramount importance in providing performance predictions to compare with observations, this prompted a need for determination of the absolute roughness of the rubber lined pipe from direct observations.

Figure 54 shows a schematic of the test length of butyl rubber lined pipe used in the absolute roughness determinations. It is a pipe section which is exactly 2m long and has an inner diameter of exactly 0.0893m to the rubber surface. The differential pressure loss was measured using a digital manometer with a sensitivity of 1 Pa over a range of +/- 3735 Pa.

The HAC was operated in closed loop configuration, by manipulation of 3-way valves so that the air delivered from the separator is fed back into the forebay (Configuration C in Figure 54). An additional thermistor was installed in this loop to monitor air temperature. The absolute pressure of the air at the outlet side of the test section was established from barometer and DPT1 observations, so that, with the thermistor observations, the air density could be established. Mass flow rate across the test section is thus very accurately measured using the Coriolis meter.

The density of the air entering the pipe can be calculated using the temperature, T, and pressure, P_{air}, measured at the inlet. The barometric pressure is measured at a different elevation from which the experiment was being performed and so an atmospheric correction is applied to the atmospheric pressure observation to allow for the elevation of the absolute roughness tests.

$$P_{\mathrm{air}} = P_{\mathrm{atm}} - \rho g H \tag{33}$$

The calculated air pressure is used with the measured air temperature at the inlet of the pipe to calculate the density of the air, ρ,

$$\rho = \frac{P_{air}}{n\mathcal{R}T} \tag{34}$$

The measured mass flow rate of air, $\dot{m}$, at the inlet is then used with air density to calculate the velocity of air, u, flowing through the pipe,

$$u = \frac{\dot{m}}{\rho A} \tag{35}$$

With the diameter of the pipe, the density of the air, and the velocity of the flow, the viscosity, μ, of the air can be calculated using REFPROP (Lemmon, Huber and McLinden, 2013) which is then used to calculate the Reynolds number, Re, of the air flow,

$$\mathrm{Re} = \frac{\rho u D}{\mu} \tag{36}$$

The friction factor, f, of the rubber lined pipe can be calculated using the Reynolds number, the inner diameter of the pipe, D, and an assumed absolute roughness, ϵ, using the Colebrook-White formula (IDELCHIK, 1994).

Then the predicted pressure drop, $\Delta P_{predicted}$, along the test section of the pipe under these conditions can be calculated,

$$\Delta P_{predicted} = f\rho\left(\frac{L}{D}\right)\frac{u^2}{2} \tag{37}$$

The sum of all the squared differences between the measured differential pressure readings and the predicted differential pressures can be estimated,

$$S = \sum_{set\ points} (\Delta P_{predicted} - \Delta P_{meaasured})^2 \tag{38}$$

An iterative procedure such as the Newton Raphson method can be used to refine the starting value of ϵ, so that S is minimized. By applying this method a single least squares estimate of ϵ applicable across all operating conditions can be obtained. Independence from the starting value for ϵ was also verified robustly via the Monte Carlo technique (Harr, 1987).

After multiple trials of passing air through the test section under similar conditions consistency is observed in the observed pressure drop compared to the predicted pressure drop. The experiment has concluded that the absolute roughness of the rubber lined pipe in the HAC Demonstrator has a significant difference from the accepted theoretical value of 0.15mm. A precise value for the absolute roughness of the rubber lined pipes of 0.058mm, plus or minus 0.002mm has been calculated using experimental data from Tables 2, 3 and 4.

Table 2: Absolute roughness experimental data for trial #1.

Set point (rpm)	Mass flow (kg/s)	Baro. P (Pa)	DP Avg (Pa)	T Probe (°K)	Density (kg/m^3)	Viscosity (Pa s)	Reynolds Number	Absolute Roughness (m)	Darcy f.f	Predicted DP (Pa)	Error^2	Sum(Error^2)
600	0.0538	98895	16.2	292.4	1.1786	1.82E-05	41958		0.0237	16.27	0.0051	
650	0.0674	98884	24.4	291.0	1.1842	1.81E-05	52745		0.0228	24.48	0.0056	
700	0.0787	98889	32.5	291.2	1.1832	1.82E-05	61555		0.0223	32.63	0.0182	
750	0.0875	98875	39.7	290.2	1.1872	1.81E-05	68660	5.8E-05	0.0219	39.62	0.0069	1.1001
800	0.0964	98850	46.6	290.1	1.1874	1.81E-05	75657		0.0217	47.43	0.6829	
850	0.1001	98848	50.9	289.2	1.1908	1.81E-05	78738		0.0215	50.72	0.0312	
880	0.1038	98836	54.7	288.3	1.1945	1.80E-05	81862		0.0214	54.11	0.3502	

Table 3: Absolute roughness experimental for data trial #2.

Set point (rpm)	Mass flow (kg/s)	Baro. P (Pa)	DP Avg (Pa)	T Probe (°K)	Density (kg/m³)	Viscosity (Pa s)	Reynolds Number	Absolute Roughness (m)	Darcy f.f	Predicted DP (Pa)	Error²	Sum(Error²)
600	0.0524	97542	16.4	292.0	1.1639	1.82E-05	40929		0.0237	15.66	0.5408	
650	0.0660	97534	24.3	292.0	1.164	1.82E-05	51491		0.0228	23.86	0.1945	
700	0.0775	97528	32.1	291.9	1.1641	1.82E-05	60503		0.0223	32.12	0.0004	
750	0.0864	97522	39.1	292.5	1.1616	1.82E-05	67361	5.6E-05	0.0219	39.4	0.0909	1.2611
800	0.0935	97519	45.3	293.0	1.1598	1.82E-05	72796		0.0217	45.7	0.1572	
850	0.0987	97511	50.2	292.6	1.1613	1.82E-05	76911		0.0215	50.45	0.0636	
880	0.1023	97509	54.2	291.3	1.1665	1.82E-05	80045		0.0214	53.74	0.2137	

Table 4: Absolute roughness experimental for data trial #3.

Set point (rpm)	Mass flow (kg/s)	Baro. P (Pa)	DP Avg (Pa)	T Probe (°K)	Density (kg/m³)	Viscosity (Pa s)	Reynolds Number	Absolute Roughness (m)	Darcy f.f	Predicted DP (Pa)	Error²	Sum(Error²)
600	0.0525	97856	16.5	291.0	1.1716	1.81E-05	41091		0.0238	15.69	0.6552	
650	0.0663	97857	24.4	291.1	1.1712	1.81E-05	51886		0.023	24.11	0.0821	
700	0.0774	97846	32	291.4	1.1701	1.82E-05	60547		0.0224	32.16	0.0253	
750	0.0868	97853	39.4	292.0	1.1676	1.82E-05	67759	0.00006	0.0221	39.86	0.2131	1.5817
800	0.0933	97849	45.8	291.4	1.1699	1.82E-05	72982		0.0219	45.54	0.0688	
850	0.0990	97852	50.3	291.7	1.1688	1.82E-05	77338		0.0217	50.88	0.3334	
880	0.1024	97859	54.5	291.1	1.1713	1.81E-05	80109		0.0216	54.05	0.2038	

The absolute roughness of the rubber lined pipes is significantly larger than that of smooth pipes which are in the range of 0.0015-0.01mm (IDELCHIK, 1994). Results from this experiment have been submitted to the Journal of Flow Measurement and Instrumentation (Sivret, 2018). The resulting absolute roughness of 0.058mm was then entered to the HAC process model to produce predictions of the HAC performance more closely representing as-built conditions.

7.7 HAC performance map

The test work described hitherto essentially was undertaken to improve the characterisation of the Dynamic Earth HAC Demonstrator, or to improve understanding of how the system operates when certain experimental realities arising from decisions taken during design and construction are accounted for, as well as determination of the behaviour of instruments. With such issues resolved, the purpose of the experimental program shifted towards trying to establish the optimum performance obtainable from the system. HAC efficiency and HAC free air delivery (FAD) can be varied, by adjusting the mass flow rate of water circulating through the system, or by adjusting the head available to the air compression side of the system. The former is manipulated by varying the number of pumps operating and their set points. The latter is manipulated by varying the amount of water that is used to charge the system.

An experimental procedure was designed to explore the limits of these two variables at the HAC Demonstrator to establish what has become known as the HAC Performance Map. The performance map data collection begins by charging the system with a high-water volume and operating both pumps. The benchmark test sequence is then executed to obtain head, efficiency and FAD over a range of pump speed set points. The benchmark test is then repeated with a different volume of water in the system. Between the benchmark tests, the water level in the system was reduced by 10cm intervals when the system was quiescent, until the water level was low enough such that when operating, there is very little compressed air production. Once air production stops, one of the pump discharge pipes to the forebay is blocked, and the corresponding pipe was electrically isolated before the benchmark tests were repeated in reverse order by increasing the water level by 10cm intervals until there is no more air production when the system is completely full of water.

According to this methodology, obtaining data to produce the complete performance map of the HAC Demonstrator requires conducting 23 individual benchmark tests, BM68 to BM90, each producing 7 set point states of operating performance. Data for these tests can be found in Appendix I: Benchmark test data and the fill volumes and available pressure heads for each benchmark can be seen in Table 5.

Table 5: HAC benchmark test fill volumes and available pressure heads for all setpoints.

		Available pressure head						
BM #	Fill Vol. (m^3)	600rpm	650rpm	700rpm	750rpm	800rpm	850rpm	880rpm
68	45.17	1.67	2.14	2.77	3.53	4.34	4.51	4.66
69	44.33	2.38	2.97	3.65	4.28	4.44	4.59	4.74
70	43.13	3.33	3.91	4.19	4.36	4.52	4.68	4.90
71	42.46	4.03	4.13	4.27	4.44	4.61	4.78	4.88
72	41.68	4.12	4.22	4.35	4.54	4.70	4.85	4.96
73	40.98	4.20	4.30	4.43	4.62	4.77	4.93	5.03
74	39.96	4.28	4.38	4.50	4.69	4.85	5.01	5.12
75	39.12	4.37	4.46	4.59	4.76	4.92	5.10	5.20
76	38.34	4.45	4.54	4.66	4.84	5.00	5.17	5.28
77	37.71	4.52	4.62	4.74	4.91	5.08	5.25	5.35
78	37.05	4.59	4.68	4.80	4.97	5.13	5.31	5.42
79	35.79	4.64	4.73	4.85	5.01	5.18	5.36	5.47
80	34.66	4.70	4.80	4.91	5.08	5.24	5.43	5.55
81	35.11	4.58	4.64	4.69	4.72	4.77	4.80	4.82
82	34.40	4.51	4.58	4.62	4.65	4.69	4.72	4.75
83	37.15	4.42	4.49	4.53	4.56	4.60	4.63	4.66
84	38.06	4.32	4.38	4.42	4.44	4.47	4.51	4.53
85	38.39	4.23	4.29	4.32	4.35	4.38	4.42	4.44
86	40.02	4.16	4.22	4.25	4.28	4.31	4.35	4.38
87	40.79	4.07	4.13	4.16	4.18	4.22	4.26	4.28
88	41.65	4.00	4.05	4.07	4.09	4.13	4.17	4.19
89	42.54	3.26	3.52	3.81	3.99	4.04	4.08	4.10
90	43.35	1.72	1.95	2.22	2.52	2.81	3.09	3.27

The calculated quantities for the performance map include the mechanical efficiency term using equation (11), the volume flow rate of water (m^3/s), the free air delivery (kg/s), differential temperature (mK) and head available for compression (m). With the exception of the HAC efficiency these quantities are readily established from the 5-minute averages of the 1 Hz data logged at each operating set point (i.e. after transients between set points have diminished, and the system operates at a new steady state).

The benchmark tests have been paired in such a way that data from single pump operation and two pump operation tests can be compared when a similar water volume was present in the HAC. The pairs are as follows: BM70/BM90, BM71/BM89, BM72/BM88, BM73/BM87, BM74/BM86, BM76/BM85, BM77/BM84, BM78/BM83 and BM80/BM81 for a total of nine pairs. The remaining 5 benchmark tests still contribute to the performance map composition but do not have a test with a similar operating water volume to compare between single and two pump operation. Set point performance from BM70 and BM90 tests has been plotted to illustrate relationships of calculated efficiency, difference in temperature along the length of the downcomer pipe and free air delivery in Figure 57.

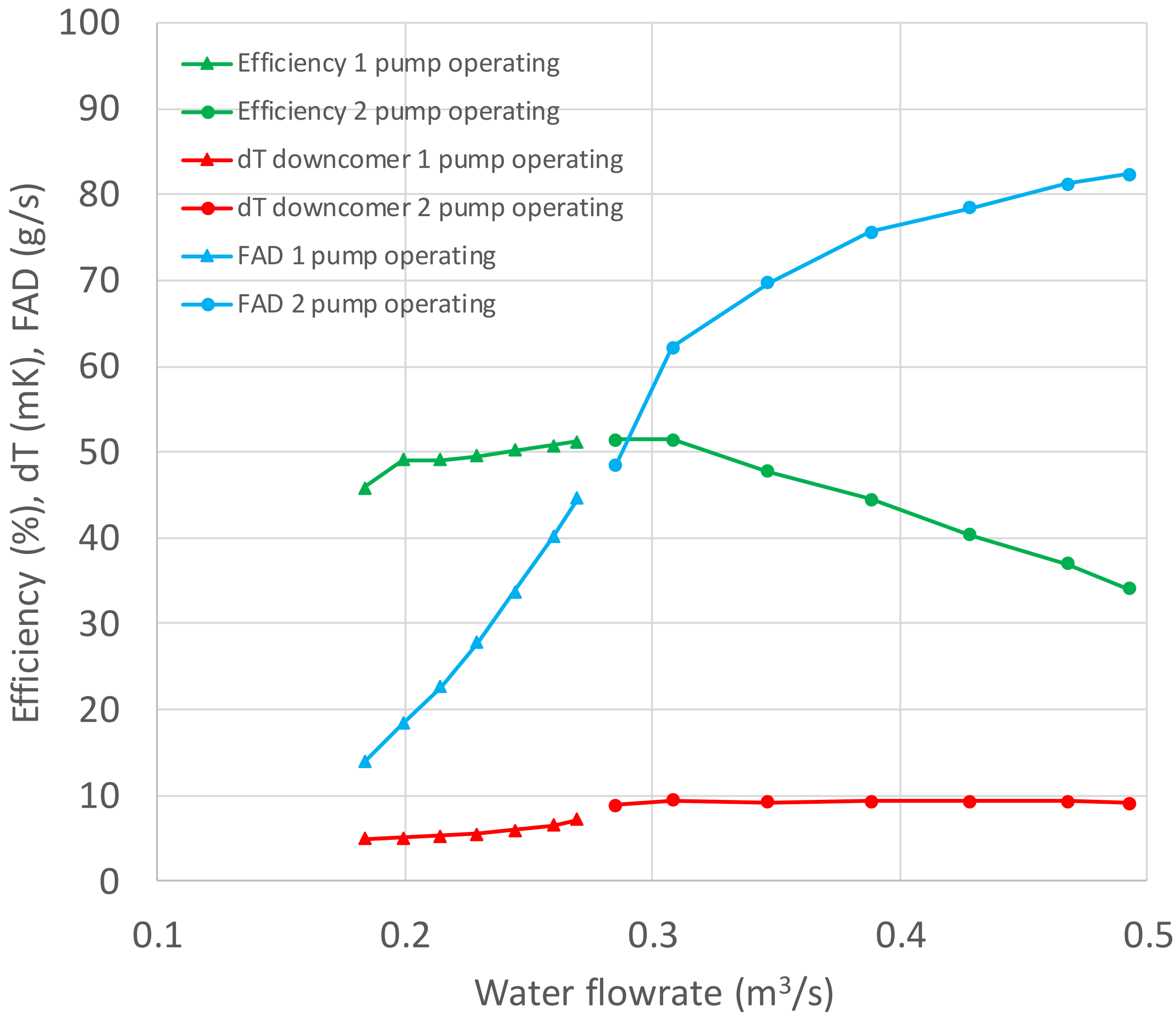

Figure 57: Efficiency, difference in temperature and free air delivery for benchmark tests BM70 and BM90 showing the comparison between single and double pump tests.

When aggregating two-pump test results with single pump test results (each with approximately the same water charge volume) the efficiency, free air delivery and differential temperature trends can be presented over a wider range of water flow rates than when considering results from either individuals in the pair alone. Observations from the curves in Figure 57 are:

- The free air delivery of the HAC monotonically increases with increasing water flow rate. This is consistent with prior modeling done by others, e.g. Millar (2014) and Young (2017) and literature results (Schulze, 1954; Rice, 1976; Chen and Rice, 1982, 1983).

- The optimal efficiency point of the system for this pair of tests lies in the 0.2-0.3m^3/s range on the water flow rate axis at just above 50% efficiency. This is consistent with the predictions made by Young et al (2015), including the prediction of an optimum.

- The differential temperature remains around 10mK across the entire range of tests. This is consistent with the ‘nearly isothermal’ hypothesis set out in the theoretical development set out by Pavese at al (2016) and model predictions of Young (2017).

The VBA scripts used to compute the volume of water inside of the HAC for pairing of the benchmark tests and the efficiency for all benchmark tests are presented in Appendix J: HAC performance map efficiency and volume VBA scripts. Appendix K: Efficiency, free air delivery and differential temperature plots shows the data for all set points across the 8 remaining different water volume configurations in a decreasing order.

The behavior evident in Figure 57, is clearly reproduced for other states of the system ranging from the maximum water volume with which the HAC Demonstrator can be charged, to the minimum water volume.

Although there is good correspondence of performance between the two pump test data and the single pump test data, each pairing does reveal a small discrepancy in each of the curves, at the locations where the curves from each individual in the pairs overlap on flow rate. The efficiency curves should ‘connect’ precisely, but a gap is evident across the entire range of test pairs. Possible reasons for this gap could be unaccounted-for head loss in the downcomer process, air leakage into the system disturbing the mass balance of air or discrepancies in the measurements when the system is adjusted for two pumps to single pump operation.

As the volume of water in the HAC decreases, the free air delivery across all flowrates can be seen to increase. This is a consequence of the greater head available to the system, set up by the pumps, when the HAC water fill volume is lower. The differential temperature across all water volumes and setpoints seems to consistently be in the range of 10mK or less.

Looking into the discrepancy between single and two pump efficiency results the first thing to be verified is the accuracy of the data provided to the calculations. Investigation revealed the most significant discrepancy in the raw observations of instruments between single and two pump configurations was in the LT1 measurement for the water level in the forebay tank. Figure 58 shows data recorded by LT1 across all benchmark tests highlighting the difference between single and two pump data.

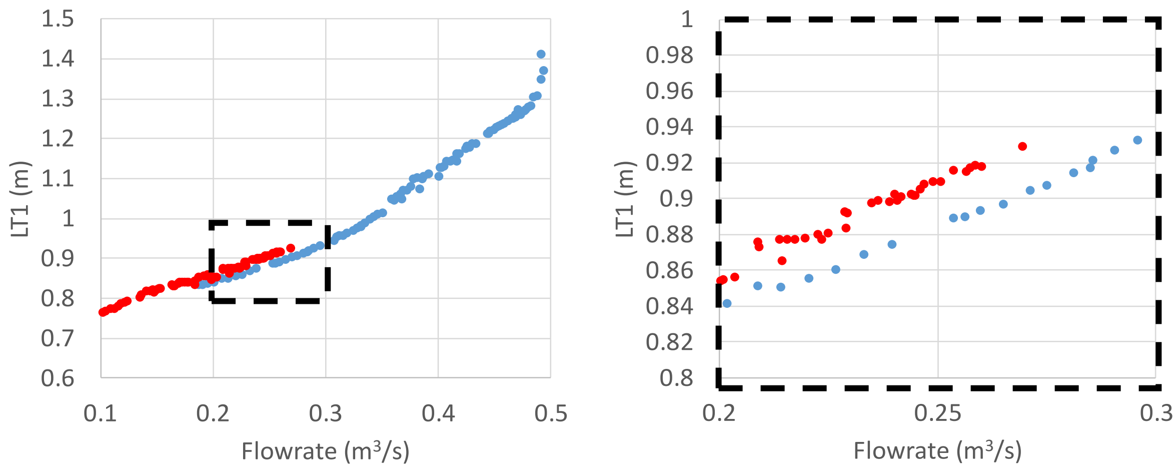

Figure 58: LT1 measurement across all benchmark tests reveals a discrepancy in LT1 measurements between single pump (red) and two pump (blue) operation.

There is a small, ~2cm, discrepancy apparent in LT1 observations when the single pump data is identified separately from the two-pump data, for identical flow rates. This precipitated forensic investigation of the reliability of the measurements taken by LT1, which resulted in them being determined to be accurate and precise. The disparity, although small, represents genuine information on differences in HAC operating performance with one and two pump operations.

To take investigations of this aspect of HAC behavior further just one step further, within the scope of this thesis, a special performance trial was undertaken with the forebay tank lid open so that the form of the water surface in the forebay tank could be visually inspected and recorded. The HAC was operated with one pump at 880rpm and a second time with two pumps at 600 rpm, so that the water flow rate of the pumps was the same, and the system was charged with the same volume of water.

As can be appreciated from the photographs of Figure 59, the specific form of the water surface in the forebay tank is quite different with one pump running and two pumps running. When observing the movement of the water in real time during the single pump trial the water is very agitated when compared to the stillness of the two-pump trial. This difference in the form of the water surface between single and two pump operation may be a possible cause of the small discrepancy between water level measurements taken across the HAC performance map tests.

Figure 59: Water surface in the forebay tank during single pump operation at 880rpm (left) and double pump operation (right).

The effect a slight difference or error in the measurement of LT1 would have on the available head is small and is not sufficient to explain the discrepancy in the calculation of efficiency between single and two pumps for the same HAC fill volume and same circulating water flow rate.

As discussed earlier in section 5.3 air leakage into the system presents a still to be resolved, but minor, uncertainty in post process calculations when balancing the mass flow rates of air entering and leaving the system. The Coriolis meter, FT4, is installed in a 4inch line that was pressure tested to over 90psig during construction and this line generally operates in overpressure of 30psig to 36psig, so it is considered unlikely that the observations from this instrument are in any way in error due to leaks. On the intake side of the system, suction pressures prevail and result in air leaking into the system after intake air is metered by FT5. For this series of tests, although leakage was significantly reduced in comparison to previous test series, the intake mass flow was known to be still subject to leakage uncertainty. As a result, the efficiency calculations utilized the mass flow rate of air out, instead mass flow of air input, and, as a consequence, will lead to slightly lower efficiency values and could also be a factor in the discrepancy between single and two pump data as seen in Figure 57 and Appendix K: Efficiency, free air delivery and differential temperature plots.

Modifications to the seals around the forebay lid are proposed that aim to eliminate intake leakage so that future performance map data collection will eliminate these uncertainties and will include strict verification of air leakage and air loss before the start of any benchmark test. It becomes clear, that irrespective of how well one considers the seal on the forebay tank is at the beginning of a series of benchmark tests, the quality of the seal deteriorates over time and subsequent tests and thus needs to be vigorously attended to in order that accurate mass flow rates of air entering the HAC can be recorded and reliable estimates of air loss can be obtained.

In one of the earlier benchmark tests (BM34), where suction air leakage could reasonably be regarded as nil due to copious taping of the lid, compressed air loss (ratio of air in to air out) figures that varied in the range: 94%-99% were observed with reducing water flow rate, as presented in Table 6.

Table 6: Air mass flow rates and air loss from BM34 to be used as a reference for minimal leakage into the HAC, compared to optimistic and pessimistic separator effectiveness.

RPM	880	850	800	750	700	650	600
Air in (kg/s)	0.0987	0.0962	0.0920	0.0847	0.0736	0.0645	0.0534
Air out (kg/s)	0.0935	0.0919	0.0883	0.0818	0.0720	0.0640	0.0531
Air loss (%)	94.672	95.495	96.009	96.572	97.704	99.353	99.360
Optimistic air loss Hutchison (2018)	94.66	95.36	96.39	97.27	98.02	98.71	99.25
Pessimistic air loss Hutchison (2018)	89.97	90.94	92.48	93.91	95.28	96.73	98.08

A model for bubble underflow at the separator of the Dynamic Earth HAC Demonstrator, resulting from the PhD work of Hutchison (2018), makes predictions of the separator effectiveness for optimistic and pessimistic scenarios. Separator effectiveness is a parameter that describes the proportion of compressed air at the separator that may be expected to pass to underflow because individual bubble sizes are small enough to be dragged from the separator to the riser pipe. Separator effectiveness is one component of separator loss. A second component is loss due to the solution of compressed air in the water of the separator, which is termed yield. Overall, compressed air loss due to both mechanisms can be quantified as the ratio of air mass flow in to air mass flow out. Hutchison's optimistic and pessimistic predictions for separator effectiveness are presented in Table 6 for comparison with experimental results.

On this basis it is possible to apply a correction to efficiency calculations for the data collected during BM68-BM90. Table 6 shows air loss increasing as the speed of the pumps increases for BM34, and a water fill level of 0.16m above the floor of the forebay tank. At the time of writing, Table 6 illustrates good correspondence between Hutchison's model of separator effectiveness in the optimistic scenario and the loss data from the HAC Demonstrator although this preliminary observation awaits repeated testing following sustained resolution of the leakage issues at the forebay. This correspondence also suggests that solubility losses are very small for the Dynamic

Earth HAC Demonstrator, a preliminary assertion nevertheless broadly confirmed by the gas solubility modeling undertaken by Young. At least on a preliminary basis, Hutchison's separator effectiveness values may be applied as a correction to accurately established air mass flow output by the HAC Demonstrator, to produce estimates of air mass flow at intake that are free of the problems of forebay tank leakage. In the HAC Demonstrator performance maps presented subsequently, we refer to the 'unadjusted efficiency' as that efficiency figure computed when Hutchison's correction is not applied, and the 'adjusted efficiency' as that efficiency computed when it is.

The unadjusted efficiency values for all set points across the benchmark tests can be seen plotted in a contour map on Figure 60 showing the relationship between the pressure head, the water flowrate and the efficiency. There is a visible optimum efficiency zone between 0.2m^3/s and 0.3m^3/s. The optimum flowrate for the HAC correlates to low rpm pump set points when operating with two pumps, and high rpm set points when operating in single pump configuration. The optimum efficiency zone also falls between 3.5m to 4.5m of pressure head which correlates to fill levels in the forebay tank of 0.669m to 0.176m with volumes of water in the system ranging from 38.5m^3 to 42.6m^3.

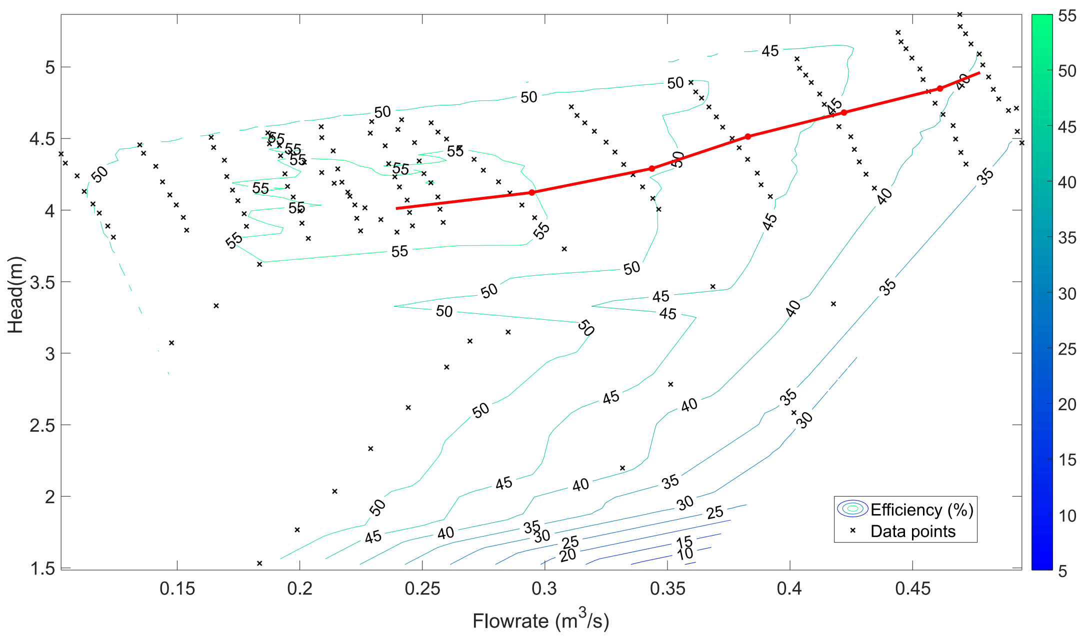

Figure 60: HAC performance map contour plot made in MATLAB, the red line represents the data for BM71 at a fill level of 0.669m above the floor in the forebay tank.

The performance map suggests a ‘ravine’ near the 3.5m head level from 0.2m^3/s to 0.4m^3/s but with the locations of data points in this portion of the map being sparse and forensic examination of the actual data values suggest that this is an artefact of the Delauney triangulation and bilinear interpolation process used in the contour algorithm. Future HAC Demonstrator tests aiming to refine this performance map will schedule additional fill volumes and rpm set points in order to ensure that the distribution of data for contouring purposes is more even. A contour plot of the free air delivery versus head and flowrate has also been prepared and can be seen in Figure 61.

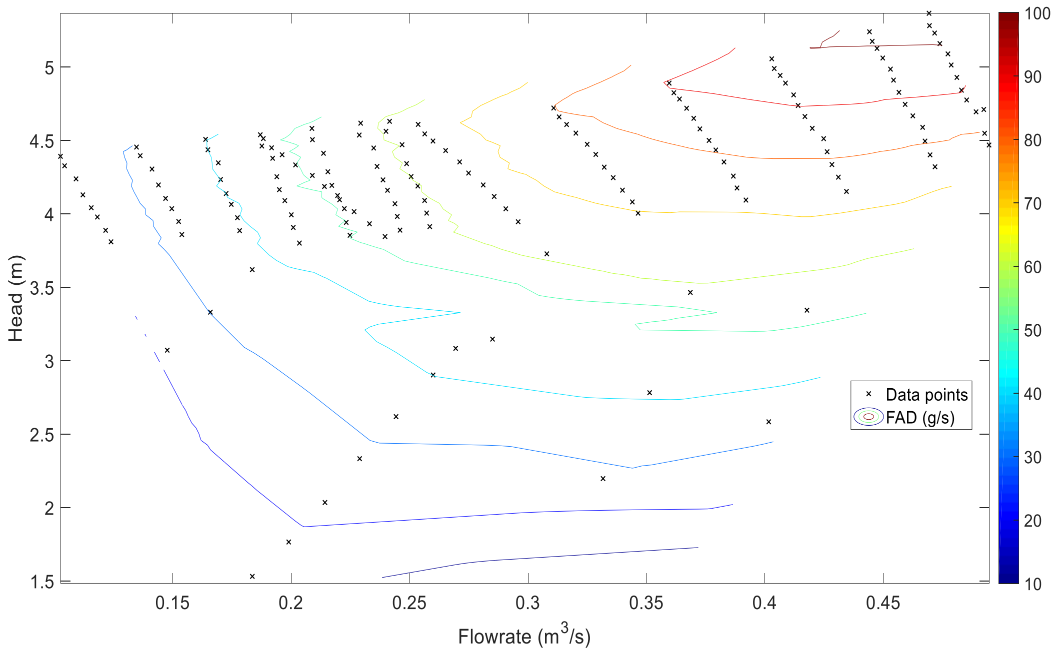

Figure 61: FAD of the performance map made in MATLAB.

The optimal operating condition in terms of free air delivery can be obtained when the head and flowrate are at its highest points. In order to optimize future HACs further analysis will require comparing the benefits of a reduced efficiency to the benefit of higher mass of free air delivered.

7.8 Characterizing the pressure in the downcomer pipe

Shortly after performance trials started, following commissioning and acceptance, comparison of modeled performance and measured performance revealed significant discrepancies in estimates of efficiency and (to a lesser extent) free air delivery. Some portion of this discrepancy arose for reasons already explained, such as the differences in flow cross section and absolute roughness of pipework due to rubber lining of the pipework, rather than ceramic-polymer coating. A second portion of discrepancy arose from the pressure drop along the air intake line, due to higher than expected minor loss factors as a consequence of installation of a dense inlet screen (to protect against bird entry), bends and fittings. This latter circumstance resulted in the pressure boundary condition at the forebay used in modelling being in error. With repeated investigation and further testing such factors were identified and corrected for. However, differences between modeled and expected performance remained that still required explanation. In this section, the progress that has been attained in explaining these differences is reported.

Sensitivity analysis undertaken with the HAC hydrodynamic model used to render the predictions of DE HAC performance made by Young et al (2015) reveals the disparities could arise from a difference between measured head and the head actually effective in compressing air in the HAC. Another way to express this idea is to state that an appreciable portion of the head set up in the HAC was being consumed in overcoming a loss mechanism that was not present in the model used to make performance predictions. By deliberately introducing an error in the head measurements carried over to the model to account for this unknown loss, correspondence between modeled and observed performance was excellent. What was remarkable, was that the magnitude of the deliberate error in head introduced to the model was the same, for every set point of every benchmark test that had been conducted to that time: 0.85 to 0.90m. This indicated that although the source of the loss was unknown at the time, it was a significant mechanism and ubiquitous in performance observations of the Dynamic Earth HAC.

The design of the Dynamic Earth HAC was based on the HAC installed within the mass concrete abutments of the Peterborough Lift Lock. Refer to Schultz (1954) for a detailed description of the facility. The design of its air water mixing head was the only part of the Peterborough Lift Lock system that was adopted essentially unchanged (other than use of modern materials) for the Dynamic Earth HAC design. Air-water mixing is a complex process and this complexity migrates to mixer design. In order to mitigate project technical risk, it was deemed sensible to utilize a design that had been proven in decades of operational use during the start up phase of the HAC Demonstrator. Given the magnitude and ubiquity of the head loss required to render observed performance to match modeled performance, as all other parts of the design had been considered in detail, it was considered plausible that the mechanism responsible for the loss could reside in the air-water mixing head.

7.8.1 Behaviour anticipated in Young (2017) downcomer model

Moving downward from the water surface toward the hydrofoil plane at the air-water mixing head inlet, the elevation pressure will reduce to exchange with static pressure and their will be an increase in dynamic pressure as the fluid accelerates toward the duct. Across the hydrofoil plane, it is expected that the static pressure drops as the water is accelerated further through the venturi-shaped spaces between the hydrofoils, which are also occupied by induced air distribution pipes that present their open ends at the elevation of these venturi-like throats (see Figure 62).

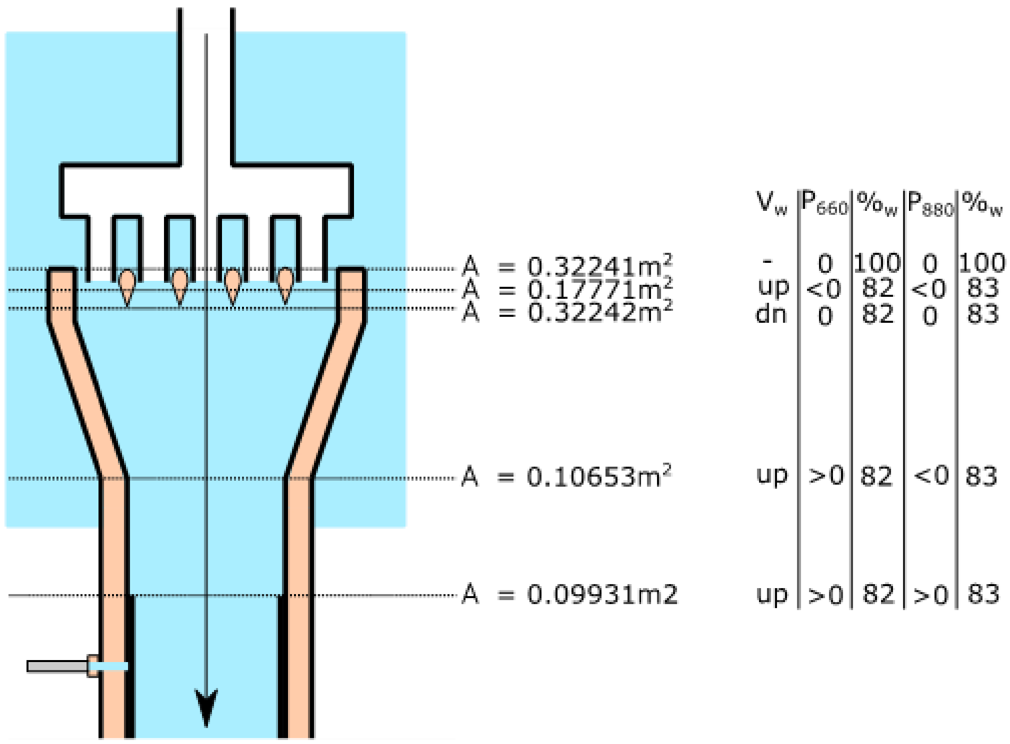

Figure 62: Geometry of the fluid path through the hydrofoil plane and into the downcomer in relation to water velocity, expected static gauge pressure and volume fraction of water.

Beyond the hydrofoil plane, the duct is convergent, so that expectation is that the mixed flow, if assumed only moderately compressible, will accelerate further so that static pressure is reduced further.

To establish greater understanding of the assumed process in the air-water mixing head it is instructive to consider the predictions of pressure, water and gas slip velocity made by the high-fidelity downcomer hydrodynamic model prepared by Young (2017) (Figure 63) which accommodates the compressibility behaviour of the gas phase of the mixed flow. The model ‘starts’ from the mid plane of the hydrofoils where the air delivery pipes present their open ends, and the air and the water mix. As the two-phase flow moves away from the hydrofoil midplane towards the trailing edge of the hydroplanes, the increase in area leads to a rapid reduction of the water velocity, and a rapid increase in gauge static pressure. The gas slip velocity at this location is low; the water and gas phases largely move with the same velocity.

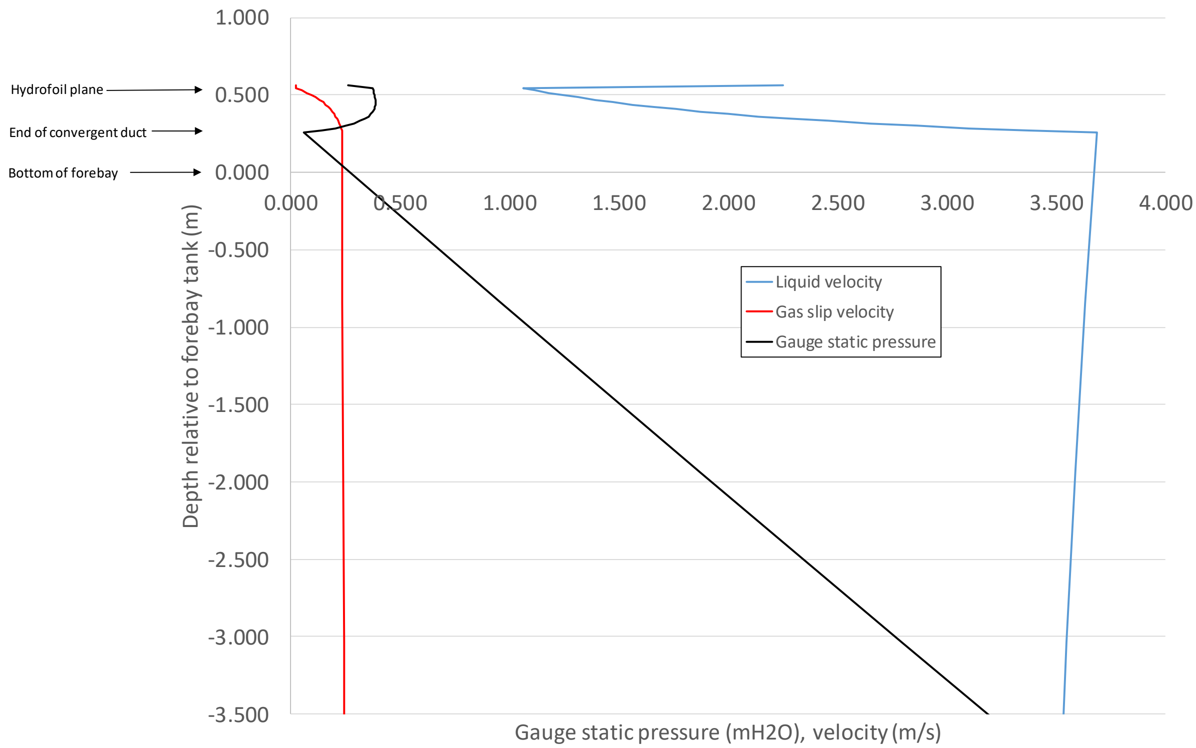

Figure 63: Gauge static pressure, water velocity and gas slip velocity in the air-water mixing head and the first 3.75m of downcomer pipe predicted by the model of Young (2017) for an operating condition with water flow rate 325 kg/s, gas mass flow rate 0.0738 kg/s, forebay absolute pressure 95,353 Pa and geometry as depicted in Figure 62.These conditions correspond to the operating condition of BM76 with pump speed set point at 700 rpm.

As the flow passes into the convergent duct section below the hydrofoil plane, the gauge static pressure reduces with pronounced curvature, and the water velocity increases dramatically. The gas slip velocity gradually increases toward a steady value of around 0.25 m/s, which is consistent with threshold value required for the HAC process evident in the experimental observations of Rice (1976) and the predictions of Millar (2014). Conceptually air bubbles attain a terminal velocity condition whereby drag forces on bubbles and buoyancy forces are in balance, and the bubbles are dragged down the downcomer by the water. Figure 63 indicates this condition is attained in the convergent duct section, just before the mixed flow arrives at the sharp geometric transition to the constant sectioned downcomer duct.

When the flow arrives at the constant sectioned downcomer duct and continues downward into the downcomer, the gauge static pressure increases, the gas slip velocity remains in its terminal condition, and the velocity of the incompressible water phase gradually reduces due to the pressurization of the gas phase (and consequently the reduction of the gas phases' occupation of the available flow cross section of the downcomer pipe). If the water flow rate established by the pumps had been higher, then the gauge static pressure at the hydrofoil mid plane would be lower, and the reduction in gauge static pressure in the convergent section of the air water mixing head would be greater, to produce strong suction conditions because flow velocity would be higher.

It currently is not possible to measure the velocity of the water and the gas slip velocity of the bubbly flow. However, the gauge static pressure of the mixed flow is shared by both phases, and so, if its observation is measured through pressure profiling in the downcomer, any deviation of measured behaviour from this detailed conceptualization in the Young (2017) model, becomes an indicator of an unaccounted-for loss mechanism in air water mixing process.

7.8.2 Experimental set up for downcomer pressure profiling

To investigate postulated losses in the air water mixing head the 4 pressure sensors installed across each of the pumps were temporarily redeployed to the first 4 sampling ports on the downcomer pipe underneath the forebay tank and the air water mixing head, so that pressure profiles could be measured for the water and air mixture during operation as seen in Figure 64. Each point forming an individual profile is the average pressure measured at the probe location over a 5-minute period, logging at 1Hz.

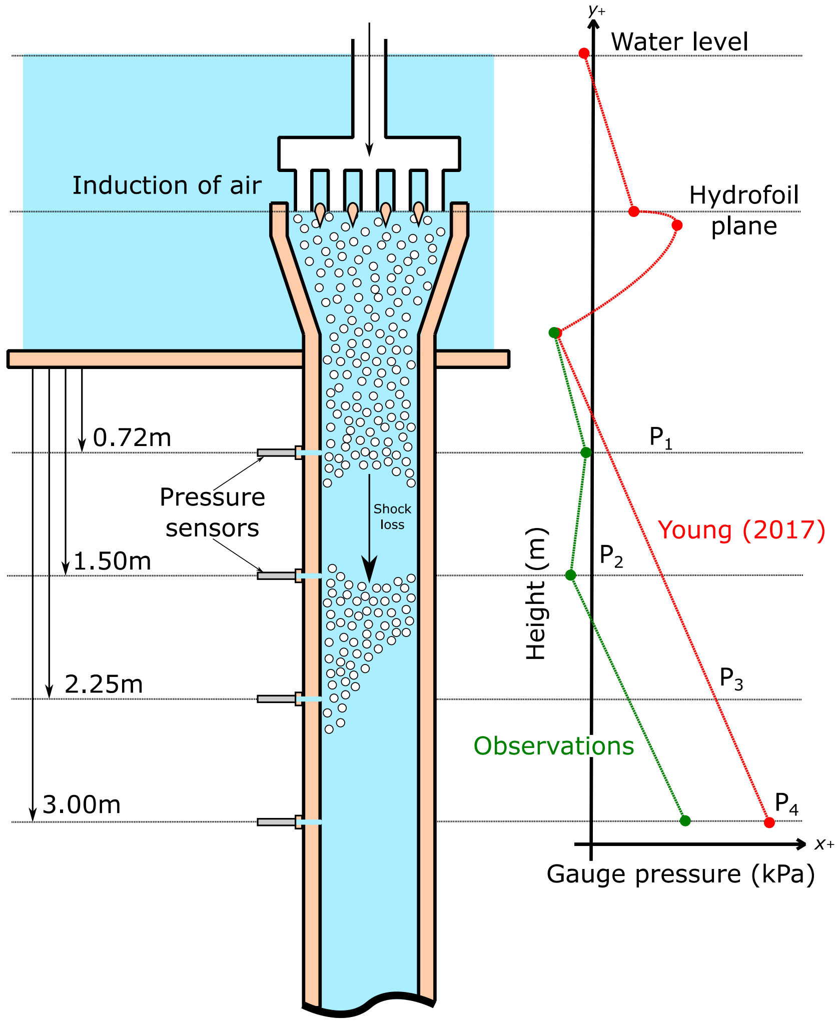

Figure 64: Experimental setup for the pressure sensors equipped to the downcomer.

The exact geometry of the fluid path is presented in Figure 62. The data was recorded throughout all benchmark tests to record the pressure profile across a wide range of pump operating speeds (thus flowrates) and HAC fill volumes (thus heads).

It was hypothesised that establishing the pressure profile of the flowing air water mixture would reveal if the pressure along the first section of the downcomer was behaving as expected (according to Young's (2017) model) or not. If not, this would indicate the presence of a loss mechanism not yet present in the models of either Young (2017) or Young et al (2015). The red pressure profile in Figure 64 is an idealized representation of the mechanisms incorporated in the Young (2017) model; the green profile postulates one possible deviation from this expected behaviour.

The work of Evan's et al (1996) indicates that some air entrainment into the water jet could occur via an annular film of air which is carried along adjacent to the water jet surface as the water plunges. Additional air is entrained at the plunging jet impact point which itself creates a so-called 'induction trumpet'. Chanson (2004) and (2007) clearly report the phenomenon of entrainment resulting from a tabular sectioned water jet free falling upon the surface of a pool already occupied by a swarm of bubbles, the latter being subject to vortical motion induced by the presence of the bottom of the pool. The tabular water jet was sometimes allowed to fall directly upon the pool surface but for differing water flow rates was also permitted to impact on the opposite side of the drop shaft from admission, before flowing vertically downward to the pool.

Chanson's results can be considered in a re-entrainment context because there may be a degree of similarity between those results and the behaviour that must be taking place within the downcomer in this work, although the 'pool' in this work is effectively unbottomed and the specific form of the water jet is unknown. If the speculated free-fall zone does in fact exist, the water jet could have an annular form that 'clings' to the downcomer wall or it could be a water core freely falling within an annulus of air. Chanson's work shows that either water jet geometry would result in entrainment of air to bubbles.

Importantly, Evans et al. (1996), describe some plunging jet air induction processes as 'self regulating', but with the air entrainment rate dependent on both the free fall length of the jet and the diameter of a confining duct. The length of the free-falling jet adjusts itself so that all of the recirculating air around the jet within the duct is entrained into the water flow. Despite the uncertainties regarding the plunging jet geometry, and the absence of any formal nozzle forming the water jet, a similar ‘self-regulating’ effect must be in play in the HAC downcomer; all the air metered entering the air inlet pipe, the forebay tank, the air-water mixing head is ultimately compressed in the downcomer.

7.8.3 Observed pressure profiles below the air water mixing head

In this section, one particular benchmark test, BM76, is selected specifically to explain the deviations from the conceptual idealization observed in pressure profiling data. BM76 had 38.34m^3 HAC water fill volume, and 2 pumps were running, enabling access to heads between 4.0 to 4.5 from pump speed set points from 600rpm to 800rpm respectively. Figure 65 shows the pressure profile data gathered while the HAC was in operation, each profile corresponding to a given pump speed and thus a given water flow rate. The Young (2017) model expectations are overlaid on the plot, for two pump speed set point cases: 700 rpm and 880 rpm.

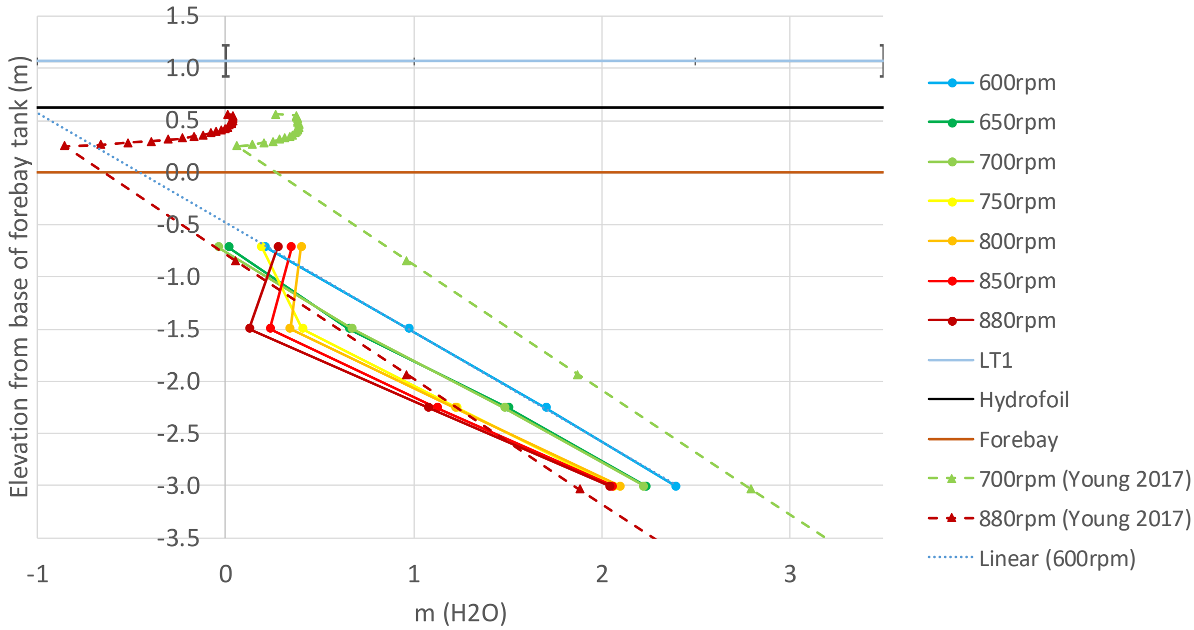

Figure 65: Experimentally established pressure profiles of the air water mixture below the forebay tank inside the downcomer for BM76 with operating conditions. LT1 shows the average elevation of the water level in the forebay tank with error bars to show the maximum and minimum elevations, the Hydrofoil displays the static elevation of the hydrofoil plane, and Forebay shows the elevation of the base of the forebay tank. 700rpm/880rpm (Young 2017) show the modelled behavior of the pressure profiles going from the hydrofoil down the downcomer, which can be compared to the measured pressure profiles.

Figure 65 shows clearly that there is a disparity in observed and modeled air-water mixing head behavior. Focusing on the 700rpm set point information first, it appears that the pressure observations of the 4 sensors, produce a rate of pressure increase that is consistent with the modeled rate of pressure increase. However, for a given depth below the forebay tank base, the pressure measured by the sensor is substantially lower than the pressure predicted by the model (approximately 1 mH_2O lower).

At the end of the convergent section of the air water mixing head, with pump speed 700 rpm, the model predicts a gauge static pressure, positive, but close to zero, whereas the uppermost pressure sensor returns a pressure of just below zero. At this speed, it appears that there is a pressure 'discontinuity' that may be consistent with free fall of the water through a continuous void of air between the end of the convergent section and the uppermost pressure sensor. If the water does enter free-fall, it will be effectively decoupled from the downcomer pipe, so gauge static pressure will be due to the gas phase and steady, and the water velocity will increase with gravitational acceleration.

Such behavior is reported in the literature by (Kobus, 1984) who refers to it as 'detrainment' of a bubbly 2 phase flow. That there may be detrainment, and that the air is definitely compressed at the HAC outlet, confirms that there must also be re-entrainment of the air in the water. Re-entrainment must occur after the water has accelerated through the air and impacted on the fluid below a detrainment zone.

For the downcomer as a whole, the downstream pressure boundary condition is at the bottom of the riser pipe in the separator, measured by DPT2. Despite this discontinuity of pressure profile at the upper part of the downcomer pipe, the lower parts of the pressure profile in the downcomer (close to the separator) must converge on the modeled pressure profile, and Figure 65 presents evidence in the observed pressure profiling of the lower probes that this convergence is starting to occur.

Turning now to the information presented for the 880rpm case, the gauge static pressure predicted at the end of the convergent section of the air-water mixing head is substantially lower than in the 700rpm, amounting to 87.9kPa (abs). A free-fall zone immediately below the convergent duct section can also be postulated, but the pressure recorded in the upper most pressure sensor is actually higher than the model predicts. This 'overpressuring' could be attributed to an impact pressure of the free-fall water jet landing on the fluid mixture around the upper pressure probe.

Such overpressures of both non-aerated and aerated water have been measured by several authors. Two examples include: May and Willoughby (1991) who report on experiments of particular interest to HAC technology and by Duarte, Schleiss and Pinheiro (2015).

It is instructive to examine the rate of pressure increase from one of the pressure sensing probes to the next, as one progresses deeper. In the modeled cases, the pressure gradients are steady in the downcomer and arise as a consequence of the pressurization expected due to a column of overlying fluid with an aggregate density consistent with the ratio of measured mass flows of air and water. For the observed data, where the pressure profile is steeper on the plot, pressure does not increase much between the space between the probes, and it may be concluded that the aggregate density of the fluid column is less than that expected of due to the ratio of the mass flows. Conversely, where the pressure profile has a shallower gradient between probes, the aggregate density of the intervening fluid may be regarded as higher. Such deliberations are appropriate to interpretation of mixture behavior in the lower parts of the profile involving the lower 3 probes. If the pressure increase arising between probes is consistent with the phase mass flow rates, then this may indicative of the air having been effectively re-entrained by the water.

To reinforce these points, using the difference in elevation between the pressure sensors and the pressures values observed, the density of the air-water mixture needed to account for such a pressure rise can be computed and such computations are presented in Table 7 for each set point of BM76. The average expected density can also be estimated based on the known mass flow rates of water and air measured by the system instrumentation.

Table 7: Densities accounting for pressure rises observed in the downcomer (kg/m^3).

RPM	600	650	700	750	800	850	880
Apparent density P1 to P2	968.12	812.67	908.26	272.73	-74.39	-143.44	-191.74
Apparent density P2 to P3	966.33	1120.20	1067.78	1091.53	1164.33	1176.79	1262.11
Apparent density P3 to P4	916.73	976.67	989.38	1104.51	1164.92	1243.13	1281.08
Expected Density	826.18	828.18	830.94	840.71	841.39	848.37	852.19

According to the mass flow rates of the air and water observed on the system, around the inlet, the expected density of the mixture should increase from 826kg/m^3 to 852kg/m^3 as the mass flow rate of water increases with the HAC set point. However, looking at the data presented in Table 7 the densities appear to be higher than is inferred from these observations.

Figure 66 shows an example of pressure profiles observed, each obtained when the HAC was operating at steady states during BM68 when the HAC contained 45.17m^3 of water with low accessible head set up by the pumps.

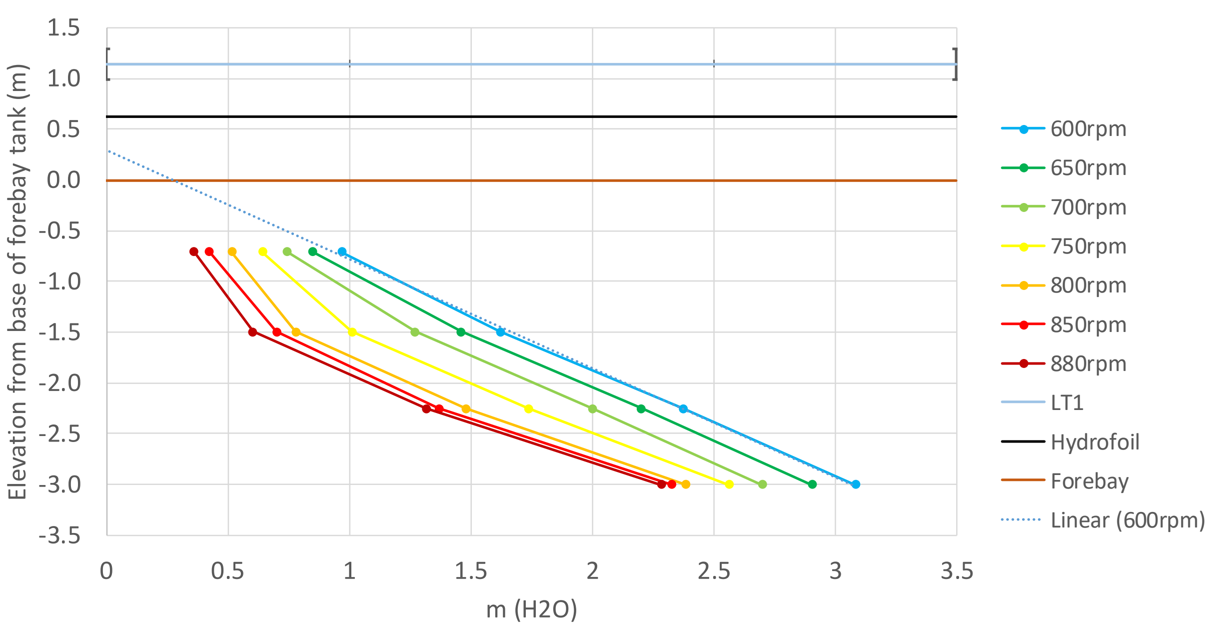

Figure 66: Pressure profile of the air water mixture below the forebay tank inside the downcomer for BM68 filled with 45.17m^3 of water.

For the 600rpm pump set point of BM68, extrapolation upward of the sensed gauge static pressure predicts zero at an elevation corresponding to the end of the convergent section of the air-water mixing head. This suggests that there may be no pressure discontinuity or free fall zone for this case. It should be noted that at the 600rpm set point of BM68, the mass flow rate of air was very low; very little compressed air was being produced. In general, the higher the water circulation flow rate, the more compressed air is produced. The pronounced upward curvature of the pressure profiles in the high flow rate set points of BM68, and the coherence of behaviour across multiple set points may simply be interpreted as being indicative of a greater mass flow of air being inducted into the air-water mixing head, so that the density of the fluid is reduced in the upper portion of the downcomer, above the pressure probes. If detrainment occurs within BM68, it seems likely that it does so above the location of the highest-pressure probe. In such cases, for the high flow rate pump set points, the upper pressure probes may sense a small amount of a free-falling water jet impact overpressure and this may account for the higher than expected mixture densities in Table 7.

Figure 67 shows an example of the time series of the pressure profiles recorded on the four sensors connected to the downcomer below the forebay tank, each obtained during BM68 when the HAC contained 45.17m^3 of water. The remaining time series pressure profiles can be seen in Appendix L: Pressure profiles.

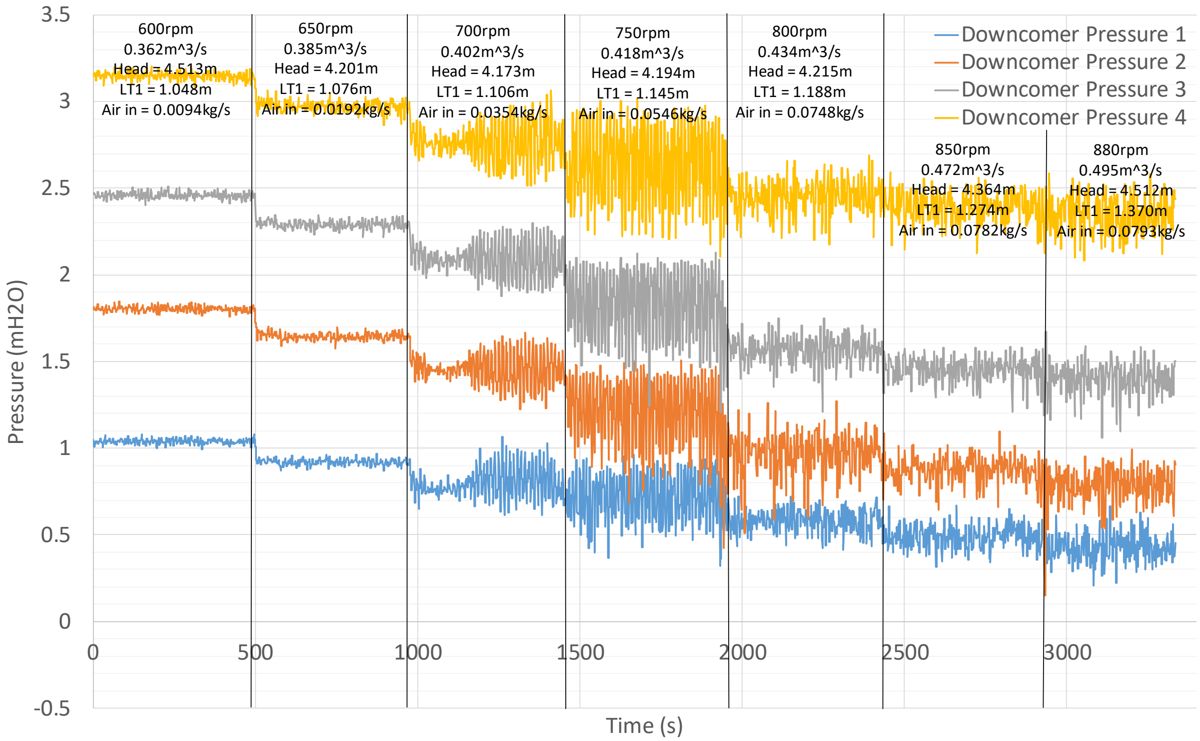

Figure 67: Time series of the pressure profile of the air water mixture below the forebay tank inside the downcomer for BM68 filled with 45.17m^3 of water.

With reference to Figure 67, for Benchmark Test BM68, the first thing to note is that the measured pressures do increase with depth after mixing as is expected in various models of the HAC downcomer compression process (e.g, Millar (2014), Young (2017)). However different regimes of flow behaviour are further evident in Figure 67.

Regime A: Between 600rpm and 700rpm (0.36 m^3/s to 0.40 m^3/s) there was so little air inducted at these set points, that the flow could be considered single liquid phase. For the 600rpm and 650rpm set points, this idea is consistent with the difference in the pressure observations from one probe to the next, as these correspond closely to the physical elevation differences between the probes. Although the pressure differences between probes remain the same for the 650rpm case, the pressures measured for the 650rpm case are lower, and this is accounted for by an increased in frictional energy loss associated with the higher velocity of the (single liquid phase) flow.

Regime B: Where the pressure time trace indicates set points with great, and sustained, variability (between 700rpm and 750rpm), it is thought that this represents the onset of significant air induction leading to appreciable bubble presence around the pressure sensing probes. The change in the form of the curve is significant for 700rpm to 750rpm set points. While appreciable air induction is secured, the bubble transport capacity of the water may still be limited for these flow conditions, leading to significant air bubble recirculation, with more recirculation measured at the deepest pressure probe. At higher heads (lower fill rates – see remaining series of curves in Appendix L: Pressure profiles), if this condition does correspond to air bubble recirculation, the recirculation behaviour develops at lower flow rates.

Regime C: Where the pressure time trace indicates set points with less variability and greater intermittency, the flow rate of the water phase is thought to be sufficiently high that it gains/possesses bubble transport capacity, so that the occurrence of bubble circulation (and associated high amplitude pressure fluctuations) diminishes. These flow conditions are thought to prevail for set points at 800rpm and upward for BM68 in Figure 67. In the progression from 800rpm to 880rpm, it is evident that the measured pressure falls, as the flow rate increases. The principal reason for this is thought to be frictional energy loss, although the drops in pressure at the same horizon from one set point to the next are much lower, than for the single liquid phase cases of Regime A. Consequently, it may be speculated that within Regime C, the transported bubbles produce a form of ‘lubrication’ for the overall flow.

Medjiade et al. (2017) presented several methods of characterisation of the flow regime of bubbly two phase flows, all be they, for upward rather than downward flows. As is the case with this work, they utilize time series observations of static pressure measurements (relative to atmospheric pressure) in order to characterise the flows. The magnitude of pressure fluctuations for four different regimes of flow were presented as follows: intermittent, 3 kPa (0.3m H_2O); homogeneous, 0.2 kPa (0.02m H_2O); transitional, 1 kPa (0.1m H_2O) and heterogeneous (5.5 kPa, 0.55m H_2O).

Clearly, the ultimate function of the complete downcomer is to pressurise the flow, and it is clear from Figure 67, that for the flow conditions represented, compression of entrained, transported bubbles starts at elevations corresponding to the third lowest probe. At approximately 0.33 m, according to Medjiade et al. (2017), the magnitude of the pressure fluctuations suggest that the two phase flow condition is a transitional state to heterogeneous flow. This seems to be consistent with independent methods of establishing the flow regime. For the flow conditions at 880rpm, the gas hold up is 0.099 whereas the threshold gas hold up at the transition to heterogeneous flow, according to Reilly et al. (1994) is 0.146. Krishna et al. (1999) compare Reilly's criterion with that of Wilkinson. For the same flow conditions at 880rpm in Figure 67, Wilkinson's threshold gas hold up is 0.02 indicating that the flow is already heterogeneous.

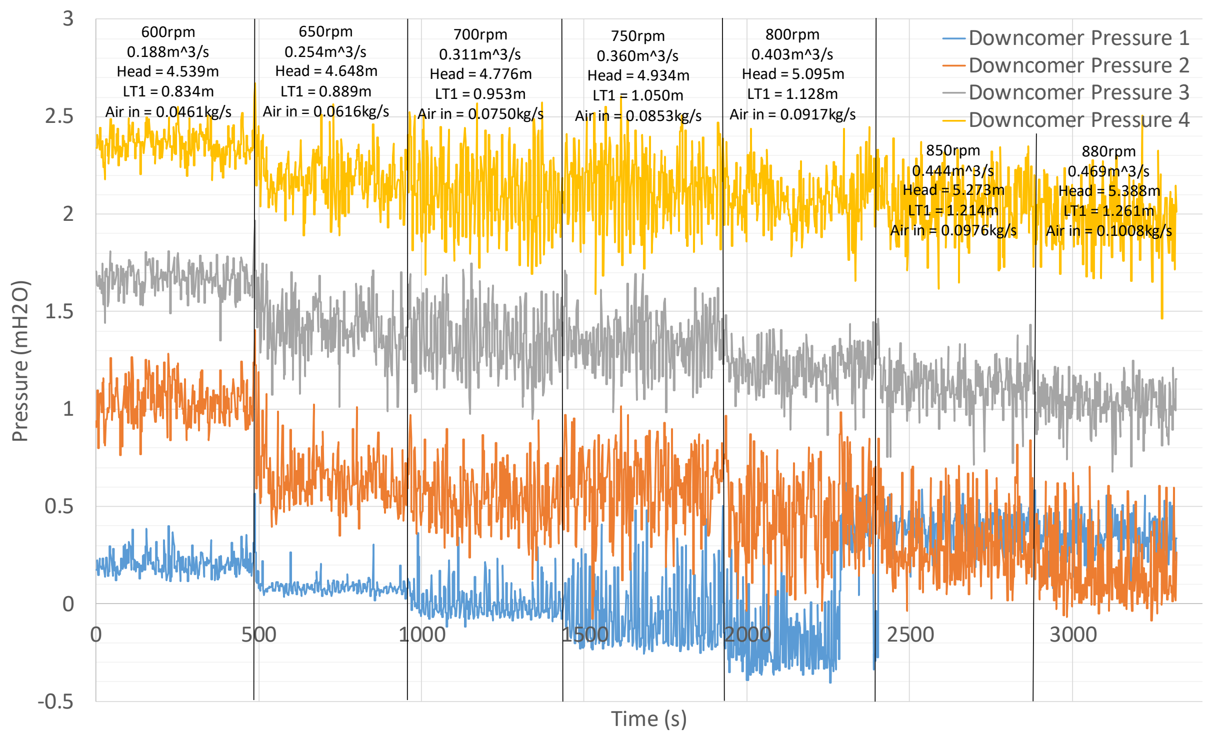

Figure 68: Time series plot of the pressure profile for BM80, fill level at -3.245m and two pumps.

In subsequent benchmark tests conducted with lower HAC fill volumes, as exemplified in Figure 68 for BM80, at high HAC heads, and at set points corresponding to higher water flow rates (850rpm, 880rpm), the pressure measured by the pressure probe with the highest elevation in the downcomer suddenly rises (within the set point), in comparison to lower flow rate set points, toward the pressure values recorded by the next probe, around 0.75m lower. This is speculated to reflect a water free fall condition occurring. If the pressure remains steady from one probe to another, the water must have become detached from the downcomer pipe, removed frictional energy loss and be in free fall. The spontaneous introduction of a loss mechanism such as this (e.g. at set point 800rpm in Figure 68), confirms a degree of self-regulating behaviour of the flow. The head and flow rate conditions set up for downcomer operation by the control system, may not result in sufficient transport capacity for the low density, low pressure bubbles in the upper reach of the downcomer. These low-pressure bubbles will be large and thus may coalesce readily to form a large void (slug) through which the water free falls and accelerates. The flow adjusts itself such that the fall height must result in a water velocity high enough to provide sufficient transport capacity for re-entrained bubbles.

So, it is suggested that the pressure profiling evidence remains consistent with the development of a pressure discontinuity even when the HAC has a high-water fill volume and head accessible across the pump set points is low.

When the evolution of pressure profile behavior is examined as the HAC fill volume is reduced and greater head becomes accessible, the evidence for the development of a pressure discontinuity grows. Discontinuous behavior perhaps begins to become noticeable in the profiles for test BM74 and is strongly evident in the profiles for test BM76.

Another trend observable when the water fill volume of the HAC decreases, and the head that can be developed by the pumps increases, is an increasingly pronounced shift in the position of these pressure profiles; the profiles for individual flow rates are displaced towards the suction condition.

7.8.4 Presentation of all pressure profiling data

Looking at the pressure profiles in Appendix L: Pressure profiles the HAC begins with a high volume of water at BM68 with two pumps running down to a low volume at BM76. BM84 to BM90 are tests run with a single pump with a low volume of water up to a high volume of water.

The benchmark tests BM77-BM83 contain a volume of water in the HAC that cannot be calibrated with a measurement from LT1, leaving the level sensor calculation using DPT2 to calibrate the pressure sensors - which could lead to errors because DPT2 experiences drift which cannot be corrected with an LT1 or LT2 observation either. This problem can be overcome with experimental methodological procedure: at rest water levels can be obtained by dipping the water level in the HAC surge pipe when the fill volume in the system means that the quiescent level of water in the system falls below the flanges of the forebay tank (out of range of LT1).

Benchmark tests performed at similar water volumes with single or double pump operation can be plotted on the same charts to present a more complete picture over a wider range of flow rates as seen in Figure 69. For example, for BM70 and BM90 combined, the linearity of the pressure profiles at low flowrates (RHS, single pump 600rpm) becomes much more distinct from the non-linearity experienced at high flowrates (LHS, double pump 880rpm).

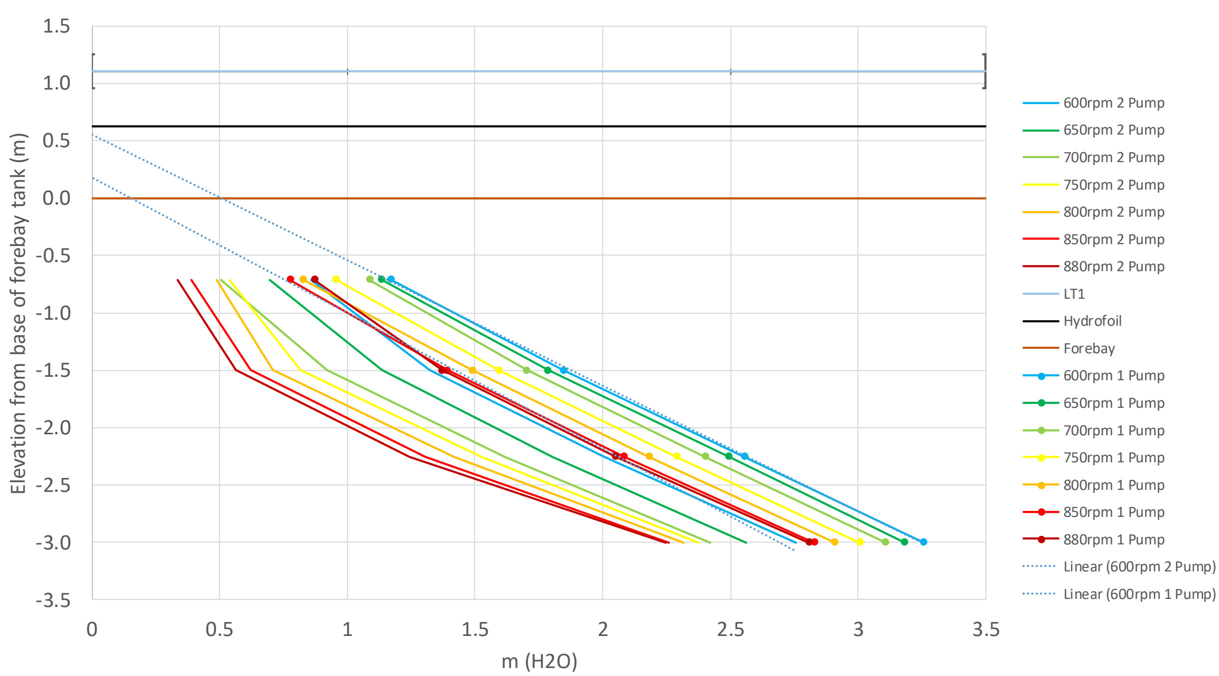

Figure 69: Pressure profile of the air water mixture below the forebay tank inside the downcomer for BM70 and BM90 combined.

7.8.5 Estimation of loss due to detrainment, free-fall and re-entrainment

Detrainment, free fall and re-entrainment processes are all phenomena that will consume the head set up by the pumps, and are loss mechanisms that need to be allowed for when determining compression efficiency of the Dynamic Earth HAC. The magnitude of the possible free fall zone can be crudely estimated from the pressure profiles, and introduced as a head loss when calculating the efficiency of the HAC. These corrections increase the fidelity of the model of the process, which formerly did not include any sort of head loss due to detrainment. Figure 70 shows the effect of estimating free fall corrections for set points in BM76 (two pumps) and BM85 (one pump) and applying these in compression efficiency calculations.

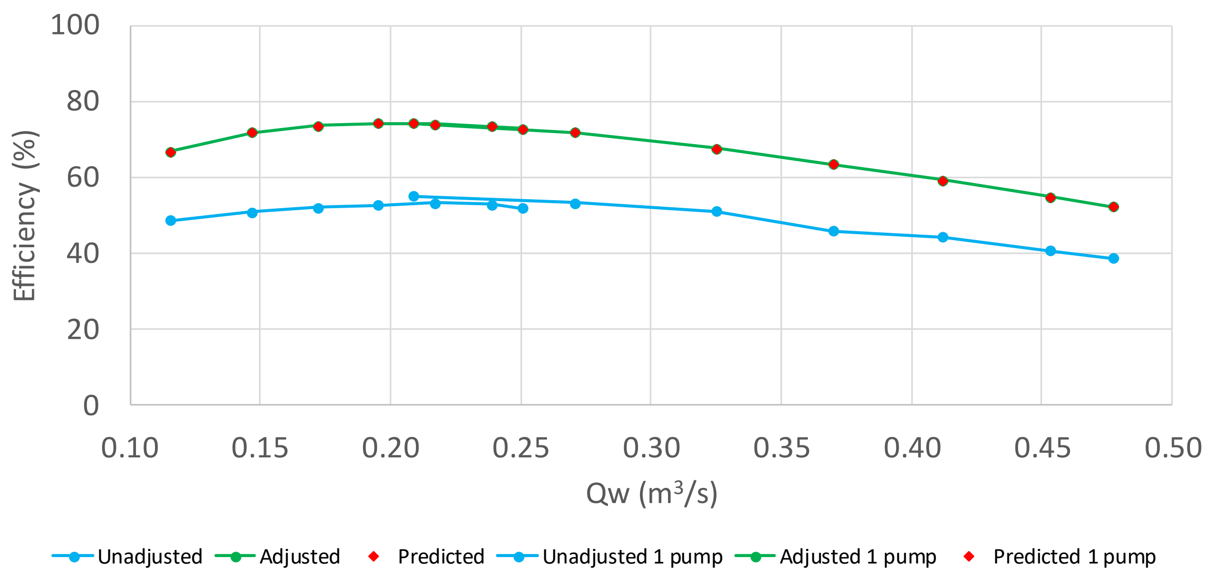

Figure 70: Observed (blue) efficiencies for BM76 and BM85 across all set points with predicted (red) and adjusted (green) efficiencies.

The corrections leading to this extent of agreement over all BM tests are presented in Figure 71. As the volume of water in the HAC decreases, the driving head increases due to a larger difference in elevation between the forebay and the tailrace water levels. The increase in driving head results in increase in head loss at low flowrates, but remains near constant at high flowrates. There also seems to be an 'optimal' (minimum) amount of headloss in the 0.2-0.3 m^3/s range, which perhaps only coincidentally falls within the the same range of flow rates as the HAC's optimal operating efficiency point, for all pairs of tests with the exception of BM70 and BM90 data set which produced very little compressed air.

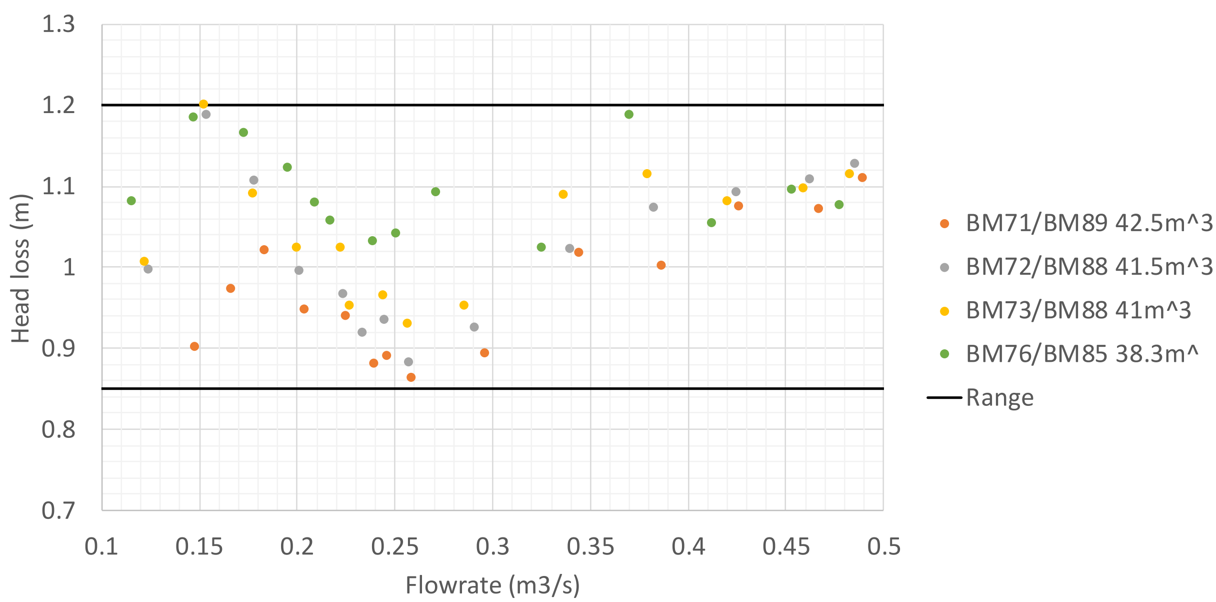

Figure 71: Estimated unaccounted for head loss in the HAC efficiency calculations across all benchmark tests which can be calibrated, sorted in pairs with matching water volumes.

7.8.6 A speculative synthesis of downcomer pressure profiling

A highly speculative mechanism for this newly established HAC head loss is presented in Figure 72 which illustrates possible locations of detrainment to create a void and lengths of the hypothesized free fall zone in the downcomer. There is still appreciable uncertainty attached to this postulation and it is only presented to illustrate the possible loss mechanisms which may be responsible for the disparities in modeled and observed pressure profiles in the downcomer. As mentioned previously, observed pressure profiles with high volumes of fill water in the HAC do not exhibit discontinuous breaks in pressure profile which could simply mean the event occurs above the pressure sensors. As the water volume in the HAC decreases and the driving head set up by the pumps increases, the location of the free fall zone may move down the downcomer so that its effects are more directly sensed by the pressure probes, especially the uppermost pressure probe.

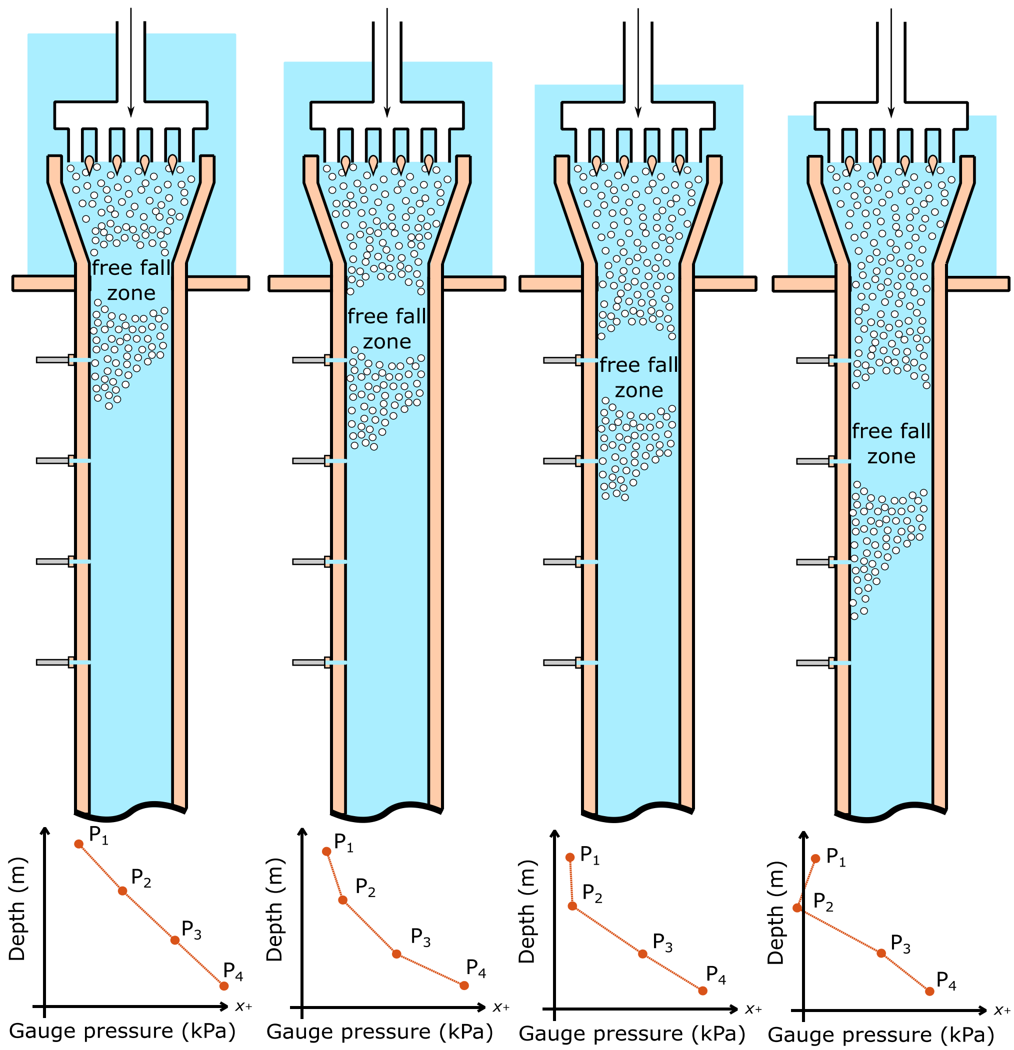

Figure 72: Estimated location and size of the free fall zone as the volume of water in the HAC decreases (left to right).

Modeling suggests that immediately below the hydroplane trailing edges, the convergent geometry of the air-water mixing head has the potential to create strong suction pressures, especially at high flow rate pump set points, where the greatest suction pressure occurs at the end of the convergent section. These cannot be directly sensed by the pressure probes because they are positioned too low in the downcomer. However, the highest-pressure probe did sense suction pressures on a few occasions. Modeling further shows the air slip velocity to be lowest and below the recognized threshold value of 0.25m/s within the convergent section of the air-water mixing head, and so it can be argued that this is the location where detrainment is most likely to initiate. However, water velocities in this zone are high, meaning that the air bubbles will be transported downward to the uniform cross section downcomer, implying detrainment initiates in the downcomer.

If water jet free-fall occurs the gas pressure in the duct around the jet would be expected to be steady. Impact of the jet would result in higher pressures than expected being sensed by probes a little below the impact point, in fluid where air had been re-entrained through the impact.

The evidence from modeling and from the BM tests undertaken, does seem to suggest that the mechanisms responsible for the hitherto unknown component of loss comprise detrainment, free-fall, water jet impact and re-entrainment. That the magnitude of loss remains within a range of 0.85 to 1.2m across all cases, and suggests that although the specific operating conditions may have some influence, the bulk of the loss may be attributable to an irreversible process that is approximately the same across all operating conditions of the HAC. The modeling reflects irreversibility in its formulation for the mixing process at the hydrofoil mid plane horizon, so is a loss that is already ‘included’ in the model. As air has to be re-entrained after detrainment, with or without free fall, and re-entrainment energy is definitely not included in the modeling (at present!) it is speculated that it is the energy consumed in re-entrainment that is primarily responsible for the bulk of the loss.

For design purposes, the fact that the magnitude of the loss generating mechanism is relatively constant across operating conditions, suggests that it may simply be allowed for through addition of a small amount of additional head set up by the circulating pumps.

7.8.7 HAC Performance Map

The HAC compression efficiencies can be recomputed allowing for the loss mechanisms speculated in the previous section; the head correction amounts required are visualized in Figure 71. Application of these corrections in the HAC efficiency calculation does not lead to proof that the HAC efficiency is as expected prior to design and construction, through comparisons between modeled and observed performance. Rather it indicates that the model (e.g. Millar (2014), Young et al (2015), Young (2017)) of gas compression in the HAC is correct where it applies upon re-entrainment and after the losses discussed in the previous section have been incurred. Experimental investigations and theoretical development are still required to properly explain the loss generating mechanism evident in the observations presented in the previous section, so that the mechanism can be inhibited, and the loss minimized. With an assumption that this can be done, the corrections in Figure 71 can be applied in the HAC efficiency calculations and the performance map for efficiency can be recompiled. This is presented below in Figure 73.

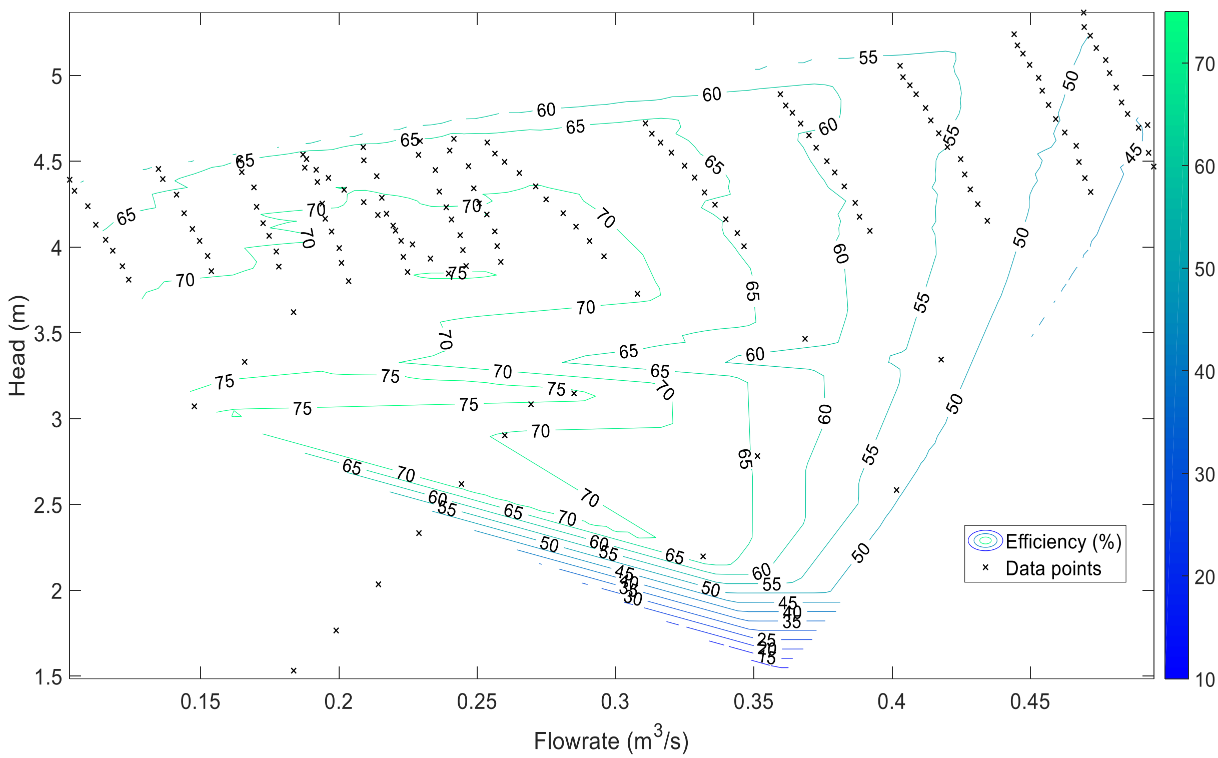

Figure 73: HAC adjusted performance map contour plot made in MATLAB.

8. Conclusions and ongoing work

8.1 State of completion and contributions

The testing and installation of instrumentation along with the design and programming of the HMI both contributed to the commissioning of the Dynamic Earth HAC Demonstrator which is now complete. The result of these efforts is that the HAC Demonstrator operates effectively and the instrumentation installed in the facility produces observations that are fully trusted as data, to support ongoing investigations. Also, standard procedures have been established for both commissioning HACs and operating HACs that will inform future HAC installations and guide other HAC operators.

The development and refinement of detailed models by others for the downcomer compression process specifically, as well as the complete HAC cycle, means that scientific experimental investigations can meaningfully proceed guided by modeling supported by formal hypothesis formulation and testing.

This is exemplified by investigations that established the reported absolute roughness of the rubber lining material protecting pipework used in the system. The results of that specific work were used not to alter the formulation of the HAC model, but to alter the value of a parameter contained within the model, so that there was a greater degree of agreement between model and observations.

As this value of absolute roughness determined is different from the one value found to be reported in the literature, it may prove of use to those designing rubber lined pipework generally. In the case of the current plant, determination of the absolute roughness of the rubber lining material has contributed to increased understanding of the mechanisms of loss incurred in the air intake system of the Dynamic Earth HAC.

The statistical process of establishing similarity of operating states of the HAC has also been established and the necessary data analysis has been automated in MATLAB scripts. The technique is founded on statistical hypothesis testing utilizing the Kolmogorov-Smirnov statistic for comparing distributions of data. It is now possible for operators of the facility to 'dial up' a specific operating condition and to know, with a defined level of confidence, how 'close' that actual operating state is, to a prior operating state. Without such metrics being established, as they have been through the work reported in this thesis, there is no scientific basis for the effects of before-and-after process interventions to be objectively evaluated. Consequently, this facility developed through the work reported in this thesis, will prove invaluable to ongoing work to improve the HAC compression process.

Software automation and data analysis methods have been developed to permit experiments to be performed rapidly, in a largely automated fashion, with little to no intervention from the operator. A PID control system design was executed in MATLAB software during HAC Commissioning, as part of the HMI script that enables the HAC to be operated completely unattended. The PID control loop maintains the water level in the separator, by means of actuation of the motorized globe valve installed on the compressed air delivery line. The data gathered from automated benchmark tests has permitted the compilation of HAC performance maps for the HAC Demonstrator, that summarise and characterise the complete operational performance of the system without any of the experimental interventions to be tested being applied. These experiments have all contributed to the understanding of losses within the system and verified many aspects of the system design.

Thus, this thesis is also the first formal report made of the post-design, post-construction operating performance of the Dynamic Earth HAC Demonstrator. The experimental results presented indicate that the predicted performance of the facility made by Young et al (2015) is very close to the performance actually observed through direct observation of the HAC in operation. Furthermore, the temperature differences between downcomer inlet to outlet obtained by direct observation are of a magnitude that verifies ‘nearly isothermal’ compression predictions made by Pavese et al (2016), which are also produced by the Young (2017) high fidelity HAC process model. In these senses, this thesis forms an important part of the evidence base for confident design of larger, commercial scale HAC installations.

Overall, through the work reported in this thesis, the Dynamic Earth HAC Demonstrator facility has been brought into a state of complete operational readiness to support an on going, high calibre, program of scientific investigation.

8.2 Ongoing work

Part of the experimental program has been completed. The characterization of pressure profiles in the downcomer pipe has revealed a potential mechanism of loss involving detrainment of air, free-fall of a water jet and re-entrainment of air. This discovery has sparked more experiments that aim to provide deeper understanding of this loss generating mechanism. In many senses the program of scientific investigation at the Dynamic Earth HAC has just started. For the Candidate, an immediate task will be to refine the HAC Demonstrator HMI by making further improvements to its functionality and by removing unnecessary computational tasks to reduce load and increase speed.

The experimental program designed for the coming months includes: conducting long duration tests of a few weeks or a month to assess performance over varying diurnal input temperature cycles, and to build up machine reliability statistics. Experiments will be conducted that will introduce a co-solute to the solute compressed gas in the water. The objective of these tests will be to determine whether the co-solutes will increase compressed air yield. The air-water mixing head currently installed in the system is one that replicates the design of a head fabricated over 100 years ago and installed in the Peterborough Lift Lock HAC. The forebay tank of the HAC Demonstrator already contains connection infrastructure to permit alternative air-water mixing head designs that aim to introduce less irreversibility into the HAC process, than the Peterborough Lift Lock design. Testing these new designs is another priority for the HAC Demonstrator at Dynamic Earth before project close out.

References

Abulnaga, B. E. (2002) ‘Slurry pipelines’, in *Slurry systems handbook*, pp. 1–34.

Chanson, H. (2004) ‘Hydraulics of Rectangular Dropshafts’, *Journal of Irrigation and Drainage Engineering*. Available at: http://staff.civil.uq.edu.au/h.chanson/reprints/jide04.pdf (Accessed: 14 April 2018).

Chanson, H. (2007) ‘Air entrainment processes in a full-scale rectangular dropshaft at large flows’, *Journal of Hydraulic Research*, 45(1), pp. 43–53. Available at: https://espace.library.uq.edu.au/data/UQ_12218/jhr06_1a.pdf?Expires=1523814358&Signature=ei~~xHy8XmdSRHcAkjMKVwPFjTYBs2niZDHWKgi34gNkNoYnNMFG2yfZX9GGGNOG0~OxRtTp3h4JXCdjlFwlYYVRRY4m-zMBZAYarqQXXZQVt6Xsvgu8IgBZP5vkj4F8i1kKK3m2Hsoy0U4Y~8f~kP~W7R0AvOQ9ONB8Df (Accessed: 14 April 2018).

Chen, L.-T. and Rice, W. (1982) ‘Some Psychometric Aspects of a Hydraulic Air Compressor (HAC)’, *Journal of Energy Resources Technology*. American Society of Mechanical Engineers, 104(3), p. 274. doi: 10.1115/1.3230415.

Chen, L.-T. and Rice, W. (1983) ‘Properties of Air Leaving a Hydraulic Air Compressor (HAC)’, *Journal of Energy Resources Technology*. American Society of Mechanical Engineers, 105(1), p. 54. doi: 10.1115/1.3230876.

Chirakalwasan, A. R. (2007) ‘Motor load and efficiency’, *Mechanical Engineering*, (1), pp. 21–33.

Clifford, T. P. (2016) ‘PhD Thesis Proposal Towards long term , high accuracy difference thermometer sets’.

Duarte, R., Schleiss, A. J. and Pinheiro, A. (2015) ‘Effect of pool confinement on pressures around a block impacted by plunging aerated jets’, *Canadian Journal of Civil Engineering*. NRC Research Press, 43(3), pp. 201–210. doi: 10.1139/cjce-2015-0246.

Electrale Innovation Ltd (2017) *Electrale Innovation Ltd – A development vehicle for low cost, low carbon gas compression using hydraulic air compressors*. Available at: https://electrale.com/ (Accessed: 15 December 2017).

Evans, G. M., Jameson, G. J. and Rielly, C. D. (1996) ‘Free jet expansion and gas entrainment characteristics of a plunging liquid jet’, *Experimental Thermal and Fluid Science*, 12(2), pp. 142–149. doi: 10.1016/0894-1777(95)00095-X.

Harr, M. E. (1987) *Reliability-Based Design in Civil Engineering.* McGraw-Hill.

Hutchison, A. (2018) *Air-water separator modeling for the hydraulic air compressor*. Laurentian

University (in preparation).

IDELCHIK, I. E. (1994) *Handbook of Hydraulic Resistance*. 3rd edition. Boca Raton, USA: CRC Press. Available at: https://www.nrc.gov/docs/ML1220/ML12209A041.pdf (Accessed: 29 March 2018).

Kobus, H. E. (1984) 'Local Air Entrainment and Detrainment', *Symposium on Scale Effects in Modelling Hydraulic Structures: Esslingen am Neckar, Germany, September 3-6, 1984*, pp. 1–10. Available at: http://elib.uni-stuttgart.de/opus/volltexte/2014/9624/pdf/kob50.pdf.

'Kolmogorov–Smirnov Test' (2008) in *The Concise Encyclopedia of Statistics*. New York, NY: Springer New York, pp. 283–287. doi: 10.1007/978-0-387-32833-1_214.

Krishna, R., Ellenberger, J. and Maretto, C. (1999) 'Flow regime transition in bubble columns', *International Communications in Heat and Mass Transfer*, 26(4), pp. 467–475. doi: 10.1016/S0735-1933(99)00032-9.

Lemmon, E. W., Huber, M. L. and McLinden, M. O. (2013) 'NIST Reference Fluid Thermodynamic and Transport Properties - REFPROP'. Available at: http://www.bldrdoc.gov/srd/upload/REFPROP9.pdf.

May, R. W. P. and Willoughby, I. R. (1991) 'Impact pressures in plunge basins to vertical falling jets', *HR Wallingford Report SR 242*. Available at: http://eprints.hrwallingford.co.uk/1108/1/SR242.pdf (Accessed: 29 December 2017).

McPherson, M. J. (2009) *Subsurface Ventilation and Environmental Engineering*. 2nd edn. Fresno: Mine Ventilation Services Inc. Available at: https://www.mvsengineering.com/index.php/products/96.

Millar, D. L. (2014) 'A review of the case for modern-day adoption of hydraulic air compressors', *Applied Thermal Engineering*. Pergamon, 69(1–2), pp. 55–77. doi: 10.1016/J.APPLTHERMALENG.2014.04.008.

Pavese, V., Millar, D. L. and Verda, V. (2016) 'Mechanical efficiency of hydraulic air compressors', *Journal of Energy Resources Technology*. American Society of Mechanical Engineers, 138(6), pp. 62005–62011. doi: 10.1115/1.4033623.

Reilly, I. G. *et al.* (1994) 'The role of gas phase momentum in determining gas holdup and hydrodynamic flow regimes in bubble column operations', *The Canadian Journal of Chemical Engineering*, 72(1), pp. 3–12. doi: 10.1002/cjce.5450720102.

Rice, W. (1976) 'Performance of Hydraulic Gas Compressors', *Journal of Fluids Engineering*. American Society of Mechanical Engineers, 98(4), p. 645. doi: 10.1115/1.3448437.

Rico, J. (2017) *Jet pump cooling for deep mines*. Available at: http://depositum.uqat.ca/729/1/Rico Paez%2C Javier.pdf (Accessed: 15 January 2018).

Riventa (2018) *FREEFLOW fixed thermodynamic pump monitoring system*. Available at: https://riventa.com/our-products/freeflow-fixed/ (Accessed: 16 January 2018).

Schulze, L. E. (1954) *Hydraulic Air Compressors*. Washington, D.C.: United States Department of the Interior.

Sivret, J. (2018) 'Experimental Estimation of the Absolute Roughness of Rubber Lined Pipes (Submitted)', *Flow measurement and Instrumentation*.

Software toolbox (2009) *TOP Server OPC & I/O Servers*. Available at: https://www.softwaretoolbox.com/topserver/ (Accessed: 15 December 2017).

Tchowa Medjiade, W., Rosenbaum Alvaro, A. and Schumpe, A. (2017) 'Flow regime transitions in a bubble column', *Chemical Engineering Science*, 170(April), pp. 263–269. doi: 10.1016/j.ces.2017.04.010.

Young, S. *et al.* (2015) 'Conceptual design of a modern-day hydraulic air compressor', in *ECOS 2015*. Pau: Energy Research Journal.

Young, S. *et al.* (2016) 'Interphase mass transfers in hydraulic air compressors for production of mine compressed air', in Canello, R. (ed.) *ENERMIN2016*. Santiago: Gecamin, pp. 87–97. Available at: http://www.gecaminpublications.com/enermin2016/.

Young, S. M. (2017) *Simulating air absorption in a hydraulic air compressor (HAC)*. Laurentian University. Available at: https://zone.biblio.laurentian.ca/handle/10219/2723.

Appendices

Use caption (References>Insert caption) with the label “Appendix” and letter numbering so they can be automatically updated and added to the List of Appendices section. Word will style them as “caption” but manually adjust to Heading 2 (remove numbering) so that they show up in the Table of Contents.

Appendix A: Process instrumentation diagram

Placeholder for the process instrumentation diagram that will be printed full sized.

Appendix B: Instrument wiring procedures

Compressed Air Flow Meter (FT4):

Controls Drawing HAC-J-87001

- Looking at the drawing there is two sets of wires coming from the Coriolis meter.
  - With two conductors and a ground used for power labelled as:
    - FT-4-L
    - FT-4-N
    - GND
  - The cable that will be used is labelled as 3C #14 TECK (3 Conductors / 14 American Wire Gauge).
  - With two conductors and a shield used for input labelled as:
    - FT-4-1
    - FT-4-2
  - The cable that will be used is labelled as 3C #16 TECK (3 Conductors / 16 American Wire Gauge).

Preparing the instrument for connection to the control panel:

1. Using the manual found on the MIRARCO server below,
   \\192.168.20.2\Projects\ERCM\Projects\HAC\Dynamic Earth HAC\Instrumentation & Equipment\FT 4 - Coriolis meter
   Identify the four connection terminals L-, L+, A, A+ which will be connected to the following wires FT-4-N, FT-4-L, FT-4-1, FT-4-2 respectively. We are using A and A+, although we originally thought this instrument was passive it seems to be active. As stated in the manual for an active connection A and A+ should be used, not A and A-. The conductors should be tightly screwed into each terminal accordingly.

Connecting the instrument to the control panel:

1. The FT-4-L conductor will then be connected to TB1 – 120VAC terminal 2A CB9.
2. The FT-4-N conductor will then be connected to TB1 – 120VAC terminal 9.
3. The FT-4-1 conductor will then be connected to TB3 terminal 7.
4. The FT-4-2 conductor will then be connected to TB3 terminal 8.

Intake Air Flow Meter (FT5):

Controls Drawing HAC-J-87002

- Looking at the drawing there is two sets of wires coming from the ultrasonic gas flow meter.
  - With two conductors and a ground used for power labelled as:
    - FT-5-L
    - FT-5-N
    - GND
  - The cable that will be used is labelled as 3C #14 TECK (3 Conductors / 14 American Wire Gauge).

  - With two conductors and a shield used for input labelled as:
    - FT-5-1
    - FT-5-2
  - The cable that will be used is labelled as 3C #16 TECK (3 Conductors / 16 American Wire Gauge).

Preparing the instrument for connection to the control panel:

1. Using the manual found on the MIRARCO server below,
   \\192.168.20.2\Projects\ERCM\Projects\HAC\Dynamic Earth HAC\Instrumentation & Equipment\FT 5 - Ultrasonic gas flow meter
   Identify the four connection terminals L-, L+, A, A+ which will be connected to the following wires FT-5-N, FT-5-L, FT-5-1, FT-5-2 respectively. We are using A and A+, although we originally thought this instrument was passive it seems to be active. As stated in the manual for an active connection A and A+ should be used, not A and A-. The conductors should be tightly screwed into each terminal accordingly.

Connecting the instrument to the control panel:

1. The FT-5-L conductor will then be connected to TB1 – 120VAC terminal 2A CB10.
2. The FT-5-N conductor will then be connected to TB1 – 120VAC terminal 10.
3. The FT-5-1 conductor will then be connected to TB4 terminal 9.
4. The FT-5-2 conductor will then be connected to TB4 terminal 10.

Forebay Tank Differential Pressure (DPT1 to DPT3):

Controls Drawing HAC-J-87010

- Looking at the drawing there is one set of wires coming from the differential pressure meter.
  - With two conductors and a shield used for power and input labelled as:
    - DPT-1-24VDC(+)
    - DPT-1-1
  - The cable that will be used is labelled as 1PR. #16 INST. TECK (1 Pair / 16 American Wire Gauge).

Preparing the instrument for connection to the control panel:

1. Using the manual found on the MIRARCO server below,
   \\192.168.20.2\Projects\ERCM\Projects\HAC\Dynamic Earth HAC\Instrumentation & Equipment\DPT 1-3 - Differential pressure
   Identify the two connection terminals 1(+) and 2(-) which will be connected to the following wires DPT-1-24VDC(+) and DPT-1-1 respectively.

Connecting the instrument to the control panel:

1. The DPT-1-24VDC(+) conductor will then be connected to TB4 – 24VDC terminal 2A FU1.
2. The DPT-1-1 conductor will then be connected to TB4 terminal 12.

Forebay Tank Differential Pressure (DPT2):

1. The DPT-2-24VDC(+) conductor will then be connected to TB4 – 24VDC terminal 2A FU2.

2. The DPT-2-1 conductor will then be connected to TB4 terminal 14.

Forebay Tank Differential Pressure (DPT3):

1. The DPT-3-24VDC(+) conductor will then be connected to TB4 – 24VDC terminal 2A FU3.
2. The DPT-3-1 conductor will then be connected to TB4 terminal 16.

Forebay Tank Level (LT1-LT3):

Controls Drawing HAC-J-87020

- Looking at the drawing there is one set of wires coming from the level sensor.
    - With two conductors and a shield used for power and input labelled as:
        - LT-1-24VDC(+)
        - LT-1-1

    - The cable that will be used is labelled as 1PR. #16 INST. TECK (1 Pair / 16 American Wire Gauge).

Preparing the instrument for connection to the control panel:

1. Using the manual found on the MIRARCO server below,
    \\192.168.20.2\Projects\ERCM\Projects\HAC\Dynamic Earth HAC\Instrumentation & Equipment\LT 1-3 - Ultrasonic level & Guided wave radar

    Identify the two connection terminals (+) and (-) which will be connected to the following wires LT-1-24VDC(+) and LT-1-1 respectively.

Connecting the instrument to the control panel:

1. The LT-1-24VDC(+) conductor will then be connected to TB5 – 24VDC terminal 2A FU1.
2. The LT-1-1 conductor will then be connected to TB4 terminal 2.

Forebay Tank Level (LT2):

1. The LT-2-24VDC(+) conductor will then be connected to TB5 – 24VDC terminal 2A FU2.
2. The LT-2-1 conductor will then be connected to TB4 terminal 4.

Forebay Tank Level (LT3):

1. The LT-3-24VDC(+) conductor will then be connected to TB5 – 24VDC terminal 2A FU3.
2. The LT-3-1 conductor will then be connected to TB4 terminal 6.

Barometric Pressure Sensor (PT17):

Controls Drawing HAC-J-87050

- Looking at the drawing there is one set of wires coming from the control valve.
    - With three conductors, used for power and input, labelled as:
        - PT-17-24DC(+)
        - PT-17-1
        - PT-17-24DC(-)
- The cable that will be used is labelled as 3C #16 TEW (3 Conductors / 16 American Wire Gauge).

Preparing the instrument for connection to the control panel:

2. Using the datasheet found on the MIRARCO server below,
   \\192.168.20.2\Projects\ERCM\Projects\HAC\Dynamic Earth HAC\Instrumentation & Equipment\PT 17 - Barometer
   Identify the three connection pins +Vs, -Vs, Vout, which will be connected to the following wires PT-17-24DC(+), PT-17-24DC(-), and PT-17-1 respectively. The conductors should be soldered to each pin accordingly.

Connecting the instrument to the control panel:

3. The PT-17-24DC(+) conductor will be connected to TB5 – 24DC terminal 2A FU8.
4. The PT-17-1 conductor will be connected to TB5 terminal 16.
5. The PT-17-24DC(-) conductor will be connected to TB – 24DC terminal 8, the one below the black boxes, not to be confused with the terminal 8 above the black boxes. This terminal is already occupied by a wire that is completing the circuit within the control panel and will need to be slotted into the same slot as the existing wire.

Air Intake Temperature and Humidity (TT-17 and GT-1 to TT-18 and GT-2):

- Looking at the manual there is one set of wires coming from the T/RH instrument.
  - With five conductors, used for Modbus power and input, labelled as:
    - Comms A (Brown)
    - Comms B (White)
    - 0V (Blue)
    - 5+ to 28+ V (Black)
    - 0V (Grey)
- Not sure which cable we are supposed to be using, but you will need a CAT cable or adapter and a M12 5pin 5wire female adapter.

Preparing the instrument for connection to the control panel:

1. Using the datasheet found on the MIRARCO server below,
   \\192.168.20.2\Projects\ERCM\Projects\HAC\Dynamic Earth HAC\Instrumentation & Equipment\TT 17-18 & GT 1 -2 - Temp and humid
   Connect all 5 coloured wires to the appropriate connection on the adapter.

Connecting the instrument to the CAT cable:

1. The Comms A (Brown) conductor will be connected to the Orange/White conductor.
2. The Comms B (White) conductor will be connected to the Orange conductor.
3. The 0V (Blue) conductor will be connected to the Blue conductor
4. The 5+ to 28+ V (Black) conductor will be connected to the Green/White conductor
5. The 0V (Grey) conductor will be connected to the Green conductor.

Connecting the instrument to the control panel:

1. Both 0V cables will then be combined and connected to another wire that will connect to a ground, TB6-24VDC terminal 1 on the control panel.

2. The 5+ to 28+ V (Black) conductor must then also be connected to another wire that will connect to the power, TB6-24VDC terminal 2A FU1. This will provide power to the instrument.
3. The CAT cable end is then plugged into one of the IDC ports on the panel.

Mechanized Control Valve (FCV1):

Controls Drawing HAC-J-87070

- Looking at the drawing there are two sets of wires coming from the control valve.
    - 120VAC INPUT, used for power, with three conductors labelled as:
        - FCV-1-L
        - FCV-1-N
        - GND
    - 4-20mA INPUT, used for signal read/write, with two conductors labelled as:
        - FCV-1-1
        - FCV-1-2
- The cable that will be used for the 120VAC INPUT is labelled as 3C #14 TECK (3 Conductors / 14 American Wire Gauge), and the cable that will be used for the 4-20mA INPUT is labelled as 1Pr. #16 INST TECK (1 Pair / 16 American Wire Gage).

Preparing the instrument for connection to the control panel:

1. Follow the instructions in section 10.2.2 Access to the connection terminals in the manual found here,
    a. http://www.burkert.com/en/Media/plm/MAN/MA/MA3360-Manual-EU-EN.pdf?id=MAN000000000000001000274112ENB.
2. Identify connection terminals,
    a. 9 and 10 which will be used to power the instrument (120VAC INPUT).
    b. 7 and 8 which will be used for read/write signals (4-20mA INPUT).

Connecting the 120VAC INPUT to the control panel:

1. Grab an appropriate length of the 3C #14 TECK cable required to extend from the control panel to where the instrument will be installed. Estimated lengths can be seen on drawing HAC-H-89000 to HAC-H-89004.
2. Strip a short section of the cover off one end of the cable exposing the two wires.
3. Strip each of the two wires allowing enough room to plug the wires into the instrument terminals.
4. Assign each of the two wires to one of the two terminals (9, 10) and insert them. Ensure they are snug.
5. Strip a short section of the cover off the other end of the cable exposing the two wires, ensure enough of the cover is removed due to the terminals on the control panel being connected to are not adjacent.
6. Strip each of the two wires allowing them enough room to connect to the control panel terminals.

7. The wire that is connected to terminal 10 on the instrument will be connected to FU14-2A on TB2 on the control panel. Loosen the screw, insert the wire, tighten the screw. Ensure the wire is not loose and is properly inserted and will not fall out of FU14-2A.
8. The wire that is connected to terminal 9 on the instrument will be connected to terminal 14 on TB2 on the control panel. Loosen the screw, insert the wire, tighten the screw. Ensure the wire is not loose and is properly inserted and will not fall out of terminal 14.

Connecting the 4-20mA INPUT to the control panel:

1. Grab an appropriate length of the 1Pr. #16 INST TECK cable required to extend from the control panel to where the instrument will be installed. Estimated lengths can be seen on drawing HAC-H-89000 to HAC-H-89004.
2. Strip a short section of the cover off one end of the cable exposing the two wires.
3. Strip each of the two wires allowing enough room to plug the wires into the instrument terminals.
4. Assign each of the two wires to one of the two terminals (7 and 8) and insert them. Ensure they are snug.
5. The wire plugged into terminal 8 will be the designated FCV-1-1 (+) wire, and the wire plugged into terminal 7 will be the designated FCV-1-2 (-) wire.
6. Strip a short section of the cover off the other end of the cable exposing the two wires.
7. Strip each of the two wires allowing them enough room to connect to the control panel terminals.
8. The FCV-1-1 (+) wire that is connected to terminal 8 on the instrument will be connected to TB7 terminal 2 on the control panel. Loosen the screw, insert FCV-1-1, tighten the screw. Ensure the wire is not loose and is properly inserted and will not fall out of TB7 terminal 2.
9. The FCV-1-2 (-) wire that is connected to terminal 7 on the instrument will be connected to TB7 terminal 3 on the control panel. Loosen the screw, insert FCV-1-2, tighten the screw. Ensure the wire is not loose and is properly inserted and will not fall out of TB7 terminal 3.

Connecting the additional output position signal from the valve:

1. Grab two wires of appropriate length and strip both ends of each wire.
2. Connect each of the wires to terminals 19 and 20 on the valve.
3. The wire connected to terminal 19 on the valve is attached to TB6 terminal 16 on the control panel.
4. The wire connected to terminal 20 on the valve is attached to TB6 terminal 15 on the control panel.

Appendix C: Dynamic Earth HAC instrument photos

FT1 – Water flowmeter

FT2 - Waterflowmeter

Motor/Pump 1

Motor/Pump 2

FT4 – Coriolis meter

FT5 – Optisonic flowmeter

DPT1 – Differential pressure sensor

DPT2 – Differential pressure sensor

DPT3 – Differential pressure sensor

LT3 – Water level sensor

LT1 – Water level sensor

LT2 – Water level sensor

TT1/GT1 – Temperature and humidity sensor

TT2/GT2 – Temperature and humidity sensor

MCV – Motorized control valve

PVRV – Pressure vacuum relief valve

	
VFD1, VFD2 – Variable frequency drives	JT – Power meters
	
CP1 – Control panel (Closed)	CP1 – Control panel (Open)

Appendix D: SQL Express procedure and automatic query script

```
% SQLtoMatFile query's SQL for all of the data tha5t was recorded between
% a specified Time1 and Time2.
function SQLtoMatFile(Time1,Time2)
% Example [Data] = SQLtoMatFile('2017-04-19 14:00:00','2017-04-19 14:30:00')
% TagMatrix contains strings for the tags that are going to be read on the
% SQL database.
TagMatrix = {'Analogue Inputs.I/O-1.DPT-1','Analogue Inputs.I/O-1.DPT-2',...
    'Analogue Inputs.I/O-1.DPT-3','Analogue Inputs.I/O-1.FT-1',...
    'Analogue Inputs.I/O-1.FT-2','Analogue Inputs.I/O-1.FT-4',...
    'Analogue Inputs.I/O-1.FT-5','Analogue Inputs.I/O-2.LT-1',...
    'Analogue Inputs.I/O-2.LT-2','Analogue Inputs.I/O-2.LT-3',...
    'Analogue Inputs.I/O-2.PT-17','Analogue Inputs.I/O-3.FCV-2',...
    'ABB_Test.VFD#1.SpeedACT-1','ABB_Test.VFD#2.SpeedACT-2',...
    'Power metering.CVM1.kW_Tot','Power metering.CVM2.kW_Tot',...
    'GTW-1 Port 1.Pump_1.In67','GTW-1 Port 1.Pump_1.In89',...
    'GTW-1 Port 1.Pump_2.In67','GTW-1 Port 1.Pump_2.In89',...
    'GTW-1 Port 1.Pump_1.RTR1','GTW-1 Port 1.Pump_1.RTR2',...
    'GTW-1 Port 1.Pump_2.RTR1','GTW-1 Port 1.Pump_2.RTR2',...
    'GTW-1 Port 1.DowncomerShaft.RTR1','GTW-1 Port 1.DowncomerShaft.RTR2',...
    'GTW-1 Port 3 (T+RH) Top.Temp/RH 1.GT1',...
    'GTW-1 Port 3 (T+RH) Top.Temp/RH 1.TT1',...
    'GTW-1 Port 4 (T+RH) Bottom.Temp/RH 2.GT2',...
    'GTW-1 Port 4 (T+RH) Bottom.Temp/RH 2.TT2',...
    'ABB_Test.VFD#1.TorqPerc-1','ABB_Test.VFD#2.TorqPerc-2',...
    'Analogue Outputs.I/O-4.FCV-1'};
VariableMatrix = {};
% Connection string, used to connect to the SQL database.
cn_str = 'PROVIDER=SQLOLEDB; Data Source=DELLT1700-2\SQLEXPRESS; Initial
Catalog=HAC; Integrated Security=SSPI;';
% Database, connects to the database and assigns it to a MATLAB variable.
DB = adodb_connect(cn_str);
% Formatting for the SQL query's.
QueryPart1 = 'SELECT TagValue FROM HAC.dbo.Nov13th2017 WHERE TagTimestamp >
''';
QueryPart2 = Time1;
QueryPart3 = ''' and TagTimestamp < ''';
QueryPart4 = Time2;
QueryPart5 = ''' and TagItemID = ''';
QueryPart7 = '''';
% Loop which performs automatic query's for the tags
for Count = 1:33
    QueryPart6 = TagMatrix{1,Count};
    SQL = strcat(QueryPart1, QueryPart2, QueryPart3, QueryPart4,...
        QueryPart5, QueryPart6, QueryPart7);
    Data = adodb_query(DB,SQL);
    Data = cell2mat(getfield(Data,'tagvalue'));
    VariableMatrix{1,Count} = Data;
end
% Assign all of the data to the corresponding MATLAB variable names for
storage.
DPT1_Data = VariableMatrix{1,1};
DPT2_Data = VariableMatrix{1,2};
DPT3_Data = VariableMatrix{1,3};
```

```
FT1_Data = VariableMatrix{1,4};
FT2_Data = VariableMatrix{1,5};
FT4_Data = VariableMatrix{1,6};
FT5_Data = VariableMatrix{1,7};
LT1_Data = VariableMatrix{1,8};
LT2_Data = VariableMatrix{1,9};
LT3_Data = VariableMatrix{1,10};
PT17_Data = VariableMatrix{1,11};
FCV2_Data = VariableMatrix{1,12};
SpeedACT1_Data = VariableMatrix{1,13};
SpeedACT2_Data = VariableMatrix{1,14};
Power1_Data = VariableMatrix{1,15};
Power2_Data = VariableMatrix{1,16};
P1P1_Data = VariableMatrix{1,17};
P1P2_Data = VariableMatrix{1,18};
P2P1_Data = VariableMatrix{1,19};
P2P2_Data = VariableMatrix{1,20};
P1T1_Data = VariableMatrix{1,21};
P1T2_Data = VariableMatrix{1,22};
P2T1_Data = VariableMatrix{1,23};
P2T2_Data = VariableMatrix{1,24};
D1T1_Data = VariableMatrix{1,25};
D1T2_Data = VariableMatrix{1,26};
GT1_Data = VariableMatrix{1,27};
TT1_Data = VariableMatrix{1,28};
GT2_Data = VariableMatrix{1,29};
TT2_Data = VariableMatrix{1,30};
TorqPerc1_Data = VariableMatrix{1,31};
TorqPerc2_Data = VariableMatrix{1,32};
FCV1_Data = VariableMatrix{1,33};
% Save all of the variables in the appropriate folder on the PC.
datetime=Time1;
datetime=strrep(datetime,':','_'); %Replace colon with underscore
datetime=strrep(datetime,'-','_');%Replace minus sign with underscore
datetime=strrep(datetime,' ','_');%Replace space with underscore
datetime=strcat('C:\HAC Data Archive\Saved States\',datetime,'.mat');
save(datetime,'DPT1_Data','DPT2_Data','DPT3_Data','FT1_Data',...
    'FT2_Data','FT4_Data','FT5_Data','LT1_Data','LT2_Data','LT3_Data',...
    'PT17_Data','FCV2_Data','SpeedACT1_Data','SpeedACT2_Data',...
    'Power1_Data','Power2_Data','P1P1_Data','P1P2_Data','P2P1_Data',...
    'P2P2_Data','P1T1_Data','P1T2_Data','P2T1_Data','P2T2_Data',...
    'D1T1_Data','D1T2_Data','GT1_Data','TT1_Data','GT2_Data','TT2_Data',...
    'TorqPerc1_Data','TorqPerc2_Data','FCV1_Data');
end
```

Appendix E: PID loop MATLAB script

```
function b = PIDLoop(app)
    % PIDLoop function sets up a timer with the following parameters,
    % and loads the required tags that are being checked on every
    % tick. A start function (@TimeStart), stop function (@TimeStop),
    % and per tick function (@PerTick) are also defined.
    Time = 1;
    b = timer('ExecutionMode','fixedRate','Period',...
        Time,'TimerFcn',...
        @PerTick,'StartFcn',@TimeStart, 'StopFcn',@TimeStop);
    load('OPCVariables.mat','DynamicHACOPC','FCV1','LT3',...
        'MainController','FCV2');
    PreviousError = 0;
    % PID loop parameters
    Kp = 25000; % Old value 75000
    Ki = 800; % Old value 3409
    Kd = 14000; % Old value 206250
    Integral = 0;
    Derivative = 0;
    % Place holder if any specific tasks need to be finished at the start of
the PID loop.
    function TimeStart(obj,evt)

    end
    % Connects to the OPC server, checks for the error between the setpoint
and the actual position of the valve
    % then runs that error through the PID function and outputs a change to
the system to approach the setpoint.
    function PerTick(obj,evt)
        connect(DynamicHACOPC);
        SeparatorSetLevel = app.SeparatorSetLevelEditField.Value;
        SeparatorLevel = PullValueFnc(LT3)/65536*2.83464;
        Error = SeparatorSetLevel - SeparatorLevel;
        Integral = Integral + Error*Time;
        Derivative = (Error - PreviousError)/Time ;
        Output = Kp*Error + Ki*Integral + Kd*Derivative;
        if Output > 4095
            Output = 4095;
        elseif Output < 0
            Output = 0;
        end
        PreviousError = Error;
        writeasync(FCV1,Output);
    end
    % Whenever the PID loop stops, the valve is closed.
    function TimeStop(obj,evt)
        connect(DynamicHACOPC);
        writeasync(FCV1,0);
        ValveError = round(PullValueFnc(FCV1)/4095*100,2) -
round(PullValueFnc(FCV2)/65536*100,2);
        while abs(ValveError) >=0.8
            app.FCV2EditField.Value =
round(double(PullValueFnc(FCV2))/65536*100,2);
```

```
            ValveError = round(PullValueFnc(FCV1)/4095*100,2) -
round(PullValueFnc(FCV2)/65536*100,2);
        end
        app.FCV2EditField.Value =
round(double(PullValueFnc(FCV2))/65536*100,2);
        app.Lamp_13.Color = [1 0 0];
    end
end
```

Appendix F: Automated benchmark test MATLAB script

```
% The HMI Benchmark Test runs on a MATLAB timer loop which is defined in the
following function.
function a = BenchmarkLoop(app)
    a = timer('ExecutionMode','fixedRate','Period',...
        1,'TimerFcn',@PerTick,...
        'StartFcn',@TimeStart, 'StopFcn',@TimeStop);
    % Load all of the necessary variables that are needed from the OPC
server.
    load('OPCVariables.mat','DynamicHACOPC','SpeedACT1','SpeedACT2',...
        'CW1','CW2','PT17','RTR1D1','FCV1','SpeedREF1','SpeedREF2',...
        'TT1');
    % Connect to the OPC server.
    connect(DynamicHACOPC);
    % Setpoints for the benchmark test.
    BenchmarkSpeeds = [600, 650, 700, 750, 800, 850, 880];
    % Number of seconds for each setpooint
    BenchmarkInterval = 480; %Loop Ticks, Benchmark Interval - 1 = Interval
Time
    NumberOfSetpoints = length(BenchmarkSpeeds);
    Count = 0;
    SpeedCount = 1;
    % Index of Saved States file location in order to record time stamps.
    FileLocation = 'C:\HAC Data Archive\Index of Saved States.xlsx';
    Sheet = 'Sheet1';
    % Parameters that will get recorded in the Index.
    xlsVector = []; %[Lid,V,Level,RPM,T,Patm,Y,M,D,H,M,S,Dialog]
    % Function that runs at the start of every benchmark test.
    function TimeStart(obj,evt)
        % Text prompt to input any specific notes for this benchmark test.
        Dialog = char(inputdlg('Notes:','Benchmark Log Notes',[1 50]));
        % Identify the location of the next entry in the Index.
        NumberOfNextEntry = string(size(xlsread(FileLocation),1) + 1);
        BMCount = xlsread(FileLocation,Sheet,'M1:M1');
        CellRange = strcat('A',NumberOfNextEntry,':','G',NumberOfNextEntry);
        % Set the speed of the VFD's to the first set point.
        SetSpeed = BenchmarkSpeeds(1,SpeedCount);
        writeasync(SpeedREF1,SetSpeed/880*20000);
        writeasync(SpeedREF2,SetSpeed/880*20000);
        % Get the timestamp for the start of the test and note it in the
Index.
        DateString = clock;
        DateString(1,6) = round(DateString(1,6),0);
        DateString = string(DateString);
        Year = num2str(double(DateString(1,1)));
        Month = num2str(double(DateString(1,2)));
        if strlength(Month) == 1
            Month = ['0',Month];
        end
        Day = num2str(double(DateString(1,3)));
        if strlength(Day) == 1
            Day = ['0',Day];
        end
        Hour = num2str(double(DateString(1,4)));
```

```
        if strlength(Hour) == 1
            Hour = ['0',Hour];
        end
        Minute = num2str(double(DateString(1,5)));
        if strlength(Minute) == 1
            Minute = ['0',Minute];
        end
        Second = num2str(double(DateString(1,6)));
        if strlength(Second) == 1
            Second = ['0',Second];
        end
        DateString = strcat('''',Year,'_',Month,'_',Day,'_',...
            Hour,'_',Minute,'_',Second);
        % Write all of the parameters to the Index
        xlsVector =
[0,app.WaterVolume,app.SeparatorSetLevelEditField.Value,SetSpeed,...
            PullValueFnc(TT1),PullValueFnc(PT17)/65536*300+800,{DateString}];
        xlswrite(FileLocation,xlsVector,Sheet,CellRange);
        CellRange3 = strcat('M',NumberOfNextEntry,':','N',NumberOfNextEntry);
        xlswrite(FileLocation,[{BMCount},{Dialog}],Sheet,CellRange3);
        SpeedCount = SpeedCount + 1;
        % Change the colour of the lamp on the HMI
        app.Lamp_15.Color = [0 1 0];
    end
    % Function that occurs every itteration of the timer.
    function PerTick(obj,evt)
        % Tracking if the final setpoint has finished, when it does it stops
the timer.
        Count = Count + 1;
        if mod(Count,BenchmarkInterval) == 0 && SpeedCount ==
NumberOfSetpoints + 1
            Count = 1;
            stop(a);
        end
        % Note all of the parameters for the HAC system in the Index at the
start of every set point.
        if mod(Count,BenchmarkInterval) == 0
            % Connect to the OPC server.
            connect(DynamicHACOPC);
            NumberOfNextEntry = string(size(xlsread(FileLocation),1) + 1);
            BMCount = xlsread(FileLocation,Sheet,'M1:M1');
            CellRange =
strcat('A',NumberOfNextEntry,':','G',NumberOfNextEntry);
            SetSpeed = BenchmarkSpeeds(1,SpeedCount);
            writeasync(SpeedREF1,SetSpeed/880*20000);
            writeasync(SpeedREF2,SetSpeed/880*20000);
            DateString = clock;
            DateString(1,6) = round(DateString(1,6),0);
            DateString = string(DateString);
            Year = num2str(double(DateString(1,1)));
            Month = num2str(double(DateString(1,2)));
            if strlength(Month) == 1
                Month = ['0',Month];
            end
            Day = num2str(double(DateString(1,3)));
```

```
            if strlength(Day) == 1
                Day = ['0',Day];
            end
            Hour = num2str(double(DateString(1,4)));
            if strlength(Hour) == 1
                Hour = ['0',Hour];
            end
            Minute = num2str(double(DateString(1,5)));
            if strlength(Minute) == 1
                Minute = ['0',Minute];
            end
            Second = num2str(double(DateString(1,6)));
            if strlength(Second) == 1
                Second = ['0',Second];
            end
            DateString = strcat('''',Year,'_',Month,'_',Day,'_',...
                Hour,'_',Minute,'_',Second);
            xlsVector =
[0,app.WaterVolume,app.SeparatorSetLevelEditField.Value,SetSpeed,...

PullValueFnc(TT1),PullValueFnc(PT17)/65536*300+800,{DateString}];
            xlswrite(FileLocation,xlsVector,Sheet,CellRange);
            SpeedCount = SpeedCount + 1;
        end
    end
    % This function runs whenever the benchmark test ends or is stopped.
    function TimeStop(obj,evt)
        % Connect to the OPC server.
        connect(DynamicHACOPC);
        NumberOfNextEntry = string(size(xlsread(FileLocation),1) + 1);
        CellRange = strcat('A',NumberOfNextEntry,':','G',NumberOfNextEntry);
        DateString = clock;
        DateString(1,6) = round(DateString(1,6),0);
        DateString = string(DateString);
        Year = num2str(double(DateString(1,1)));
        Month = num2str(double(DateString(1,2)));
        if strlength(Month) == 1
            Month = ['0',Month];
        end
        Day = num2str(double(DateString(1,3)));
        if strlength(Day) == 1
            Day = ['0',Day];
        end
        Hour = num2str(double(DateString(1,4)));
        if strlength(Hour) == 1
            Hour = ['0',Hour];
        end
        Minute = num2str(double(DateString(1,5)));
        if strlength(Minute) == 1
            Minute = ['0',Minute];
        end
        Second = num2str(double(DateString(1,6)));
        if strlength(Second) == 1
            Second = ['0',Second];
        end
```

```
        DateString = strcat('''',Year,'_',Month,'_',Day,'_',...
            Hour,'_',Minute,'_',Second);
        xlsVector = [0,0,0,0,0,0,{DateString}];
        xlswrite(FileLocation,xlsVector,Sheet,CellRange);
        writeasync(SpeedREF1,BenchmarkSpeeds(1,1)/880*20000);
        writeasync(SpeedREF2,BenchmarkSpeeds(1,1)/880*20000);
        app.Lamp_15.Color = [1 0 0];
    end
end
```

Appendix G: Data collection and analysis MATLAB script

```
% RawMatToMat takes an existing .mat file and converts all of the raw sets
% of data into measurements.
function RawMatToMat(Filename)
% Creating a string to load the desired file.
LoadFilename = strcat('C:\HAC Data Archive\Saved States\',Filename,'.mat');
load(LoadFilename,'DPT1_Data','DPT2_Data','DPT3_Data','FT1_Data',...
    'FT2_Data','FT4_Data','FT5_Data','LT1_Data','LT2_Data','LT3_Data',...
    'PT17_Data','FCV2_Data','SpeedACT1_Data','SpeedACT2_Data',...
    'Power1_Data','Power2_Data','P1P1_Data','P1P2_Data','P2P1_Data',...
    'P2P2_Data','P1T1_Data','P1T2_Data','P2T1_Data','P2T2_Data',...
    'D1T1_Data','D1T2_Data','GT1_Data','TT1_Data','GT2_Data','TT2_Data',...
    'TorqPerc1_Data','TorqPerc2_Data','FCV1_Data');
% Load the constants needed for conversion from an excel file.
Constants = xlsread('C:\HAC Data Archive\Constants','J2:J15');
% Load all of the polynomial constants for the temperature and pressure
% conversions.
Poly1 =  xlsread('C:\HAC Data Archive\Constants','B19:C19'); %in67P1
Poly2 = xlsread('C:\HAC Data Archive\Constants','B20:C20'); %in89P1
Poly3 = xlsread('C:\HAC Data Archive\Constants','B21:C21'); %in67P2
Poly4 = xlsread('C:\HAC Data Archive\Constants','B22:C22'); %in89P2
Poly5 = xlsread('C:\HAC Data Archive\Constants','B23:I23'); %RTR1P1
Poly6 = xlsread('C:\HAC Data Archive\Constants','B24:I24'); %RTR2P1
Poly7 = xlsread('C:\HAC Data Archive\Constants','B26:I26'); %RTR1P2
Poly8 = xlsread('C:\HAC Data Archive\Constants','B27:I27'); %RTR2P2
Poly9 =  xlsread('C:\HAC Data Archive\Constants','B29:I29'); %RTR1D1
Poly10 =  xlsread('C:\HAC Data Archive\Constants','B30:I30'); %RTR2D1
% Converts all of the raw data into measurements using the constants.
DPT1_Data = double(DPT1_Data)./65536.*Constants(1,1)-3000; % Pa
DPT2_Data = double(DPT2_Data)./65536.*Constants(2,1); % kPa
DPT3_Data = double(DPT3_Data)./65536.*Constants(3,1); % kPa
FT1_Data = double(FT1_Data)./65536.*Constants(4,1); % m3/s
FT2_Data = double(FT2_Data)./65536.*Constants(5,1); % m3/s
FT4_Data = double(FT4_Data)./65536.*Constants(6,1); % kg/s
FT5_Data = double(FT5_Data)./65536.*Constants(7,1); % m/s
LT1_Data = double(LT1_Data)./65536.*Constants(8,1); % m
LT2_Data = double(LT2_Data)./65536.*Constants(9,1); % m
LT3_Data = double(LT3_Data)./65536.*Constants(10,1); % m
PT17_Data = double(PT17_Data)./65536.*Constants(11,1)+800; % mbar
FCV2_Data = double(FCV2_Data)./65536.*Constants(12,1); % Percentage
FCV1_Data = double(FCV1_Data)./4095.*Constants(12,1);
SpeedACT1_Data = double(SpeedACT1_Data)./20000.*Constants(13,1); % rpm
SpeedACT2_Data = double(SpeedACT2_Data)./20000.*Constants(14,1); % rpm
Power1_Data = Power1_Data; % kW
Power2_Data = Power2_Data; % kW
TorqPerc1_Data = double(TorqPerc1_Data)./100; % Percentage
TorqPerc2_Data = double(TorqPerc2_Data)./100; % Percentage
P1P1_Data = polyval(Poly1,double(P1P1_Data)); % bar Pump1 Suction
P1P2_Data = polyval(Poly2,double(P1P2_Data)); % bar Pump1 Discharge
P2P1_Data = polyval(Poly3,double(P2P1_Data)); % bar Pump2 Suction
P2P2_Data = polyval(Poly4,double(P2P2_Data)); % bar Pump2 Discharge
P1T1_Data = polyval(Poly5,double(P1T1_Data)); % C
P1T2_Data = polyval(Poly6,double(P1T2_Data)); % C
P2T1_Data = polyval(Poly7,double(P2T1_Data)); % C
```

```
P2T2_Data = polyval(Poly8,double(P2T2_Data)); % C
D1T1_Data = polyval(Poly9,double(D1T1_Data)); % C
D1T2_Data = polyval(Poly10,double(D1T2_Data)); % C
GT1_Data = double(GT1_Data)./10; % Percentage
TT1_Data = double(TT1_Data)./10; % C
GT2_Data = double(GT2_Data)./10;  % Percentage
TT2_Data = double(TT2_Data)./10; % C
% Takes all of the measurements to calculate other quantities.
% Establishing a matrix size that will be consistent throughout all of the
% following calculations, 10 less to eliminate any chance of errors in
% dimensioning.
Size = length(DPT1_Data)-10;
% Elevation constants
LT1ReferenceReading = 0; % m
LT2ReferenceReading = 0; % m
LT3ReferenceReading = 0.598; % m
LT1ReferenceElevation = 298.328; % m old:298.33
LT2ReferenceElevation = 293.3177; % m old:293.333
LT3ReferenceElevation = 273.218; % m old:273.028
% Other constants
StandardAirDensity = 1.2; % kg/m3
Gravity = 9.80665; % m/s^2
FT5_Diameter = 0.09717; % m
CalibrationCoefficient = 1.025; % Used for FT5 calibration
% Establishing empty matrices for the following CoolProp calculations.
InletAirDensity_Data = zeros(Size,1);
InletPump1WaterDensity_Data = zeros(Size,1);
InletPump2WaterDensity_Data = zeros(Size,1);
OutletPump1WaterDensity_Data = zeros(Size,1);
OutletPump2WaterDensity_Data = zeros(Size,1);
% For loop that will calculate all of the required densities from the
% measured pressures, temperatures, and humidities using CoolProp.
for x = 1:Size
    InletAirDensity_Data(x,1) = 1/CoolProp.HAPropsSI('Vha','P',...
        PT17_Data(x,1)/0.01-134, 'T', TT1_Data(x,1)+273.15, 'RH',...
        GT1_Data(x,1)/100); % kg moist air/m3
    InletPump1WaterDensity_Data(x,1) = CoolProp.PropsSI('D','P',...
        abs(P1P1_Data(x,1))*100000, 'T',P1T1_Data(x,1)+273.15,'water');
    % kg/m3
    InletPump2WaterDensity_Data(x,1) = CoolProp.PropsSI('D','P',...
        abs(P2P1_Data(x,1))*100000, 'T',P2T1_Data(x,1)+273.15,'water');
    % kg/m3
    OutletPump1WaterDensity_Data(x,1) = CoolProp.PropsSI('D','P',...
        abs(P1P2_Data(x,1))*100000, 'T',P1T2_Data(x,1)+273.15,'water');
    % kg/m3
    OutletPump2WaterDensity_Data(x,1) = CoolProp.PropsSI('D','P',...
        abs(P2P2_Data(x,1))*100000, 'T',P2T2_Data(x,1)+273.15,'water');
    % kg/m3
end
% Calculated quantities
FT5_EffectiveDiameter = FT5_Diameter*CalibrationCoefficient;
InletVolumeFlowRate_Data =
FT5_Data(1:Size).*(FT5_EffectiveDiameter^2)./4.*pi();
InletMassFlowRate_Data = InletVolumeFlowRate_Data.*InletAirDensity_Data; %
kg/s
```

```
Pump1DifferentialPressure_Data = (P1P2_Data(1:Size) - ...
    P1P1_Data(1:Size)).*1000; % mbar
Pump2DifferentialPressure_Data = (P2P2_Data(1:Size) - ...
    P2P1_Data(1:Size)).*1000;% mbar
Pump1DifferentialTemperature_Data = (P1T2_Data(1:Size) - ...
    P1T1_Data(1:Size)).*1000; % mK
Pump2DifferentialTemperature_Data = (P2T2_Data(1:Size) - ...
    P2T1_Data(1:Size)).*1000; % mK
DowncomerDifferentialTemperature_Data = (D1T2_Data(1:Size) - ...
    D1T1_Data(1:Size)).*1000; % mK
Pump1MassFlowRate_Data = FT1_Data(1:Size)...
    .*InletPump1WaterDensity_Data; % kg/s
Pump2MassFlowRate_Data = FT2_Data(1:Size)...
    .*InletPump2WaterDensity_Data; % kg/s
DPT2Level = DPT2_WaterLevel(FT1_Data,FT2_Data,D1T1_Data,PT17_Data,...
    DPT2_Data);
LT1Elevation = sum(LT1_Data)/length(LT1_Data)+ LT1ReferenceReading + ...
    LT1ReferenceElevation; % m AD
LT2Elevation = sum(LT2_Data)/length(LT2_Data)+ LT2ReferenceReading + ...
    LT2ReferenceElevation; % m AD
LT3Elevation = sum(LT3_Data)/length(LT3_Data)+ LT3ReferenceReading + ...
    LT3ReferenceElevation; % m AD
DPT2Elevation = DPT2Level + LT2ReferenceReading + ...
    LT2ReferenceElevation; % m
AvailableHead = LT1Elevation - LT2Elevation; % m
AvailableHead2 = LT1Elevation - DPT2Elevation;% m
Depth = LT2Elevation - LT3Elevation; % m
Depth2 = DPT2Elevation - LT3Elevation; % m
TotalWaterFlowRate = sum(FT1_Data)/length(FT1_Data) + ...
    sum(FT2_Data)/length(FT2_Data); % m3/s
AverageAirFlowOut = sum(FT4_Data)/length(FT4_Data); %kg/s
AverageFAD = AverageAirFlowOut/StandardAirDensity*2119; % Scfm
AverageHydroPower = 10*AvailableHead*TotalWaterFlowRate; % kW
AveragePowerSupplied = sum(Power1_Data)/length(Power1_Data) + ...
    sum(Power2_Data)/length(Power2_Data); % kW
PumpEfficiency = AverageHydroPower/AveragePowerSupplied*100; % Percentage
AverageDeliveryPressure = sum(DPT3_Data)/length(DPT3_Data) + ...
    sum(PT17_Data)/length(PT17_Data)/10; % kPa (a)
AverageFlowWork = log(AverageDeliveryPressure/(sum(PT17_Data)/...
    length(PT17_Data)/10))/...
    log((sum(D1T2_Data)/length(D1T2_Data)+273.15)/(sum(D1T1_Data)/...
    length(D1T1_Data)+273.15))*287.056*(sum...
    (DowncomerDifferentialTemperature_Data)/length...
    (DowncomerDifferentialTemperature_Data))/1000;
AveragePneumaticPower = AverageFlowWork*AverageAirFlowOut/1000;
OverallEfficiency = AveragePneumaticPower/...
    AveragePowerSupplied*100; % Percentage
% Matrix containing a snapshot of the data contained in this file. This
% matrix is later converted into a .txt file.
MyData=[
    sum(SpeedACT2_Data)/length(SpeedACT2_Data),
    AvailableHead,
    AvailableHead2,
    Depth,
    Depth2,
```

```
    sum(FT1_Data)/length(FT1_Data),
    sum(FT2_Data)/length(FT2_Data),
    sum(InletMassFlowRate_Data)/length(InletMassFlowRate_Data),
    sum(FT4_Data)/length(FT4_Data),
    AveragePowerSupplied,
    ((sum(PT17_Data)/length(PT17_Data))/0.01-134)/1000,
    sum(TT2_Data)/length(TT2_Data),
    sum(GT2_Data)/length(GT2_Data),
    sum(DPT1_Data)/length(DPT1_Data),
    AverageDeliveryPressure,
    (sum(D1T1_Data)/length(D1T1_Data)+273.15),
    (sum(D1T2_Data)/length(D1T2_Data)+273.15),
    sum(DowncomerDifferentialTemperature_Data)/length...
    (DowncomerDifferentialTemperature_Data),
    sum(LT1_Data)/length(LT1_Data),
    sum(LT2_Data)/length(LT2_Data),
    DPT2Level,
    sum(LT3_Data)/length(LT3_Data),
    sum(DPT2_Data)/length(DPT2_Data),
    sum(DPT3_Data)/length(DPT3_Data),
    sum(P1P1_Data)/length(P1P1_Data),
    sum(P1P2_Data)/length(P1P2_Data),
    sum(P2P1_Data)/length(P2P1_Data),
    sum(P2P2_Data)/length(P2P2_Data)];
% Save all of the converted and calculated quantities in a new file.
SaveFilename = strcat('C:\HAC Data Archive\Computed Values\',Filename,...
    '-Adj.mat');
save(SaveFilename,'DPT1_Data','DPT2_Data','DPT3_Data','FT1_Data',...
    'FT2_Data','FT4_Data','FT5_Data','LT1_Data','LT2_Data','LT3_Data',...
    'PT17_Data','FCV2_Data','SpeedACT1_Data','SpeedACT2_Data',...
    'Power1_Data','Power2_Data','P1P1_Data','P1P2_Data','P2P1_Data',...
    'P2P2_Data','P1T1_Data','P1T2_Data','P2T1_Data','P2T2_Data',...
    'D1T1_Data','D1T2_Data','GT1_Data','TT1_Data','GT2_Data','TT2_Data',...
    'InletVolumeFlowRate_Data','InletAirDensity_Data',...
    'InletMassFlowRate_Data','InletPump1WaterDensity_Data',...
    'InletPump2WaterDensity_Data','OutletPump1WaterDensity_Data',...
    'OutletPump2WaterDensity_Data','Pump1DifferentialPressure_Data',...
    'Pump2DifferentialPressure_Data','Pump1DifferentialTemperature_Data',...
    'Pump2DifferentialTemperature_Data','Pump1MassFlowRate_Data',...
    'Pump2MassFlowRate_Data','DowncomerDifferentialTemperature_Data',...
    'LT1Elevation','LT2Elevation','LT3Elevation','AvailableHead',...
    'Depth','TotalWaterFlowRate','AverageFAD','AverageHydroPower',...
    'AveragePowerSupplied','PumpEfficiency','AverageDeliveryPressure',...
    'AverageFlowWork','AveragePneumaticPower','OverallEfficiency',...
    'TorqPerc1_Data','TorqPerc2_Data','FCV1_Data','DPT2Level','MyData',...
    'AvailableHead2','DPT2Elevation','Depth2');
End

% Automatic SQL query for the data collected during a specified
% benchmark test. The benchmark test is identified by opening the Index of
% Benchmark Tests and identifying the row number of that entry on the excel
% sheet.
function BenchmarkTestQuerySQL(RowNumber)
% Time stamps recorded in the spread sheet are stored in variables.
TimeStampRange = strcat('G',string(RowNumber),':G',string(RowNumber+7));
```

```
BMNumberRange = strcat('M',string(RowNumber),':M',string(RowNumber));
[Blank, TimeStamps] = xlsread('C:\HAC Data Archive\Index of Saved States',...
    TimeStampRange);
BMNumber = string(xlsread('C:\HAC Data Archive\Index of Saved States',...
    BMNumberRange));
% For loop to establish all 8 time frames that need to be queried for this
% particular benchmark test.
for x = 1:8
    DateTime = regexp(string(TimeStamps(x,1)),'_','split')';
    Year{x,1} = DateTime(1,1);
    Month{x,1} = DateTime(2,1);
    Day{x,1} = DateTime(3,1);
    Hour(x,1) = double(DateTime(4,1));
    Minute(x,1) = double(DateTime(5,1));
    % Formatting to ensure the saved files have the appropriate names.
    if Hour(x,1) < 10
        if Minute(x,1) < 10
            SQLTimes{x,1} = strcat(Year{x,1},'-',Month{x,1},'-',Day{x,1},...
                {' 0'},string(Hour(x,1)),':0',string(Minute(x,1)),':00');
            ConvertTimes{x,1} =
strcat(Year{x,1},'_',Month{x,1},'_',Day{x,1}...
                ,{'_0'},string(Hour(x,1)),'_0',string(Minute(x,1)),'_00');
        end
        if Minute(x,1) >= 10
            SQLTimes{x,1} = strcat(Year{x,1},'-',Month{x,1},'-',Day{x,1},...
                {' 0'},string(Hour(x,1)),':',string(Minute(x,1)),':00');
            ConvertTimes{x,1} =
strcat(Year{x,1},'_',Month{x,1},'_',Day{x,1}...
                ,{'_0'},string(Hour(x,1)),'_',string(Minute(x,1)),'_00');
        end
    end
    if Hour(x,1) >= 10
        if Minute(x,1) < 10
            SQLTimes{x,1} = strcat(Year{x,1},'-',Month{x,1},'-',Day{x,1},...
                {' '},string(Hour(x,1)),':0',string(Minute(x,1)),':00');
            ConvertTimes{x,1} =
strcat(Year{x,1},'_',Month{x,1},'_',Day{x,1}...
                ,{'_'},string(Hour(x,1)),'_0',string(Minute(x,1)),'_00');
        end
        if Minute(x,1) >= 10
            SQLTimes{x,1} = strcat(Year{x,1},'-',Month{x,1},'-',Day{x,1},...
                {' '},string(Hour(x,1)),':',string(Minute(x,1)),':00');
            ConvertTimes{x,1} =
strcat(Year{x,1},'_',Month{x,1},'_',Day{x,1}...
                ,{'_'},string(Hour(x,1)),'_',string(Minute(x,1)),'_00');
        end
    end
    Minute(x,1) = Minute(x,1) + 3;
    if double(DateTime(5,1)) + 3 > 59
        Minute(x,1) = Minute(x,1) - 60;
        Hour(x,1) = Hour(x,1) + 1;
    end
    if Hour(x,1) < 10
        if Minute(x,1) < 10
```

```
            SQLPlus3Times{x,1} = strcat(Year{x,1},'-',Month{x,1},'-
',Day{x,1},...
                {' 0'},string(Hour(x,1)),':0',string(Minute(x,1)),':00');
            ConvertPlus3Times{x,1} = strcat(Year{x,1},'_',Month{x,1},'_',...
Day{x,1},{'_0'},string(Hour(x,1)),'_0',string(Minute(x,1)),...
                '_00');
        end
        if Minute(x,1) >= 10
            SQLPlus3Times{x,1} = strcat(Year{x,1},'-',Month{x,1},'-
',Day{x,1},...
                {' 0'},string(Hour(x,1)),':',string(Minute(x,1)),':00');
            ConvertPlus3Times{x,1} = strcat(Year{x,1},'_',Month{x,1},...

'_',Day{x,1},{'_0'},string(Hour(x,1)),'_',string(Minute(x,1))...
                ,'_00');
        end
    end
    if Hour(x,1) >= 10
        if Minute(x,1) < 10
            SQLPlus3Times{x,1} = strcat(Year{x,1},'-',Month{x,1},'-
',Day{x,1},...
                {' '},string(Hour(x,1)),':0',string(Minute(x,1)),':00');
            ConvertPlus3Times{x,1} = strcat(Year{x,1},'_',Month{x,1},'_',...
                Day{x,1},{'_'},string(Hour(x,1)),'_0',string(Minute(x,1)),...
                '_00');
        end
        if Minute(x,1) >= 10
            SQLPlus3Times{x,1} = strcat(Year{x,1},'-',Month{x,1},'-
',Day{x,1},...
                {' '},string(Hour(x,1)),':',string(Minute(x,1)),':00');
            ConvertPlus3Times{x,1} = strcat(Year{x,1},'_',Month{x,1},'_',...
                Day{x,1},{'_'},string(Hour(x,1)),'_',string(Minute(x,1)),...
                '_00');
        end
    end
end
% Individual query for each of the 7 set points, and one overall query for
% the entire test using the established time frames.
disp('Querying raws for the entire test, start to finish.')
SQLtoMatFile(SQLTimes{1,1},SQLTimes{8,1});
disp('Querying raws for 600rpm data.')
SQLtoMatFile(SQLPlus3Times{1,1},SQLTimes{2,1});
disp('Querying raws for 650rpm data.')
SQLtoMatFile(SQLPlus3Times{2,1},SQLTimes{3,1});
disp('Querying raws for 700rpm data.')
SQLtoMatFile(SQLPlus3Times{3,1},SQLTimes{4,1});
disp('Querying raws for 750rpm data.')
SQLtoMatFile(SQLPlus3Times{4,1},SQLTimes{5,1});
disp('Querying raws for 800rpm data.')
SQLtoMatFile(SQLPlus3Times{5,1},SQLTimes{6,1});
disp('Querying raws for 850rpm data.')
SQLtoMatFile(SQLPlus3Times{6,1},SQLTimes{7,1});
disp('Querying raws for 880rpm data.')
SQLtoMatFile(SQLPlus3Times{7,1},SQLTimes{8,1});
% Converting all of the raw values taken from the query to measurements
```

```
% using the RawMatToMat function.
disp('Converting raws for the entire test, start to finish.')
RawMatToMat(ConvertTimes{1,1})
disp('Converting raws for 600rpm data.')
RawMatToMat(ConvertPlus3Times{1,1})
disp('Converting raws for 650rpm data.')
RawMatToMat(ConvertPlus3Times{2,1})
disp('Converting raws for 700rpm data.')
RawMatToMat(ConvertPlus3Times{3,1})
disp('Converting raws for 750rpm data.')
RawMatToMat(ConvertPlus3Times{4,1})
disp('Converting raws for 800rpm data.')
RawMatToMat(ConvertPlus3Times{5,1})
disp('Converting raws for 850rpm data.')
RawMatToMat(ConvertPlus3Times{6,1})
disp('Converting raws for 880rpm data.')
RawMatToMat(ConvertPlus3Times{7,1})
% Opening all of those converted files, collecting the MyData matrices and
% combining them for an overall matrix that will contain the important
% variables for all tests in one place for this benchmark test. Then saving
% that matrix in its own MATLAB file.
disp('Creating compiled process data file.')
Data000 = [0;0;0;0;0;0;0;0;0;0;0;0;0;0;0;0;0;0;0;0;0;0;0;0;0;0;0;0];
load(strcat('C:\HAC Data Archive\Computed Values\',ConvertPlus3Times{1,1},...
    '-Adj.mat'),'MyData');
Data600 = MyData;
load(strcat('C:\HAC Data Archive\Computed Values\',ConvertPlus3Times{2,1},...
    '-Adj.mat'),'MyData');
Data650 = MyData;
load(strcat('C:\HAC Data Archive\Computed Values\',ConvertPlus3Times{3,1},...
    '-Adj.mat'),'MyData');
Data700 = MyData;
load(strcat('C:\HAC Data Archive\Computed Values\',ConvertPlus3Times{4,1},...
    '-Adj.mat'),'MyData');
Data750 = MyData;
load(strcat('C:\HAC Data Archive\Computed Values\',ConvertPlus3Times{5,1},...
    '-Adj.mat'),'MyData');
Data800 = MyData;
load(strcat('C:\HAC Data Archive\Computed Values\',ConvertPlus3Times{6,1},...
    '-Adj.mat'),'MyData');
Data850 = MyData;
load(strcat('C:\HAC Data Archive\Computed Values\',ConvertPlus3Times{7,1},...
    '-Adj.mat'),'MyData');
Data880 = MyData;
Data = [Data000,Data600,Data650,Data700,Data750,Data800,Data850,Data880];
MetaData = {BMNumber,SQLTimes{1,1},string(datetime)};
save(strcat('C:\HAC Data Archive\Process Data\Data from
BM',BMNumber,'.mat'),...
    'Data','MetaData');
disp('Finished.')
end
% Converts a desired benchmark test MATLAB file containing all of the
% important quantities from a MATLAB matrix to a .txt file.
function Data2Text(BMNumber)
% Identify which file needs to be opened.
```

```
Filename = strcat('C:\HAC Data Archive\Process Data\Data from BM',BMNumber);
load(Filename,'Data','MetaData');
FileID = strcat('C:\HAC Data Archive\Text Files\Data from
BM',BMNumber,'.txt');
% Formatting for the .txt file
MetaFormat = ' %s\r\n';
MetaFormats = {strcat('Benchmark#',MetaFormat);...
    strcat('Date of BM',MetaFormat);...
    strcat('Date Published',MetaFormat)};
Format = '%4.2f\t%4.2f\t%4.2f\t%4.2f\t%4.2f\t%4.2f\t%4.2f\t%4.2f';
Formats = {strcat('\r\n','RPM:',Format);...
    strcat('\r\n','Head (LT2):',Format);...
    strcat('\r\n','Head (DPT2):',Format);...
    strcat('\r\n','Depth (LT2):',Format);...
    strcat('\r\n','Depth (DPT2):',Format);...
    strcat('\r\n','Flowrate 1:',Format);...
    strcat('\r\n','Flowrate 2:',Format);...
    strcat('\r\n','Inlet Mass Flow Rate:',Format);...
    strcat('\r\n','Outlet Mass Flow Rate:',Format);...
    strcat('\r\n','Power Supplied:',Format);...
    strcat('\r\n','P atm:',Format);...
    strcat('\r\n','TT1:',Format);...
    strcat('\r\n','GT1:',Format);...
    strcat('\r\n','DPT1:',Format);...
    strcat('\r\n','Average Delivery Pressure:',Format);...
    strcat('\r\n','D1T1:',Format);...
    strcat('\r\n','D1T1:',Format);...
    strcat('\r\n','Diff. T:',Format);...
    strcat('\r\n','LT1:',Format);...
    strcat('\r\n','LT2:',Format);...
    strcat('\r\n','LT2 (DPT2):',Format);...
    strcat('\r\n','LT3:',Format);...
    strcat('\r\n','DPT2:',Format);...
    strcat('\r\n','DPT3:',Format);...
    strcat('\r\n','Downcomer P1:',Format);...
    strcat('\r\n','Downcomer P2:',Format);...
    strcat('\r\n','Downcomer P3:',Format);...
    strcat('\r\n','Downcomer P4:',Format)};
% Take all of the information from the MATLAB file and print it into a .txt
% file.
for x = 1:3
    fprintf(fopen(FileID,'a'),MetaFormats{x,1},MetaData{1,x});
end
for x = 1:28
    fprintf(fopen(FileID,'a'),Formats{x,1},Data(x,1:8));
end
fclose('all');
end
```

Appendix H: KS statistic MATLAB script

```
% Function to calculate the KS statistic between every quantity for two
% separate benchmark tests.
function ksStatistic(Time1,Time2,Sig,Speed)
% First set of data
DataSet1 = load(strcat('C:\HAC Data Archive\Saved States\',Time1));
DataSet2 = load(strcat('C:\HAC Data Archive\Saved States\',Time2));
LT1_Data1 = sort(getfield(DataSet1,'LT1_Data'));
LT2_Data1 = sort(getfield(DataSet1,'LT2_Data'));
LT3_Data1 = sort(getfield(DataSet1,'LT3_Data'));
DPT1_Data1 = sort(getfield(DataSet1,'DPT1_Data'));
DPT2_Data1 = sort(getfield(DataSet1,'DPT2_Data'));
DPT3_Data1 = sort(getfield(DataSet1,'DPT3_Data'));
Power1_Data1 = sort(getfield(DataSet1,'Power1_Data'));
Power2_Data1 = sort(getfield(DataSet1,'Power2_Data'));
FT1_Data1 = sort(getfield(DataSet1,'FT1_Data'));
FT2_Data1 = sort(getfield(DataSet1,'FT2_Data'));
FT4_Data1 = sort(getfield(DataSet1,'FT4_Data'));
FT5_Data1 = sort(getfield(DataSet1,'FT5_Data'));
FCV2_Data1 = sort(getfield(DataSet1,'FCV2_Data'));
SpeedACT1_Data1 = sort(getfield(DataSet1,'SpeedACT1_Data'));
SpeedACT2_Data1 = sort(getfield(DataSet1,'SpeedACT2_Data'));
PT17_Data1 = sort(getfield(DataSet1,'PT17_Data'));
RTR1D1_Data1 = sort(getfield(DataSet1,'D1T1_Data'));
RTR2D1_Data1 = sort(getfield(DataSet1,'D1T2_Data'));
RTR1P1_Data1 = sort(getfield(DataSet1,'P1T1_Data'));
RTR2P1_Data1 = sort(getfield(DataSet1,'P1T2_Data'));
RTR1P2_Data1 = sort(getfield(DataSet1,'P2T1_Data'));
RTR2P2_Data1 = sort(getfield(DataSet1,'P2T2_Data'));
in67P1_Data1 = sort(getfield(DataSet1,'P1P1_Data'));
in89P1_Data1 = sort(getfield(DataSet1,'P1P2_Data'));
in67P2_Data1 = sort(getfield(DataSet1,'P2P1_Data'));
in89P2_Data1 = sort(getfield(DataSet1,'P2P2_Data'));
GT1_Data1 = sort(getfield(DataSet1,'GT1_Data'));
TT1_Data1 = sort(getfield(DataSet1,'TT1_Data'));
GT2_Data1 = sort(getfield(DataSet1,'GT2_Data'));
TT2_Data1 = sort(getfield(DataSet1,'TT2_Data'));
% Second set of data
LT1_Data2 = sort(getfield(DataSet2,'LT1_Data'));
LT2_Data2 = sort(getfield(DataSet2,'LT2_Data'));
LT3_Data2 = sort(getfield(DataSet2,'LT3_Data'));
DPT1_Data2 = sort(getfield(DataSet2,'DPT1_Data'));
DPT2_Data2 = sort(getfield(DataSet2,'DPT2_Data'));
DPT3_Data2 = sort(getfield(DataSet2,'DPT3_Data'));
Power1_Data2 = sort(getfield(DataSet2,'Power1_Data'));
Power2_Data2 = sort(getfield(DataSet2,'Power2_Data'));
FT1_Data2 = sort(getfield(DataSet2,'FT1_Data'));
FT2_Data2 = sort(getfield(DataSet2,'FT2_Data'));
FT4_Data2 = sort(getfield(DataSet2,'FT4_Data'));
FT5_Data2 = sort(getfield(DataSet2,'FT5_Data'));
FCV2_Data2 = sort(getfield(DataSet2,'FCV2_Data'));
SpeedACT1_Data2 = sort(getfield(DataSet2,'SpeedACT1_Data'));
SpeedACT2_Data2 = sort(getfield(DataSet2,'SpeedACT2_Data'));
PT17_Data2 = sort(getfield(DataSet2,'PT17_Data'));
```

```
RTR1D1_Data2 = sort(getfield(DataSet2,'D1T1_Data'));
RTR2D1_Data2 = sort(getfield(DataSet2,'D1T2_Data'));
RTR1P1_Data2 = sort(getfield(DataSet2,'P1T1_Data'));
RTR2P1_Data2 = sort(getfield(DataSet2,'P1T2_Data'));
RTR1P2_Data2 = sort(getfield(DataSet2,'P2T1_Data'));
RTR2P2_Data2 = sort(getfield(DataSet2,'P2T2_Data'));
in67P1_Data2 = sort(getfield(DataSet2,'P1P1_Data'));
in89P1_Data2 = sort(getfield(DataSet2,'P1P2_Data'));
in67P2_Data2 = sort(getfield(DataSet2,'P2P1_Data'));
in89P2_Data2 = sort(getfield(DataSet2,'P2P2_Data'));
GT1_Data2 = sort(getfield(DataSet2,'GT1_Data'));
TT1_Data2 = sort(getfield(DataSet2,'TT1_Data'));
GT2_Data2 = sort(getfield(DataSet2,'GT2_Data'));
TT2_Data2 = sort(getfield(DataSet2,'TT2_Data'));
% Data is all placed into a matrix.
DataSet1 = {LT1_Data1; LT2_Data1; LT3_Data1; DPT1_Data1; DPT2_Data1;
DPT3_Data1; Power1_Data1; Power2_Data1; FT1_Data1; ...
FT2_Data1; FT4_Data1; FT5_Data1; FCV2_Data1; SpeedACT1_Data1;
SpeedACT2_Data1; PT17_Data1; RTR1D1_Data1; ...
RTR2D1_Data1; RTR1P1_Data1; RTR2P1_Data1; RTR1P2_Data1; RTR2P2_Data1;
in67P1_Data1; in89P1_Data1; in67P2_Data1; ...
in89P2_Data1; GT1_Data1; TT1_Data1; GT2_Data1; TT2_Data1};
DataSet2 = {LT1_Data2; LT2_Data2; LT3_Data2; DPT1_Data2; DPT2_Data2;
DPT3_Data2; Power1_Data2; Power2_Data2; FT1_Data2; ...
FT2_Data2; FT4_Data2; FT5_Data2; FCV2_Data2; SpeedACT1_Data2;
SpeedACT2_Data2; PT17_Data2; RTR1D1_Data2; ...
RTR2D1_Data2; RTR1P1_Data2; RTR2P1_Data2; RTR1P2_Data2; RTR2P2_Data2;
in67P1_Data2; in89P1_Data2; in67P2_Data2; ...
in89P2_Data2; GT1_Data2; TT1_Data2; GT2_Data2; TT2_Data2};

HMatrix = [];
pMatrix = [];
DMatrix = [];
% Loop which computes the KS statistic between each data set.
for n = 1:30
    Data1 = DataSet1{n,1}';
    Data2 = DataSet2{n,1}';
    %Data1 = Data1(2:length(Data1));
    %Data2 = Data2(2:length(Data2));
    %Data1 = sort(xlsread('C:\HAC Data Archive\Index of Saved
States','KSTest','A2:A99999'))';
    %Data2 = sort(xlsread('C:\HAC Data Archive\Index of Saved
States','KSTest','B2:B99999'))';
    %Data1 = [];
    %Data2 = [];
    %for x = 1:1000000
    %Data1 = [Data1,sum(rand(1,10))/10];
    %Data2 = [Data2,sum(rand(1,10))/10];
    %end
    %Data1 = sort(Data1);
    %Data2 = sort(Data2);
    %histogram(Data1);
    %figure;
    %histogram(Data2);
    %mean1 = mean(Data1);
```

```
%mean2 = mean(Data2);
%std1 = std(Data1);
%std2 = std(Data2);

n1 = length(Data1);
n2 = length(Data2);
y1 = [1:n1]/n1;
y2 = [1:n2]/n2;
Fn1 = 0;
Fn2 = 0;
j1 = 1;
j2 = 1;
d1 = 0;
d2 = 0;
dt = 0;
N = 0;
D = 0;
while (j1 < n1 && j2 < n2)
    d1 = Data1(1,j1);
    d2 = Data2(1,j2);
    if d1 <= d2
        j1 = j1 + 1;
        Fn1 = j1/n1;
        while (j1 < n1 && d1 == Data1(1,j1))
            j1 = j1 + 1;
            Fn1 = j1/n1;
        end
    end
    if d2 <= d1
        j2 = j2 + 1;
        Fn2 = j2/n2;
        while (j2 < n2 && d2 == Data2(1,j2))
            j2 = j2 + 1;
            Fn2 = j2/n2;
        end
    end
    dt = abs(Fn2 - Fn1);
    if dt > D
        D = dt;
    end
end
N = sqrt((n1*n2)/(n1+n2));
z = (N+0.12+0.11/N)*D;
if z < 0
    disp('Bad z in KSdist');
end
if z == 0
    p = 1;
end
if z < 1.18
    y = exp(-1.23370055013616983/z^2);
    p = 1 - 2.25675833419102515*sqrt(-log(y))*(y+y^9+y^25+y^49);
end
if z >= 1.18
    x = exp(-2*z^2);
```

```
        p = 2*(x-x^4+x^9);
    end
    if p < Sig
        H = 1;
    else
        H = 0;
    end
    HMatrix = [HMatrix;H];
    pMatrix = [pMatrix;p];
    DMatrix = [DMatrix;D];
    %figure;
    %plot(Data1,y1,Data2,y2);
end
% Results are printed and saved in an excel document
FileLocation = 'C:\HAC Data Archive\KSResults.xlsx';
Sheet = 'KS Statistic';
NumberOfNextEntry1 = string(size(xlsread(FileLocation),1) + 2);
NumberOfNextEntry2 = string(size(xlsread(FileLocation),1) + 4);
CellRange1 = strcat('B',NumberOfNextEntry1,':','D',NumberOfNextEntry2);
CellRange2 = strcat('E',NumberOfNextEntry1,':','AH',NumberOfNextEntry2);
TimeAndSpeed = {Time1, Time2, Speed};
xlsVector = [HMatrix';pMatrix';DMatrix']
%xlswrite(FileLocation,TimeAndSpeed,Sheet,CellRange1);
%xlswrite(FileLocation,xlsVector,Sheet,CellRange2);
end
```

Appendix I: Benchmark test data

BM68									
Fill level	0.965								m
RPM	0.0000	599.9685	650.0009	699.9860	749.9830	799.9910	849.9997	880.4088	rpm
Head (LT2)	4.1004	4.1532	4.2011	4.1727	4.1939	4.2148	4.3638	4.5124	m
Head (DPT2)	1.0321	1.6703	2.1358	2.7700	3.5301	4.3388	4.5067	4.6550	m
Depth (LT2)	19.3740	21.9183	21.8975	21.9564	21.9736	21.9964	21.9333	21.8811	m
Depth (DPT2)	22.4430	24.4012	23.9628	23.3591	22.6374	21.8724	21.7903	21.7385	m
Flowrate 2	0.2586	0.3616	0.3847	0.4016	0.4177	0.4344	0.4718	0.4946	m3/s
Inlet mfr	0.0006	0.0094	0.0192	0.0354	0.0546	0.0748	0.0782	0.0793	kg/s
Outlet mfr	0.0000	0.0008	0.0182	0.0340	0.0528	0.0739	0.0758	0.0761	kg/s
Power	9.7404	13.8279	17.3729	21.5826	26.6063	32.2475	37.5734	41.2575	kW
P atm	97.7120	97.6994	97.7117	97.7121	97.7169	97.7261	97.7364	97.7326	kPa
TT 1	11.4000	11.2000	11.2376	11.2913	11.3929	11.4836	11.6000	11.7000	C
GT1	0.0000	0.0000	0.0000	0.0000	0.0000	0.0000	0.0000	0.0000	%
DPT1	-81.3820	-101.5228	-147.1068	-282.6660	-532.2056	-900.7674	-981.4653	-1007.5813	Pa
Avg Del. Pr.	344.3000	341.3897	337.4818	332.0179	325.4361	318.6803	318.6466	318.6265	Kpa
D1T1	286.3400	286.3702	286.3998	286.4374	286.4851	286.5443	286.6162	286.6966	K
D1T2	286.3400	286.3742	286.4049	286.4441	286.4931	286.5534	286.6251	286.7054	K
Diff. T	2.1227	4.0664	5.0324	6.6641	8.0283	9.0541	8.9551	8.7412	mK
LT1	0.9611	1.0483	1.0758	1.1061	1.1446	1.1882	1.2741	1.3704	m
LT2	1.8999	1.9054	1.8850	1.9437	1.9609	1.9836	1.9207	1.8683	m
LT2 (DPT2)	5.0033	4.3883	3.9502	3.3464	2.6248	1.8596	1.7777	1.7257	m
LT3	1.7000	1.6998	1.7002	1.7000	1.7000	1.6999	1.7001	1.6999	m
DPT2	252.5900	241.5891	237.6425	231.9946	225.1894	217.9789	217.8596	217.7963	kPa
DPT3	254.5300	243.5562	239.6362	234.1718	227.5852	220.8202	220.7762	220.7599	kPa
Down. Pr. 1	0.1710	0.1018	0.0901	0.0798	0.0697	0.0573	0.0482	0.0420	bar
Down. Pr. 2	0.2592	0.1767	0.1610	0.1425	0.1169	0.0943	0.0864	0.0770	bar
Down. Pr. 3	0.3238	0.2409	0.2242	0.2043	0.1785	0.1533	0.1423	0.1373	bar
Down. Pr. 4	0.3951	0.3085	0.2910	0.2708	0.2575	0.2401	0.2346	0.2300	bar

RPM	600	650	700	750	800	850	880
Down. Pr. 1 Void Fraction (m3/m3)	0.0193	0.0370	0.0640	0.0930	0.1202	0.1173	0.1145
Down. Pr. 2 Void Fraction (m3/m3)	0.0181	0.0347	0.0606	0.0893	0.1166	0.1135	0.1111
Down. Pr. 3 Void Fraction (m3/m3)	0.0172	0.0330	0.0577	0.0850	0.1112	0.1085	0.1057
Down. Pr. 4 Void Fraction (m3/m3)	0.0163	0.0313	0.0548	0.0800	0.1041	0.1011	0.0984

BM69									
Fill level	0.868								m
RPM	0.0000	599.9559	649.9966	699.9842	749.9835	799.9819	849.9836	880.4236	rpm
Head (LT2)	4.0109	4.1266	4.0759	4.0719	4.1574	4.2952	4.4433	4.5857	m
Head (DPT2)	0.4966	2.3835	2.9682	3.6510	4.2801	4.4361	4.5878	4.7351	m
Depth (LT2)	19.4210	21.8774	21.9621	22.0014	21.9781	21.9160	21.8381	21.7872	m
Depth (DPT2)	22.9360	23.6205	23.0697	22.4223	21.8554	21.7751	21.6936	21.6377	m
Flowrate 2	0.0833	0.3316	0.3513	0.3685	0.3920	0.4310	0.4697	0.4927	m3/s
Inlet mfr	0.0007	0.0299	0.0429	0.0588	0.0745	0.0775	0.0813	0.0826	kg/s
Outlet mfr	0.0000	0.0291	0.0419	0.0587	0.0737	0.0762	0.0787	0.0794	kg/s
Power	3.7208	14.4729	18.1190	22.3080	27.2300	32.1609	37.6456	41.2908	kW
P atm	97.7500	97.7600	97.7752	97.7717	97.7619	97.7570	97.7445	97.7348	kPa
TT 1	11.2000	11.4617	11.5532	11.6593	11.7695	11.8919	11.9735	12.0143	C
GT1	0.0000	0.0000	0.0000	0.0000	0.0000	0.0000	0.0000	0.0000	%
DPT1	-116.0500	-260.1081	-401.3186	-624.0772	-926.8857	-997.0689	-1092.0548	-1123.2028	Pa
Avg Del. Pr.	347.2900	333.5024	328.5418	322.6524	317.7454	317.6619	317.6591	317.5966	Kpa
D1T1	286.7400	286.7557	286.7893	286.8315	286.8844	286.9480	287.0230	287.1063	K
D1T2	286.7100	286.7622	286.7968	286.8401	286.8934	286.9572	287.0321	287.1152	K
Diff. T	-31.3040	6.4472	7.5044	8.6731	9.0207	9.1264	9.0941	8.9028	mK
LT1	0.8671	0.9808	1.0150	1.0503	1.1125	1.1883	1.2586	1.3499	m
LT2	1.9280	1.8645	1.9494	1.9887	1.9654	1.9034	1.8255	1.7745	m
LT2 (DPT2)	5.4301	3.6076	3.0570	2.4096	1.8427	1.7625	1.6810	1.6251	m
LT3	1.7000	1.6999	1.7000	1.7000	1.7000	1.7001	1.7001	1.7000	m
DPT2	251.7500	233.5028	228.3776	222.2841	217.0893	216.9527	216.8597	216.7587	kPa
DPT3	253.6400	235.6085	230.6326	224.7466	219.8495	219.7709	219.7806	219.7278	kPa
Down. Pr. 1	0.1626	0.0971	0.0864	0.0784	0.0620	0.0568	0.0463	0.0412	bar
Down. Pr. 2	0.2504	0.1642	0.1463	0.1274	0.1054	0.0901	0.0841	0.0764	bar
Down. Pr. 3	0.3148	0.2248	0.2055	0.1847	0.1623	0.1509	0.1400	0.1336	bar
Down. Pr. 4	0.3862	0.2918	0.2785	0.2630	0.2427	0.2385	0.2319	0.2282	bar

RPM	600	650	700	750	800	850	880
Down. Pr. 1 Void Fraction (m3/m3)	0.0644	0.0861	0.1105	0.1306	0.1251	0.1221	0.1193
Down. Pr. 2 Void Fraction (m3/m3)	0.0609	0.0819	0.1062	0.1261	0.1217	0.1183	0.1158
Down. Pr. 3 Void Fraction (m3/m3)	0.0580	0.0781	0.1015	0.1205	0.1159	0.1130	0.1105
Down. Pr. 4 Void Fraction (m3/m3)	0.0551	0.0739	0.0957	0.1135	0.1085	0.1054	0.1027

BM70									
Fill level	0.761								m
RPM	0.0000	599.9727	650.0085	699.9911	749.9861	800.0015	849.9932	880.5218	rpm
Head (LT2)	3.9104	3.9383	3.9704	4.0587	4.2270	4.3790	4.5269	4.7395	m
Head (DPT2)	1.3960	3.3333	3.9138	4.1909	4.3623	4.5221	4.6816	4.8971	m
Depth (LT2)	19.3930	22.0018	21.9991	21.9749	21.9009	21.8234	21.7460	21.6947	m
Depth (DPT2)	21.9070	22.6068	22.0557	21.8427	21.7656	21.6803	21.5914	21.5371	m
Flowrate 2	0.1346	0.2850	0.3079	0.3464	0.3882	0.4283	0.4676	0.4924	m3/s
Inlet mfr	0.0007	0.0482	0.0618	0.0696	0.0758	0.0794	0.0839	0.0855	kg/s
Outlet mfr	0.0000	0.0486	0.0622	0.0697	0.0757	0.0785	0.0813	0.0824	kg/s
Power	7.1178	15.0347	18.6638	22.7047	27.2187	32.2372	37.8317	41.8841	kW
P atm	97.6950	97.6990	97.6955	97.7046	97.7027	97.7160	97.6970	97.7151	kPa
TT 1	11.5000	11.9000	11.9701	12.0764	12.1675	12.2205	12.3000	12.4000	C
GT1	0.0000	0.0000	0.0000	0.0000	0.0000	0.0000	0.0000	0.0000	%
DPT1	-149.6300	-488.7279	-702.6851	-853.1019	-987.9757	-1072.9894	-1178.8579	-1212.0596	Pa
Avg Del. Pr.	337.8100	323.0630	318.1534	316.7526	316.7481	316.6805	316.6176	316.6370	Kpa
D1T1	287.1600	287.1969	287.2334	287.2788	287.3336	287.3988	287.4755	287.5614	K
D1T2	287.1000	287.2058	287.2429	287.2881	287.3429	287.4082	287.4848	287.5705	K
Diff. T	-66.5640	8.8929	9.4550	9.2266	9.2840	9.3343	9.3073	9.1042	mK
LT1	0.7616	0.9171	0.9465	1.0107	1.1050	1.1794	1.2500	1.4112	m
LT2	1.8972	1.9891	1.9864	1.9623	1.8883	1.8107	1.7334	1.6820	m
LT2 (DPT2)	4.4501	2.5941	2.0430	1.8300	1.7529	1.6676	1.5787	1.5244	m
LT3	1.7000	1.7000	1.6999	1.7000	1.7001	1.7000	1.7001	1.7000	m
DPT2	250.6800	222.9699	217.8453	216.2697	216.1361	215.9628	215.8030	215.7509	kPa
DPT3	252.5400	225.2300	220.3239	218.9140	218.9115	218.8306	218.7865	218.7878	kPa
Down. Pr. 1	0.1518	0.0910	0.0753	0.0566	0.0599	0.0549	0.0451	0.0399	bar
Down. Pr. 2	0.2395	0.1472	0.1288	0.1079	0.0975	0.0871	0.0787	0.0729	bar
Down. Pr. 3	0.3040	0.2045	0.1849	0.1664	0.1574	0.1469	0.1361	0.1297	bar
Down. Pr. 4	0.3752	0.2760	0.2569	0.2430	0.2387	0.2330	0.2272	0.2261	bar

RPM	600	650	700	750	800	850	880
Down. Pr. 1 Void Fraction (m3/m3)	0.1153	0.1357	0.1379	0.1343	0.1289	0.1264	0.1233
Down. Pr. 2 Void Fraction (m3/m3)	0.1102	0.1299	0.1323	0.1302	0.1255	0.1229	0.1199
Down. Pr. 3 Void Fraction (m3/m3)	0.1054	0.1245	0.1264	0.1242	0.1196	0.1173	0.1145
Down. Pr. 4 Void Fraction (m3/m3)	0.1000	0.1181	0.1194	0.1169	0.1121	0.1094	0.1063

BM71									
Fill level	0.669								m
RPM	0.0000	599.9764	650.0107	699.9922	749.9889	799.9895	849.9836	880.5693	rpm
Head (LT2)	3.7747	3.8999	4.0081	4.1411	4.3094	4.4672	4.6153	4.7215	m
Head (DPT2)	1.0761	4.0316	4.1323	4.2670	4.4430	4.6091	4.7756	4.8809	m
Depth (LT2)	19.4400	21.9976	21.9478	21.8883	21.8138	21.7386	21.6606	21.6109	m
Depth (DPT2)	22.1380	21.8658	21.8236	21.7624	21.6802	21.5967	21.5003	21.4515	m
Flowrate 2	0.0774	0.2396	0.2958	0.3440	0.3866	0.4262	0.4666	0.4891	m3/s
Inlet mfr	0.0007	0.0526	0.0627	0.0687	0.0757	0.0796	0.0846	0.0859	kg/s
Outlet mfr	0.0000	0.0549	0.0659	0.0713	0.0784	0.0817	0.0854	0.0860	kg/s
Power	4.2100	15.1046	18.8466	22.9429	27.5240	32.5140	38.2951	41.8919	kW
P atm	98.6590	98.6617	98.6649	98.6668	98.6672	98.6739	98.6677	98.6634	kPa
TT 1	10.8770	11.4433	11.7228	11.8406	11.9587	12.0653	12.1630	12.2473	C
GT1	0.0000	0.0000	0.0000	0.0000	0.0000	0.0000	0.0000	0.0000	%
DPT1	-53.2610	-456.3293	-633.1969	-756.4007	-915.7629	-1010.0597	-1134.4382	-1178.7255	Pa
Avg Del. Pr.	340.4200	316.4076	316.7874	316.8763	316.8815	316.7938	316.7204	316.7245	Kpa
D1T1	287.0800	287.0895	287.1171	287.1541	287.2010	287.2593	287.3299	287.4104	K
D1T2	287.1800	287.0983	287.1256	287.1628	287.2102	287.2686	287.3391	287.4195	K
Diff. T	100.7000	8.7868	8.4736	8.7605	9.2484	9.3364	9.2270	9.1117	mK
LT1	0.6706	0.8744	0.9328	1.0064	1.1004	1.1827	1.2528	1.3094	m
LT2	2.0000	1.9848	1.9350	1.8756	1.8012	1.7258	1.6477	1.5982	m
LT2 (DPT2)	4.6661	1.8531	1.8109	1.7496	1.6677	1.5839	1.4874	1.4387	m
LT3	1.7000	1.7000	1.7000	1.7000	1.7001	1.6999	1.6999	1.7000	m
DPT2	249.7800	215.2230	215.4231	215.4501	215.2774	215.1103	214.8937	214.8497	kPa
DPT3	251.6500	217.6120	217.9885	218.0756	218.0803	217.9859	217.9186	217.9272	kPa
Down. Pr. 1	0.1510	0.0700	0.0544	0.0576	0.0676	0.0637	0.0535	0.0493	bar
Down. Pr. 2	0.2396	0.1469	0.1326	0.1109	0.1057	0.0923	0.0869	0.0800	bar
Down. Pr. 3	0.3033	0.2017	0.1893	0.1697	0.1646	0.1541	0.1436	0.1367	bar
Down. Pr. 4	0.3757	0.2702	0.2619	0.2468	0.2457	0.2422	0.2360	0.2321	bar

RPM	600	650	700	750	800	850	880
Down. Pr. 1 Void Fraction (m3/m3)	0.1460	0.1436	0.1359	0.1326	0.1277	0.1256	0.1226
Down. Pr. 2 Void Fraction (m3/m3)	0.1374	0.1349	0.1302	0.1286	0.1248	0.1221	0.1195
Down. Pr. 3 Void Fraction (m3/m3)	0.1319	0.1292	0.1244	0.1228	0.1188	0.1167	0.1141
Down. Pr. 4 Void Fraction (m3/m3)	0.1257	0.1226	0.1175	0.1156	0.1112	0.1089	0.1061

BM72									
Fill level	0.577								m
RPM	0.0000	599.9786	650.0092	699.9935	749.9742	799.9888	850.0089	880.6412	rpm
Head (LT2)	3.6929	3.9757	4.0863	4.2158	4.3931	4.5425	4.6886	4.7956	m
Head (DPT2)	0.9887	4.1186	4.2204	4.3474	4.5394	4.6981	4.8534	4.9616	m
Depth (LT2)	19.4680	21.9160	21.8638	21.8052	21.7340	21.6561	21.5808	21.5313	m
Depth (DPT2)	22.1730	21.7732	21.7297	21.6736	21.5878	21.5005	21.4160	21.3653	m
Flowrate 2	0.0625	0.2331	0.2906	0.3398	0.3827	0.4248	0.4624	0.4851	m3/s
Inlet mfr	0.0008	0.0528	0.0647	0.0714	0.0783	0.0835	0.0884	0.0901	kg/s
Outlet mfr	0.0000	0.0546	0.0666	0.0729	0.0792	0.0839	0.0870	0.0882	kg/s
Power	4.0364	14.8750	18.7026	22.8177	27.3888	32.7557	38.1195	41.7147	kW
P atm	98.6580	98.6505	98.6482	98.6532	98.6584	98.6630	98.6614	98.6633	kPa
TT 1	11.6000	12.0535	12.2000	12.3000	12.3768	12.4631	12.5327	12.6064	C
GT1	0.0000	0.0000	0.0000	0.0000	0.0000	0.0000	0.0000	0.0000	%
DPT1	-89.0580	-495.6419	-695.0072	-837.4258	-987.1083	-1114.9962	-1243.2938	-1295.5780	Pa
Avg Del. Pr.	340.6200	315.3682	315.7765	315.9815	315.9140	315.8754	315.8673	315.8175	Kpa
D1T1	287.4300	287.4499	287.4822	287.5228	287.5745	287.6371	287.7124	287.7972	K
D1T2	287.3800	287.4591	287.4906	287.5320	287.5836	287.6466	287.7220	287.8066	K
Diff. T	-54.5460	9.1269	8.4338	9.1901	9.0639	9.5512	9.5871	9.3851	mK
LT1	0.5775	0.8688	0.9272	0.9980	1.1041	1.1756	1.2464	1.3039	m
LT2	2.0000	1.9033	1.8512	1.7925	1.7213	1.6434	1.5681	1.5186	m
LT2 (DPT2)	4.6812	1.7605	1.7171	1.6609	1.5750	1.4878	1.4033	1.3526	m
LT3	1.7000	1.7000	1.7001	1.7000	1.7000	1.7000	1.7000	1.7000	m
DPT2	248.8800	214.2410	214.4297	214.5113	214.2978	214.1307	213.9775	213.9144	kPa
DPT3	250.7700	216.5837	216.9943	217.1944	217.1216	217.0785	217.0718	217.0202	kPa
Down. Pr. 1	0.1430	0.0649	0.0451	0.0589	0.0547	0.0627	0.0540	0.0467	bar
Down. Pr. 2	0.2308	0.1446	0.1288	0.1092	0.0973	0.0848	0.0793	0.0749	bar
Down. Pr. 3	0.2937	0.1999	0.1852	0.1688	0.1593	0.1500	0.1399	0.1331	bar
Down. Pr. 4	0.3667	0.2690	0.2567	0.2430	0.2413	0.2385	0.2330	0.2292	bar

RPM	600	650	700	750	800	850	880
Down. Pr. 1 Void Fraction (m3/m3)	0.1508	0.1509	0.1420	0.1393	0.1338	0.1315	0.1292
Down. Pr. 2 Void Fraction (m3/m3)	0.1417	0.1412	0.1364	0.1346	0.1314	0.1288	0.1262
Down. Pr. 3 Void Fraction (m3/m3)	0.1360	0.1353	0.1303	0.1282	0.1248	0.1227	0.1204
Down. Pr. 4 Void Fraction (m3/m3)	0.1295	0.1285	0.1234	0.1207	0.1169	0.1144	0.1120

BM73									
Fill level	0.480								m
RPM	0.0000	599.9787	650.0061	699.9855	749.9668	799.9813	849.9775	880.7965	rpm
Head (LT2)	3.5999	4.0540	4.1673	4.2859	4.4701	4.6116	4.7671	4.8639	m
Head (DPT2)	0.5975	4.2013	4.3044	4.4324	4.6207	4.7684	4.9318	5.0286	m
Depth (LT2)	19.4870	21.8295	21.7770	21.7262	21.6523	21.5754	21.4957	21.4430	m
Depth (DPT2)	22.4900	21.6822	21.6398	21.5797	21.5017	21.4185	21.3310	21.2783	m
Flowrate 2	0.0361	0.2266	0.2857	0.3360	0.3793	0.4200	0.4592	0.4830	m3/s
Inlet mfr	0.0006	0.0531	0.0657	0.0724	0.0801	0.0867	0.0912	0.0932	kg/s
Outlet mfr	0.0000	0.0542	0.0672	0.0732	0.0803	0.0860	0.0896	0.0906	kg/s
Power	2.4054	14.7598	18.6735	22.8169	27.3964	32.5428	38.0776	41.9265	kW
P atm	98.6300	98.6174	98.6077	98.5941	98.5891	98.5777	98.5654	98.5488	kPa
TT 1	12.0000	12.4030	12.5849	12.6535	12.7007	12.8000	12.9000	13.0000	C
GT1	0.0000	0.0000	0.0000	0.0000	0.0000	0.0000	0.0000	0.0000	%
DPT1	-119.4700	-528.0381	-744.5295	-886.6368	-1054.6650	-1216.0867	-1336.4258	-1401.0428	Pa
Avg Del. Pr.	343.4500	314.4045	314.8230	314.9964	315.0014	314.9908	314.9425	314.9206	Kpa
D1T1	287.8300	287.8442	287.8792	287.9230	287.9780	288.0440	288.1231	288.2121	K
D1T2	287.7800	287.8536	287.8875	287.9320	287.9869	288.0537	288.1327	288.2217	K
Diff. T	-53.3510	9.2942	8.3566	9.0202	8.8254	9.6507	9.6227	9.5523	mK
LT1	0.4788	0.8605	0.9212	0.9891	1.0994	1.1640	1.2397	1.2839	m
LT2	2.0000	1.8168	1.7643	1.7135	1.6396	1.5628	1.4829	1.4303	m
LT2 (DPT2)	4.9763	1.6695	1.6271	1.5671	1.4890	1.4059	1.3183	1.2656	m
LT3	1.7000	1.7000	1.7000	1.7000	1.7000	1.7001	1.7000	1.7000	m
DPT2	247.8400	213.2759	213.4785	213.5250	213.3888	213.2321	213.0712	213.0057	kPa
DPT3	249.7000	215.6530	216.0813	216.2683	216.2783	216.2791	216.2430	216.2378	kPa
Down. Pr. 1	0.1325	0.0594	0.0363	0.0525	0.0438	0.0596	0.0504	0.0447	bar
Down. Pr. 2	0.2205	0.1422	0.1235	0.0972	0.0907	0.0822	0.0746	0.0703	bar
Down. Pr. 3	0.2840	0.1969	0.1824	0.1605	0.1536	0.1453	0.1369	0.1302	bar
Down. Pr. 4	0.3562	0.2650	0.2526	0.2379	0.2337	0.2346	0.2285	0.2261	bar

RPM	600	650	700	750	800	850	880
Down. Pr. 1 Void Fraction (m3/m3)	0.1562	0.1564	0.1462	0.1449	0.1402	0.1367	0.1340
Down. Pr. 2 Void Fraction (m3/m3)	0.1464	0.1459	0.1411	0.1394	0.1377	0.1340	0.1312
Down. Pr. 3 Void Fraction (m3/m3)	0.1406	0.1396	0.1343	0.1328	0.1310	0.1275	0.1250
Down. Pr. 4 Void Fraction (m3/m3)	0.1340	0.1328	0.1269	0.1251	0.1226	0.1190	0.1163

BM74									
Fill level	0.378								m
RPM	0.0000	599.9720	650.0062	699.9827	749.9841	800.0070	849.9868	880.8295	rpm
Head (LT2)	3.5700	4.1347	4.2424	4.3665	4.5357	4.6924	4.8472	4.9472	m
Head (DPT2)	0.8840	4.2821	4.3829	4.5040	4.6863	4.8492	5.0138	5.1154	m
Depth (LT2)	19.4510	21.7437	21.6948	21.6388	21.5694	21.4940	21.4113	21.3554	m
Depth (DPT2)	22.1370	21.5963	21.5543	21.5013	21.4188	21.3372	21.2448	21.1872	m
Flowrate 2	0.0504	0.2204	0.2811	0.3322	0.3764	0.4169	0.4565	0.4810	m3/s
Inlet mfr	0.0005	0.0536	0.0668	0.0760	0.0817	0.0886	0.0932	0.0958	kg/s
Outlet mfr	0.0000	0.0539	0.0677	0.0761	0.0813	0.0882	0.0917	0.0934	kg/s
Power	3.3609	14.6863	18.6324	22.7929	27.4917	32.5225	38.2033	42.0648	kW
P atm	98.5220	98.5078	98.4953	98.4862	98.4760	98.4730	98.4584	98.4492	kPa
TT 1	12.4000	12.7862	12.9552	13.0168	13.1000	13.2000	13.3000	13.4000	C
GT1	0.0000	0.0000	0.0000	0.0000	0.0000	0.0000	0.0000	0.0000	%
DPT1	-154.1200	-565.5934	-796.1525	-989.2000	-1123.7604	-1301.8706	-1432.8353	-1505.5233	Pa
Avg Del. Pr.	339.9600	313.3528	313.7714	314.0738	313.9922	314.0266	313.9707	313.9206	Kpa
D1T1	288.2600	288.2762	288.3139	288.3607	288.4193	288.4886	288.5717	288.6652	K
D1T2	288.2000	288.2855	288.3224	288.3697	288.4281	288.4984	288.5815	288.6748	K
Diff. T	-57.9520	9.3213	8.4796	9.0106	8.8385	9.8416	9.8137	9.6737	mK
LT1	0.3790	0.8554	0.9143	0.9824	1.0821	1.1633	1.2356	1.2795	m
LT2	2.0000	1.7310	1.6821	1.6263	1.5567	1.4812	1.3987	1.3426	m
LT2 (DPT2)	4.6311	1.5836	1.5417	1.4887	1.4061	1.3244	1.2321	1.1744	m
LT3	1.7000	1.7000	1.7001	1.7002	1.7000	1.6999	1.7000	1.7000	m
DPT2	246.7300	212.3654	212.5739	212.6909	212.5181	212.3680	212.1629	212.0601	kPa
DPT3	248.6400	214.7110	215.1420	215.4535	215.3822	215.4196	215.3783	215.3374	kPa
Down. Pr. 1	0.1216	0.0547	0.0273	0.0394	0.0361	0.0549	0.0488	0.0428	bar
Down. Pr. 2	0.2093	0.1387	0.1165	0.1053	0.0826	0.0701	0.0622	0.0600	bar
Down. Pr. 3	0.2732	0.1944	0.1762	0.1664	0.1467	0.1408	0.1315	0.1252	bar
Down. Pr. 4	0.3452	0.2619	0.2473	0.2394	0.2268	0.2274	0.2235	0.2203	bar

RPM	600	650	700	750	800	850	880
Down. Pr. 1 Void Fraction (m3/m3)	0.1619	0.1624	0.1558	0.1495	0.1447	0.1405	0.1382
Down. Pr. 2 Void Fraction (m3/m3)	0.1516	0.1513	0.1478	0.1439	0.1429	0.1389	0.1362
Down. Pr. 3 Void Fraction (m3/m3)	0.1455	0.1446	0.1411	0.1369	0.1351	0.1315	0.1293
Down. Pr. 4 Void Fraction (m3/m3)	0.1387	0.1374	0.1338	0.1290	0.1267	0.1227	0.1203

BM75									
Fill level	0.279								m
RPM	0.0000	599.9742	650.0039	699.9799	749.9833	800.0061	849.9932	880.7701	rpm
Head (LT2)	3.4800	4.2197	4.3298	4.4532	4.6173	4.7672	4.9382	5.0389	m
Head (DPT2)	0.7606	4.3727	4.4639	4.5908	4.7648	4.9241	5.0971	5.2000	m
Depth (LT2)	19.4530	21.6536	21.6006	21.5470	21.4781	21.4019	21.3160	21.2578	m
Depth (DPT2)	22.1720	21.5006	21.4665	21.4094	21.3306	21.2450	21.1571	21.0967	m
Flowrate 2	0.0421	0.2141	0.2749	0.3286	0.3725	0.4140	0.4543	0.4786	m3/s
Inlet mfr	0.0008	0.0532	0.0669	0.0775	0.0826	0.0909	0.0959	0.0986	kg/s
Outlet mfr	0.0000	0.0534	0.0677	0.0780	0.0825	0.0902	0.0941	0.0961	kg/s
Power	2.8909	14.6036	18.5789	22.8685	27.4652	32.6329	38.3196	42.1209	kW
P atm	98.4120	98.4159	98.4113	98.3988	98.3841	98.3732	98.3659	98.3603	kPa
TT 1	12.6000	13.1111	13.3000	13.4000	13.5000	13.6000	13.7000	13.7980	C
GT1	0.0000	0.0000	0.0000	0.0000	0.0000	0.0000	0.0000	0.0000	%
DPT1	-184.4400	-583.9348	-821.3597	-1049.3362	-1170.6224	-1380.3923	-1520.7498	-1602.1974	Pa
Avg Del. Pr.	340.0500	312.2428	312.6919	312.9892	312.9648	313.0044	312.9943	312.9099	Kpa
D1T1	288.7200	288.7243	288.7644	288.8130	288.8733	288.9452	289.0316	289.1277	K
D1T2	288.6300	288.7336	288.7729	288.8217	288.8824	288.9553	289.0416	289.1378	K
Diff. T	-95.4800	9.3307	8.5267	8.7117	9.1245	10.0536	9.9968	10.0844	mK
LT1	0.2791	0.8504	0.9075	0.9772	1.0724	1.1462	1.2311	1.2737	m
LT2	2.0000	1.6409	1.5879	1.5344	1.4654	1.3893	1.3032	1.2451	m
LT2 (DPT2)	4.6596	1.4879	1.4539	1.3968	1.3179	1.2323	1.1444	1.0840	m
LT3	1.7000	1.7000	1.7001	1.7000	1.7000	1.7000	1.7000	1.7000	m
DPT2	245.7400	211.3567	211.6292	211.7278	211.5802	211.4011	211.2459	211.1113	kPa
DPT3	247.6600	213.6929	214.1466	214.4564	214.4467	214.4972	214.4944	214.4156	kPa
Down. Pr. 1	0.1105	0.0450	0.0227	0.0147	0.0316	0.0537	0.0461	0.0411	bar
Down. Pr. 2	0.1983	0.1333	0.1074	0.0988	0.0731	0.0666	0.0555	0.0491	bar
Down. Pr. 3	0.2628	0.1887	0.1697	0.1616	0.1404	0.1381	0.1274	0.1189	bar
Down. Pr. 4	0.3341	0.2556	0.2421	0.2338	0.2207	0.2228	0.2174	0.2151	bar

RPM	600	650	700	750	800	850	880
Down. Pr. 1 Void Fraction (m3/m3)	0.1666	0.1666	0.1636	0.1531	0.1491	0.1452	0.1428
Down. Pr. 2 Void Fraction (m3/m3)	0.1555	0.1557	0.1529	0.1480	0.1476	0.1441	0.1418
Down. Pr. 3 Void Fraction (m3/m3)	0.1492	0.1485	0.1457	0.1404	0.1395	0.1360	0.1341
Down. Pr. 4 Void Fraction (m3/m3)	0.1423	0.1410	0.1383	0.1323	0.1310	0.1272	0.1247

BM76									
Fill level	0.176								m
RPM	0.0000	599.9791	649.9928	699.9916	749.9805	799.9861	849.9872	880.7246	rpm
Head (LT2)	3.3854	4.3065	4.4129	4.5341	4.6985	4.8545	5.0165	5.0909	m
Head (DPT2)	0.6389	4.4481	4.5402	4.6602	4.8370	4.9968	5.1721	5.2760	m
Depth (LT2)	19.4510	21.5674	21.5147	21.4606	21.3954	21.3131	21.2354	21.2013	m
Depth (DPT2)	22.1970	21.4259	21.3874	21.3345	21.2569	21.1708	21.0799	21.0163	m
Flowrate 2	0.0353	0.2089	0.2711	0.3250	0.3699	0.4121	0.4530	0.4772	m3/s
Inlet mfr	0.0010	0.0494	0.0627	0.0738	0.0794	0.0878	0.0925	0.0951	kg/s
Outlet mfr	0.0000	0.0520	0.0666	0.0782	0.0829	0.0919	0.0958	0.0979	kg/s
Power	2.4966	14.7488	18.8242	23.1005	27.6947	32.9262	38.6149	42.3767	kW
P atm	96.1790	96.1930	96.2121	96.2349	96.2522	96.2626	96.2792	96.2857	kPa
TT 1	10.0000	11.1003	11.4463	11.6238	11.7376	11.8789	11.9919	12.1000	C
GT1	0.0000	0.0000	0.0000	0.0000	0.0000	0.0000	0.0000	0.0000	%
DPT1	-53.4610	-441.7309	-656.2700	-881.8748	-1001.4926	-1217.0758	-1340.2852	-1422.5267	Pa
Avg Del. Pr.	338.1100	309.3496	309.8674	310.2184	310.2039	310.2310	310.2071	310.1516	Kpa
D1T1	287.2000	286.9444	286.9759	287.0139	287.0656	287.1288	287.2061	287.2936	K
D1T2	287.4000	286.9534	286.9843	287.0222	287.0744	287.1383	287.2156	287.3032	K
Diff. T	203.6500	8.9411	8.3777	8.2395	8.7365	9.5604	9.4750	9.5935	mK
LT1	0.1864	0.8509	0.9046	0.9717	1.0710	1.1446	1.2289	1.2693	m
LT2	2.0000	1.5547	1.5020	1.4479	1.3829	1.3004	1.2227	1.1887	m
LT2 (DPT2)	4.6848	1.4132	1.3747	1.3218	1.2443	1.1580	1.0671	1.0037	m
LT3	1.7000	1.7000	1.7000	1.7000	1.7001	1.6999	1.7000	1.7001	m
DPT2	245.0900	210.6400	210.8728	211.0075	210.8814	210.7059	210.5299	210.3618	kPa
DPT3	246.9900	213.0227	213.5214	213.8495	213.8177	213.8344	213.7939	213.7319	kPa
Down. Pr. 1	0.0795	0.0120	-0.0072	-0.0128	0.0101	0.0305	0.0255	0.0183	bar
Down. Pr. 2	0.1677	0.0977	0.0666	0.0684	0.0422	0.0357	0.0254	0.0145	bar
Down. Pr. 3	0.2306	0.1581	0.1384	0.1363	0.1119	0.1108	0.1014	0.0969	bar
Down. Pr. 4	0.3036	0.2251	0.2097	0.2086	0.1926	0.1960	0.1923	0.1906	bar

RPM	600	650	700	750	800	850	880
Down. Pr. 1 Void Fraction (m3/m3)	0.1665	0.1660	0.1644	0.1537	0.1500	0.1454	0.1433
Down. Pr. 2 Void Fraction (m3/m3)	0.1551	0.1560	0.1534	0.1495	0.1493	0.1454	0.1438
Down. Pr. 3 Void Fraction (m3/m3)	0.1480	0.1473	0.1453	0.1412	0.1404	0.1364	0.1341
Down. Pr. 4 Void Fraction (m3/m3)	0.1408	0.1396	0.1376	0.1326	0.1314	0.1271	0.1246

BM77									
Fill level	<0.164 (Below flanges)								m
RPM	0.0000	599.9757	650.0095	699.9822	749.9794	799.9971	849.9819	880.6799	rpm
Head (LT2)	3.3661	4.3743	4.4805	4.6019	4.7667	4.9321	5.0899	5.1812	m
Head (DPT2)	1.4165	4.5199	4.6176	4.7365	4.9060	5.0769	5.2479	5.3464	m
Depth (LT2)	19.4010	21.4900	21.4394	21.3860	21.3187	21.2335	21.1570	21.1018	m
Depth (DPT2)	21.3510	21.3443	21.3023	21.2513	21.1794	21.0887	20.9990	20.9366	m
Flowrate 2	0.0380	0.2018	0.2652	0.3202	0.3669	0.4087	0.4497	0.4738	m3/s
Inlet mfr	0.0010	0.0471	0.0613	0.0738	0.0825	0.0896	0.0933	0.0966	kg/s
Outlet mfr	0.0000	0.0502	0.0657	0.0784	0.0870	0.0938	0.0975	0.1002	kg/s
Power	2.7075	14.4569	18.6171	22.9127	27.6190	32.8012	38.5359	42.1466	kW
P atm	96.3260	96.3397	96.3594	96.3701	96.3769	96.3908	96.4069	96.4210	kPa
TT 1	11.2980	11.7641	11.9856	12.1000	12.1889	12.2661	12.3468	12.4359	C
GT1	0.0000	0.0000	0.0000	0.0000	0.0000	0.0000	0.0000	0.0000	%
DPT1	-62.7440	-403.9649	-629.1891	-883.7299	-1095.5842	-1277.0995	-1384.1619	-1482.9564	Pa
Avg Del. Pr.	330.3400	308.5596	309.0330	309.4618	309.6150	309.5922	309.5461	309.4710	Kpa
D1T1	287.2900	287.3286	287.3596	287.3990	287.4501	287.5118	287.5877	287.6743	K
D1T2	287.2600	287.3377	287.3682	287.4073	287.4585	287.5214	287.5972	287.6839	K
Diff. T	-23.1810	9.0503	8.5429	8.2974	8.3240	9.6484	9.5820	9.6600	mK
LT1	0.1617	0.8413	0.8970	0.9648	1.0624	1.1426	1.2240	1.2599	m
LT2	2.0000	1.4774	1.4268	1.3732	1.3059	1.2209	1.1443	1.0890	m
LT2 (DPT2)	3.8674	1.3317	1.2897	1.2386	1.1667	1.0761	0.9864	0.9238	m
LT3	1.7000	1.7001	1.7001	1.7000	1.6999	1.7001	1.7001	1.6999	m
DPT2	235.8600	209.7693	209.9617	210.1179	210.0654	209.8318	209.6663	209.5032	kPa
DPT3	237.7200	212.0859	212.5396	212.9577	213.1041	213.0674	213.0052	212.9160	kPa
Down. Pr. 1	-0.0073	0.0057	-0.0075	-0.0160	-0.0149	0.0301	0.0238	0.0190	bar
Down. Pr. 2	0.0763	0.0876	0.0515	0.0545	0.0607	0.0399	0.0222	0.0103	bar
Down. Pr. 3	0.1403	0.1507	0.1301	0.1274	0.1248	0.1107	0.1012	0.0928	bar
Down. Pr. 4	0.2120	0.2182	0.2037	0.2019	0.2036	0.1946	0.1938	0.1884	bar

RPM	600	650	700	750	800	850	880
Down. Pr. 1 Void Fraction (m3/m3)	0.1654	0.1661	0.1668	0.1633	0.1537	0.1475	0.1461
Down. Pr. 2 Void Fraction (m3/m3)	0.1545	0.1580	0.1571	0.1531	0.1525	0.1478	0.1472
Down. Pr. 3 Void Fraction (m3/m3)	0.1471	0.1483	0.1482	0.1454	0.1439	0.1383	0.1373
Down. Pr. 4 Void Fraction (m3/m3)	0.1399	0.1403	0.1400	0.1370	0.1349	0.1287	0.1273

BM78									
Fill level	<0.164 (Below flanges)								m
RPM	0.0000	599.9728	650.0042	699.9863	749.9724	800.0035	849.9787	880.7795	rpm
Head (LT2)	3.7480	4.4356	4.5411	4.6634	4.8313	4.9814	5.1603	5.2556	m
Head (DPT2)	2.8881	4.5892	4.6823	4.7951	4.9686	5.1294	5.3137	5.4179	m
Depth (LT2)	19.1790	21.4260	21.3747	21.3171	21.2474	21.1740	21.0826	21.0286	m
Depth (DPT2)	20.0390	21.2723	21.2335	21.1854	21.1101	21.0260	20.9292	20.8663	m
Flowrate 2	0.0830	0.1962	0.2599	0.3163	0.3639	0.4064	0.4473	0.4716	m3/s
Inlet mfr	0.0010	0.0463	0.0608	0.0739	0.0829	0.0900	0.0946	0.0976	kg/s
Outlet mfr	0.0000	0.0494	0.0654	0.0788	0.0883	0.0949	0.0996	0.1026	kg/s
Power	6.0399	14.3398	18.5075	22.8891	27.5925	32.8323	38.5187	42.3020	kW
P atm	96.4780	96.4894	96.4961	96.5117	96.5367	96.5547	96.5765	96.5966	kPa
TT 1	11.5000	12.1401	12.3000	12.4000	12.5000	12.6000	12.7000	12.7943	C
GT1	0.0000	0.0000	0.0000	0.0000	0.0000	0.0000	0.0000	0.0000	%
DPT1	-68.4350	-392.2356	-630.0718	-894.8469	-1117.8899	-1305.7220	-1437.3546	-1535.7614	Pa
Avg Del. Pr.	317.8800	307.9429	308.4305	308.8472	309.0346	309.0463	308.9584	308.9028	Kpa
D1T1	287.4700	287.7181	287.7473	287.7854	287.8361	287.8977	287.9737	288.0604	K
D1T2	287.6500	287.7268	287.7561	287.7940	287.8445	287.9071	287.9833	288.0702	K
Diff. T	182.1800	8.6423	8.8957	8.5498	8.4067	9.4618	9.6641	9.8275	mK
LT1	0.1634	0.8385	0.8929	0.9575	1.0557	1.1323	1.2197	1.2612	m
LT2	2.0000	1.4132	1.3621	1.3044	1.2347	1.1612	1.0698	1.0159	m
LT2 (DPT2)	2.5540	1.2596	1.2209	1.1727	1.0974	1.0132	0.9164	0.8537	m
LT3	1.7000	1.6999	1.7001	1.7000	1.7000	1.6999	1.6999	1.7000	m
DPT2	225.0200	209.0058	209.2189	209.4092	209.3290	209.1684	208.9252	208.7597	kPa
DPT3	226.9600	211.3195	211.8004	212.2015	212.3640	212.3576	212.2479	212.1722	kPa
Down. Pr. 1	-0.0062	0.0063	-0.0069	-0.0142	-0.0182	0.0246	0.0266	0.0201	bar
Down. Pr. 2	0.0049	0.0871	0.0516	0.0476	0.0521	0.0425	0.0185	0.0064	bar
Down. Pr. 3	0.0330	0.1475	0.1276	0.1247	0.1207	0.1103	0.0987	0.0931	bar
Down. Pr. 4	0.1059	0.2160	0.2011	0.1980	0.1998	0.1972	0.1899	0.1852	bar

RPM	600	650	700	750	800	850	880
Down. Pr. 1 Void Fraction (m3/m3)	0.1669	0.1677	0.1685	0.1655	0.1558	0.1496	0.1477
Down. Pr. 2 Void Fraction (m3/m3)	0.1560	0.1596	0.1599	0.1559	0.1535	0.1507	0.1494
Down. Pr. 3 Void Fraction (m3/m3)	0.1488	0.1502	0.1503	0.1475	0.1452	0.1409	0.1389
Down. Pr. 4 Void Fraction (m3/m3)	0.1414	0.1421	0.1422	0.1389	0.1358	0.1313	0.1292

BM79									
Fill level	<0.164 (Below flanges)								m
RPM	0.0000	599.9802	650.0076	699.9791	749.9683	799.9978	849.9955	880.7704	rpm
Head (LT2)	3.6205	4.4852	4.5904	4.7166	4.8778	5.0335	5.2086	5.3129	m
Head (DPT2)	3.5173	4.6364	4.7312	4.8468	5.0114	5.1765	5.3615	5.4681	m
Depth (LT2)	19.2310	21.3732	21.3221	21.2630	21.1928	21.1175	21.0283	20.9661	m
Depth (DPT2)	19.3340	21.2220	21.1814	21.1328	21.0592	20.9746	20.8754	20.8109	m
Flowrate 2	0.0861	0.1917	0.2564	0.3131	0.3615	0.4039	0.4453	0.4694	m3/s
Inlet mfr	0.0009	0.0457	0.0608	0.0736	0.0836	0.0900	0.0956	0.0987	kg/s
Outlet mfr	0.0000	0.0485	0.0652	0.0788	0.0891	0.0954	0.1007	0.1044	kg/s
Power	5.2565	14.3153	18.4816	22.9071	27.6037	32.7557	38.5050	42.3127	kW
P atm	96.7200	96.7345	96.7364	96.7402	96.7478	96.7549	96.7609	96.7735	kPa
TT 1	11.2450	12.2448	12.4636	12.6000	12.7172	12.8128	12.9330	13.0279	C
GT1	0.0000	0.0000	0.0000	0.0000	0.0000	0.0000	0.0000	0.0000	%
DPT1	-80.5920	-390.9701	-632.0930	-906.5206	-1146.7026	-1321.8788	-1486.9199	-1591.7245	Pa
Avg Del. Pr.	311.5500	307.6077	308.0481	308.5002	308.6891	308.6715	308.6141	308.5255	Kpa
D1T1	287.6400	288.0117	288.0398	288.0766	288.1271	288.1897	288.2654	288.3537	K
D1T2	287.9700	288.0201	288.0487	288.0852	288.1357	288.1984	288.2752	288.3637	K
Diff. T	336.1600	8.4991	8.9528	8.6611	8.5305	8.6520	9.8387	9.9583	mK
LT1	0.1642	0.8353	0.8895	0.9566	1.0476	1.1280	1.2138	1.2561	m
LT2	2.0000	1.3605	1.3094	1.2503	1.1802	1.1047	1.0155	0.9535	m
LT2 (DPT2)	1.8867	1.2092	1.1686	1.1201	1.0466	0.9618	0.8626	0.7983	m
LT3	1.7000	1.6999	1.7000	1.7000	1.7000	1.6999	1.6999	1.7001	m
DPT2	214.8600	208.4675	208.6619	208.8438	208.7861	208.6139	208.3517	208.1651	kPa
DPT3	216.7800	210.7392	211.1778	211.6259	211.8073	211.7826	211.7193	211.6180	kPa
Down. Pr. 1	-0.0035	0.0068	-0.0042	-0.0130	-0.0193	-0.0103	0.0269	0.0212	bar
Down. Pr. 2	0.0070	0.0838	0.0478	0.0426	0.0491	0.0408	0.0202	0.0068	bar
Down. Pr. 3	-0.0020	0.1475	0.1246	0.1229	0.1211	0.1105	0.0982	0.0895	bar
Down. Pr. 4	0.0093	0.2153	0.2008	0.1980	0.1978	0.1944	0.1913	0.1855	bar

RPM	600	650	700	750	800	850	880
Down. Pr. 1 Void Fraction (m3/m3)	0.1680	0.1689	0.1690	0.1677	0.1613	0.1514	0.1495
Down. Pr. 2 Void Fraction (m3/m3)	0.1576	0.1616	0.1612	0.1582	0.1544	0.1523	0.1514
Down. Pr. 3 Void Fraction (m3/m3)	0.1500	0.1520	0.1512	0.1493	0.1459	0.1427	0.1412
Down. Pr. 4 Void Fraction (m3/m3)	0.1426	0.1435	0.1428	0.1409	0.1368	0.1328	0.1310

BM80									
Fill level	<0.164 (Below flanges)								m
RPM	0.0000	599.9769	650.0052	699.9876	749.9729	799.9996	850.0009	880.7704	rpm
Head (LT2)	3.6825	4.5389	4.6484	4.7759	4.9341	5.0946	5.2729	5.3876	m
Head (DPT2)	3.6576	4.6989	4.7952	4.9068	5.0767	5.2423	5.4262	5.5524	m
Depth (LT2)	19.1950	21.3182	21.2636	21.2002	21.1389	21.0560	20.9642	20.8970	m
Depth (DPT2)	19.2200	21.1582	21.1168	21.0693	20.9964	20.9084	20.8109	20.7322	m
Flowrate 2	0.0000	0.1883	0.2536	0.3108	0.3596	0.4029	0.4441	0.4693	m3/s
Inlet mfr	0.0004	0.0461	0.0616	0.0750	0.0853	0.0917	0.0976	0.1008	kg/s
Outlet mfr	0.0000	0.0494	0.0663	0.0804	0.0912	0.0979	0.1037	0.1082	kg/s
Power	5.4806	14.3752	18.5844	23.0006	27.6550	32.8627	38.6790	42.6754	kW
P atm	97.9560	97.9664	97.9855	97.9766	97.9603	97.9542	97.9537	97.9546	kPa
TT 1	10.0000	11.1758	11.4295	11.6000	11.7202	11.8151	11.9410	12.0377	C
GT1	0.0000	0.0000	0.0000	0.0000	0.0000	0.0000	0.0000	0.0000	%
DPT1	-31.0290	-355.3398	-590.7941	-862.3736	-1109.4478	-1295.3188	-1457.9218	-1557.0994	Pa
Avg Del. Pr.	311.5500	308.2422	308.7026	309.1147	309.3141	309.2943	309.1985	308.9687	Kpa
D1T1	285.0600	286.9416	286.9658	286.9958	287.0432	287.1033	287.1758	287.2614	K
D1T2	286.9600	286.9503	286.9746	287.0043	287.0518	287.1117	287.1856	287.2712	K
Diff. T	1895.8000	8.7577	8.7780	8.4852	8.5989	8.3552	9.7977	9.8011	mK
LT1	0.1658	0.8340	0.8891	0.9532	1.0499	1.1275	1.2142	1.2614	m
LT2	1.9543	1.3054	1.2510	1.1876	1.1261	1.0432	0.9516	0.8841	m
LT2 (DPT2)	1.7555	1.1454	1.1042	1.0567	0.9836	0.8955	0.7984	0.7193	m
LT3	1.7000	1.6999	1.7001	1.7001	1.6999	1.6998	1.7001	1.6999	m
DPT2	213.2500	207.8441	208.0294	208.2218	208.1713	207.9783	207.7304	207.4218	kPa
DPT3	215.1800	210.1418	210.5830	211.0041	211.2198	211.2061	211.1108	210.8800	kPa
Down. Pr. 1	0.0081	0.0204	0.0082	-0.0001	-0.0065	-0.0001	0.0381	0.0341	bar
Down. Pr. 2	0.0198	0.1021	0.0617	0.0525	0.0594	0.0445	0.0301	0.0159	bar
Down. Pr. 3	0.0108	0.1636	0.1378	0.1314	0.1320	0.1175	0.1087	0.1008	bar
Down. Pr. 4	0.0110	0.2308	0.2139	0.2064	0.2088	0.2018	0.2020	0.1934	bar

RPM	600	650	700	750	800	850	880
Down. Pr. 1 Void Fraction (m3/m3)	0.1677	0.1681	0.1685	0.1671	0.1605	0.1509	0.1486
Down. Pr. 2 Void Fraction (m3/m3)	0.1570	0.1609	0.1613	0.1582	0.1546	0.1519	0.1508
Down. Pr. 3 Void Fraction (m3/m3)	0.1499	0.1516	0.1516	0.1494	0.1458	0.1425	0.1407
Down. Pr. 4 Void Fraction (m3/m3)	0.1427	0.1433	0.1434	0.1411	0.1368	0.1327	0.1310

BM81									
Fill level	<0.164 (Below flanges)								m
RPM	0.0000	599.9794	650.0090	699.9852	749.9747	799.9952	849.9859	880.3377	rpm
Head (LT2)	3.5810	4.3667	4.4335	4.4871	4.5239	4.5607	4.5934	4.6135	m
Head (DPT2)	3.5563	4.5779	4.6410	4.6933	4.7248	4.7680	4.8037	4.8165	m
Depth (LT2)	19.2650	21.4226	21.3929	21.3702	21.3548	21.3381	21.3219	21.3109	m
Depth (DPT2)	19.2900	21.2114	21.1854	21.1641	21.1538	21.1309	21.1116	21.1078	m
Flowrate 2	0.0000	0.1026	0.1347	0.1639	0.1870	0.2088	0.2293	0.2416	m3/s
Inlet mfr	0.0004	0.0216	0.0298	0.0375	0.0436	0.0497	0.0543	0.0567	kg/s
Outlet mfr	0.0000	0.0220	0.0318	0.0398	0.0467	0.0531	0.0579	0.0607	kg/s
Power	2.7300	7.3541	9.4201	11.6007	13.9124	16.4588	19.1799	21.0911	kW
P atm	97.9780	97.9633	97.9564	97.9428	97.9392	97.9240	97.9146	97.9149	kPa
TT 1	10.4000	11.1279	11.3292	11.5000	11.6483	11.7411	11.8007	11.9000	C
GT1	0.0000	0.0000	0.0000	0.0000	0.0000	0.0000	0.0000	0.0000	%
DPT1	-69.9550	-147.0395	-211.7166	-290.7299	-365.2533	-446.1485	-513.9644	-555.8077	Pa
Avg Del. Pr.	312.0400	308.2787	308.2951	308.3594	308.5540	308.6490	308.7573	308.8578	Kpa
D1T1	286.1100	287.1671	287.1723	287.1859	287.2067	287.2326	287.2637	287.3020	K
D1T2	287.0600	287.1758	287.1807	287.1941	287.2134	287.2393	287.2723	287.3110	K
Diff. T	947.7400	8.7569	8.4552	8.1522	6.6313	6.7446	8.5077	9.0245	mK
LT1	0.1595	0.7664	0.8033	0.8345	0.8557	0.8759	0.8923	0.9013	m
LT2	1.9723	1.4099	1.3801	1.3577	1.3421	1.3254	1.3092	1.2981	m
LT2 (DPT2)	1.8141	1.1988	1.1726	1.1515	1.1411	1.1182	1.0989	1.0950	m
LT3	1.7000	1.7001	1.6999	1.7001	1.7000	1.7000	1.7000	1.6999	m
DPT2	213.7500	208.1406	208.0980	208.0976	208.2109	208.2519	208.3126	208.3708	kPa
DPT3	215.6900	210.1814	210.2048	210.2826	210.4808	210.5909	210.7086	210.8089	kPa
Down. Pr. 1	0.0079	0.0534	0.0442	0.0397	0.0261	0.0178	0.0119	0.0101	bar
Down. Pr. 2	0.0197	0.1319	0.1307	0.1256	0.0946	0.0851	0.0645	0.0524	bar
Down. Pr. 3	0.0107	0.1756	0.1758	0.1776	0.1571	0.1521	0.1396	0.1281	bar
Down. Pr. 4	0.0108	0.2354	0.2363	0.2423	0.2249	0.2198	0.2153	0.2069	bar

RPM	600	650	700	750	800	850	880
Down. Pr. 1 Void Fraction (m3/m3)	0.0984	0.1134	0.1244	0.1314	0.1351	0.1368	0.1387
Down. Pr. 2 Void Fraction (m3/m3)	0.0921	0.1055	0.1159	0.1240	0.1277	0.1308	0.1338
Down. Pr. 3 Void Fraction (m3/m3)	0.0889	0.1018	0.1113	0.1180	0.1210	0.1231	0.1258
Down. Pr. 4 Void Fraction (m3/m3)	0.0849	0.0972	0.1060	0.1121	0.1150	0.1162	0.1185

BM82									
Fill level	<0.164 (Below flanges)								m
RPM	0.0000	599.9834	650.0030	699.9896	749.9705	799.9913	849.9743	880.3477	rpm
Head (LT2)	3.8955	4.3039	4.3741	4.4187	4.4538	4.4905	4.5267	4.5457	m
Head (DPT2)	3.8335	4.5135	4.5823	4.6226	4.6483	4.6915	4.7228	4.7484	m
Depth (LT2)	19.1130	21.4874	21.4582	21.4380	21.4237	21.4057	21.3891	21.3797	m
Depth (DPT2)	19.1750	21.2778	21.2500	21.2341	21.2291	21.2048	21.1931	21.1770	m
Flowrate 2	0.0000	0.1044	0.1363	0.1649	0.1876	0.2090	0.2288	0.2400	m3/s
Inlet mfr	0.0004	0.0219	0.0303	0.0373	0.0434	0.0490	0.0535	0.0558	kg/s
Outlet mfr	0.0000	0.0225	0.0320	0.0398	0.0464	0.0522	0.0572	0.0594	kg/s
Power	4.9955	7.3562	9.4251	11.6256	13.9111	16.4936	19.2353	21.0754	kW
P atm	97.9110	97.9085	97.9041	97.9036	97.9060	97.9098	97.9036	97.8982	kPa
TT 1	11.3000	11.6000	11.7000	11.8000	11.9000	11.9372	12.0000	12.0909	C
GT1	0.0000	0.0000	0.0000	0.0000	0.0000	0.0000	0.0000	0.0000	%
DPT1	-87.9070	-171.6390	-246.1829	-316.6182	-382.4474	-461.8510	-534.9669	-562.9092	Pa
Avg Del. Pr.	311.3200	308.8815	308.8889	308.9312	309.0941	309.2741	309.3487	309.4221	Kpa
D1T1	287.1000	287.3019	287.3118	287.3275	287.3502	287.3778	287.4109	287.4498	K
D1T2	287.2800	287.3103	287.3204	287.3361	287.3572	287.3846	287.4190	287.4587	K
Diff. T	180.5400	8.3853	8.6919	8.5836	7.0159	6.8392	8.1015	8.9576	mK
LT1	0.1649	0.7682	0.8093	0.8337	0.8543	0.8732	0.8930	0.9024	m
LT2	2.0000	1.4747	1.4455	1.4253	1.4108	1.3930	1.3766	1.3670	m
LT2 (DPT2)	1.7271	1.2650	1.2373	1.2214	1.2162	1.1921	1.1805	1.1643	m
LT3	1.7000	1.7000	1.7000	1.7000	1.6998	1.7000	1.7001	1.7000	m
DPT2	216.9500	208.7743	208.7336	208.7521	208.8448	208.9275	208.9489	208.9934	kPa
DPT3	218.9300	210.8390	210.8508	210.8936	211.0541	211.2303	211.3111	211.3899	kPa
Down. Pr. 1	0.0083	0.0574	0.0489	0.0406	0.0252	0.0180	0.0113	0.0099	bar
Down. Pr. 2	0.0190	0.1338	0.1335	0.1296	0.0980	0.0882	0.0713	0.0575	bar
Down. Pr. 3	0.0099	0.1783	0.1786	0.1813	0.1603	0.1551	0.1462	0.1339	bar
Down. Pr. 4	0.0423	0.2375	0.2386	0.2466	0.2280	0.2257	0.2192	0.2120	bar

RPM	600	650	700	750	800	850	880
Down. Pr. 1 Void Fraction (m3/m3)	0.1006	0.1141	0.1255	0.1363	0.1355	0.1411	0.1387
Down. Pr. 2 Void Fraction (m3/m3)	0.0943	0.1064	0.1166	0.1283	0.1277	0.1341	0.1332
Down. Pr. 3 Void Fraction (m3/m3)	0.0910	0.1027	0.1120	0.1221	0.1211	0.1263	0.1252
Down. Pr. 4 Void Fraction (m3/m3)	0.0870	0.0981	0.1067	0.1161	0.1148	0.1195	0.1179

BM83									
Fill level	<0.164 (Below flanges)								m
RPM	0.0000	599.9710	650.0081	699.9901	749.9803	799.9926	849.9876	880.3415	rpm
Head (LT2)	3.6670	4.2257	4.2985	4.3410	4.3748	4.4106	4.4496	4.4704	m
Head (DPT2)	2.7303	4.4244	4.4910	4.5336	4.5648	4.5989	4.6344	4.6569	m
Depth (LT2)	19.2230	21.5723	21.5437	21.5219	21.5073	21.4900	21.4712	21.4609	m
Depth (DPT2)	20.1590	21.3736	21.3513	21.3292	21.3174	21.3017	21.2864	21.2743	m
Flowrate 2	0.0000	0.1092	0.1413	0.1693	0.1922	0.2137	0.2348	0.2468	m3/s
Inlet mfr	0.0006	0.0230	0.0318	0.0390	0.0453	0.0504	0.0551	0.0577	kg/s
Outlet mfr	0.0000	0.0236	0.0331	0.0407	0.0470	0.0528	0.0576	0.0602	kg/s
Power	4.7428	7.5402	9.5956	11.7436	14.0881	16.6029	19.3249	21.1527	kW
P atm	97.9290	97.9175	97.8865	97.8682	97.8782	97.8845	97.8977	97.8814	kPa
TT 1	10.2560	10.5983	10.8444	11.0000	11.1000	11.2000	11.3000	11.3182	C
GT1	0.0000	0.0000	0.0000	0.0000	0.0000	0.0000	0.0000	0.0000	%
DPT1	-35.2580	-124.8666	-187.3967	-268.9936	-332.4230	-404.7013	-479.7551	-521.0881	Pa
Avg Del. Pr.	321.0700	309.8691	309.8311	309.9431	310.0937	310.1934	310.3523	310.4444	Kpa
D1T1	286.4500	286.4007	286.4120	286.4261	286.4471	286.4726	286.5031	286.5404	K
D1T2	286.6700	286.4096	286.4204	286.4340	286.4534	286.4791	286.5115	286.5492	K
Diff. T	222.9800	8.8695	8.3763	7.8998	6.2797	6.5276	8.4129	8.7455	mK
LT1	0.1639	0.7749	0.8194	0.8398	0.8592	0.8776	0.8978	0.9083	m
LT2	2.0000	1.5595	1.5312	1.5092	1.4946	1.4773	1.4586	1.4482	m
LT2 (DPT2)	2.7262	1.3608	1.3387	1.3165	1.3047	1.2890	1.2737	1.2616	m
LT3	1.7000	1.6999	1.7002	1.7000	1.7000	1.7000	1.7000	1.7000	m
DPT2	233.9600	209.7338	209.6809	209.7254	209.8188	209.9123	209.9872	210.0442	kPa
DPT3	235.8600	211.8176	211.8106	211.9409	212.0816	212.1749	212.3206	212.4290	kPa
Down. Pr. 1	0.0087	0.0632	0.0548	0.0418	0.0242	0.0199	0.0101	0.0084	bar
Down. Pr. 2	0.0745	0.1381	0.1385	0.1279	0.0989	0.0939	0.0702	0.0618	bar
Down. Pr. 3	0.1381	0.1832	0.1810	0.1807	0.1643	0.1589	0.1462	0.1392	bar
Down. Pr. 4	0.2112	0.2438	0.2417	0.2451	0.2314	0.2302	0.2206	0.2178	bar

RPM	600	650	700	750	800	850	880
Down. Pr. 1 Void Fraction (m3/m3)	0.1049	0.1236	0.1291	0.1364	0.1380	0.1406	0.1401
Down. Pr. 2 Void Fraction (m3/m3)	0.0986	0.1154	0.1202	0.1282	0.1297	0.1336	0.1339
Down. Pr. 3 Void Fraction (m3/m3)	0.0951	0.1117	0.1154	0.1218	0.1232	0.1258	0.1258
Down. Pr. 4 Void Fraction (m3/m3)	0.0908	0.1067	0.1100	0.1158	0.1168	0.1189	0.1185

BM84									
Fill level	0.189								m
RPM	0.0000	599.9695	650.0057	699.9868	749.9775	799.9923	849.9891	880.3049	rpm
Head (LT2)	3.4190	4.1480	4.2200	4.2611	4.2917	4.3302	4.3705	4.3933	m
Head (DPT2)	1.2530	4.3155	4.3827	4.4201	4.4391	4.4731	4.5091	4.5282	m
Depth (LT2)	19.3700	21.6519	21.6227	21.6027	21.5888	21.5704	21.5514	21.5396	m
Depth (DPT2)	21.5360	21.4843	21.4600	21.4438	21.4414	21.4276	21.4128	21.4046	m
Flowrate 2	0.0000	0.1121	0.1440	0.1702	0.1939	0.2155	0.2363	0.2487	m3/s
Inlet mfr	0.0011	0.0234	0.0318	0.0384	0.0454	0.0507	0.0556	0.0588	kg/s
Outlet mfr	0.0000	0.0241	0.0332	0.0399	0.0468	0.0525	0.0574	0.0603	kg/s
Power	2.5481	7.5101	9.5694	11.6926	14.0688	16.7068	19.4802	21.3298	kW
P atm	97.8840	97.9263	97.9202	97.9197	97.9175	97.9167	97.9308	97.9185	kPa
TT 1	11.2000	10.9715	11.1852	11.2846	11.3178	11.4000	11.4570	11.5000	C
GT1	0.0000	0.0000	0.0000	0.0000	0.0000	0.0000	0.0000	0.0000	%
DPT1	-58.4430	-160.7678	-219.9078	-291.4529	-365.6585	-433.4788	-503.2973	-553.8292	Pa
Avg Del. Pr.	333.9600	310.6371	310.6186	310.7375	310.9048	311.0333	311.1946	311.2658	Kpa
D1T1	286.5400	286.5449	286.5545	286.5698	286.5913	286.6173	286.6487	286.6856	K
D1T2	286.5500	286.5534	286.5631	286.5778	286.5978	286.6238	286.6564	286.6939	K
Diff. T	10.5500	8.4749	8.6125	7.9772	6.5250	6.4437	7.7041	8.3748	mK
LT1	0.1898	0.7768	0.8199	0.8408	0.8575	0.8776	0.8989	0.9098	m
LT2	2.0000	1.6391	1.6102	1.5900	1.5761	1.5576	1.5387	1.5268	m
LT2 (DPT2)	4.0885	1.4715	1.4475	1.4310	1.4287	1.4148	1.4001	1.3919	m
LT3	1.7000	1.6999	1.7002	1.7000	1.7000	1.6999	1.7000	1.7000	m
DPT2	245.0700	210.5783	210.5091	210.5199	210.6735	210.7185	210.7656	210.8078	kPa
DPT3	246.9200	212.5768	212.5645	212.6838	212.8533	212.9826	213.1299	213.2132	kPa
Down. Pr. 1	0.0959	0.0673	0.0626	0.0472	0.0291	0.0208	0.0163	0.0122	bar
Down. Pr. 2	0.1847	0.1408	0.1419	0.1335	0.1086	0.0985	0.0849	0.0762	bar
Down. Pr. 3	0.2465	0.1875	0.1892	0.1861	0.1702	0.1635	0.1572	0.1521	bar
Down. Pr. 4	0.3210	0.2477	0.2462	0.2537	0.2372	0.2317	0.2284	0.2253	bar

RPM	600	650	700	750	800	850	880
Down. Pr. 1 Void Fraction (m3/m3)	0.1406	0.1484	0.1528	0.1603	0.1620	0.1627	0.1637
Down. Pr. 2 Void Fraction (m3/m3)	0.1326	0.1394	0.1427	0.1503	0.1521	0.1538	0.1554
Down. Pr. 3 Void Fraction (m3/m3)	0.1279	0.1345	0.1371	0.1434	0.1447	0.1455	0.1465
Down. Pr. 4 Void Fraction (m3/m3)	0.1224	0.1290	0.1306	0.1366	0.1377	0.1381	0.1388

BM85									
Fill level	0.285								m
RPM	0.0000	599.9766	650.0087	699.9872	749.9771	799.9984	849.9911	880.3111	rpm
Head (LT2)	3.7096	4.0631	4.1320	4.1707	4.1974	4.2336	4.2746	4.2978	m
Head (DPT2)	2.4264	4.2281	4.2913	4.3247	4.3509	4.3802	4.4175	4.4402	m
Depth (LT2)	19.3180	21.7424	21.7130	21.6933	21.6854	21.6666	21.6468	21.6351	m
Depth (DPT2)	20.6010	21.5774	21.5537	21.5393	21.5320	21.5201	21.5039	21.4927	m
Flowrate 2	0.0000	0.1156	0.1470	0.1726	0.1950	0.2172	0.2388	0.2506	m3/s
Inlet mfr	0.0008	0.0236	0.0318	0.0386	0.0446	0.0506	0.0555	0.0576	kg/s
Outlet mfr	0.0003	0.0246	0.0331	0.0400	0.0460	0.0520	0.0571	0.0590	kg/s
Power	4.3003	7.5372	9.5302	11.6818	14.0671	16.6325	19.4852	21.3002	kW
P atm	97.9100	97.8966	97.8860	97.9085	97.8937	97.8788	97.8740	97.8625	kPa
TT 1	11.2380	11.2695	11.3205	11.4000	11.5000	11.5000	11.6000	11.6060	C
GT1	0.0000	0.0000	0.0000	0.0000	0.0000	0.0000	0.0000	0.0000	%
DPT1	-67.8100	-168.8272	-230.4607	-311.0669	-376.8104	-448.1473	-512.5042	-553.1798	Pa
Avg Del. Pr.	324.6800	311.5865	311.5628	311.6937	311.8534	311.9690	312.0748	312.1552	Kpa
D1T1	286.6800	286.7050	286.7138	286.7288	286.7497	286.7751	286.8061	286.8416	K
D1T2	286.7100	286.7134	286.7224	286.7366	286.7563	286.7817	286.8135	286.8505	K
Diff. T	26.1780	8.4072	8.6992	7.8061	6.5832	6.6122	7.4521	8.8167	mK
LT1	0.2850	0.7824	0.8220	0.8412	0.8600	0.8772	0.8984	0.9099	m
LT2	2.0000	1.7296	1.7003	1.6808	1.6728	1.6539	1.6341	1.6224	m
LT2 (DPT2)	3.1452	1.5646	1.5410	1.5267	1.5193	1.5073	1.4912	1.4800	m
LT3	1.7000	1.6998	1.7000	1.7002	1.7001	1.6999	1.7000	1.7000	m
DPT2	245.9700	211.5034	211.4417	211.4680	211.5656	211.6356	211.6776	211.6864	kPa
DPT3	247.7900	213.5559	213.5428	213.6512	213.8257	213.9562	214.0668	214.1587	kPa
Down. Pr. 1	0.1048	0.0719	0.0715	0.0486	0.0304	0.0237	0.0192	0.0109	bar
Down. Pr. 2	0.1941	0.1442	0.1476	0.1333	0.1126	0.1073	0.0978	0.0808	bar
Down. Pr. 3	0.2557	0.1924	0.1985	0.1885	0.1733	0.1694	0.1641	0.1558	bar
Down. Pr. 4	0.3302	0.2520	0.2513	0.2527	0.2422	0.2389	0.2353	0.2292	bar

RPM	600	650	700	750	800	850	880
Down. Pr. 1 Void Fraction (m3/m3)	0.1374	0.1447	0.1518	0.1569	0.1603	0.1607	0.1603
Down. Pr. 2 Void Fraction (m3/m3)	0.1297	0.1363	0.1419	0.1468	0.1498	0.1507	0.1513
Down. Pr. 3 Void Fraction (m3/m3)	0.1251	0.1312	0.1361	0.1402	0.1429	0.1432	0.1427
Down. Pr. 4 Void Fraction (m3/m3)	0.1197	0.1262	0.1299	0.1333	0.1358	0.1360	0.1352

BM86									
Fill level	0.365								m
RPM	0.0000	599.9757	650.0083	699.9849	749.9777	799.9959	849.9866	880.2792	rpm
Head (LT2)	3.3811	4.0014	4.0657	4.1017	4.1299	4.1682	4.2104	4.2394	m
Head (DPT2)	0.3029	4.1646	4.2214	4.2510	4.2764	4.3110	4.3468	4.3759	m
Depth (LT2)	19.4400	21.8091	21.7814	21.7635	21.7503	21.7327	21.7121	21.6998	m
Depth (DPT2)	22.5180	21.6459	21.6257	21.6141	21.6039	21.5899	21.5757	21.5633	m
Flowrate 2	0.0000	0.1182	0.1496	0.1747	0.1973	0.2196	0.2407	0.2535	m3/s
Inlet mfr	0.0016	0.0238	0.0311	0.0373	0.0445	0.0498	0.0547	0.0571	kg/s
Outlet mfr	0.0000	0.0250	0.0327	0.0388	0.0462	0.0512	0.0565	0.0595	kg/s
Power	0.7348	7.5632	9.5716	11.6832	14.0324	16.6540	19.4346	21.3588	kW
P atm	97.6880	97.5842	97.5870	97.5720	97.5422	97.5518	97.5547	97.5631	kPa
TT 1	10.3000	11.0000	11.1815	11.3000	11.4000	11.4946	11.5332	11.6000	C
GT1	0.0000	0.0000	0.0000	0.0000	0.0000	0.0000	0.0000	0.0000	%
DPT1	-83.7520	-182.6797	-243.8455	-299.8976	-377.5020	-449.9464	-520.0226	-562.0131	Pa
Avg Del. Pr.	343.3200	311.9092	311.9325	312.0388	312.1939	312.3143	312.4473	312.5721	Kpa
D1T1	286.6900	286.7043	286.7138	286.7293	286.7510	286.7769	286.8084	286.8449	K
D1T2	286.6900	286.7129	286.7228	286.7376	286.7578	286.7836	286.8157	286.8528	K
Diff. T	0.6559	8.5645	8.9498	8.3225	6.7547	6.7670	7.3730	7.8624	mK
LT1	0.3648	0.7874	0.8243	0.8423	0.8575	0.8778	0.8995	0.9161	m
LT2	2.0000	1.7963	1.7689	1.7509	1.7378	1.7199	1.6994	1.6870	m
LT2 (DPT2)	5.0672	1.6331	1.6132	1.6016	1.5914	1.5771	1.5630	1.5505	m
LT3	1.7000	1.6999	1.7002	1.7001	1.7003	1.7000	1.7000	1.6999	m
DPT2	246.7700	212.1875	212.1637	212.2180	212.2894	212.3420	212.4011	212.4076	kPa
DPT3	248.5900	214.1910	214.2115	214.3327	214.5177	214.6285	214.7585	214.8749	kPa
Down. Pr. 1	0.1096	0.0737	0.0752	0.0598	0.0292	0.0234	0.0195	0.0156	bar
Down. Pr. 2	0.1996	0.1438	0.1503	0.1404	0.1140	0.1054	0.0996	0.0938	bar
Down. Pr. 3	0.2612	0.1896	0.2033	0.1949	0.1743	0.1697	0.1645	0.1618	bar
Down. Pr. 4	0.3358	0.2533	0.2650	0.2609	0.2422	0.2380	0.2349	0.2349	bar

RPM	600	650	700	750	800	850	880
Down. Pr. 1 Void Fraction (m3/m3)	0.1361	0.1399	0.1449	0.1556	0.1572	0.1582	0.1575
Down. Pr. 2 Void Fraction (m3/m3)	0.1286	0.1318	0.1358	0.1453	0.1471	0.1482	0.1477
Down. Pr. 3 Void Fraction (m3/m3)	0.1242	0.1267	0.1303	0.1387	0.1400	0.1409	0.1401
Down. Pr. 4 Void Fraction (m3/m3)	0.1185	0.1211	0.1242	0.1320	0.1332	0.1338	0.1328

BM87									
Fill level	0.450								m
RPM	0.0000	599.9774	650.0111	699.9880	749.9782	800.0017	849.9818	880.2659	rpm
Head (LT2)	3.4621	3.9201	3.9792	4.0120	4.0384	4.0846	4.1269	4.1509	m
Head (DPT2)	0.0011	4.0744	4.1344	4.1604	4.1799	4.2221	4.2555	4.2774	m
Depth (LT2)	19.4250	21.8964	21.8698	21.8539	21.8387	21.8187	21.7991	21.7876	m
Depth (DPT2)	22.8860	21.7421	21.7146	21.7056	21.6973	21.6811	21.6705	21.6612	m
Flowrate 2	0.0000	0.1217	0.1525	0.1773	0.2001	0.2225	0.2438	0.2563	m3/s
Inlet mfr	0.0003	0.0265	0.0332	0.0404	0.0469	0.0521	0.0573	0.0600	kg/s
Outlet mfr	0.0000	0.0255	0.0323	0.0396	0.0457	0.0506	0.0558	0.0584	kg/s
Power	0.0621	7.6985	9.6719	11.7800	14.0500	16.6649	19.4751	21.3385	kW
P atm	96.2730	96.2594	96.2393	96.2261	96.2220	96.2232	96.2226	96.2138	kPa
TT 1	9.7274	10.0064	10.1623	10.2128	10.3000	10.3195	10.4000	10.4000	C
GT1	0.0000	0.0000	0.0000	0.0000	0.0000	0.0000	0.0000	0.0000	%
DPT1	-41.4080	-163.3196	-232.3805	-311.2397	-388.0773	-454.2868	-536.4401	-587.4532	Pa
Avg Del. Pr.	345.8700	311.6034	311.6225	311.7701	311.9390	312.0662	312.1721	312.2685	Kpa
D1T1	284.9400	285.0015	285.0166	285.0378	285.0638	285.0944	285.1308	285.1719	K
D1T2	284.9300	285.0098	285.0252	285.0450	285.0701	285.1007	285.1374	285.1793	K
Diff. T	-8.5268	8.2616	8.5945	7.2162	6.3452	6.2648	6.6440	7.4112	mK
LT1	0.4518	0.7933	0.8259	0.8429	0.8542	0.8802	0.9029	0.9157	m
LT2	2.0000	1.8836	1.8570	1.8411	1.8260	1.8059	1.7863	1.7750	m
LT2 (DPT2)	5.4610	1.7293	1.7018	1.6928	1.6846	1.6684	1.6578	1.6486	m
LT3	1.7000	1.6999	1.6999	1.6999	1.7000	1.7000	1.7000	1.7001	m
DPT2	247.6400	213.1946	213.1000	213.1799	213.2742	213.3096	213.4086	213.4447	kPa
DPT3	249.4600	215.2100	215.2492	215.4100	215.5831	215.7090	215.8155	215.9207	kPa
Down. Pr. 1	0.1040	0.0601	0.0644	0.0363	0.0185	0.0123	0.0098	0.0039	bar
Down. Pr. 2	0.1948	0.1335	0.1400	0.1194	0.1062	0.0980	0.0934	0.0860	bar
Down. Pr. 3	0.2565	0.1799	0.1902	0.1730	0.1634	0.1576	0.1549	0.1512	bar
Down. Pr. 4	0.3311	0.2423	0.2545	0.2417	0.2324	0.2281	0.2254	0.2246	bar

RPM	600	650	700	750	800	850	880
Down. Pr. 1 Void Fraction (m3/m3)	0.1483	0.1476	0.1570	0.1634	0.1642	0.1649	0.1653
Down. Pr. 2 Void Fraction (m3/m3)	0.1398	0.1389	0.1467	0.1520	0.1530	0.1539	0.1544
Down. Pr. 3 Void Fraction (m3/m3)	0.1349	0.1337	0.1408	0.1454	0.1461	0.1467	0.1467
Down. Pr. 4 Void Fraction (m3/m3)	0.1288	0.1275	0.1338	0.1382	0.1386	0.1392	0.1389

BM88									
Fill level	0.550								m
RPM	0.0000	599.9738	650.0070	699.9947	749.9784	799.9949	849.9910	880.2756	rpm
Head (LT2)	3.5614	3.8374	3.8919	3.9248	3.9519	3.9943	4.0389	4.0660	m
Head (DPT2)	0.0002	3.9960	4.0455	4.0722	4.0936	4.1284	4.1688	4.1916	m
Depth (LT2)	19.4340	21.9804	21.9568	21.9416	21.9260	21.9061	21.8857	21.8745	m
Depth (DPT2)	22.9950	21.8217	21.8031	21.7942	21.7843	21.7721	21.7558	21.7489	m
Flowrate 2	0.0000	0.1240	0.1538	0.1782	0.2009	0.2233	0.2448	0.2572	m3/s
Inlet mfr	0.0003	0.0266	0.0326	0.0392	0.0459	0.0513	0.0560	0.0591	kg/s
Outlet mfr	0.0000	0.0254	0.0317	0.0384	0.0448	0.0500	0.0547	0.0576	kg/s
Power	0.0636	7.6220	9.5361	11.6449	13.9222	16.5217	19.3837	21.2047	kW
P atm	96.1910	96.1854	96.1807	96.1693	96.1550	96.1435	96.1402	96.1296	kPa
TT 1	10.2000	10.2552	10.4000	10.4000	10.5000	10.5000	10.5869	10.6000	C
GT1	0.0000	0.0000	0.0000	0.0000	0.0000	0.0000	0.0000	0.0000	%
DPT1	-63.3300	-181.6121	-231.5714	-307.2155	-383.2994	-467.1412	-544.2240	-595.3530	Pa
Avg Del. Pr.	346.7800	312.3529	312.3870	312.5190	312.6561	312.7826	312.8998	312.9913	Kpa
D1T1	285.1700	285.2268	285.2414	285.2616	285.2867	285.3160	285.3513	285.3912	K
D1T2	285.1700	285.2353	285.2501	285.2691	285.2931	285.3225	285.3579	285.3982	K
Diff. T	-2.0077	8.4749	8.7012	7.5312	6.3786	6.4117	6.6315	6.9922	mK
LT1	0.5511	0.7948	0.8255	0.8433	0.8550	0.8775	0.9016	0.9176	m
LT2	2.0000	1.9677	1.9440	1.9288	1.9134	1.8935	1.8731	1.8619	m
LT2 (DPT2)	5.5612	1.8091	1.7903	1.7815	1.7717	1.7594	1.7432	1.7362	m
LT3	1.7000	1.7000	1.6999	1.7000	1.7001	1.7000	1.7000	1.7001	m
DPT2	248.6200	213.9818	213.9704	214.0498	214.1292	214.2029	214.2497	214.3077	kPa
DPT3	250.4600	216.0336	216.0723	216.2157	216.3671	216.5051	216.6256	216.7277	kPa
Down. Pr. 1	0.1128	0.0643	0.0681	0.0484	0.0226	0.0173	0.0143	0.0106	bar
Down. Pr. 2	0.2037	0.1351	0.1407	0.1280	0.1117	0.1051	0.0979	0.0963	bar
Down. Pr. 3	0.2653	0.1826	0.1934	0.1828	0.1692	0.1641	0.1591	0.1576	bar
Down. Pr. 4	0.3398	0.2446	0.2581	0.2495	0.2364	0.2324	0.2287	0.2271	bar

RPM	600	650	700	750	800	850	880
Down. Pr. 1 Void Fraction (m3/m3)	0.1458	0.1439	0.1511	0.1594	0.1611	0.1609	0.1620
Down. Pr. 2 Void Fraction (m3/m3)	0.1377	0.1357	0.1417	0.1482	0.1499	0.1502	0.1508
Down. Pr. 3 Void Fraction (m3/m3)	0.1328	0.1303	0.1358	0.1417	0.1431	0.1431	0.1437
Down. Pr. 4 Void Fraction (m3/m3)	0.1268	0.1243	0.1293	0.1348	0.1361	0.1359	0.1365

BM89									
Fill level	0.650								m
RPM	0.0000	599.9760	650.0105	699.9832	749.9813	799.9975	849.9867	880.2534	rpm
Head (LT2)	3.6646	3.8309	3.8501	3.8644	3.8699	3.9060	3.9490	3.9736	m
Head (DPT2)	-0.0015	3.2580	3.5168	3.8068	3.9874	4.0405	4.0756	4.0995	m
Depth (LT2)	19.4360	22.0087	22.0063	22.0028	22.0092	21.9979	21.9792	21.9679	m
Depth (DPT2)	23.1020	22.5816	22.3396	22.0604	21.8917	21.8635	21.8526	21.8420	m
Flowrate 2	0.0000	0.1477	0.1659	0.1836	0.2035	0.2248	0.2460	0.2585	m3/s
Inlet mfr	0.0002	0.0251	0.0311	0.0378	0.0454	0.0504	0.0547	0.0579	kg/s
Outlet mfr	0.0000	0.0242	0.0301	0.0368	0.0443	0.0491	0.0539	0.0563	kg/s
Power	0.0575	7.6600	9.4510	11.5303	13.8817	16.3786	19.1592	21.0208	kW
P atm	96.1250	96.1205	96.1207	96.1244	96.1410	96.1607	96.1468	96.1229	kPa
TT 1	10.3000	10.4195	10.4949	10.5513	10.6284	10.7000	10.7688	10.8000	C
GT1	0.0000	0.0000	0.0000	0.0000	0.0000	0.0000	0.0000	0.0000	%
DPT1	-80.3310	-187.4631	-242.9158	-302.8921	-391.4270	-467.1011	-537.0810	-588.0133	Pa
Avg Del. Pr.	347.7100	319.7783	317.6010	315.0675	313.7048	313.6883	313.8284	313.8723	Kpa
D1T1	285.3900	285.4416	285.4555	285.4746	285.4997	285.5289	285.5635	285.6029	K
D1T2	285.3800	285.4496	285.4640	285.4826	285.5063	285.5353	285.5702	285.6098	K
Diff. T	-11.7740	8.0242	8.3988	7.9751	6.5892	6.4503	6.6849	6.9061	mK
LT1	0.6543	0.8166	0.8335	0.8441	0.8561	0.8810	0.9052	0.9186	m
LT2	2.0000	1.9960	1.9937	1.9901	1.9965	1.9853	1.9665	1.9553	m
LT2 (DPT2)	5.6661	2.5689	2.3270	2.0477	1.8790	1.8508	1.8398	1.8293	m
LT3	1.7000	1.7000	1.7001	1.6999	1.7000	1.7000	1.6999	1.7001	m
DPT2	249.6400	221.5583	219.3034	216.6938	215.1976	215.1077	215.2045	215.2289	kPa
DPT3	251.4500	223.5238	221.3463	218.8091	217.4298	217.3936	217.5476	217.6154	kPa
Down. Pr. 1	0.1221	0.0855	0.0802	0.0695	0.0281	0.0237	0.0200	0.0204	bar
Down. Pr. 2	0.2129	0.1582	0.1519	0.1417	0.1181	0.1110	0.1061	0.1012	bar
Down. Pr. 3	0.2772	0.2126	0.2066	0.1966	0.1731	0.1688	0.1643	0.1615	bar
Down. Pr. 4	0.3489	0.2799	0.2739	0.2628	0.2432	0.2384	0.2357	0.2333	bar

RPM	600	650	700	750	800	850	880
Down. Pr. 1 Void Fraction (m3/m3)	0.1173	0.1284	0.1404	0.1557	0.1569	0.1565	0.1574
Down. Pr. 2 Void Fraction (m3/m3)	0.1105	0.1211	0.1324	0.1446	0.1460	0.1457	0.1472
Down. Pr. 3 Void Fraction (m3/m3)	0.1059	0.1161	0.1269	0.1385	0.1396	0.1393	0.1404
Down. Pr. 4 Void Fraction (m3/m3)	0.1008	0.1105	0.1209	0.1315	0.1326	0.1321	0.1331

BM90									
Fill level	0.750								m
RPM	0.0000	599.9797	649.9988	699.9886	749.9816	800.0039	849.9907	880.2767	rpm
Head (LT2)	3.7597	3.8463	3.8915	3.9411	4.0034	3.9261	3.9424	3.9512	m
Head (DPT2)	0.0030	1.7178	1.9516	2.2209	2.5191	2.8057	3.0891	3.2705	m
Depth (LT2)	19.4340	22.0127	21.9796	21.9473	21.9032	21.9987	21.9988	22.0009	m
Depth (DPT2)	23.1910	24.1412	23.9195	23.6676	23.3875	23.1191	22.8520	22.6817	m
Flowrate 2	0.0000	0.1836	0.1990	0.2143	0.2289	0.2443	0.2599	0.2694	m3/s
Inlet mfr	0.0003	0.0143	0.0184	0.0232	0.0284	0.0343	0.0410	0.0456	kg/s
Outlet mfr	0.0000	0.0139	0.0184	0.0226	0.0278	0.0337	0.0402	0.0446	kg/s
Power	0.0565	7.1051	8.8163	10.7710	13.0325	15.6675	18.5840	20.4841	kW
P atm	96.1250	96.1148	96.1145	96.1163	96.1144	96.1206	96.1231	96.1334	kPa
TT 1	10.6720	10.6000	10.6431	10.6899	10.7362	10.7848	10.8631	10.9158	C
GT1	0.0000	0.0000	0.0000	0.0000	0.0000	0.0000	0.0000	0.0000	%
DPT1	-88.4900	-133.2277	-159.5985	-196.5942	-244.1140	-294.3849	-361.6777	-420.6400	Pa
Avg Del. Pr.	348.6200	335.2604	333.2257	330.9245	328.3727	325.9515	323.5593	322.0869	Kpa
D1T1	285.6100	285.6483	285.6596	285.6758	285.6972	285.7242	285.7572	285.7922	K
D1T2	285.6100	285.6531	285.6646	285.6810	285.7027	285.7301	285.7637	285.7994	K
Diff. T	-0.8558	4.8785	5.0376	5.2367	5.5196	5.9344	6.4720	7.2205	mK
LT1	0.7494	0.8359	0.8482	0.8655	0.8837	0.9019	0.9181	0.9291	m
LT2	2.0000	2.0000	1.9671	1.9347	1.8906	1.9861	1.9861	1.9882	m
LT2 (DPT2)	5.7567	4.1285	3.9069	3.6549	3.3749	3.1064	2.8393	2.6690	m
LT3	1.7000	1.7000	1.7002	1.7000	1.7001	1.7000	1.7000	1.7000	m
DPT2	250.5200	237.0835	235.0309	232.6915	230.0789	227.5965	225.1396	223.5714	kPa
DPT3	252.3600	239.0115	236.9772	234.6743	232.1242	229.6969	227.3022	225.8195	kPa
Down. Pr. 1	0.1315	0.1029	0.0992	0.0944	0.0817	0.0690	0.0640	0.0733	bar
Down. Pr. 2	0.2223	0.1826	0.1766	0.1685	0.1578	0.1475	0.1380	0.1360	bar
Down. Pr. 3	0.2865	0.2422	0.2362	0.2272	0.2161	0.2056	0.1959	0.1928	bar
Down. Pr. 4	0.3583	0.3094	0.3021	0.2947	0.2847	0.2752	0.2673	0.2653	bar

RPM	600	650	700	750	800	850	880
Down. Pr. 1 Void Fraction (m3/m3)	0.0565	0.0666	0.0775	0.0887	0.1004	0.1118	0.1182
Down. Pr. 2 Void Fraction (m3/m3)	0.0528	0.0624	0.0727	0.0832	0.0940	0.1051	0.1122
Down. Pr. 3 Void Fraction (m3/m3)	0.0503	0.0594	0.0694	0.0794	0.0897	0.1004	0.1073
Down. Pr. 4 Void Fraction (m3/m3)	0.0478	0.0565	0.0659	0.0754	0.0851	0.0951	0.1016

Appendix J: HAC performance map efficiency and volume VBA scripts

```
Function HAC_Fio(LT1, LT2)
ElevationForebayFloor = 298.328 'm
ElevationTailraceFloor = 293.318 'm
g = 9.81 'm/s^2
HAC_Fio = g * (ElevationForebayFloor + LT1 - (ElevationTailraceFloor + LT2)) 'J/kg
End Function

Function HAC_VdP(Patm, DPT1, D1T1, dT, LT1, DPT2)
ElevationCollarFloor = 287.468 'm
ElevationSeparatorFloor = 271.007 'm
ElevationForebayFloor = 298.328 'm
HeightfromSeparatorFloorToDPT2 = 4.663 'm
AirDensity = 1.2 'kg/m^3
g = 9.81 'm/s^2
R = 287.058 'Gas Constant, J/kgK
p3 = DPT2 + (ElevationCollarFloor - ElevationSeparatorFloor - _
   HeightfromSeparatorFloorToDPT2) * g * AirDensity / 1000 + Patm 'Pa
P1 = (ElevationCollarFloor - (ElevationForebayFloor + LT1)) * g * AirDensity / _
   1000 + Patm + DPT1 / 1000 'Pa
t3 = D1T1 + dT / 1000 'K
t1 = D1T1 'K
HAC_VdP = Application.WorksheetFunction.ln(p3 / P1) / _
   Application.WorksheetFunction.ln(t3 / t1) * R * (t3 - t1) 'J/kg
End Function

Function HAC_Efficiency(Vw, mg, Fio, VdP)
WaterDensity = 999
mw = Vw * WaterDensity
HAC_Efficiency = VdP * mg / mw / Fio * 100
End Function
Function HAC_Volume(LT1, LT2, LT3)
ForebayVolume_1 = 1.36517 'm^3 when LT1 reads 0.16m
ForebayVolume_2 = 17.0647 'm^3 when LT1 reads 2m
TailraceVolume_1 = 0 'm^3 when LT2 reads 2m
TailraceVolume_2 = 17.4373 'm^3 when LT2 reads 2m
TailraceVolume_3 = 18.9675 'm^3 when LT2 reads 2m
TailraceVolume_4 = 19.1117 'm^3 when LT2 reads 2m
SeparatorVolume_1 = 9.93365 'm^3 when LT3 reads 2.148m
SeparatorVolume_2 = 12.5027 'm^3 when LT3 reads 2.848m

ForebayHeight_1 = 0.16 'm
ForebayHeight_2 = 2 'm
TailraceHeight_1 = 0 'm
```

```
TailraceHeight_2 = 2 'm
TailraceHeight_3 = 4.987 'm
TailraceHeight_4 = 6.987 'm
SeparatorHeight_1 = 2.148 'm
SeparatorHeight_2 = 2.848 'm

LT3 = 2.298 'm Separator Set Level

VolumeForebay = LT1 / ForebayHeight_2 * ForebayVolume_2
VolumeSeparator = (LT3 - SeparatorHeight_1) / (SeparatorHeight_2 - SeparatorHeight_1) * _
   (SeparatorVolume_2 - SeparatorVolume_1) + SeparatorVolume_1
VolumePipes = 7.45304 'm^3
If LT2 > TailraceHeight_3 Then
VolumeTailrace = (LT2 - TailraceHeight_3) / (TailraceHeight_4 - TailraceHeight_3) * _
   (TailraceVolume_4 - TailraceVolume_3) + TailraceVolume_3
Else
If LT2 > TailraceHeight_2 Then
   VolumeTailrace = (LT2 - TailraceHeight_2) / (TailraceHeight_3 - TailraceHeight_2) * _
   (TailraceVolume_3 - TailraceVolume_2) + TailraceVolume_2
   Else
      VolumeTailrace = LT2 / TailraceHeight_2 * TailraceVolume_2
   End If
End If

HAC_Volume = VolumeForebay + VolumeSeparator + VolumeTailrace + VolumePipes
End Function
```

Appendix K: Efficiency, free air delivery and differential temperature plots

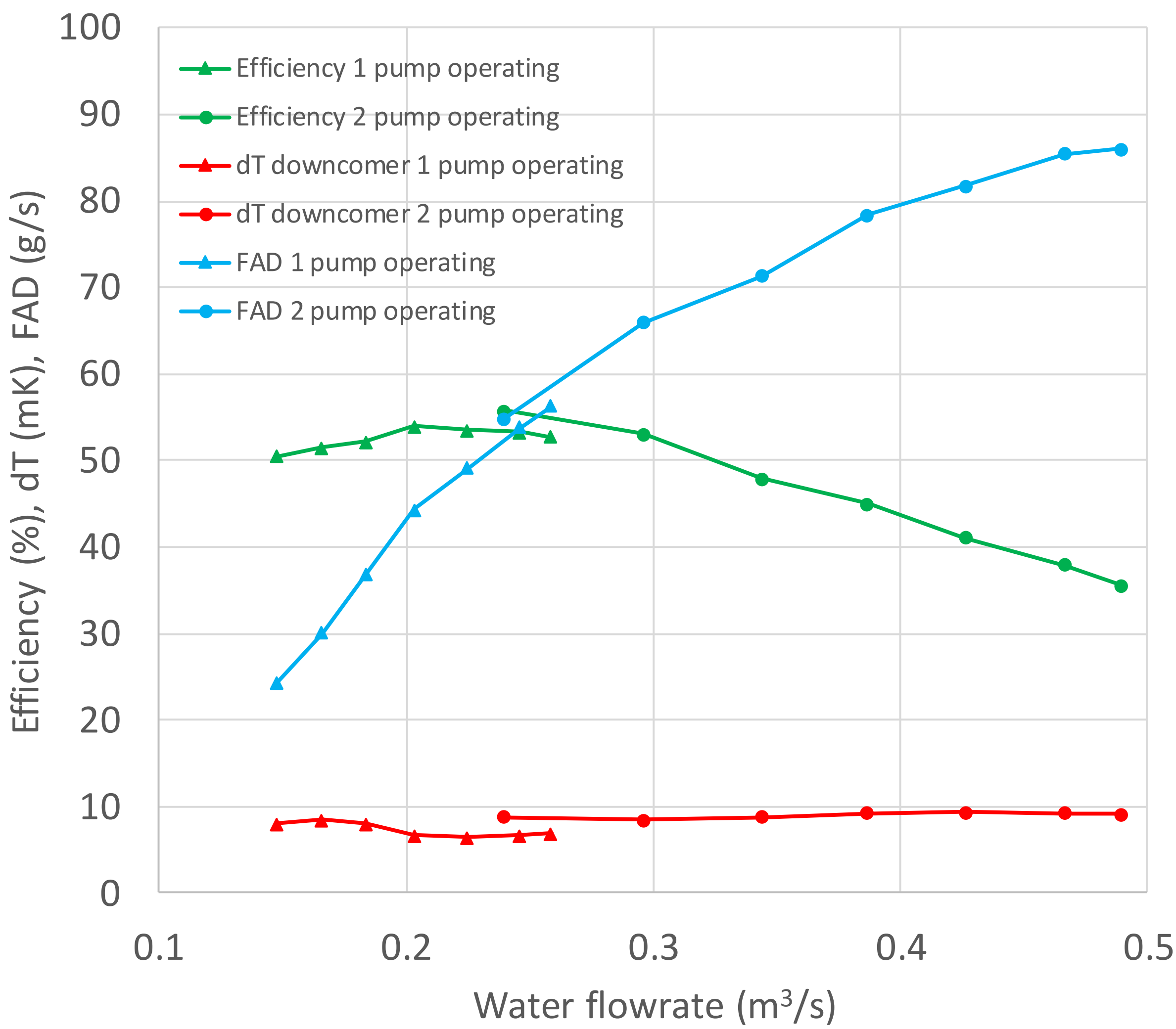

K1: Efficiency, difference in temperature and free air delivery for benchmark tests BM71 and BM89 showing the comparison between single and double pump tests.

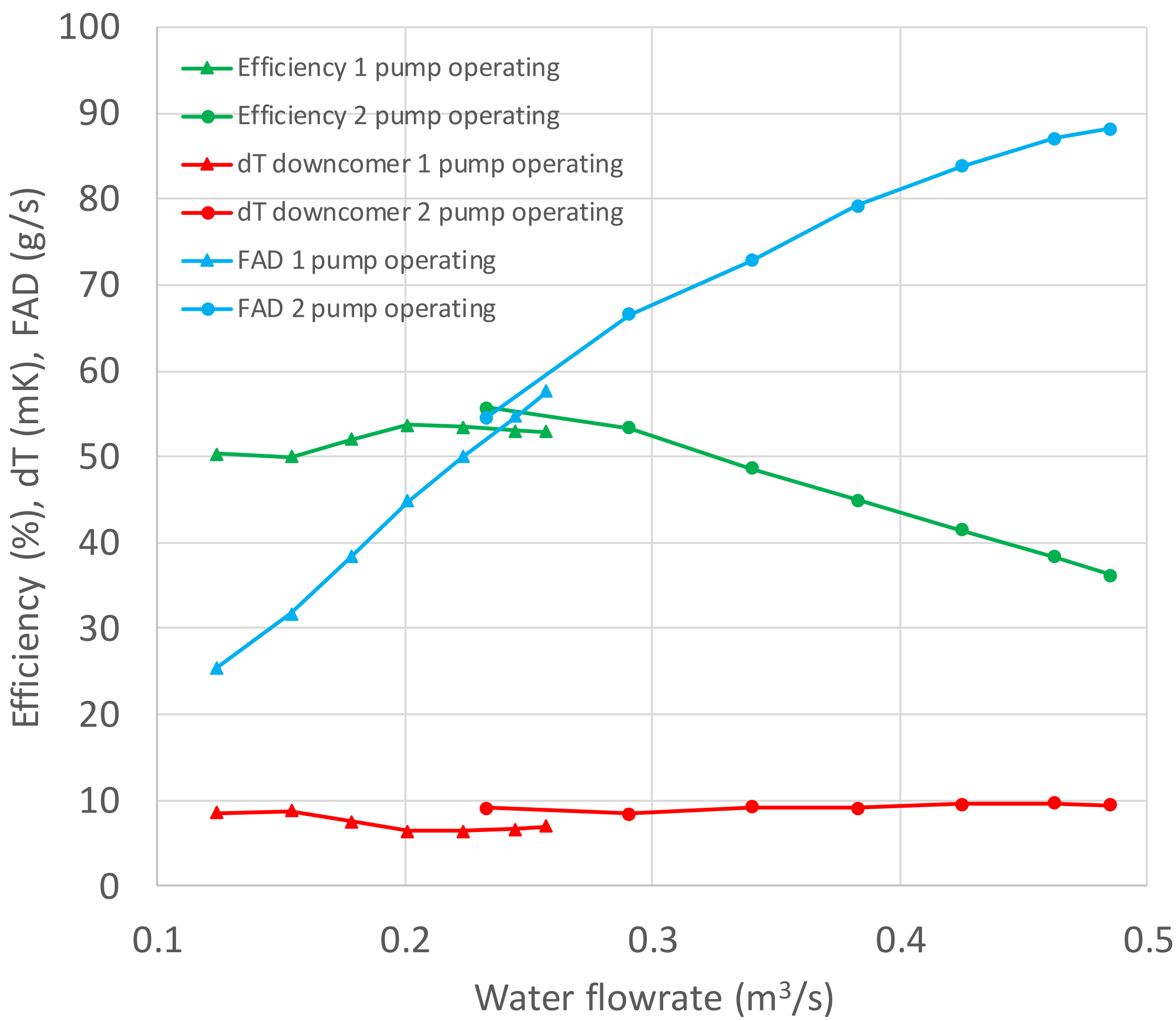

K2: Efficiency, difference in temperature and free air delivery for benchmark tests BM72 and BM88 showing the comparison between single and double pump tests.

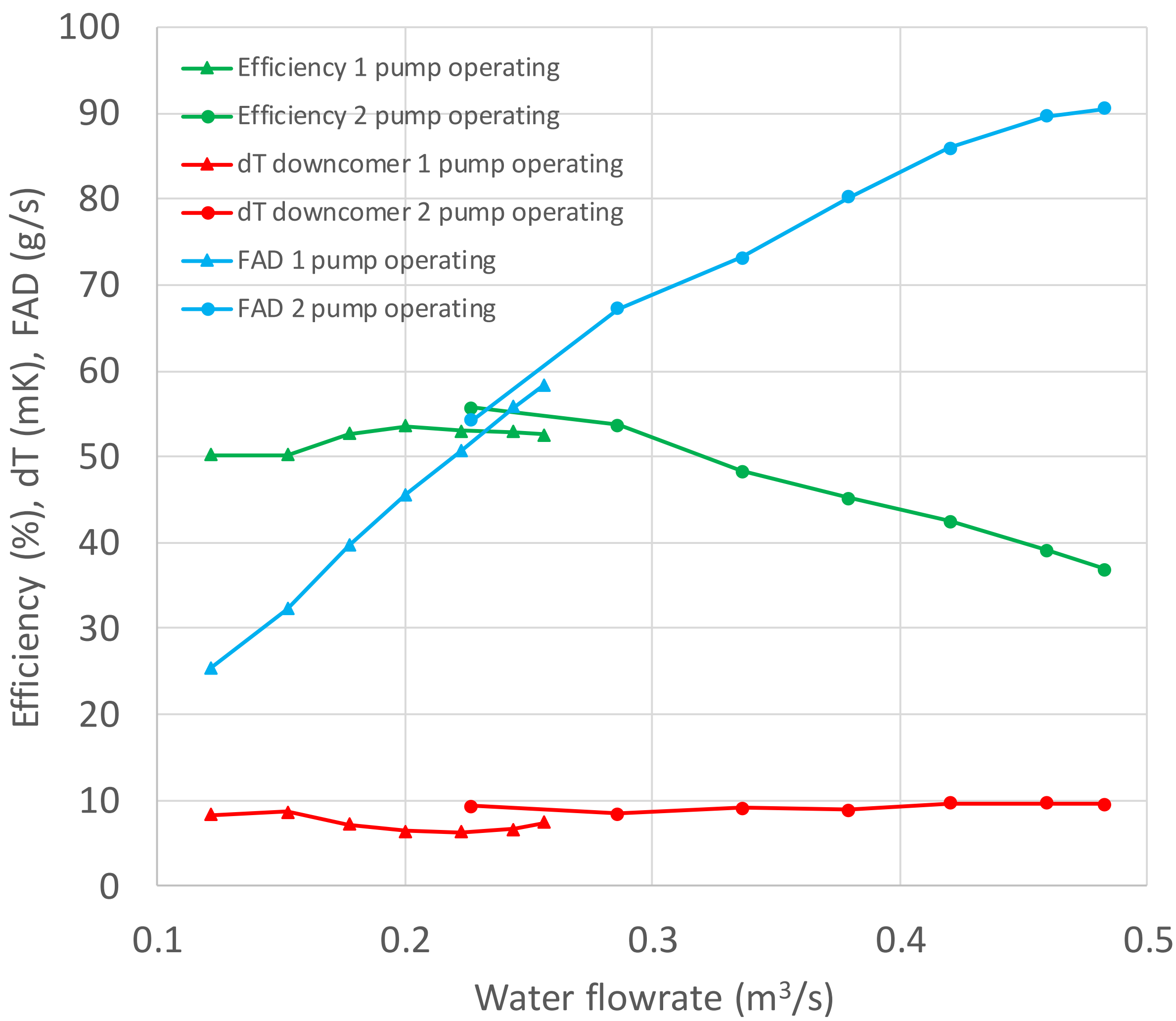

K3: Efficiency, difference in temperature and free air delivery for benchmark tests BM73 and BM87 showing the comparison between single and double pump tests.

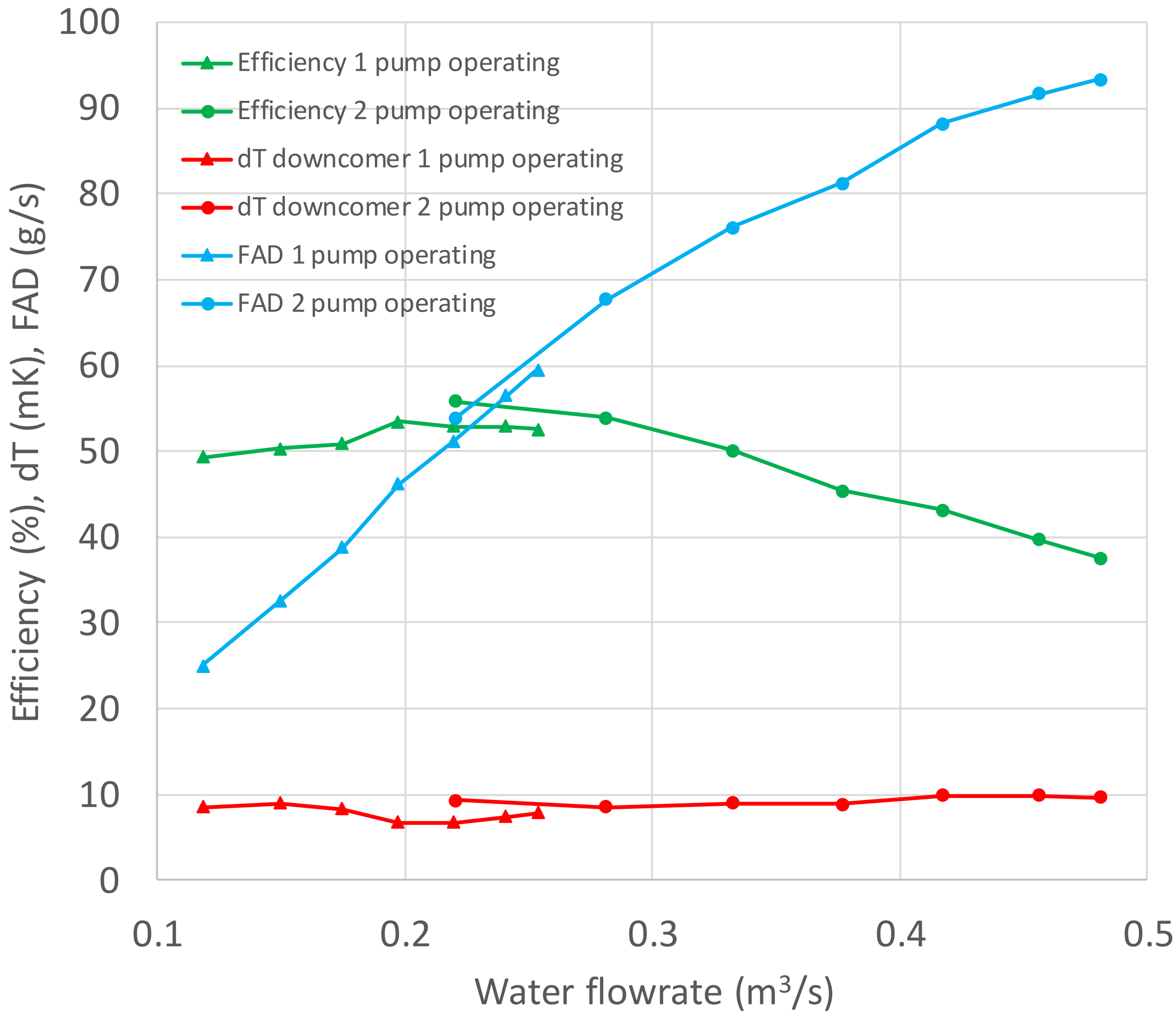

K4: Efficiency, difference in temperature and free air delivery for benchmark tests BM74 and BM86 showing the comparison between single and double pump tests.

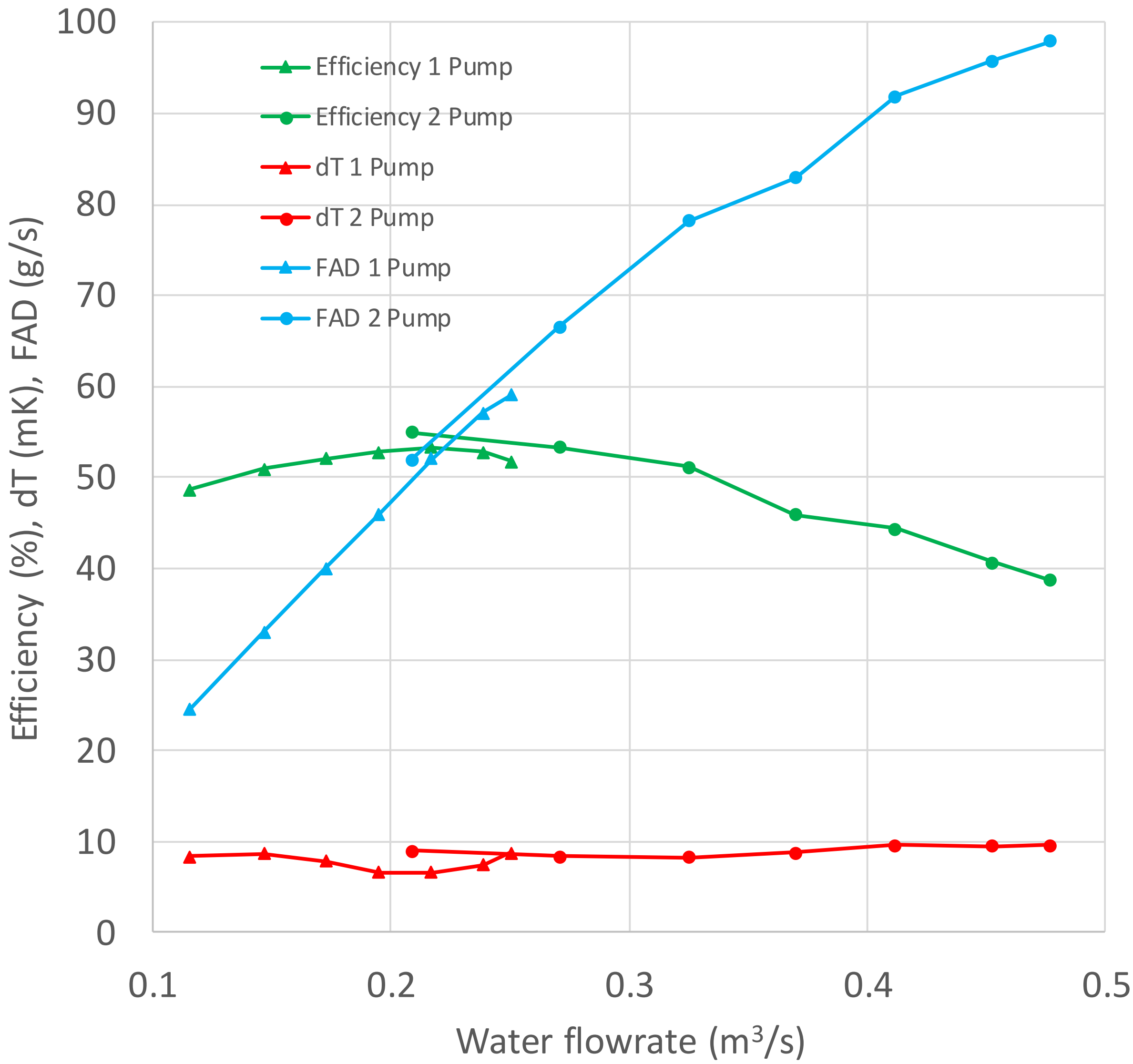

K5: Efficiency, difference in temperature and free air delivery for benchmark tests BM76 and BM85 showing the comparison between single and double pump tests.

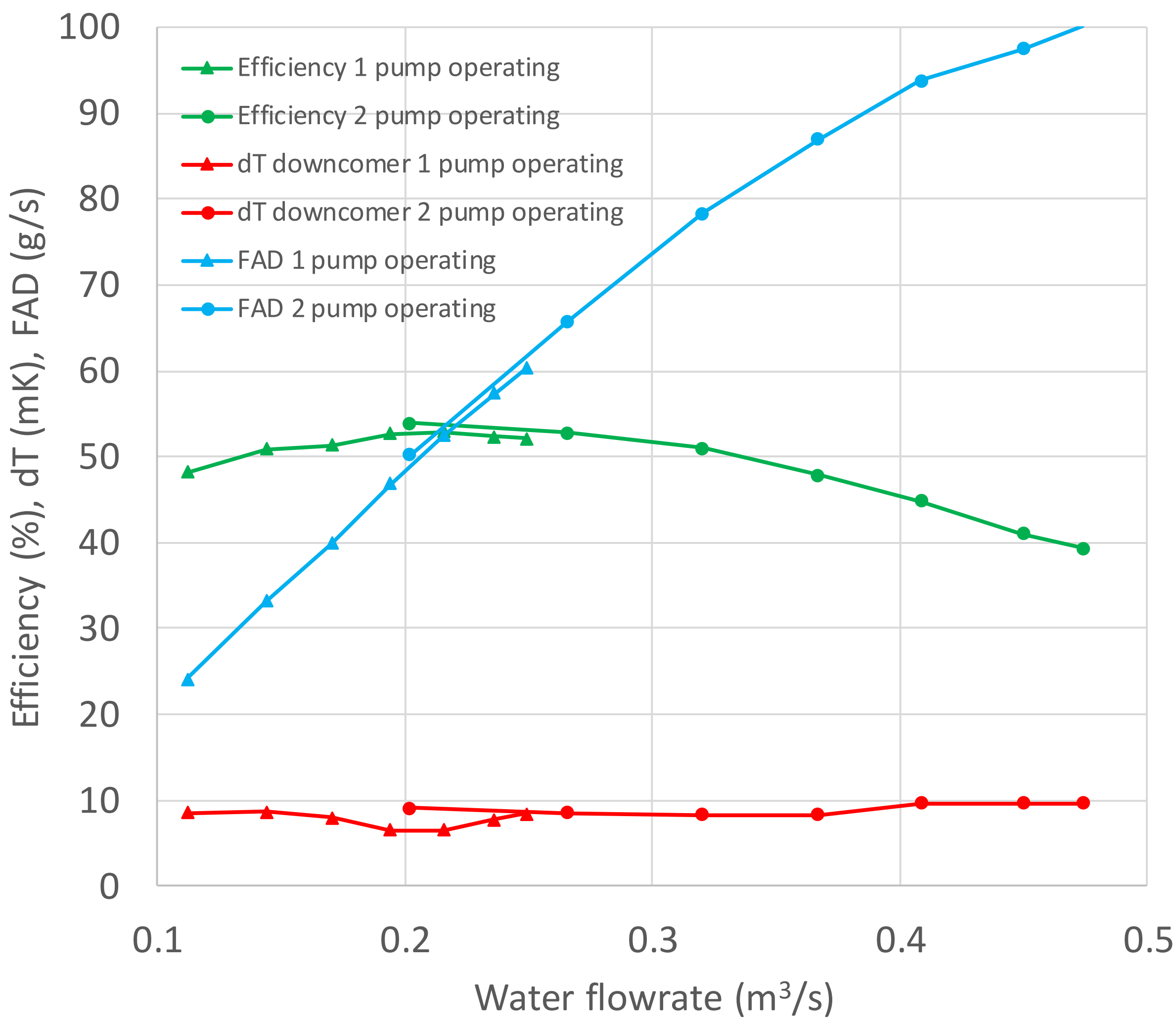

K6: Efficiency, difference in temperature and free air delivery for benchmark tests BM77 and BM84 showing the comparison between single and double pump tests.

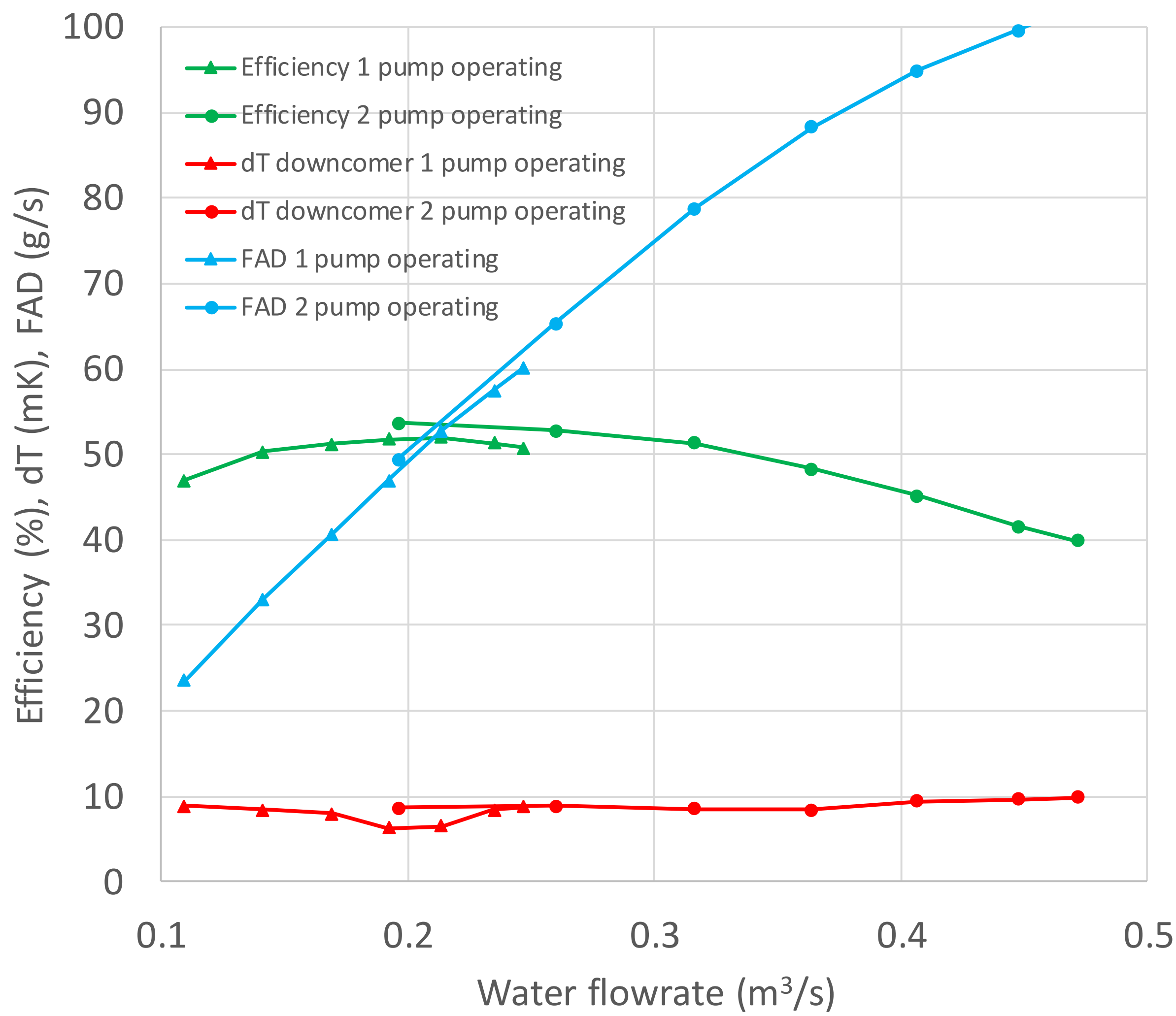

K7: Efficiency, difference in temperature and free air delivery for benchmark tests BM78 and BM83 showing the comparison between single and double pump tests.

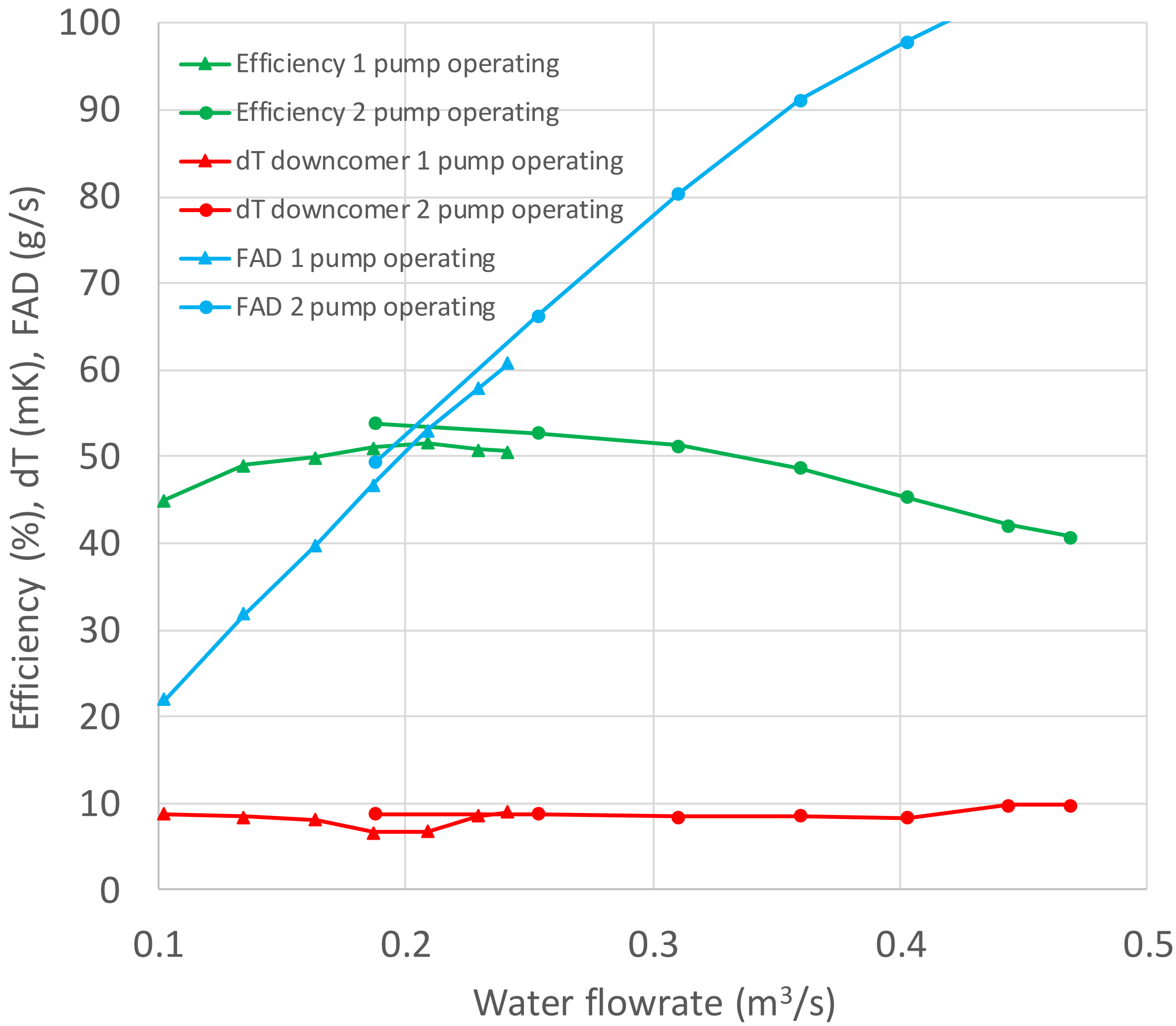

K8: Efficiency, difference in temperature and free air delivery for benchmark tests BM80 and BM81 showing the comparison between single and double pump tests.

Appendix L: Pressure profiles

Fill level denoted by square brackets (ex: [-1.000m]) indicate estimated fill level using DPT2.

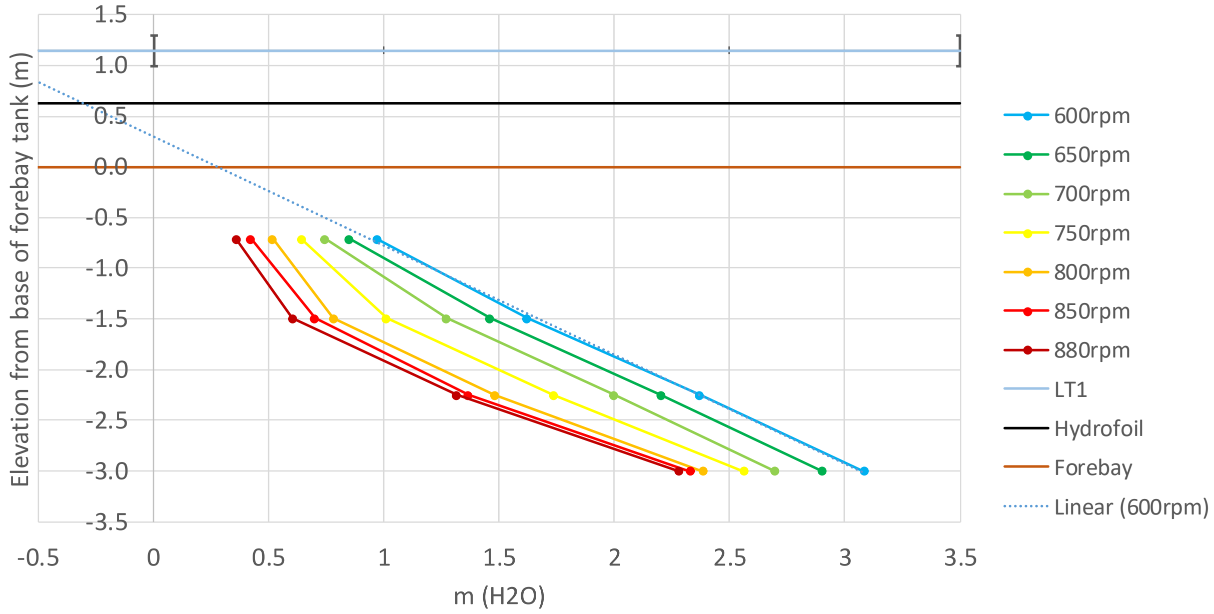

L1: Pressure profile for BM68, fill level at 0.965m and two pumps.

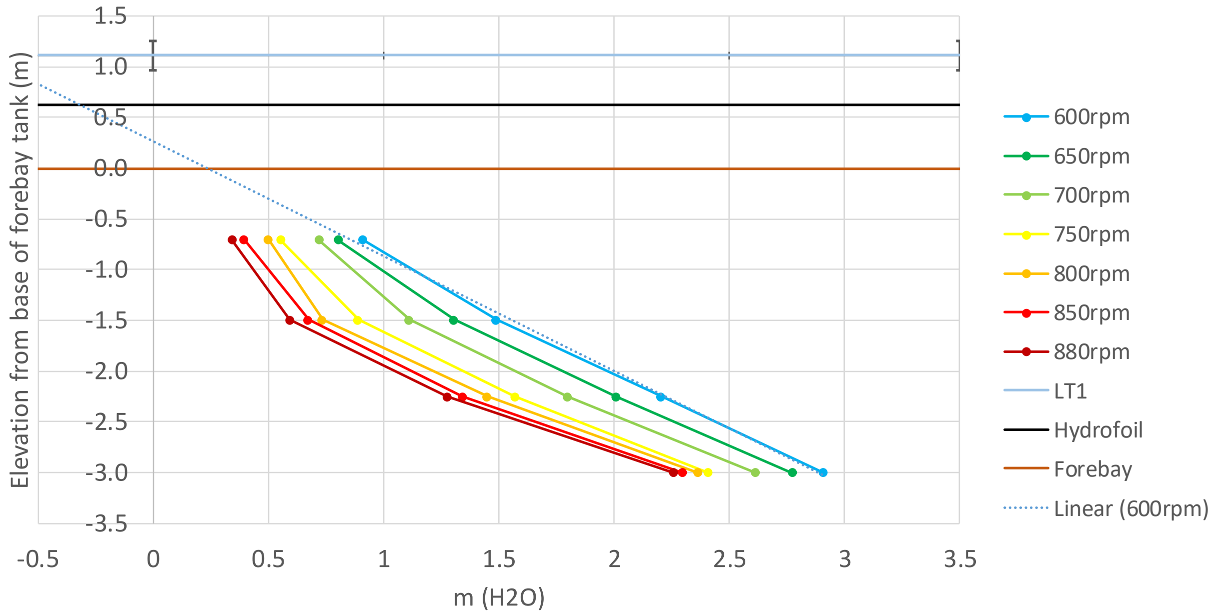

L2: Pressure profile for BM69, fill level at 0.8675m and two pumps.

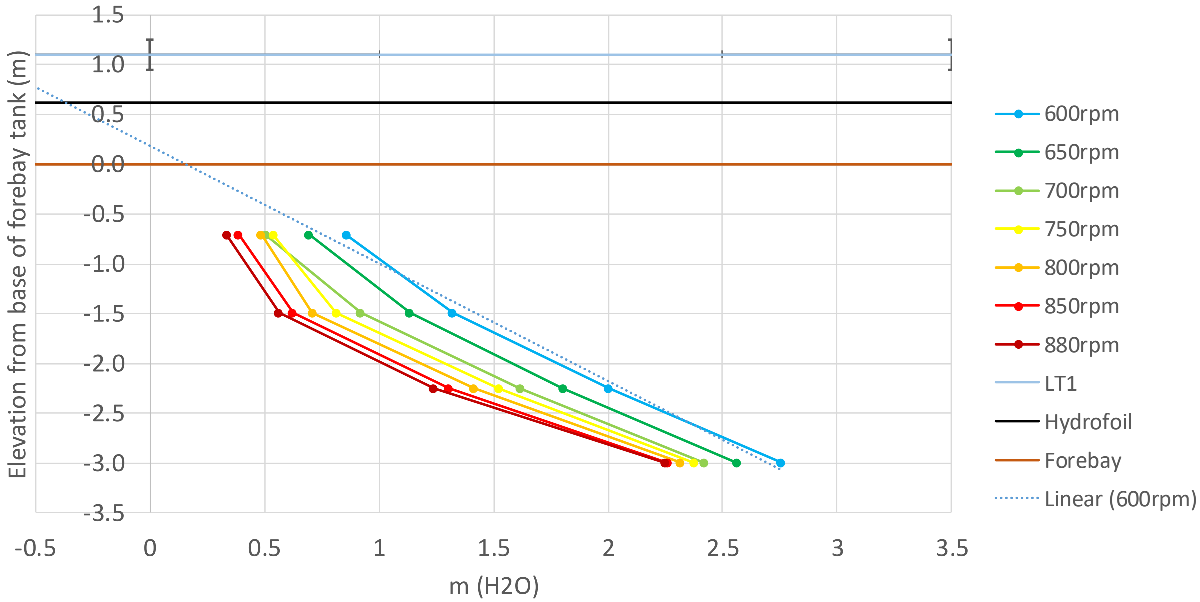

L3: Pressure profile for BM70, fill level at 0.7614m and two pumps.

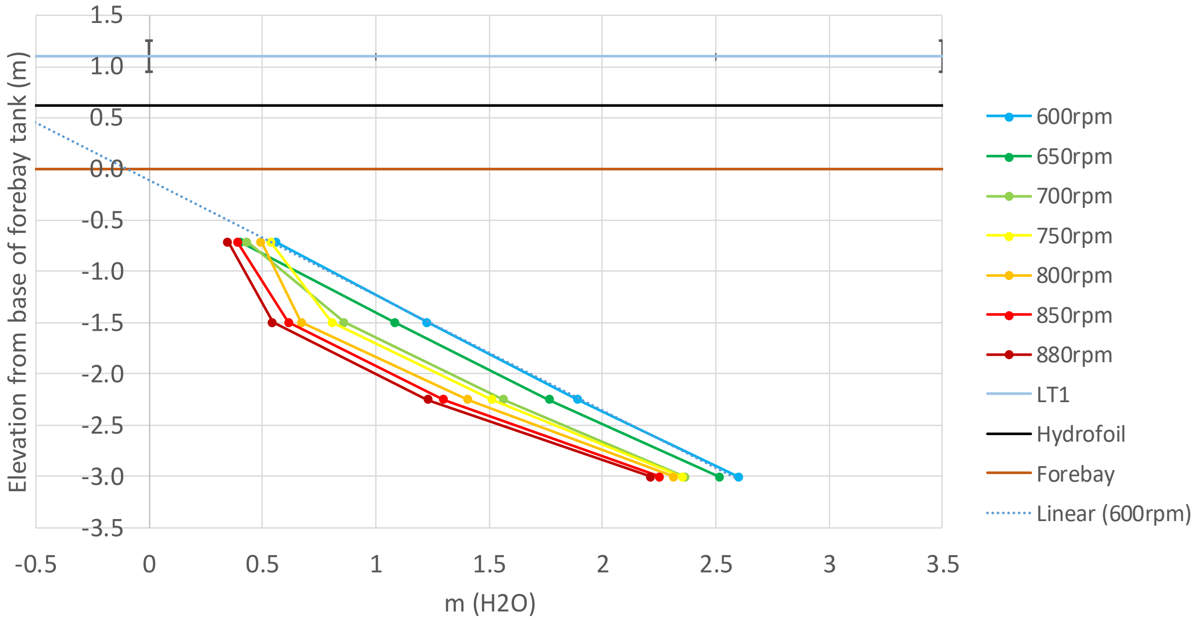

L4: Pressure profile for BM71, fill level at 0.6690m and two pumps.

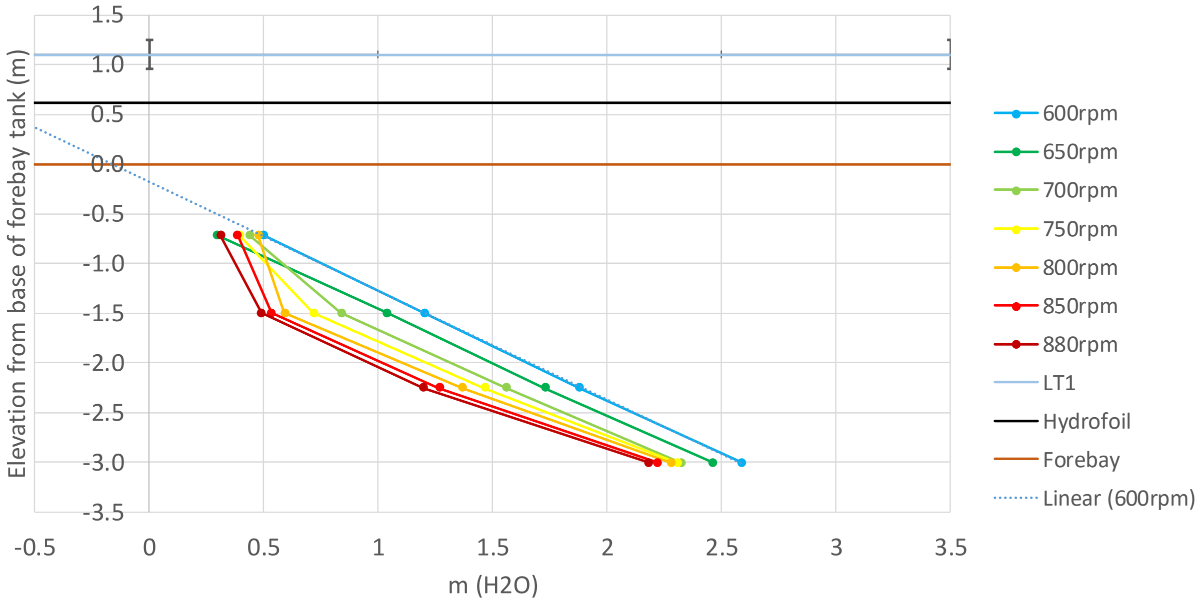

L5: Pressure profile for BM72, fill level at 0.5771m and two pumps.

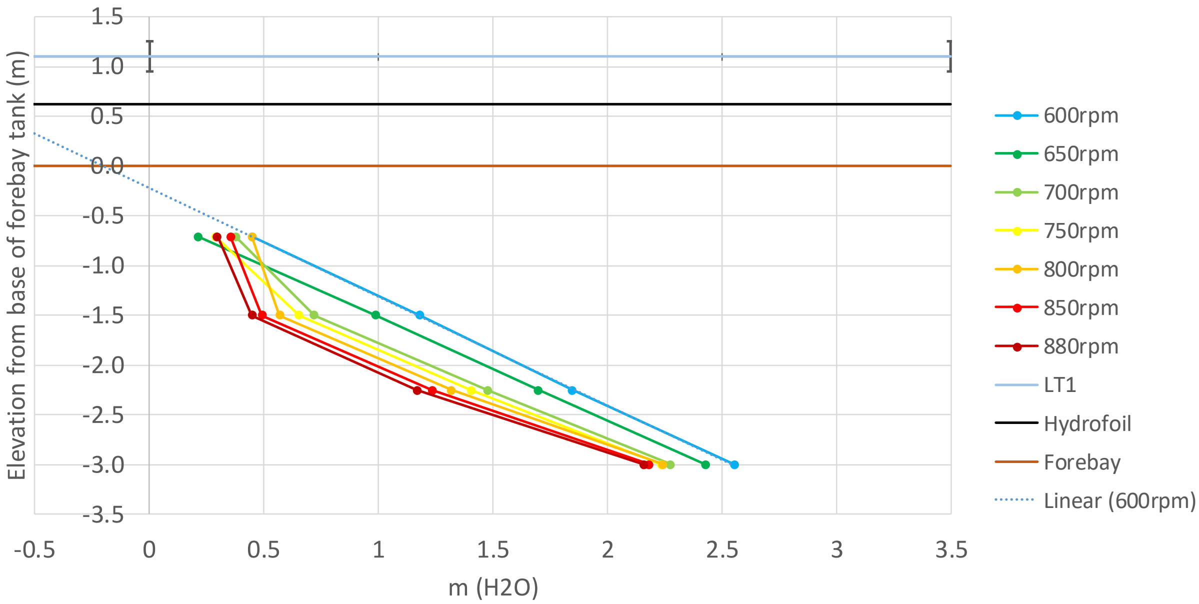

L6: Pressure profile for BM73, fill level at 0.4797m and two pumps.

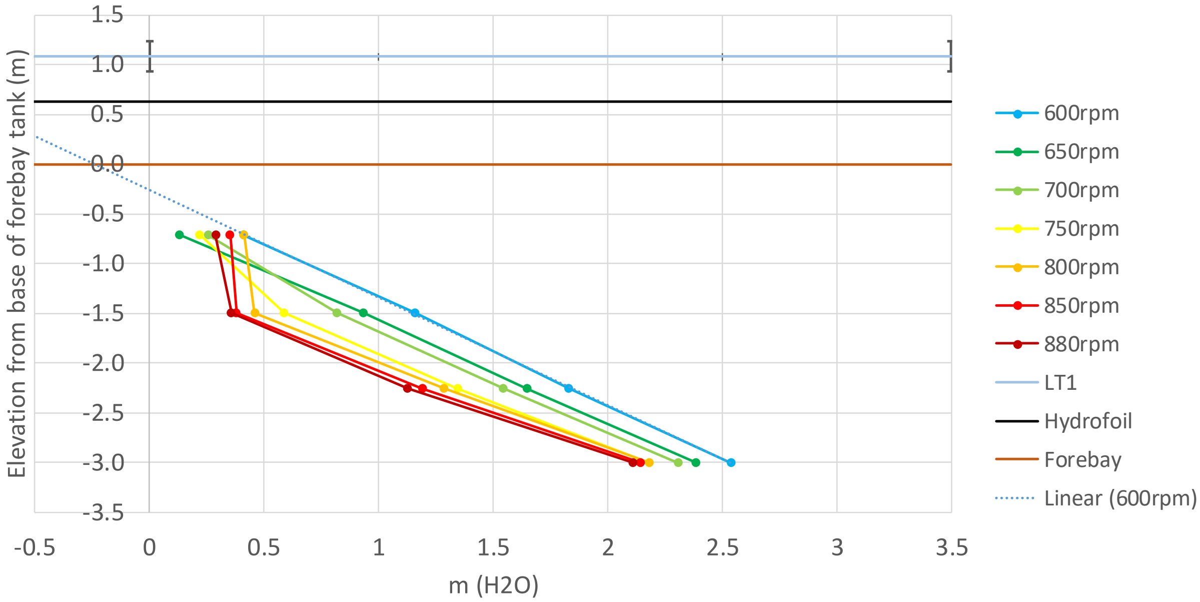

L7: Pressure profile for BM74, fill level at 0.3776m and two pumps.

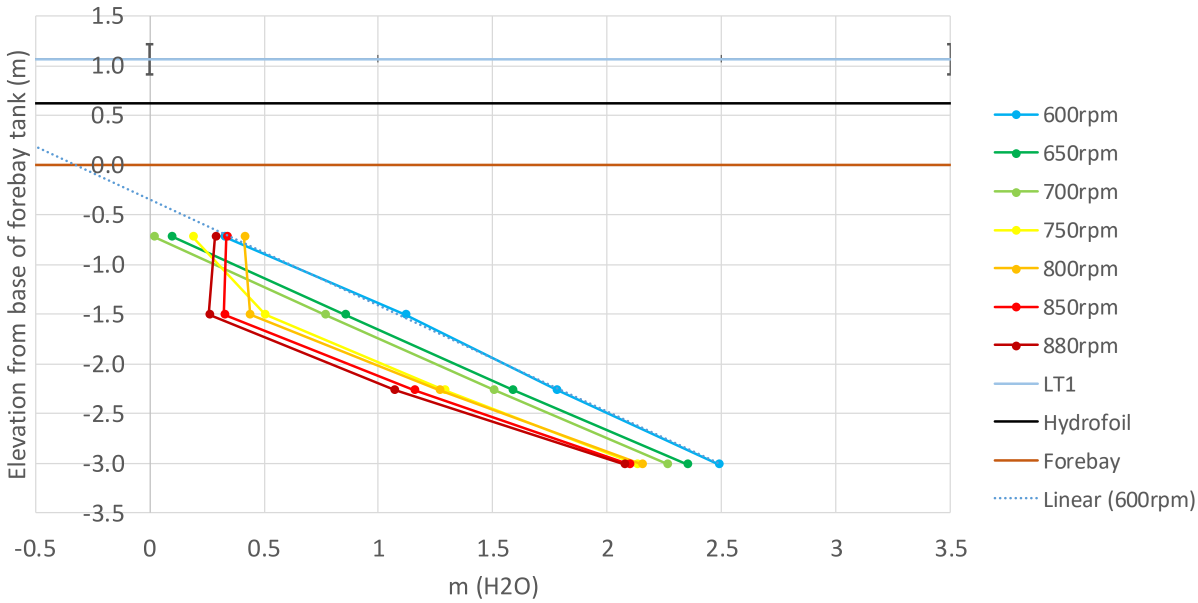

L8: Pressure profile for BM75, 0.2793m and two pumps.

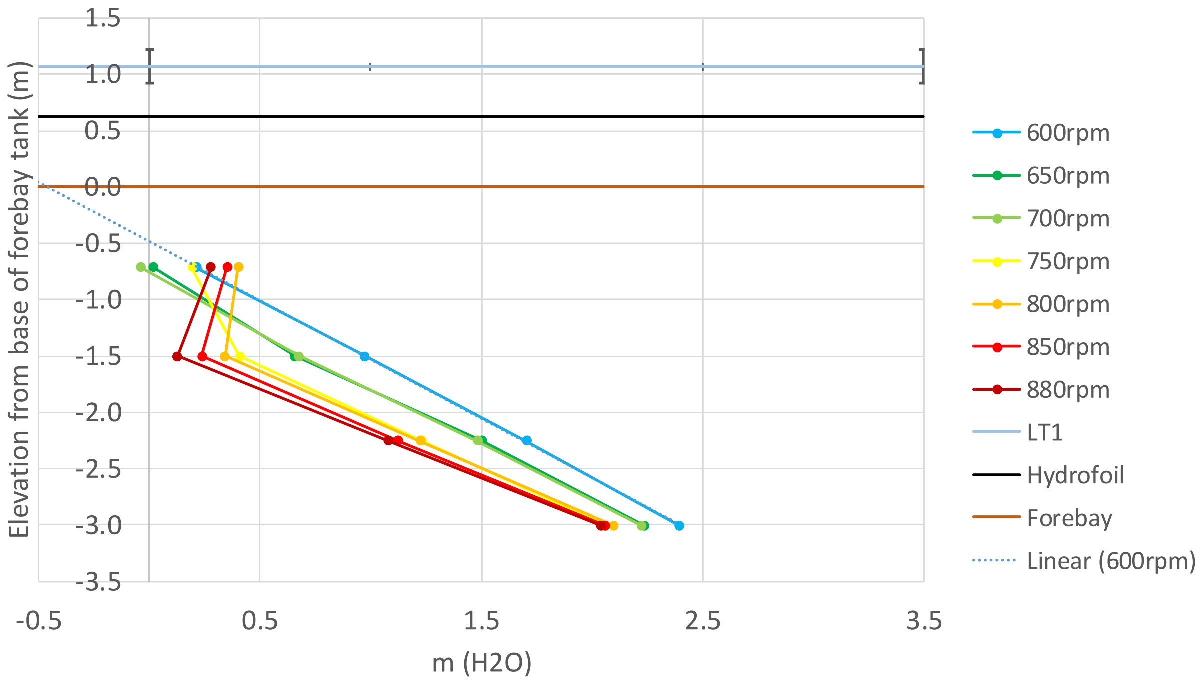

L9: Pressure profile for BM76, fill level at 0.1763m and two pumps.

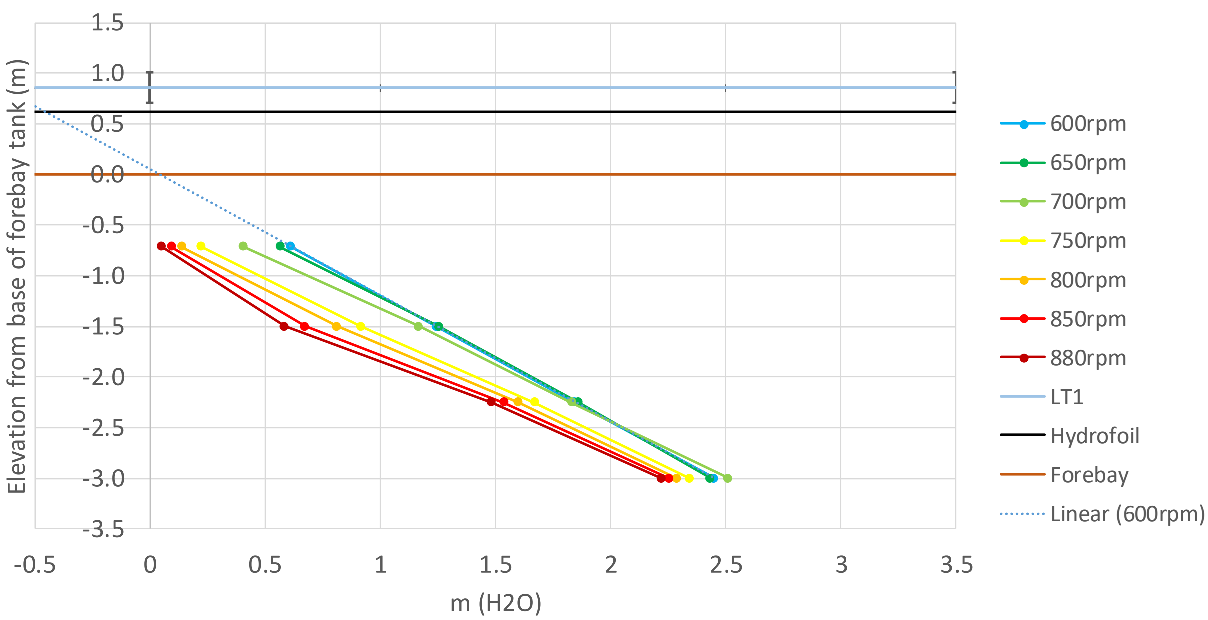

L10: Pressure profile for BM84, fill level at 0.189m and single pump.

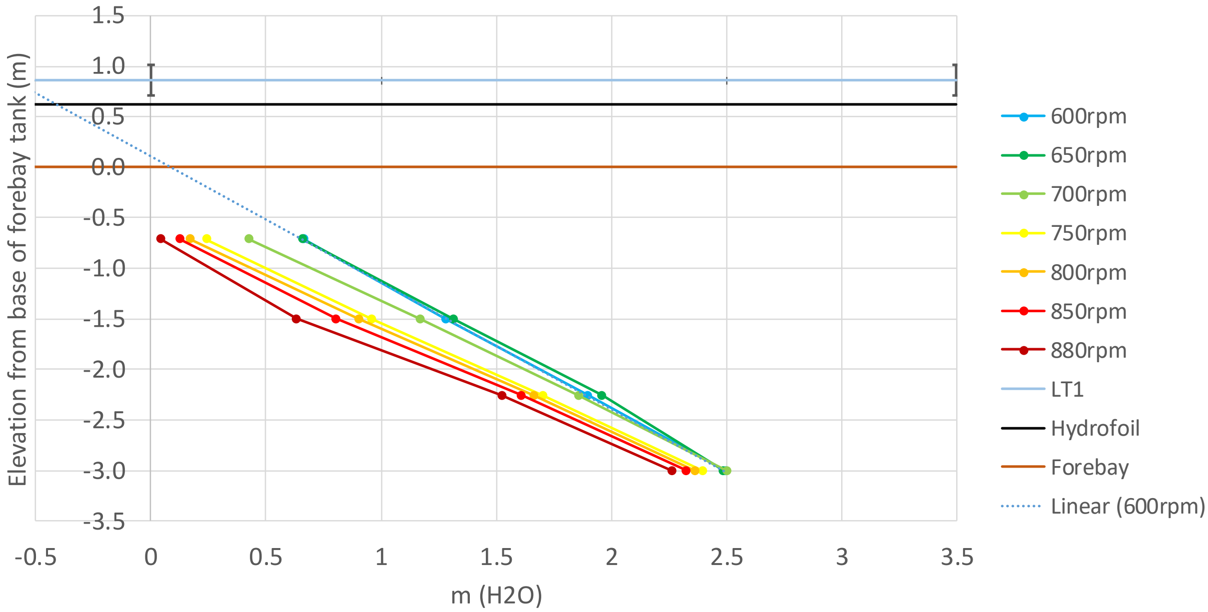

L11: Pressure profile for BM85, fill level at 0.285m and single pump.

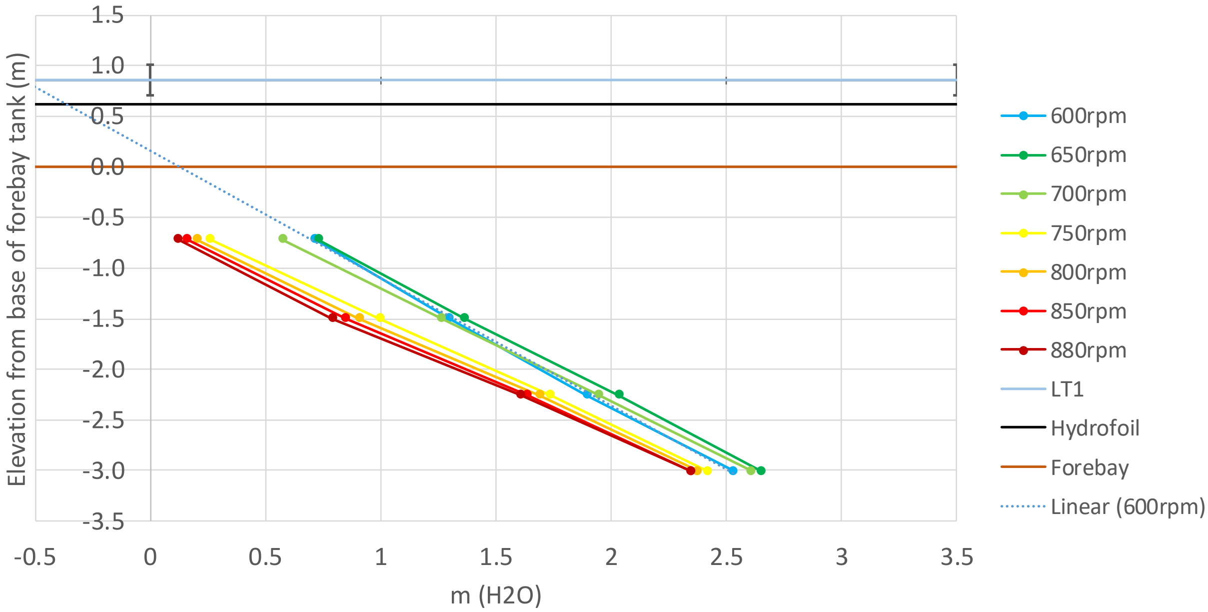

L12: Pressure profile for BM86, fill level at 0.3648m and single pump.

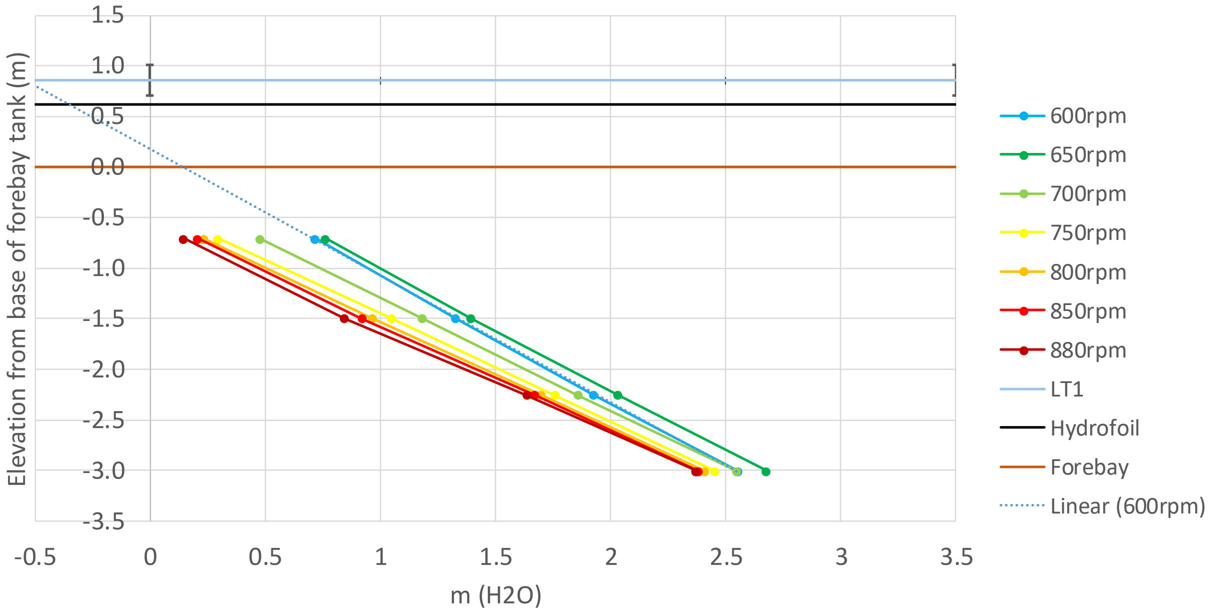

L13: Pressure profile for BM87, fill level at 0.450m and single pump.

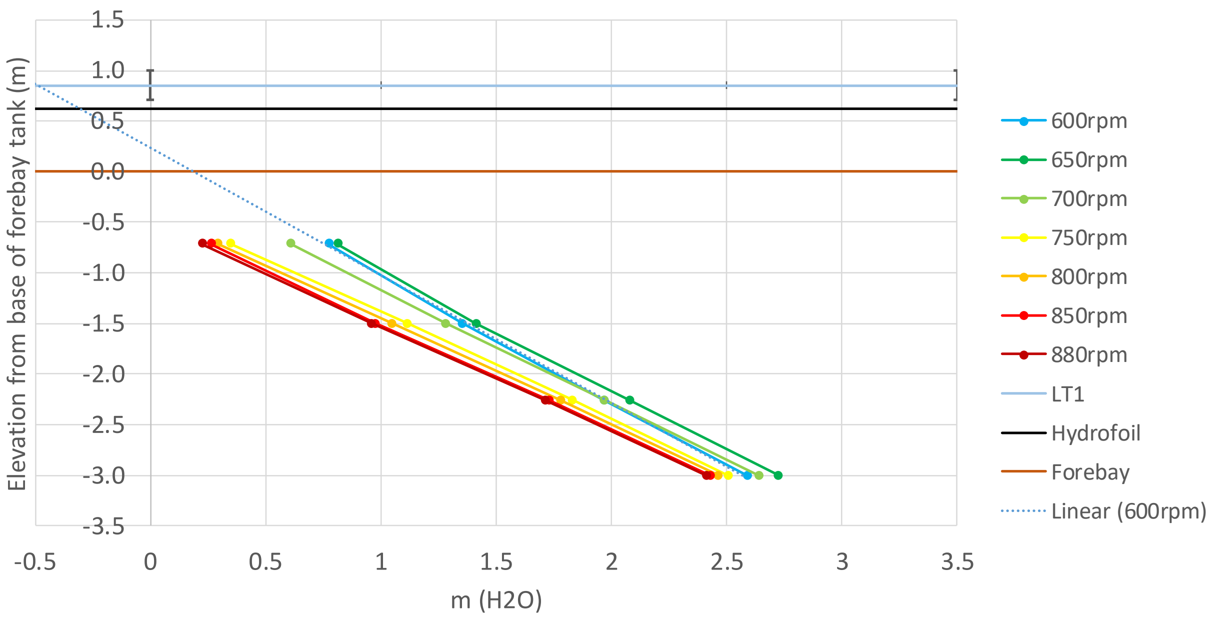

L14: Pressure profile for BM88, fill level at 0.550m and single pump.

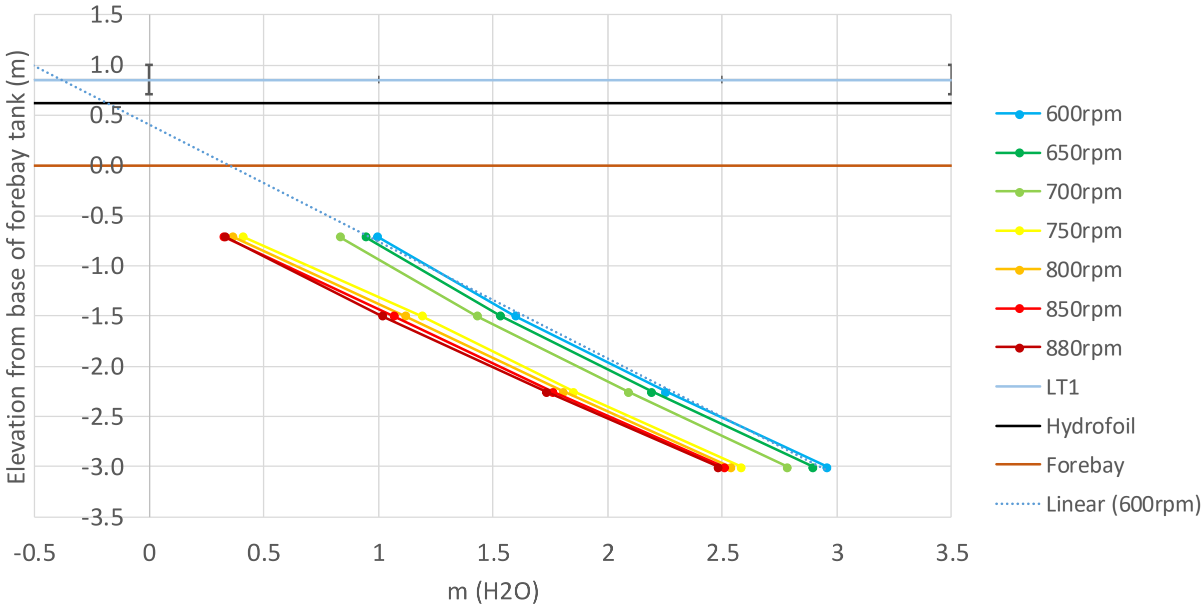

L15: Pressure profile for BM89, fill level at 0.650m and single pump.

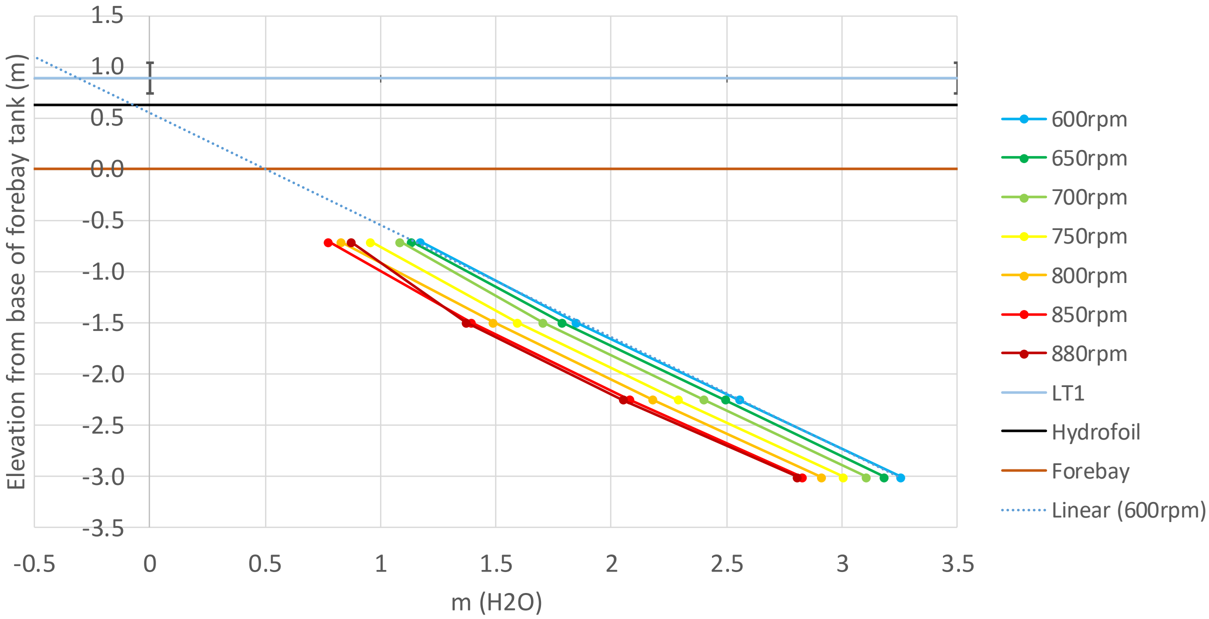

L16: Pressure profile for BM90, fill level at 0.750m and single pump.

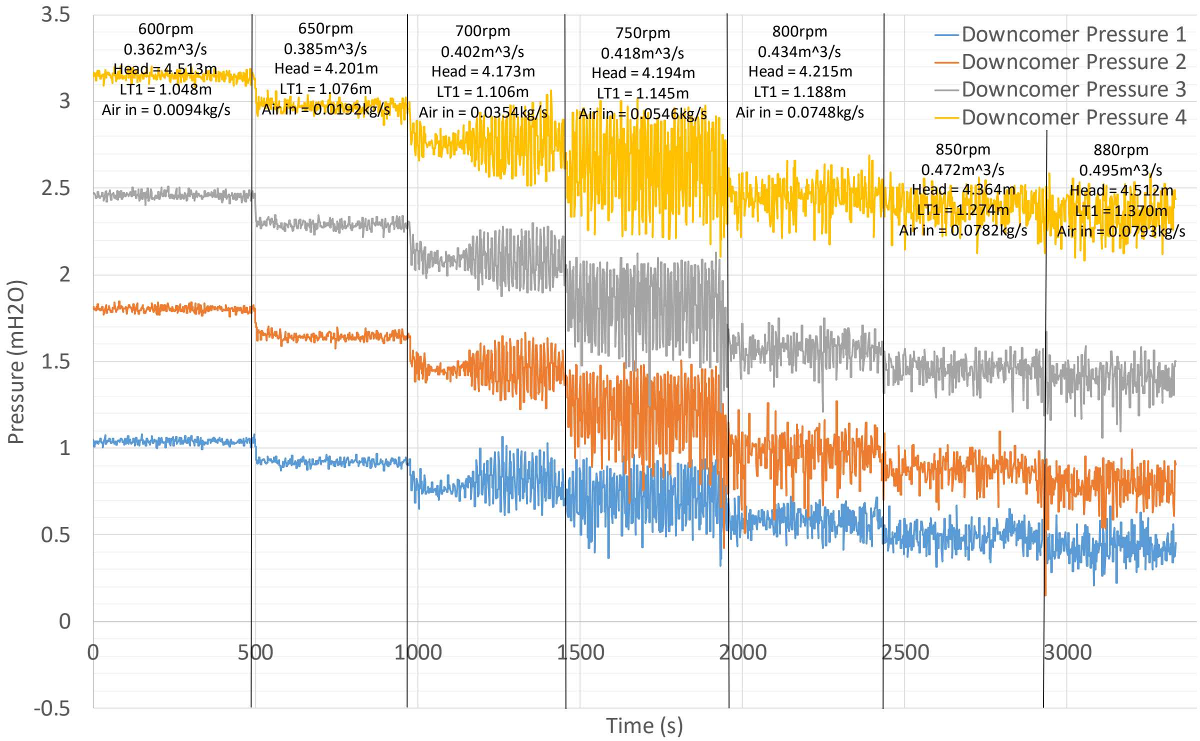

L17: Time series plot of the pressure profile for BM68, fill level at 0.965m and two pumps.

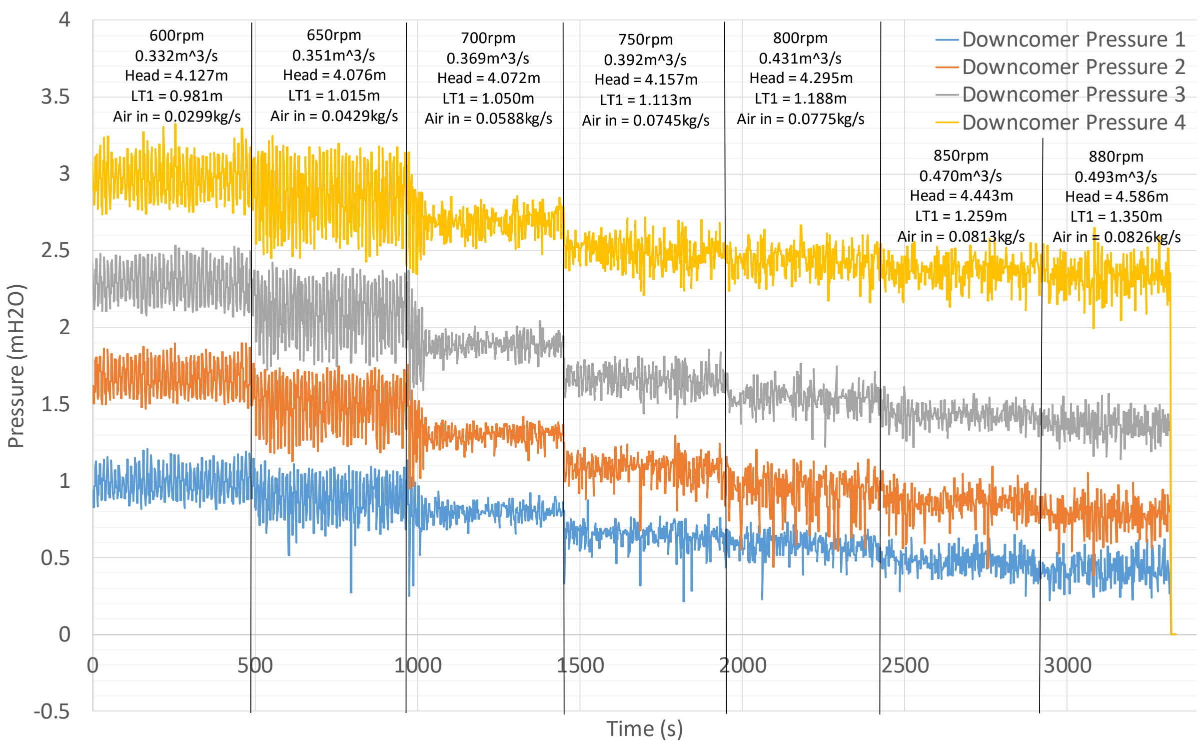

L18: Time series plot of the pressure profile for BM69, fill level at 0.8675m and two pumps.

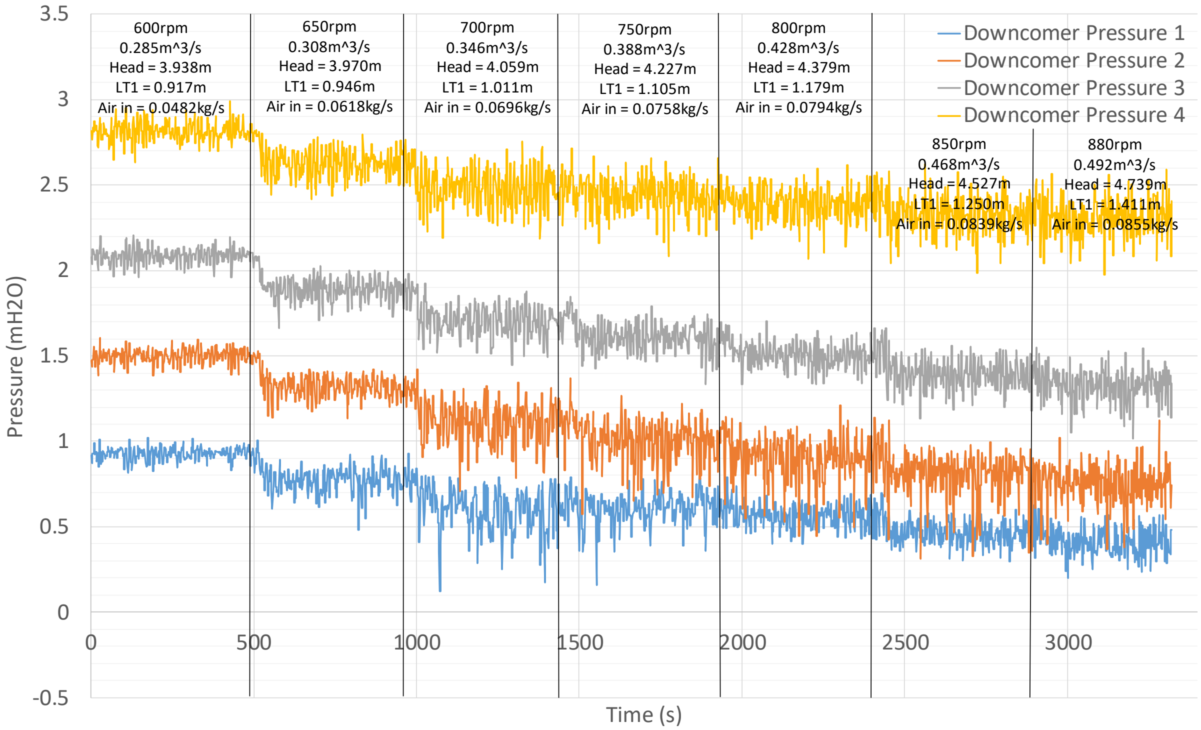

L19: Time series plot of the pressure profile for BM70, fill level at 0.7614m and two pumps.

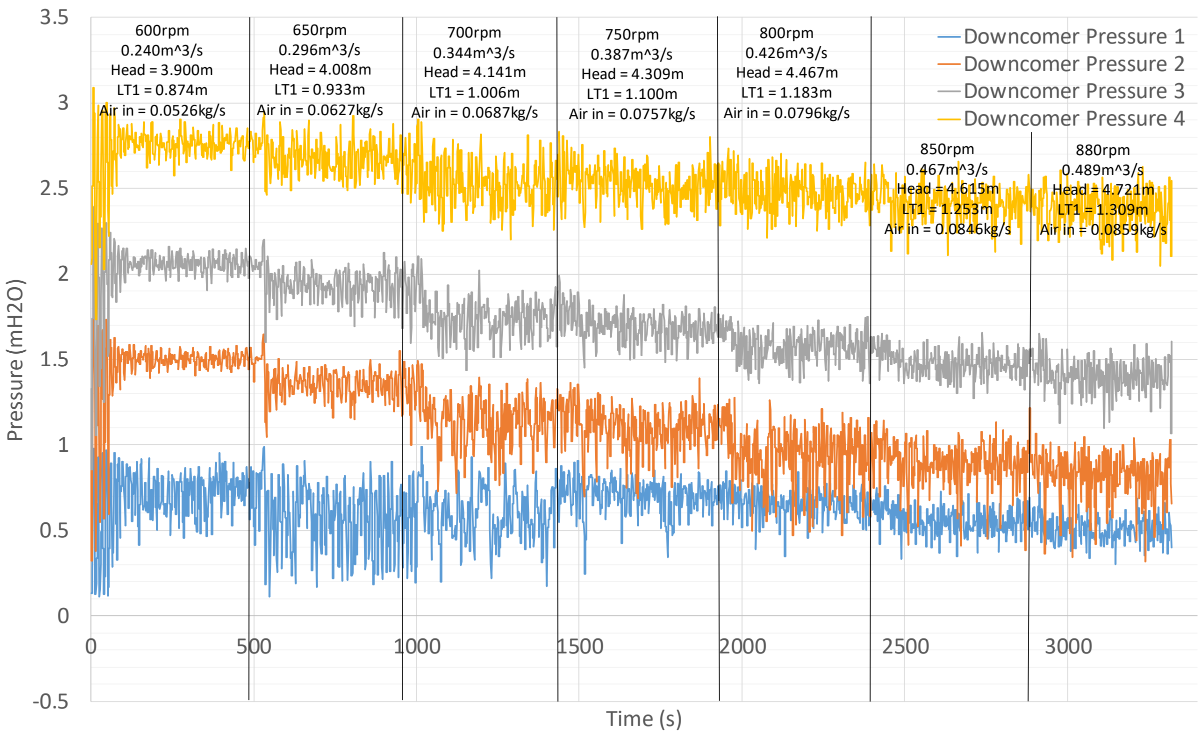

L20: Time series plot of the pressure profile for BM71, fill level at 0.6690m and two pumps.

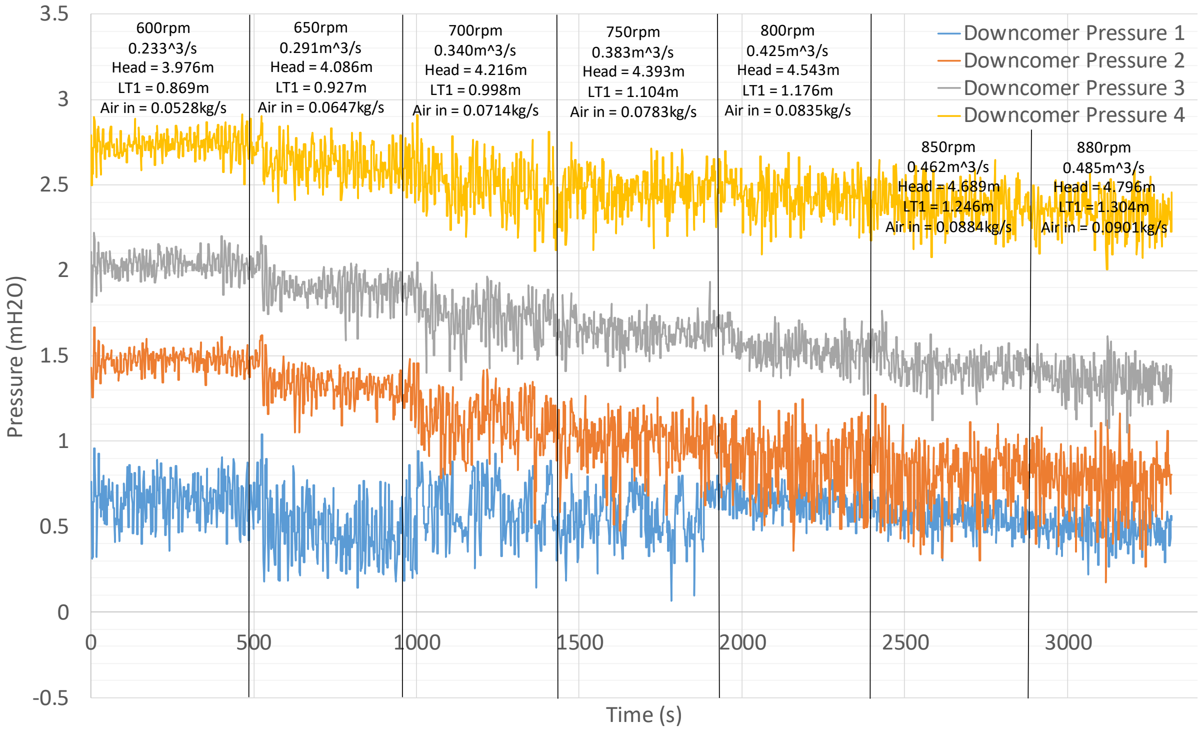

L21: Time series plot of the pressure profile for BM72, fill level at 0.5771m and two pumps.

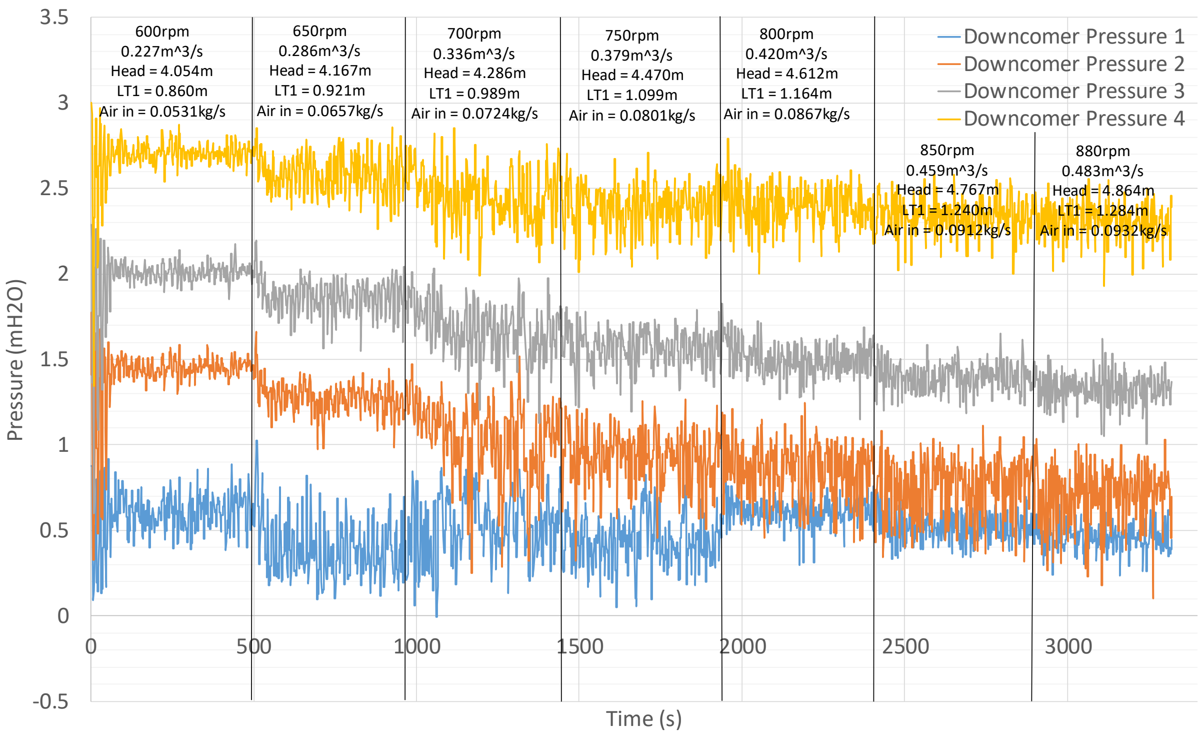

L22: Time series plot of the pressure profile for BM73, fill level at 0.4791m and two pumps.

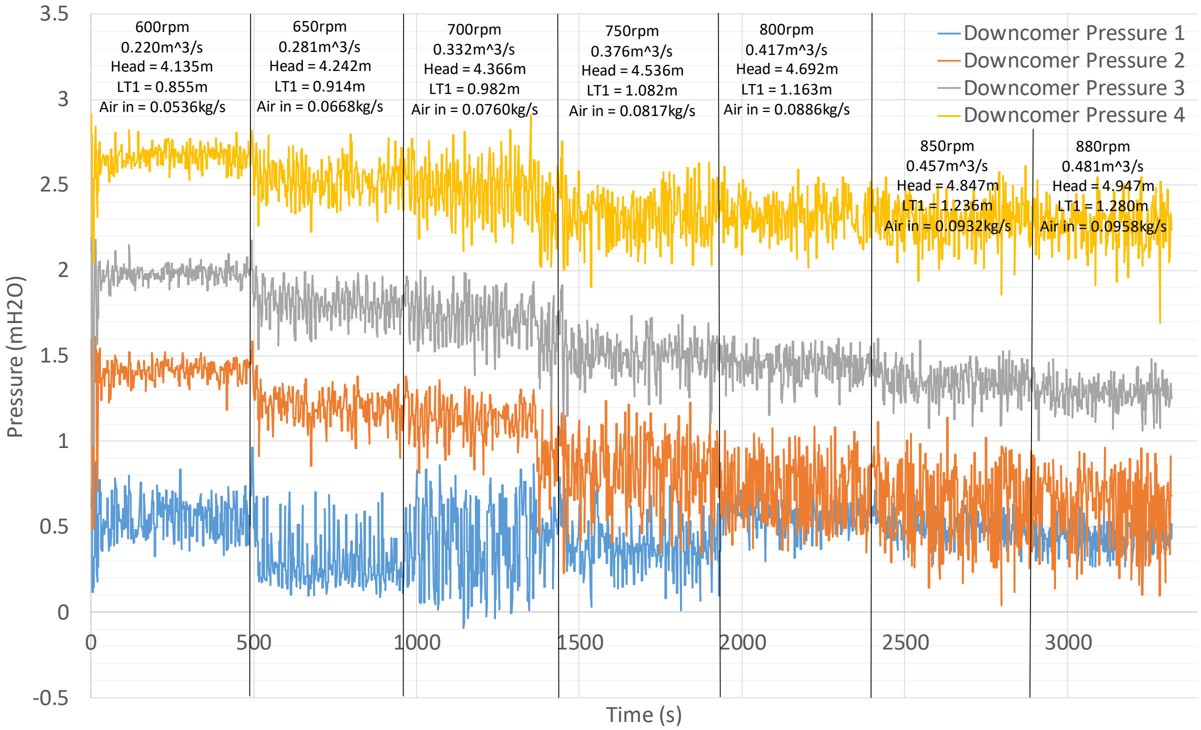

L23: Time series plot of the pressure profile for BM74, fill level at 0.3776m and two pumps.

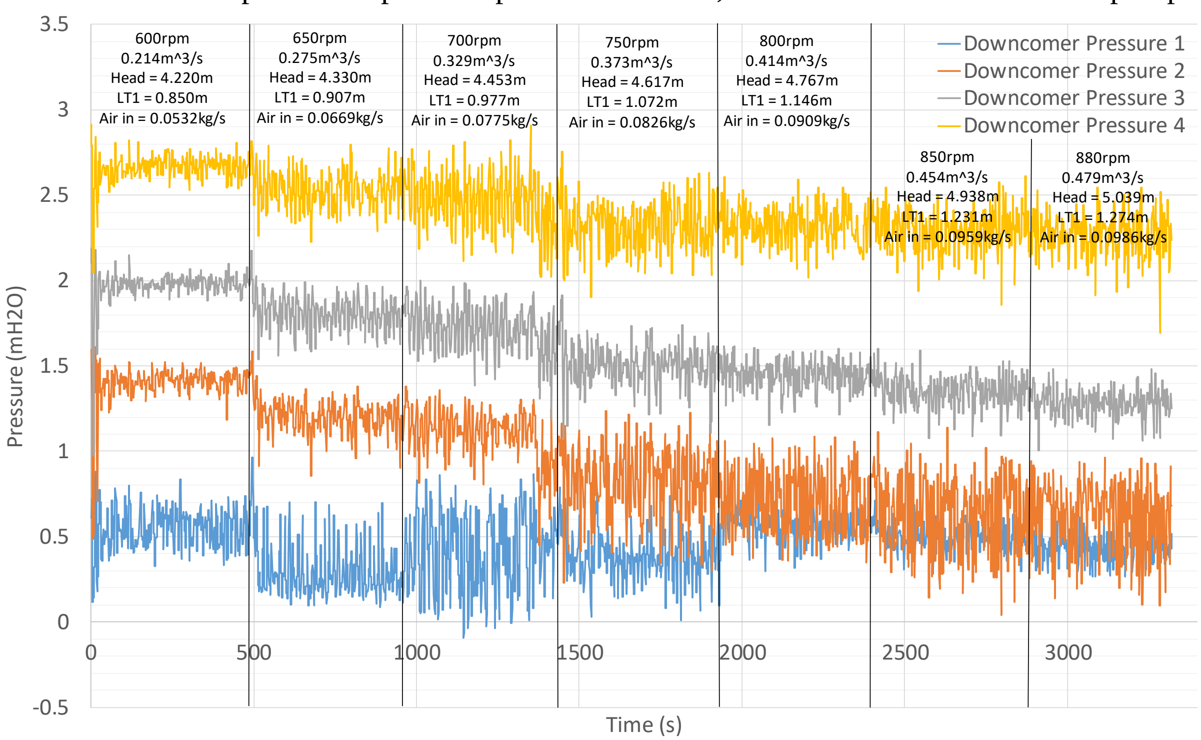

L24: Time series plot of the pressure profile for BM75, fill level at 0.2793m and two pumps.

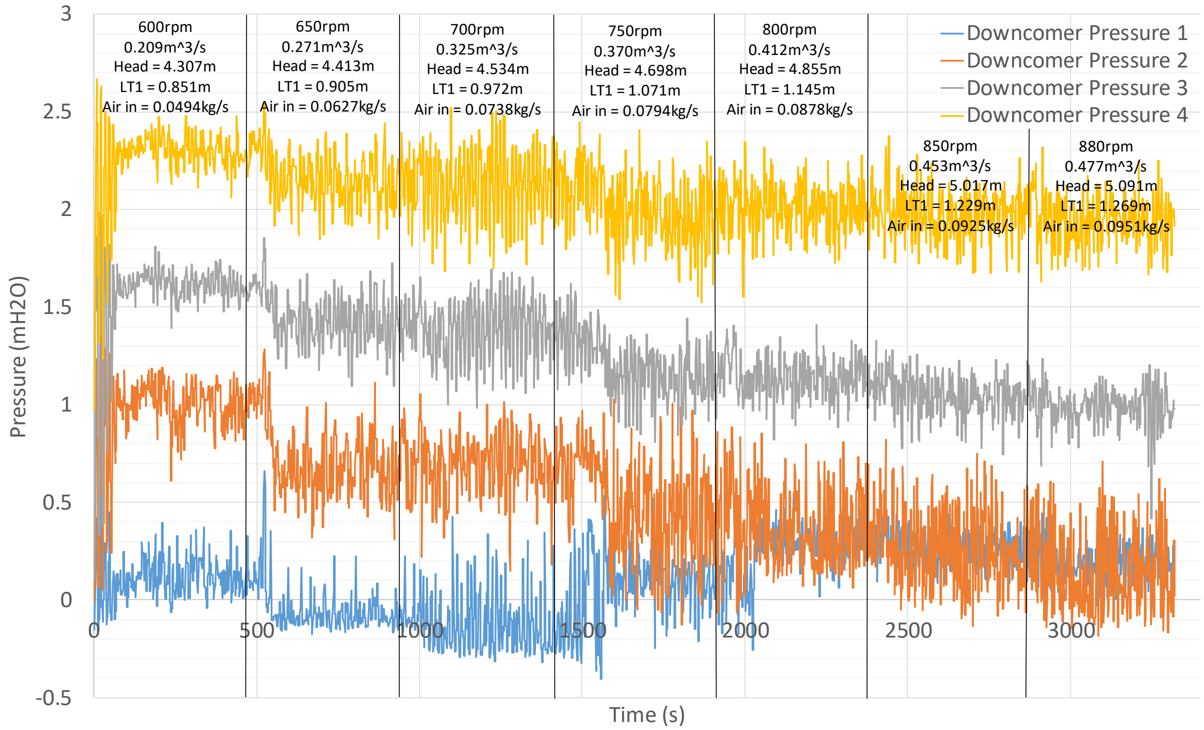

L25: Time series plot of the pressure profile for BM76, fill level at 0.1763m and two pumps.

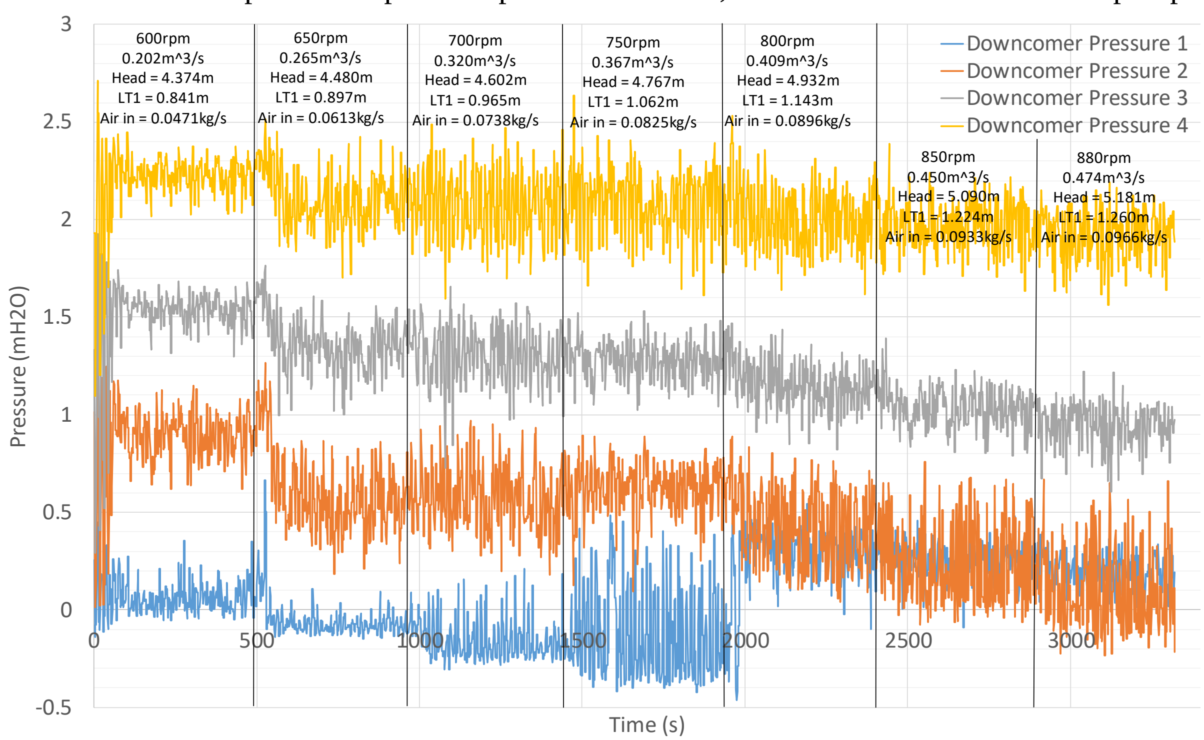

L26: Time series plot of the pressure profile for BM77, fill level at [-1.132m] and two pumps.

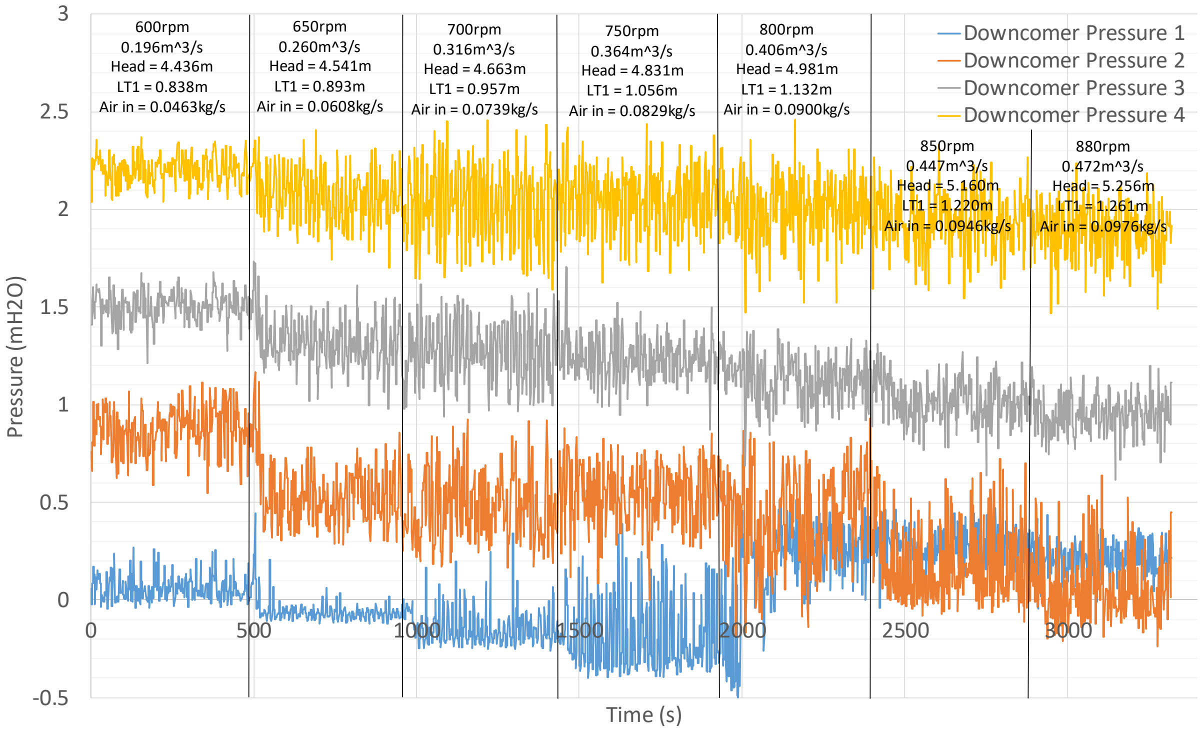

L27: Time series plot of the pressure profile for BM78, fill level at [-2.446m] and two pumps.

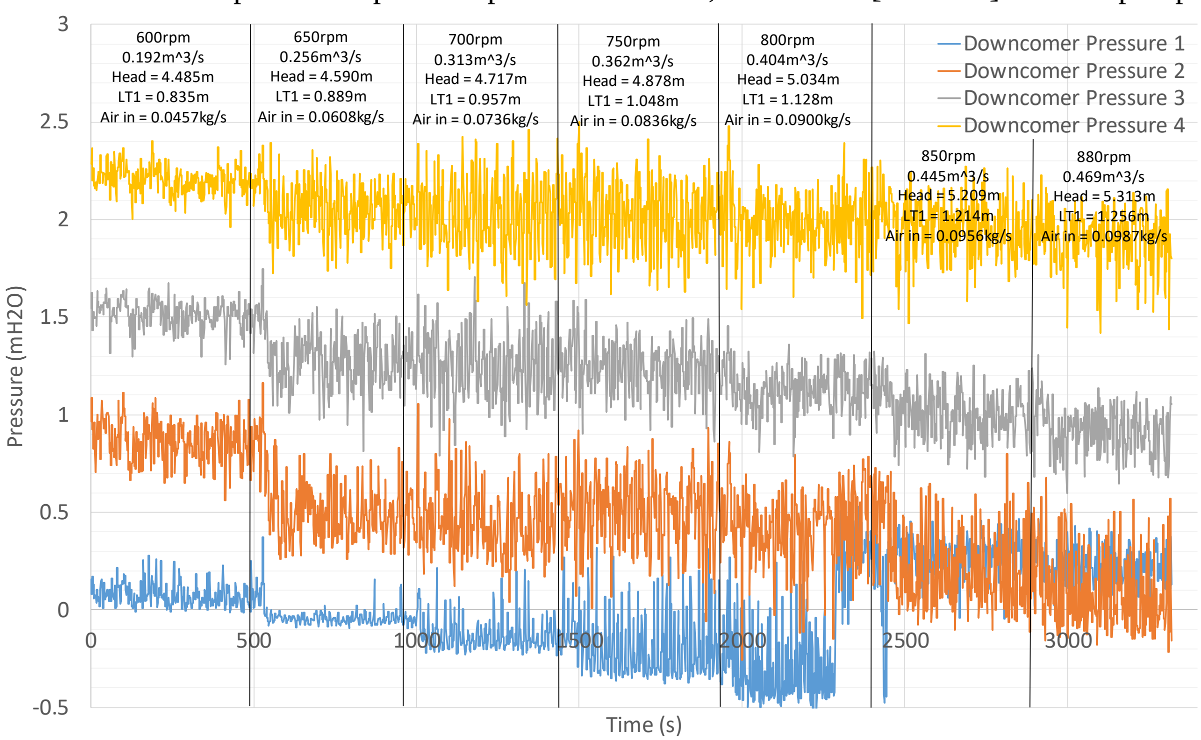

L28: Time series plot of the pressure profile for BM79, fill level at [-3.113m] and two pumps.

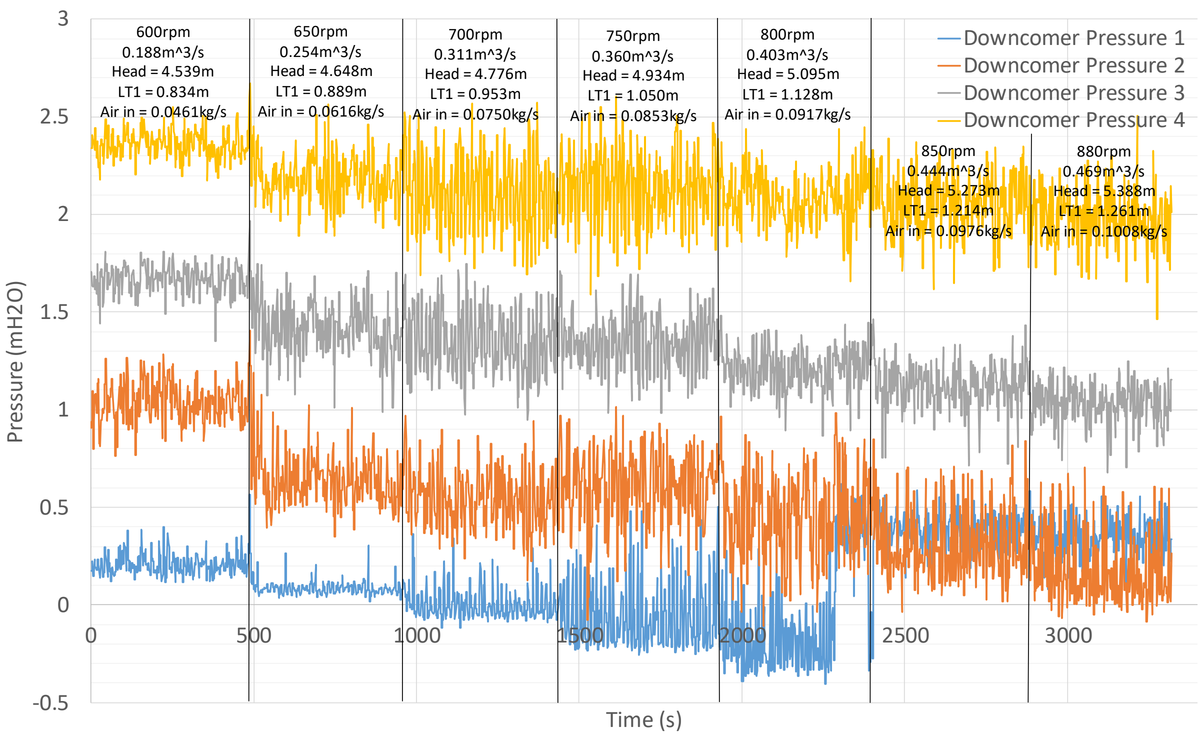

L29: Time series plot of the pressure profile for BM80, fill level at [-3.245m] and two pumps.

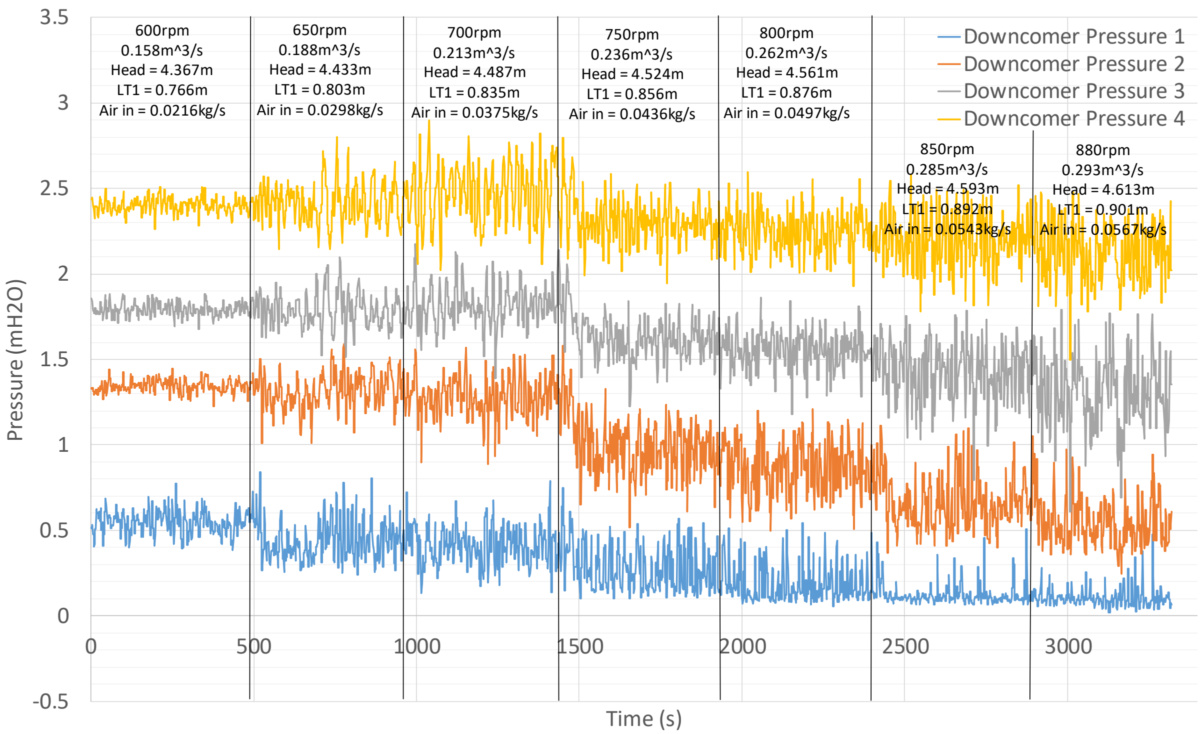

L30: Time series plot of the pressure profile for BM81, fill level at [-3.186m] and single pump.

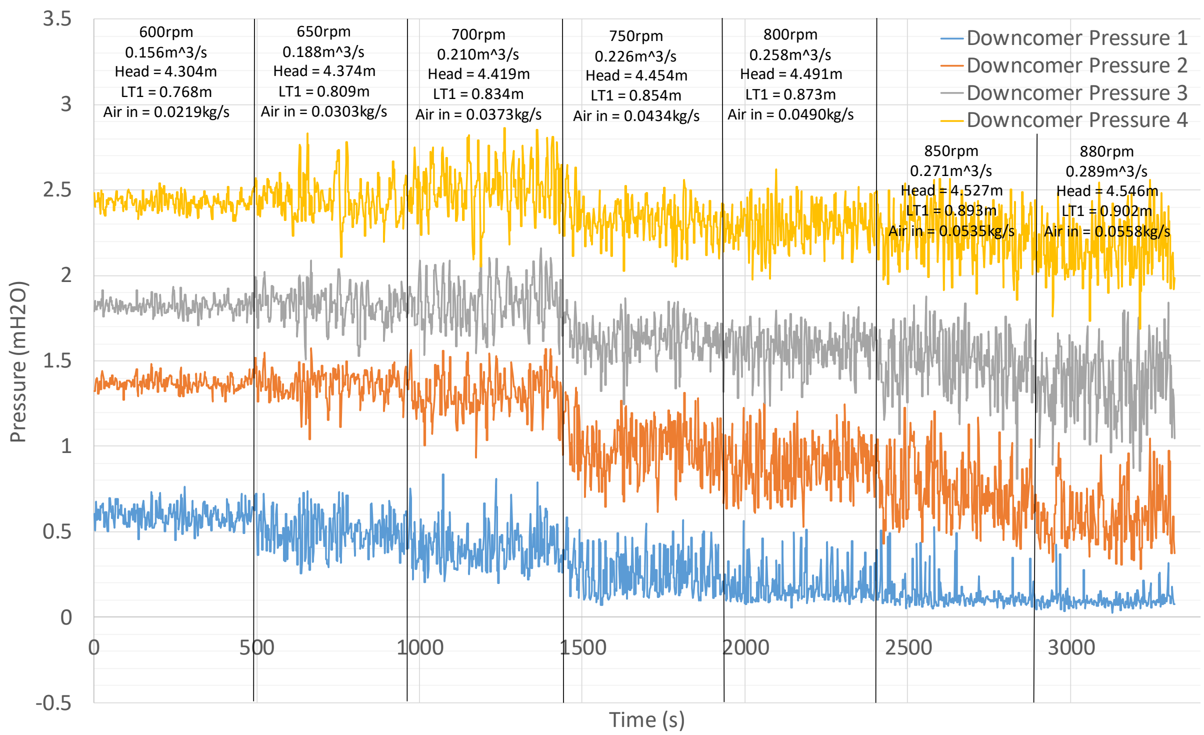

L31: Time series plot of the pressure profile for BM82, fill level at [-3.273m] and single pump.

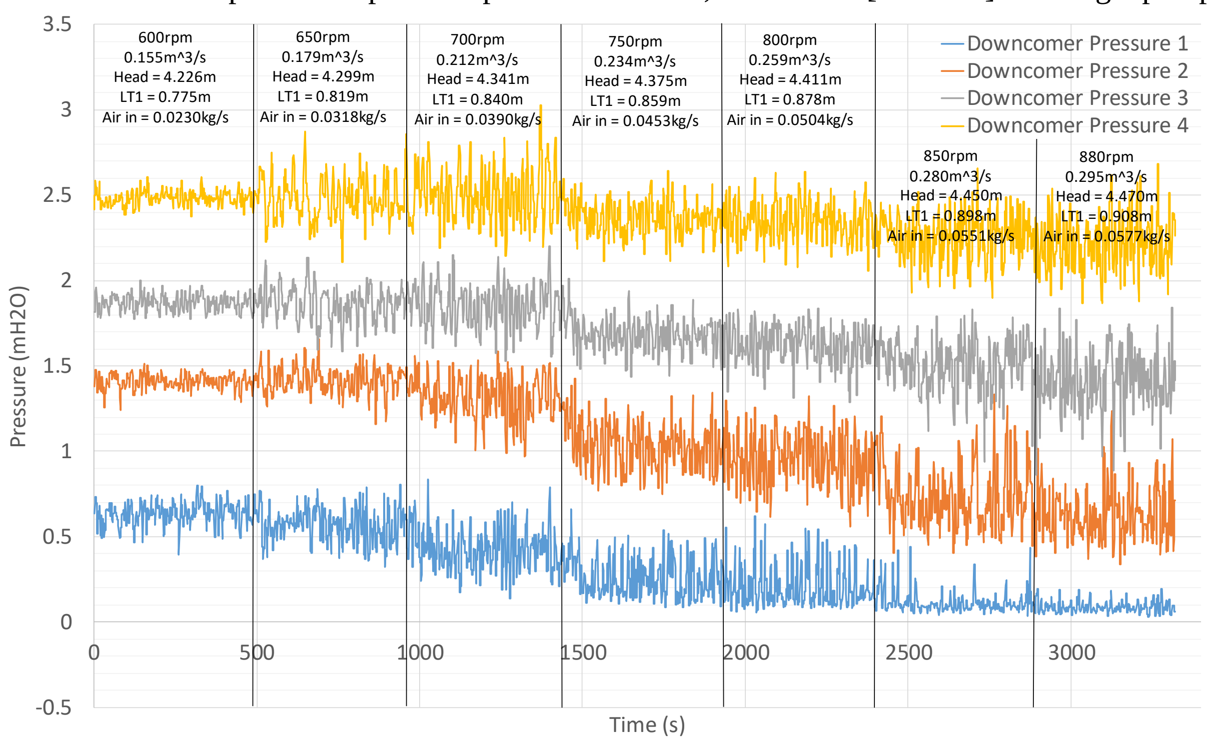

L32: Time series plot of the pressure profile for BM83, fill level at [-2.274m] and single pump.

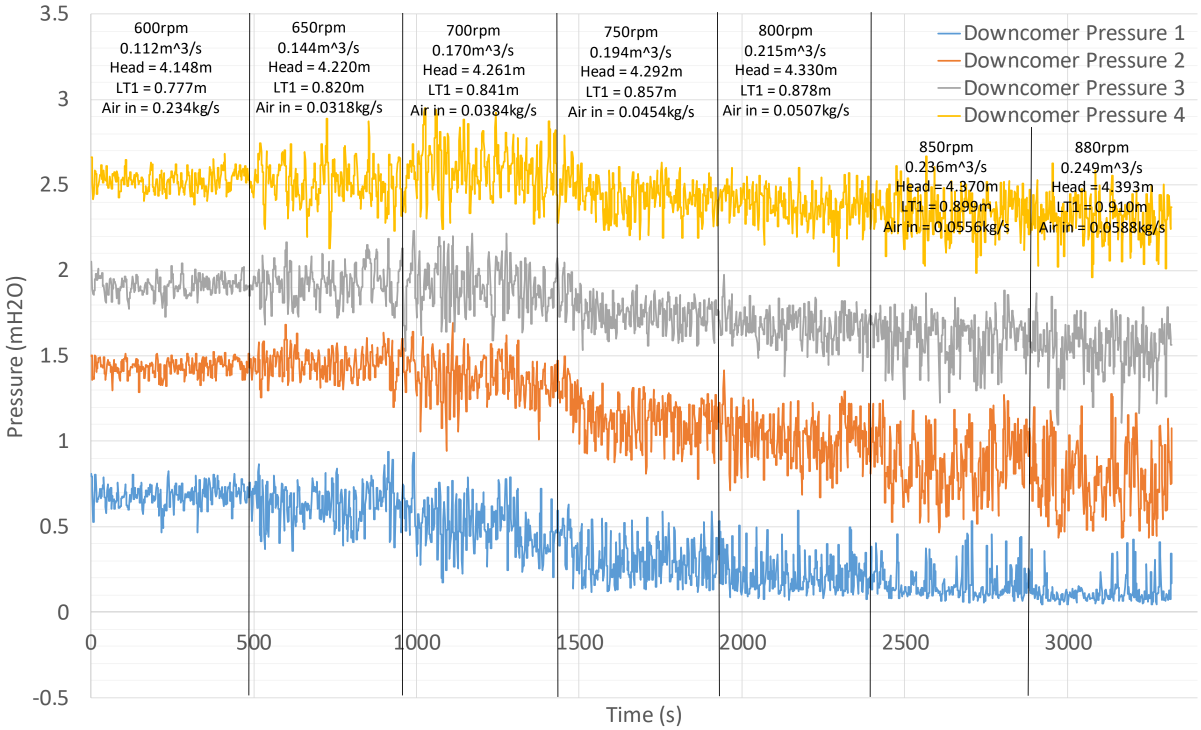

L33: Time series plot of the pressure profile for BM84, fill level at 0.189m and single pump.

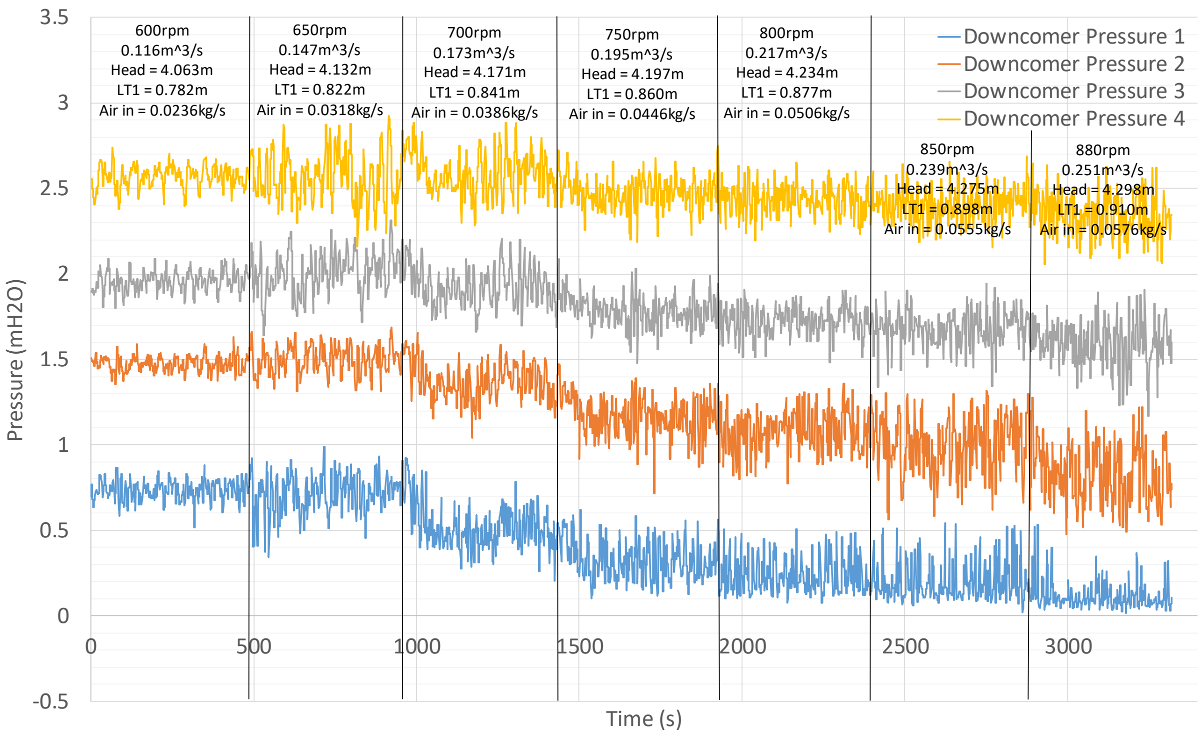

L34: Time series plot of the pressure profile for BM85, fill level at 0.285m and single pump.

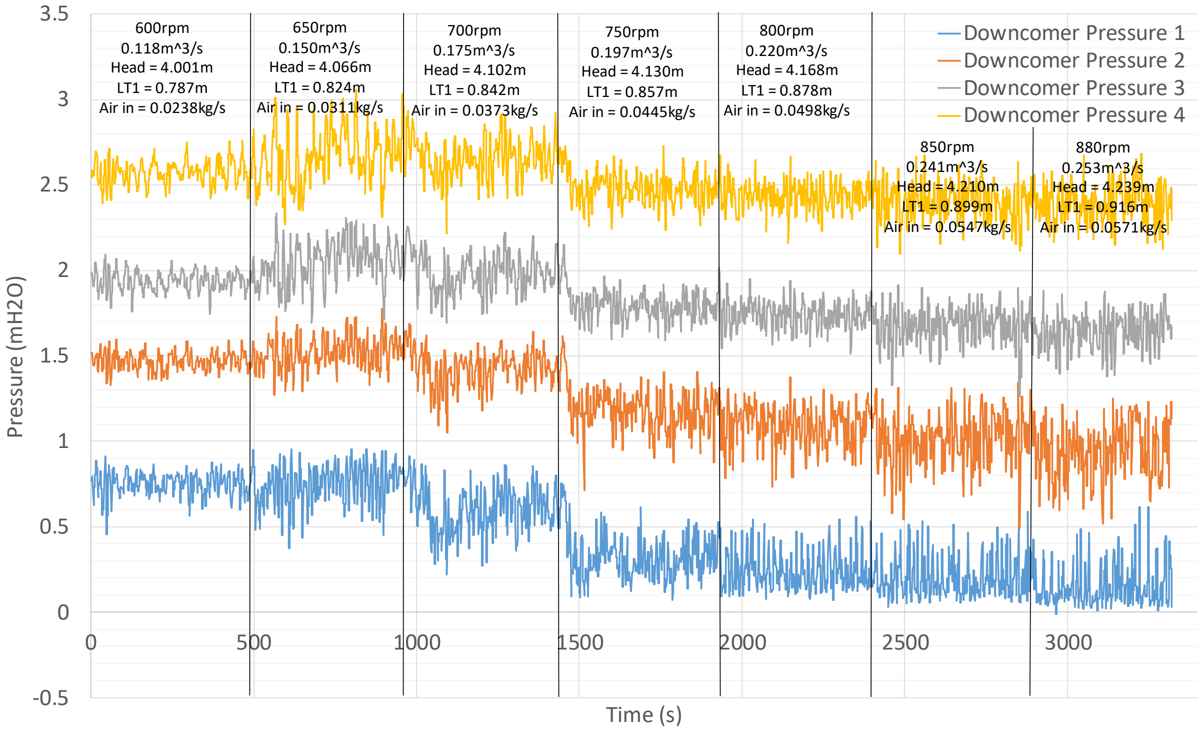

L35: Time series plot of the pressure profile for BM86, fill level 0.3648m and single pump.

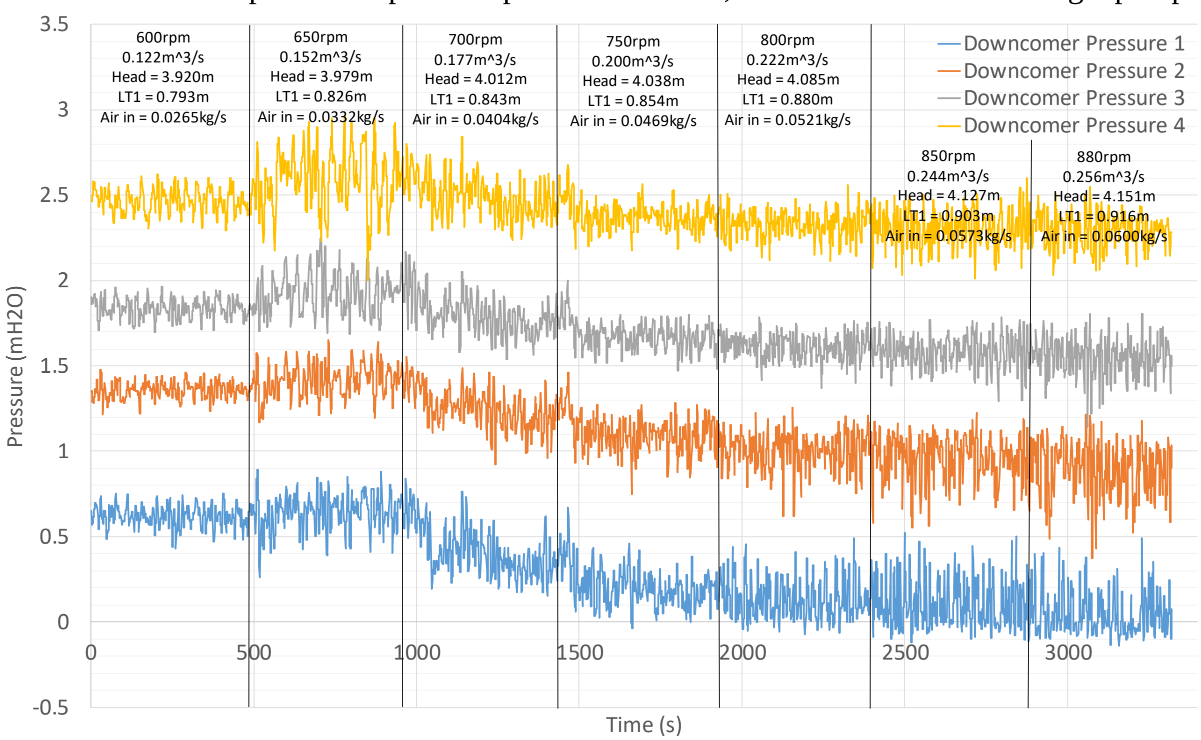

L36: Time series plot of the pressure profile for BM87, fill level 0.450m and single pump.

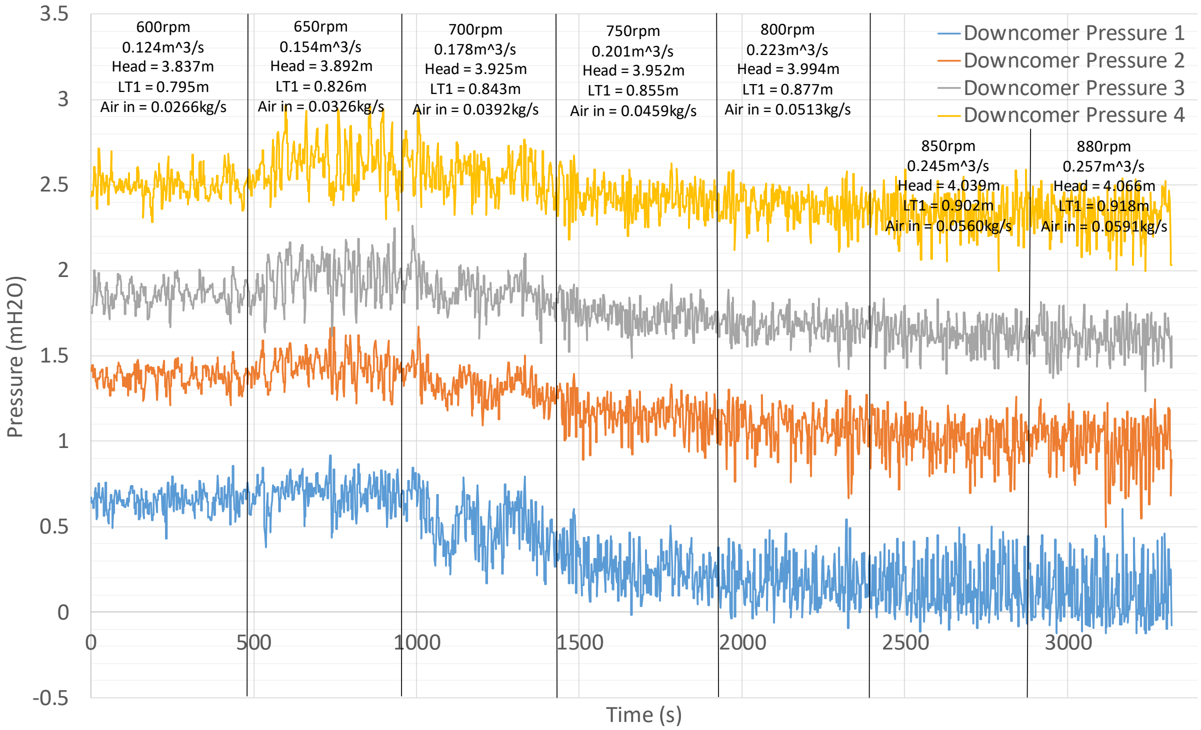

L37: Time series plot of the pressure profile for BM88, fill level 0.550m and single pump.

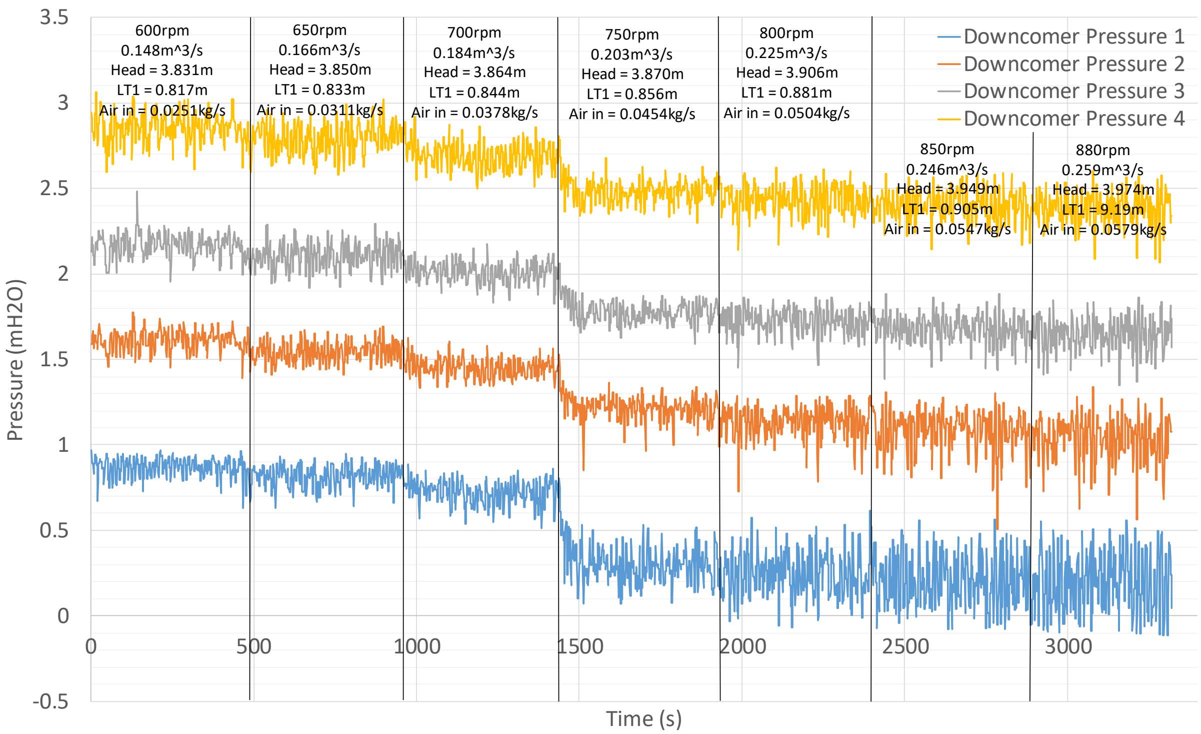

L38: Time series plot of the pressure profile for BM89, fill level 0.650m and single pump.

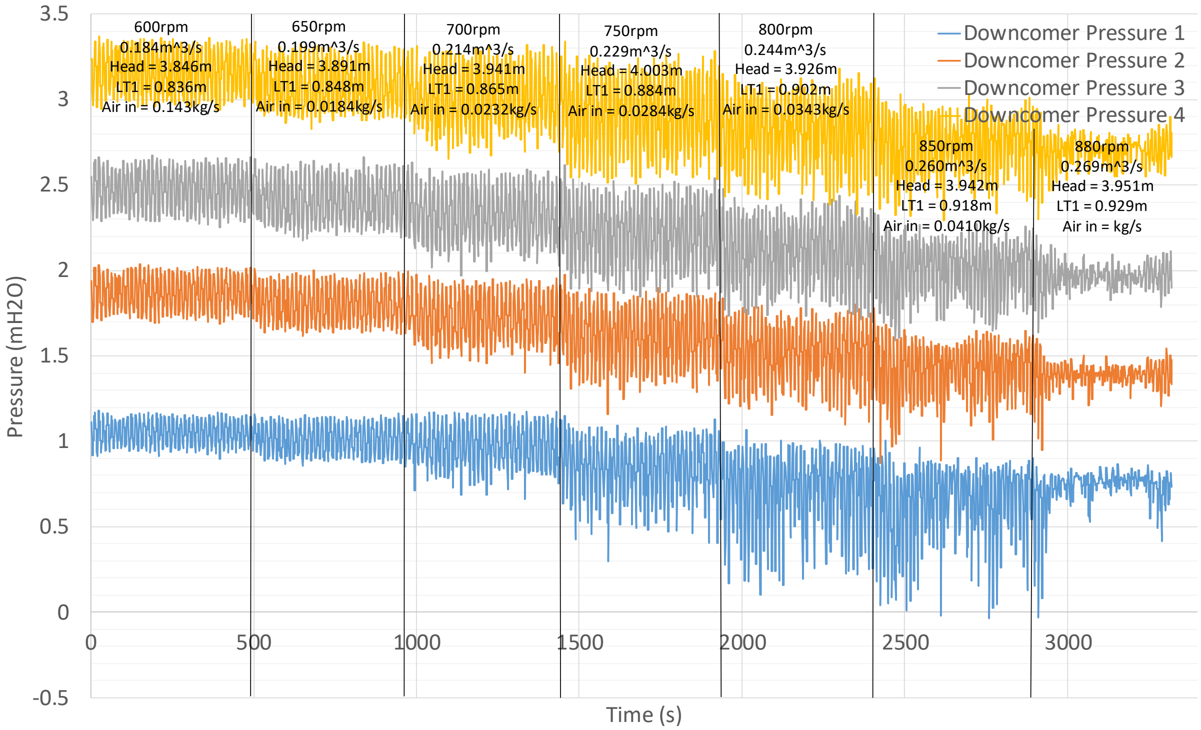

L39: Time series plot of the pressure profile for BM90, fill level 0.750m and single pump.

Appendix M: Dynamic Earth HAC start-up procedure

HAC System Startup Procedure`

1. Turn on the Server by flipping the CB01 breaker within the Control Panel. The colour indicator on the breaker should be red to indicate it is ON.
2. Press the E-Stop reset button on the front of the Control Panel.
3. Turn on both VFD's by flipping their respective breakers labelled VFD-1 and VFD-2.
4. If the LED on the VFD's is flashing red, simply press the reset button on the VFD manually. This should stop the light from flashing red to flashing green.
5. Check if all of the instruments are properly communicating with the Server by opening the TOPServer software. Then open the OPC Quick Client accessible from the Tools drop down menu. Cycle through the following tabs on the left and check if the tags on the right side of the screen are reading values:

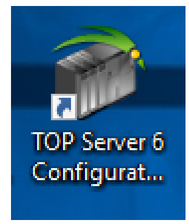

   a. ABB_Test.VFD#1
   b. ABB_Test.VFD#2
   c. Analogue Inputs.I/O-1
   d. Analogue Inputs.I/O-2
   e. Analogue Inputs.I/O-3
   f. Analogue Outputs.I/O-4
   g. GTW-1 Port 1.DowncomerShaft
   h. GTW-1 Port 1.Pump_1
   i. GTW-1 Port 1.Pump_2
   j. GTW-1 Port 3 (T+RH) Top.Temp/RH 1
   k. GTW-1 Port 3 (T+RH) Top.Temp/RH 2
   l. Power metering.CVM1
   m. Power metering.CVM2

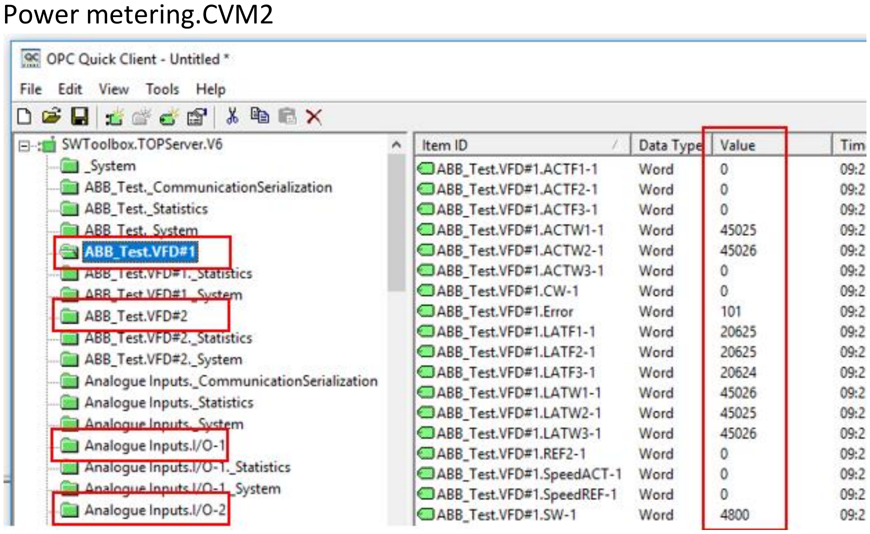

6. Any "Unknown" readings would indicate there is an issue with the communication between the Server and the respective instrument. If any the tags on one of those Devices is reading "Unknown" the likely solution would be to simply reboot the server by flipping the CB01 breaker OFF and ON again, and repeating steps 4-6.
7. To log data to the SQL Server, you must ensure the Data Logger Runtime is running. You can check this by clicking the arrow on the far right of the task bar revealing the hidden icons. The Data Logger icon should read "OPC Data Logger – Runtime Mode Enabled". If Runtime is not enabled but the Icon is there, simply right click on it and initiate the runtime. If the Icon is not there, double click on the Data Logger Notification Shortcut on the desktop to make it appear in the hidden icons. If the computer was recently restarted you will need to Start the data logger service by right clicking on the icon in the hidden icon tab once you have opened it, then proceed to start runtime after the service has been started.

8. A compiled version of the HMI should be located on the desktop, simply double click on this icon to start up the app.

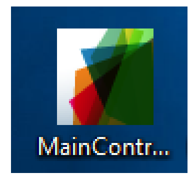

9. Click *Start* on the *GUI Loop*. After a short delay the tags below and the graphs should be updating every second, and the lamp should have changed to green to indicate it is running.
10. Set the desired speed of both VFD's by changing the text in the *VFD-1 Controller (rpm)* and *VFD-2 Controller (rpm)* text boxes. Then click on both the *Set Speed VFD-1* and *Set Speed VFD-2* buttons, the green lamp should change to yellow to indicate the process is in happening and back to green upon completion. *SpeedREF1* and *SpeedREF2* should have both been updated to the desired speed.
11. Press the *Ready/Stop* button to Ready the VFD's for operation. The LED's on the physical VFD's should stop flashing green and simply be a solid green after pressing the *Ready/Stop* button.
12. Press *Start* on the HMI to start the VFD's at the desired set speed.
13. Carefully watch the level in the Separator Tank decrease on the right graph indicated by a green line of data points. **Once the Separator Level falls below 1.7m**, or the set point, turn on the *PID Loop* by pressing the *Start PID* loop button.
14. The system is now automatically regulating the control valve to maintain a set separator level. Adjustments made to the VFD speeds can be done periodically and the PID system will control the valve accordingly to maintain the separator set point. It takes roughly 1-2 minutes to reach stability depending on the variation in VFD speed.
15. To stop the system simply press the *Ready/Stop* button. This will stop both the PID Loop and the VFD's and will close the Control Valve. A 0.5-0.6% value on *FCV-2 (%)* indicates the valve is in the closed position.
16. Benchmark tests can be performed by pressing start/stop benchmark test on the HMI once the system is operating in a steady state condition. The benchmark test takes about 56 minutes with 7 set points each being held for 8 minutes.